University of Alberta

Petrogenesis of the Northern Alberta Kimberlite Province

by

Donald Roy Eccles ©

A thesis submitted to the Faculty of Graduate Studies and Research in partial fulfillment of the requirements for the degree of Master of Science

Department of Earth and Atmospheric Sciences

Edmonton, Alberta

Spring 2004

Library and
Archives Canada

Published Heritage
Branch

395 Wellington Street
Ottawa ON K1A 0N4
Canada

Bibliothèque et
Archives Canada

Direction du
Patrimoine de l'édition

395, rue Wellington
Ottawa ON K1A 0N4
Canada

Your file Votre référence
ISBN: 0-612-96471-X
Our file Notre référence
ISBN: 0-612-96471-X

The author has granted a non-exclusive license allowing the Library and Archives Canada to reproduce, loan, distribute or sell copies of this thesis in microform, paper or electronic formats.

L'auteur a accordé une licence non exclusive permettant à la Bibliothèque et Archives Canada de reproduire, prêter, distribuer ou vendre des copies de cette thèse sous la forme de microfiche/film, de reproduction sur papier ou sur format électronique.

The author retains ownership of the copyright in this thesis. Neither the thesis nor substantial extracts from it may be printed or otherwise reproduced without the author's permission.

L'auteur conserve la propriété du droit d'auteur qui protège cette thèse. Ni la thèse ni des extraits substantiels de celle-ci ne doivent être imprimés ou aturement reproduits sans son autorisation.

In compliance with the Canadian Privacy Act some supporting forms may have been removed from this thesis.

Conformément à la loi canadienne sur la protection de la vie privée, quelques formulaires secondaires ont été enlevés de cette thèse.

While these forms may be included in the document page count, their removal does not represent any loss of content from the thesis.

Bien que ces formulaires aient inclus dans la pagination, il n'y aura aucun contenu manquant.

Canada

Abstract

Ultramafic rocks have been discovered in three separate areas of northern Alberta. Pyroclastic (juvenile lapilli-bearing olivine tuff), serpentine to carbonate-bearing serpentine kimberlitic rocks are by far the dominant rock type in the northern Alberta kimberlite province.

The Mountain Lake pipes are not archetypal kimberlite, and are classified as alkali olivine basalt/basanite. The majority of the Buffalo Head Hills and Birch Mountains kimberlites are derived from low degree partial melts that resemble South African Group I kimberlite. The kimberlite fields can be distinguished from one another by their primitive to evolved magmatic signatures, which reflect differences in the mineralogy and composition of the source region related to magmatic differentiation processes.

This is important from the viewpoint of diamond exploration because the majority of the more primitive Buffalo Head Hills kimberlites are diamondiferous, whereas the evolved Birch Mountains pipes are mostly barren of diamonds.

Dedication

This thesis is dedicated to Karena, Allison, Meghan and Thomas.

Thank you for your positive guidance, support, love and enthusiasm.
Without these, this thesis would not have been possible.

For your presence, I am forever grateful.

Acknowledgements

Rick Richardson, Reg Olson and Mark Fenton of the Alberta Geological Survey and Bob Luth, Larry Heaman, Thomas Stachel and Rob Creaser of the University of Alberta are thanked for their intuitive discussion with regard to the direction and goals of this thesis. On a historical note, Rick's continued encouragement to register for post-graduate studies was a major factor in the decision to undertake this thesis – thank you. Bob and Larry acted as co-supervisors and are thanked not only for their genuine interest in this study, but also for their seemingly unknowing capacity to teach the values of professionalism and dedication.

Several exploration companies are thanked for their roles in the discovery of kimberlitic occurrences in northern Alberta and for providing samples of Alberta kimberlitic rocks. These include: Alberta Energy Company (now EnCana Corporation), Ashton Mining of Canada Inc., Kennecott Canada Exploration Inc., Monopros Limited (De Beers), Montello Resources Ltd., New Blue Ribbon Resources Ltd. (now Blue Diamond Mining Corporation), Pure Gold Resources Ltd. and Redwood Resources Ltd.

Several individuals played key roles during the construction of this thesis. Andrew Skupinski of Tatra Mineralogical Services and Barbara Scott Smith of Scott-Smith Petrological Inc. are thanked for their insightful and patient responses to the many petrological questions. Dinu Pana and Glen Prior of the Alberta Geological Survey of Alberta are thanked for editorial notes on the basement of Alberta and pyroclastic deposits, respectively. Sergei Matveev and Diane Caird at the University of Alberta are thanked for operation of the electron microprobe and X-ray diffraction analysis, respectively. Lastly, many thanks to Mike Dufresne of APEX Geoscience Ltd. for the always enjoyable discussion 'sessions' on the geological setting of northern Alberta.

Table of Contents

1 Introduction ... 1
1.1 Major- and trace-element geochemistry ... 1
1.2 Petrographic Characteristics ... 3
1.3 Radiogenic Isotopes ... 3
2 Geological Setting of the Northern Alberta Kimberlite Province ... 4
2.1 Precambrian Basement ... 5
2.2 Proterozoic Strata ... 8
2.3 Paleozoic to Jurassic Platformal Succession ... 9
2.4 Mid-Jurassic to Paleocene Foreland Basin Succession ... 9
2.5 Late Tertiary to Quaternary Sand and Gravel Deposits ... 10
2.6 Quaternary ... 11
2.7 Major Structures and Tectonic Features ... 11
3 Northern Alberta Kimberlite Province: Discoveries and General Geology ... 13
3.1 Mountain Lake Cluster ... 13
3.2 Buffalo Head Hills Kimberlite Field ... 17
3.3 Birch Mountains Field ... 18
4 Sample Selection and Analytical Techniques ... 20
4.1 Whole-Rock Geochemistry ... 23
4.2 Petrography ... 23
4.3 Isotope Geochemistry ... 24
4.3.1 Whole-rock Sm-Nd, Rb-Sr and Pb-Pb ... 24
4.3.2 U-Pb Perovskite ... 25
4.3.3 Rb-Sr Phlogopite ... 26
5 Criteria Used for Classification of Alberta Kimberlitic rocks ... 27
5.1 Comparative Rock Descriptions for Geochemical Classification ... 27
5.2 Petrographic Nomenclature and Terminology of Kimberlite ... 29
5.2.1 Nomenclature ... 29
5.2.2 Textural- and Mineraological-Genetic Classifications ... 33
6 Whole-Rock Geochemistry ... 34
6.1 Contamination and Alteration ... 34
6.2 Major Element Geochemistry ... 37
6.2.1 Mountain Lake ... 37
6.2.2 Buffalo Head Hills ... 46
6.2.3 Birch Mountains ... 47
6.2.4 Major-Element Comparisons of the Buffalo Head Hills and Birch Mountains with Kimberlites Worldwide ... 48
6.3 Compatible- and Incompatible-Trace Element Geochemistry ... 50
6.3.1 Compatible-Trace Element Variation Between Magmas ... 50
6.3.2 Incompatible-Trace Element Variation Between Magmas ... 53
6.3.3 Mountain Lake ... 55
6.3.4 Buffalo Head Hills ... 57
6.3.5 Birch Mountains ... 60
6.4 Linear Relationships Using Multi-Element Principal-Component Analysis ... 62
6.4.1 Introduction to Principal Component Analysis ... 62
6.4.2 Results of Principal Component Analysis Results ... 63
6.4.3 Kimberlite Trend ... 65
6.4.4 Mountain Lake Trend ... 68
6.5 Geochemistry and Diamond Content ... 68
7 Selection of Pipes for Detailed Petrography and Isotopic Analysis ... 70

8 Textural-Genetic Classification and Petrographic Summary 70
9 Mineralogical Summary 76
9.1 Olivine 76
9.2 Serpentine 78
9.3 Carbonate 79
9.4 Phlogopite 79
9.5 Apatite 80
9.6 Perovskite 80
9.7 Opaque Minerals 81
10 Radiogenic Isotopes 81
10.1 Considerations for Country Rock Contamination 83
10.2 Considerations for Mantle Metasomatism 89
10.3 Whole-Rock Isotopic Tracing 90
10.4 Emplacement Age Results 92
10.5 Temporal and Spatial Associations between Western North America Kimberlite Fields 100
11 Discussion: Petrogenetic Considerations for the Northern Alberta Kimberlite Province 102
11.1 Evolution of Kimberlitic Magma 102
11.1.1 Source Composition 103
11.1.2 Magmatic Differentiation 103
11.1.2.1 Partial Melting 104
11.1.2.2 Mantle Metasomatism 105
11.1.2.3 Crystal Fractionation 106
11.2 Geodynamic Controls for Kimberlite Emplacement 108
11.2.1 Mantle Plume Hotspot Tracks 108
11.2.2 Subduction 109
11.2.3 Structure 110
12 Final Observations and Conclusions 113
12.1 General 113
12.2 Petrological Characteristics 115
12.3 Petrogenesis 116
13 References 118
Appendix 1. Major-element geochemical data from bulk rock samples collected from selected pipes in the Mountain Lake, Buffalo Head Hills and Birch Mountains fields. 132
Appendix 2. Trace-element geochemical data from bulk rock samples collected from selected pipes in the Mountain Lake, Buffalo Head Hills and Birch Mountains fields. 134
Appendix 3. Petrographic Characteristics of Individual Samples 136
Appendix 3. 1 Samples ABK01, ABK02 and ABK03 (Kimberlite K4, Buffalo Head Hills) 136
Appendix 3.1. 1 Sample ABK01 (Kimberlite K4A, Buffalo Head Hills) 136
Appendix 3.1. 2 Sample ABK02 (Kimberlite K4B, Buffalo Head Hills) 139
Appendix 3.1. 3 Sample ABK03 (Kimberlite K4C, Buffalo Head Hills) 140
Appendix 3. 2 Samples ABK05 and ABK29 (Kimberlite K6, Buffalo Head Hills) 143
Appendix 3. 3 Samples ABK59 and ABK68 (Legend Kimberlite, Birch Mountains) 149
Appendix 3. 4 Samples ABK75 and ABK76 (Phoenix Kimberlite, Birch Mountains) 154
Appendix 3. 5. Samples ABK81 and ABK82 (Kendu Pipe, Birch Mountains) 157
Appendix 4. Electron microprobe backscatter and X-ray elemental images. 164
Appendix 5. Bulk-rock X-ray diffractograms. 169

List of Tables

Table 1. Sample summary with type of geochemical analyses performed. 21
Table 2. Mineralogical comparisons between kimberlites, orangeites and lamproites (modified after Mitchell, 1995). 32
Table 3. Duplicate samples from northern Alberta kimberlitic rocks with geochemical data and relative error. 35
Table 4. Comparison of selected major elements in northern Alberta kimberlitic rocks with average kimberlite, olivine/madupitic lamproite, olivine melilitite, olivine minette and basanite. 40
Table 5. Selected trace and major elements and element ratios from Alberta kimberlitic rocks and, for comparison, worldwide kimberlite, olivine melilitite and Sweet Grass minette. 52
Table 6. Relative contributions of selected major and trace elements to principal components 1 to 5: A) PC scores with positive values in bold; and B) relative contribution expressed as percentages with values greater than 35% in bold. Because only components 1 to 5 are presented, the percentages for individual elements does not add up to 100. 66
Table 7. Samples selected for detailed petrography and whole-rock isotope analysis. 72
Table 8. Summary of the properties, infilling and classification of selected northern Alberta kimberlitic pipes. 73
Table 9. Results of northern Alberta kimberlitic whole-rock isotopic analysis. 82
Table 10. Sample location and description of isotopic analysis on mineral separates from kimberlitic rocks in northern Alberta. 93
Table 11. Results of U-Pb perovskite, U-Pb rutile and Rb-Sr phlogopite isotopic analysis for northern Alberta kimberlitic rocks. 94
Table 12. Age compilation for northern Alberta kimberlitic rocks. 101

List of Figures

Figure 1. Generalized bedrock geology of northern Alberta with kimberlitic rock occurrences. 2
Figure 2. Inferred Precambrian basement terranes in northern Alberta with kimberlitic rock locations. 6
Figure 3. Distribution of kimberlitic rocks in northern Alberta. 14
Figure 4. Plot of contamination index of Clement (1982) versus ilmenite index of Taylor et al. (1994) for northern Alberta kimberlitic whole-rock compositions. Contaminated rocks (C.I. >1.5) are labelled and include macroscopic observations. Dashed line represents a C.I. of 1.5; vectors show trends for kimberlite contamination by granitic and siliceous crustal rocks, Fe- and Ti-oxide (ilmenite) accumulation, and olivine accumulation (Taylor et al., 1994). See section 5.1 in text for sources of comparative data. Abbreviation: DIM, diamond-indicator minerals. 38
Figure 5. Whole-rock Al_2O_3 versus SiO_2 for kimberlitic rocks from northern Alberta. Arrows indicate alteration (serpentinization and carbonate enrichment) and crustal contamination (shale, siltstone, sandstone and felsic rocks) vectors for northern Alberta. See section 5.1 in text for sources of comparative data. 39
Figure 6. Major-element whole-rock variation diagrams with SiO_2 for kimberlitic rocks from northern Alberta. 42
Figure 7. SiO_2 versus peralkalinity index (molar $[K_2O+Na_2O]/Al_2O_3$) for northern Alberta kimberlitic whole-rock compositions. Dashed line represents a peralkalinity value of 1.0. Solid vectors or polygons represent the three groups of potassic lavas recognized by Barton (1979): RPT, Roman Province type lavas; LHT, Leucite Hills type lavas; TAT, Toro-Ankole type lavas. See section 5.1 in text for sources of comparative data. 43

Figure 8. Alkali classification plots for northern Alberta kimberlitic whole-rock compositions: A) K_2O versus Na_2O; B) total alkalis versus SiO_2 (TAS classification); C) $CaO+Na_2O+K_2O$ versus $SiO_2+Al_2O_3$. See section 5.1 in text for sources of comparative data. 45

Figure 9. Plot of Mg# versus SiO_2, K_2O and TiO_2 for northern Alberta kimberlitic whole-rock compositions. Fields for South African Group I and Group II kimberlites are from Clement (1982) and Smith et al. (1985b). See section 5.1 in text for sources of comparative data. 49

Figure 10. Plot of TiO_2 versus K_2O for northern Alberta kimberlitic whole-rock compositions. Fields for kimberlite and related rock types are from Taylor et al. (1994). See section 5.1 in text for sources of comparative data. 51

Figure 11. Compatible-element distribution diagram for northern Alberta kimberlitic whole-rock compositions. A) Mountain Lake; B) Buffalo Head Hills; C) Birch Mountains; and D) Average kimberlite, melilitite, alkali olivine basalt and tholeiitic basalt compiled from Mitchell (1986) shown for comparison. Pyrolite abundance from Jagoutz et al. (1979). 54

Figure 12. Incompatible-element distribution diagram for whole-rock compositions from the Mountain Lake pipes. A) Mountain Lake samples; and B) Mountain Lake field with average kimberlite (Mitchell, 1986; Muramatsu, 1983), Montana alnöite (Hearn, 1986), Sweet Grass minette (Buhlmann et al., 2000), Roman Province–type lavas from Mount Ernici and Mount Vulsini (*from* Mitchell, 1995; *after* Peccerillo et al., 1988), South African melilitite (Rogers et al., 1992) and Wapiti Formation sedimentary rocks sampled adjacent to the Mountain Lake pipes (Dufresne et al., 2001) shown for comparison. Primitive mantle values from McDonough and Sun (1995). 56

Figure 13. Chondrite-normalized rare-earth element patterns for northern Alberta kimberlitic whole-rock compositions: A) Mountain Lake; B) Buffalo Head Hills; and C) Birch Mountains. Shaded pattern represents average worldwide kimberlite (Mitchell 1986); Roman Province–type lavas from Ernici, Italy (Civetta et al., 1981); olivine minette from Sweet Grass Hills, Alberta (Kjarsgaard, 1994; Buhlmann et al., 2000); and alnöite from Montana (Hearn, 1986). Chondrite values from Taylor and McLennan (1985). 58

Figure 14. Incompatible-element distribution diagram for whole-rock compositions from the Buffalo Head Hills. A) Buffalo Head Hills samples; and B) Selected Buffalo Head Hills groups with average kimberlite (Mitchell, 1986; Muramatsu, 1983) and Group I and Group II kimberlite (Smith et al., 1985b) shown for comparison. Primitive mantle values from McDonough and Sun (1995). 59

Figure 15. Incompatible-element distribution diagram for whole-rock compositions from the Birch Mountains. A) Birch Mountains samples; and B) Selected Birch Mountains groups with average kimberlite (Mitchell, 1986; Muramatsu, 1983) and Group I and Group II kimberlite (Smith et al., 1985b) shown for comparison. Primitive mantle values from McDonough and Sun (1995). 61

Figure 16. Screeplot showing the fraction of total variance in the data as represented by each Principal Component. 64

Figure 17. Principal-component analysis of selected major and trace elements from northern Alberta kimberlitic whole-rock compositions. Arrows indicate line of descent directions for primitive (P) to metasomatically enriched (E) kimberlite, and the direction for kimberlite contamination and/or Mountain Lake hybrid-type rocks. Kimberlite values from Jericho, Northwest Territories (Price et al., 2000) and South Africa (Smith et al., 1985b). 67

Figure 18. Whole-rock geochemical groups used for selection of pipes for detailed petrography and isotopic analysis. 71

Figure 19. Modal distribution of olivine, as determined in thin section, from selected northern Alberta kimberlitic pipes. 77

Figure 20. Nd-Sr isotope variations from selected kimberlitic rocks in northern Alberta. 84

Figure 21. Isotopic composition of Pb from kimberlitic rocks in northern Alberta. 85

Figure 22. Composite isotope-mixing diagrams for Buffalo Head Hills kimberlites with selected Sr (ppm) and initial $^{87}Sr/^{86}Sr$ values for continental plutonic rock (270, 0.7140), Devonian carbonate (245, 0.7085), clastic sediment (170, 0.7165), Cretaceous-Tertiary aquifers (6.4, 0.7080), worldwide carbonatites (10 000, 0.7032) and high-$^{87}Sr/^{86}Sr$ carbonatite (7 750, 0.7052). See text for references. Stars represent kimberlite samples. 86
Figure 23. Composite isotope-mixing diagrams for Birch Mountains kimberlites with selected Sr (ppm) and initial $^{87}Sr/^{86}Sr$ values for continental plutonic rock (270, 0.7140), Devonian carbonate (245, 0.7085), clastic sediment (170, 0.7165), Cretaceous-Tertiary aquifers (6.4, 0.7080), worldwide carbonatites (10 000, 0.7032) and high-$^{87}Sr/^{86}Sr$ carbonatite (7 750, 0.7052). See text for references. Stars represent kimberlite samples. 87
Figure 24. U-Pb concordia diagram for perovskite and rutile from selected kimberlitic rocks in northern Alberta. 96
Figure 25. Rb-Sr isochron diagram for whole-rock and phlogopite macrocrysts from selected kimberlitic rocks in northern Alberta. 99
Figure 26. Whole rock MgO versus SiO_2 for kimberlitic rock samples from nothern Alberta. Average olivine, phlogopite, garnet and clinopyroxene are from a variety of northern Alberta pipes (Creighton and Eccles, 2003; Eccles, unpublished data). 107
Figure 27. Hypothetical evolution of the crust in northern Alberta (Ross and Eaton, 2002; reproduced with permission from the Canadian Journal of Earth Sciences). 112

List of Appendix 3 Table

Table A3- 1. Summary of X-ray diffraction analysis on selected whole-rock northern Alberta kimberlitic rocks. 137

List of Appendix 3 Figures

Figure A3- 1. Photomicrographs of sample ABK01, K4A pipe, Buffalo Head Hills: A) scan of polished thin section; B) representative matrix; and C) elongate, blocky quartz textures indicative of secondary, hydrothermal emplacement. Abbreviation: FOV, field of view. 138
Figure A3- 2. Photomicrographs of sample ABK02, K4B pipe, Buffalo Head Hills: A) scan of polished thin section; B) representative matrix; C) curvilinear lapillus; D) comparison between lapillus matrix and matrix that encompasses lapillus; and D) pyrite nucleating on dolomite. Abbreviation: FOV, field of view. 141
Figure A3- 3. Backscatter image of representative area from sample ABK02, K4B pipe, Buffalo Head Hills. 142
Figure A3- 4. Photomicrographs of sample ABK03, K4C pipe, Buffalo Head Hills: A) scan of polished thin section; B) and C) selected images of tabular serpentine under plane and crossed polars, respectively. Abbreviation: FOV, field of view. 144
Figure A3- 5. Scanned images of polished thin sections from samples ABK05 and ABK29, K6 pipe, Buffalo Head Hills. Abbreviation: FOV, field of view. 146
Figure A3- 6. Variation between juvenile lapilli from the K6 pipe, Buffalo Head Hills: A) large, curvilinear lapillus; and B) ash- to lapilli-sized juvenile pyroclasts. Abbreviation: FOV, field of view. 147
Figure A3- 7. Ash- and lapilli-sized juvenile pyroclasts from the K6 pipe, Buffalo Head Hills: A) in hand sample; and B) photomicrograph mosaic capturing the entire pyroclast, in plane-polarized light. Abbreviation: FOV, field of view. 148
Figure A3- 8. Photomicrographs of sample ABK05, K6 pipe, Buffalo Head Hills: A) backscatter image of representative matrix; B) perovskite; C) dendritic crystals of ilmenite; and

D) intergrown ilmenite (light grey) and chromite (dark grey). Abbreviation: FOV, field of view. 150
Figure A3- 9. Mantle xenolith from sample ABK29, K6 pipe, Buffalo Head Hills: A) expanded view of the xenolith in contact with kimberlite; B) clinopyroxene and orthopyroxene; and C) IUGS classifcation of ultramafic rocks. Abbreviation: FOV, field of view. 151
Figure A3- 10. Basement xenolith from sample ABK29, K6 pipe, Buffalo Head Hills. Abbreviation: FOV, field of view. 152
Figure A3- 11. Photomicrographs of sample ABK59, Legend pipe, Birch Mountains: A) scan of polished thin section; B) blowup of image A, with lapillus; C) lapillus; D) hexagonal apatite; E) needle-textured sulphide mineral (?pyrite); and F) ilmenite. Abbreviation: FOV, field of view. 155
Figure A3- 12. Photomicrographs of sample ABK76, Phoenix pipe, Birch Mountains: A) scan of polished thin section; B) enlargement of image A; C) lapillus; D) matrix perovskite and phlogopite; and E) and F) atoll-textured spinel. Abbreviation: FOV, field of view. 156
Figure A3- 13. Backscatter image of representative area from sample ABK76, Phoenix pipe, Birch Mountains. 158
Figure A3- 14. Photomicrographs of sample ABK81, Kendu pipe, Birch Mountains: A) scan of polished thin section; B) juvenile lapillus in an aphanitic matrix; C) matrix comparison between pyroclast and matrix external to autolith; and D) magnified image of an lapillus. Abbreviation: FOV, field of view. 160
Figure A3- 15. Photomicrographs of the Kendu pipe, Birch Mountains: A) microphenocrystic kimberlitic rock haloes around altered basement xenoliths; B) and C) pelletal-textured lapilli with tangentially aligned phlogopite crystals; and D) matrix microsegregation textures. Abbreviation: FOV, field of view. 161
Figure A3- 16. Photomicrographs of mantle minerals from the Kendu pipe, Birch Mountains. Abbreviation: FOV, field of view. 163

1 Introduction

To September 2003, 48 ultramafic pipes, which comprise mainly volcaniclastic crater facies kimberlite with varying amounts of mantle material, have been discovered in three separate areas of northern Alberta (Figure 1). The northern Alberta pipes, hereafter referred to as the northern Alberta kimberlite province (NAKP), are distributed as follows:

- 2 pipes directly north of Mountain Lake in northwestern Alberta;
- 38 pipes in the Buffalo Head Hills area of north-central Alberta, which are located approximately 175 km northeast of Mountain Lake; and
- 8 pipes in the Birch Mountains area of northeastern Alberta, which are located approximately 85 km east-northeast of the Buffalo Head Hills field.

Thus, the three areas may be referred to as the Mountain Lake (ML) cluster, and Buffalo Head Hills (BHH) and Birch Mountains (BM) 'fields' within the NAKP.

This thesis is the first study to compare the three northern Alberta kimberlite fields and documents the petrographic (e.g., mineralogy and texture), and geochemical (e.g., major and trace element, isotopic) characteristics of the pipes. The thesis is divided into three main sections: whole-rock geochemistry, petrography, and isotopic geochemistry, each of which is now introduced.

1.1 Major- and trace-element geochemistry

Major- and trace-element geochemical studies of kimberlites are hindered by the ubiquitous presence of crustal, xenolithic and xenocrystic material. Because pipes in northern Alberta are dominated by pyroclastic and resedimented volcaniclastic rocks (e.g., Leckie et al., 1997; Carlson et al., 1998; Wood et al., 1998), one might expect that bulk geochemistry is of limited potential for the purpose of rock classification.

As noted by Mitchell (1986), and Mitchell and Bergman (1991), however, ultramafic alkaline rocks such as kimberlites are characterized by elevated contents of first- and second-period transition elements, alkali and alkaline earth elements, and lanthanides relative to common igneous and sedimentary rocks. A number of these elements are relatively immobile during weathering and deuteric alteration processes, because they are hosted in insoluble relict primary and secondary phases, or are insoluble in low-temperature fluids. The absolute abundance of many of these elements may therefore change slightly, but the ratios of these elements should

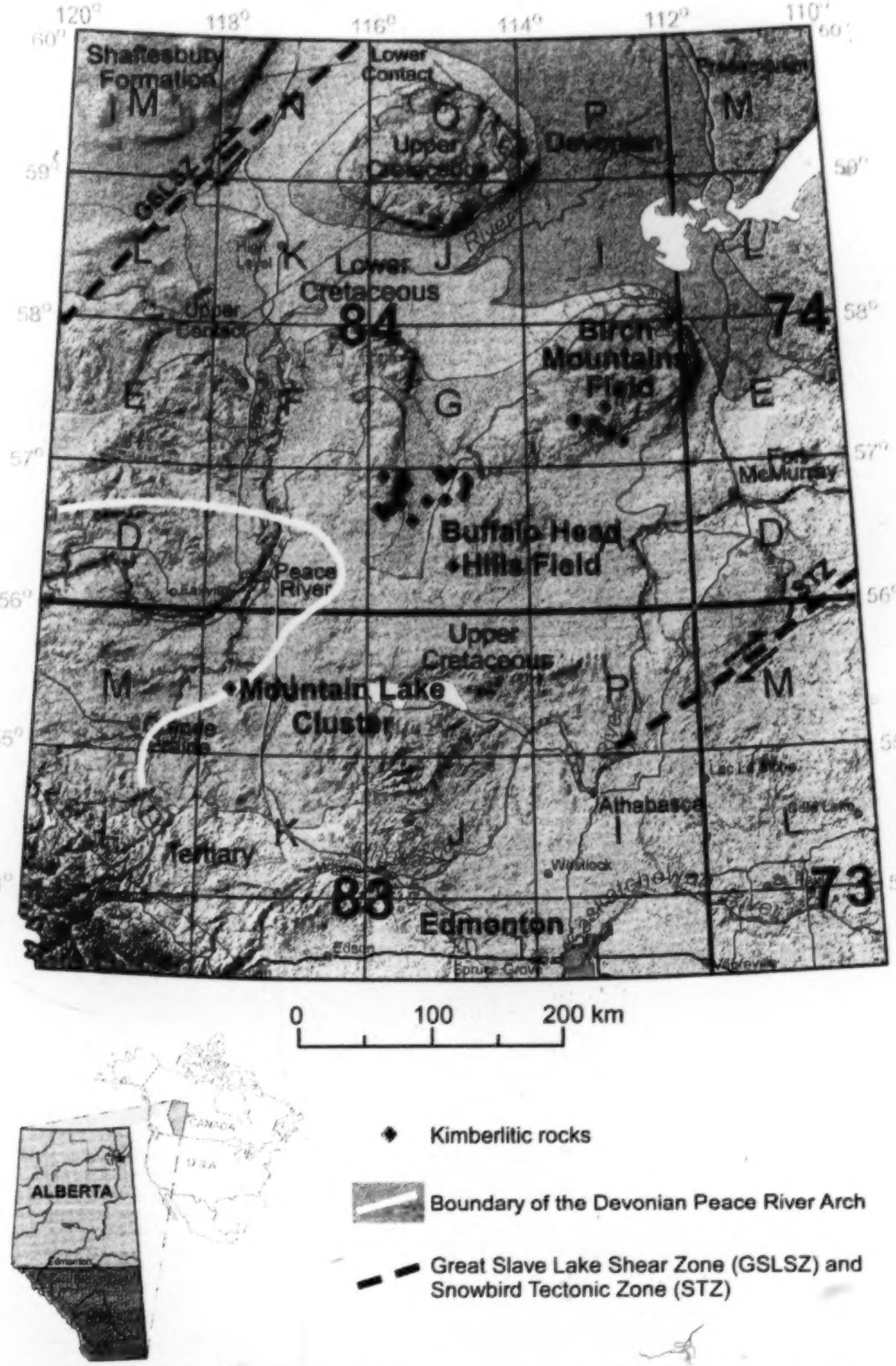
120°
118°
116°
114°
112°
110°
60°
59°
58°
57°
56°
55°
54°
Shaftesbury Formation
Lower Contact
Precambrian
M
N
O
P
M
Upper Cretaceous
Devonian
GSLSZ
L
K
J
I
L
Lower Cretaceous
Upper Contact
84
74
Birch Mountains Field
E
F
G
E
Fort McMurray
D
Buffalo Head Hills Field
D
Peace River
STZ
Upper Cretaceous
M
Mountain Lake Cluster
P
M
Tertiary
K
J
I
L
Athabasca
Lac La Biche
83
73
Edmonton
Spruce Grove
0
100
200 km
ALBERTA
CANADA
USA
Kimberlitic rocks
Boundary of the Devonian Peace River Arch
Great Slave Lake Shear Zone (GSLSZ) and Snowbird Tectonic Zone (STZ)

Figure 1. Generalized bedrock geology of northern Alberta with kimberlitic rock occurrences (Hamilton et al., 1999).

remain unchanged. Therefore, bulk-rock geochemistry may be particularly useful in assessing the character of volcaniclastic and epiclastic sedimentary rocks in crater facies, where highly altered rocks may be difficult to identify by optical or electron beam methods.

Given that the Alberta pipes are variably altered, the first part of this thesis determines if whole-rock geochemistry could provide useful information on northern Alberta kimberlitic rock. To place these geochemical data in context, the compositions of the Alberta samples are compared to each other, and to kimberlite and other alkali rock types worldwide.

The results of the geochemical analysis and interpretation form the basis for the selection of kimberlite samples for detailed petrography and isotopic analysis.

1.2 Petrographic Characteristics

Kimberlites are hybrid rocks that typically contain mantle- and crustal-derived xenoliths and xenocrysts, as well as a variety of primary phases crystallized from the host magma, which itself may be derived from several mantle sources (Clement, 1982). Kimberlite mineralogy is further complicated by the possibility that xenolithic material may be incorporated into the kimberlite melt either at different points during its ascent from the mantle to surface, or locally near the surface because of final emplacement processes.

Because the contribution of any of these sources varies widely among different kimberlites, kimberlite rocks are best characterized by identification and description of the given assemblage of primary minerals. Once the mineralogical assemblage of the kimberlite has been identified, it may be described by mineralogical-genetic nomenclature (e.g., Skinner and Clement, 1979; Scott Smith, 1995). During the last 15 years, the mineralogical-genetic classification has provided petrologists with the most reliable and effective means to classify kimberlite and lamproite and of distinguishing them from other ultramafic/alkaline volcanic rocks (e.g., Jaques et al., 1986; Mitchell, 1986; Mitchell and Bergman, 1991; Scott Smith 1992).

The main objective of the petrographic section is to complement the whole-rock geochemical analysis of selected kimberlites in northern Alberta with optical mineralogical observations.

1.3 Radiogenic Isotopes

Isotopic tracers represent a particularly powerful tool for geochemical studies of mantle-derived kimberlite magma. On the basis that variations in isotopic composition represent derivation from isotopically heterogeneous sources, any major differences in isotopic character between kimberlitic rocks in the NAKP may reflect substantial differences in their mantle source rocks and may shed light on their genesis.

In addition to mantle processes, radiogenic isotopes can provide reliable data on the emplacement age of individual pipes. Knowledge of the ages of kimberlite and related rock intrusions, clusters and provinces provides a basis for evaluating the controls on magma genesis and eruption mechanisms (e.g., le Roex, 1986; Heaman et al., 2003). Furthermore, variations in diamond content relative to emplacement age can help to direct exploration companies to areas of high diamond potential.

Because kimberlitic rocks were only discovered in Alberta during the last decade, little to no research has been reported on their isotopic compositions. To date, no whole-rock Rb-Sr, Sm-Nd or Pb-Pb isotopic ratios have been reported and few emplacement ages have been reported. The latter is particularly true for the BHH field, where emplacement U-Pb perovskite ages between 86 ± 3 Ma and 88 ± 5 Ma are reported from only three of the 38 pipes (Carlson et al., 1999).

The primary objective of the radiogenic isotope study is to sample, analyze and report on the isotopic compositions of selected NAKP pipes. The results are intended to help constrain the emplacement age of selected NAKP pipes and constrain the mantle source(s), and thus, the genesis of Alberta kimberlite.

2 Geological Setting of the Northern Alberta Kimberlite Province

The exposed geology of northern Alberta ranges from Archean to Recent in age, and can be divided into broad northwesterly trending belts, which decrease in age to the southwest (Figure 1; Hamilton et al., 1999). In simplest terms, Archean and Paleoproterozoic shield rocks and Mesoproterozoic Athabasca Group sedimentary rocks are exposed in the northeast corner of Alberta. To the southwest, a major sedimentary basin called the Western Canada Sedimentary Basin (WCSB), forms a northwest-trending trough in front of the Cordilleran Fold and Thrust Belt. In Alberta, this basin is a wedge of Phanerozoic strata above Precambrian crystalline basement, with the Phanerozoic sedimentary rocks tapering from a maximum thickness of about 6000 m just east of the Rocky Mountains foothills front to a zero-edge in the northeast along the Canadian Shield (Mossop and Shetsen, 1994). The Phanerozoic strata have been deposited in the WCSB in two fundamentally different tectonosedimentary environments: a passive continental margin in the Late Proterozoic to Middle Jurassic, and a foreland basin in Middle Jurassic to Oligocene time.

An overview of the geological setting of the NAKP was recently published by Eccles et al. (2003), and is summarized below.

2.1 Precambrian Basement

Approximately 5000 wells have penetrated through WCSB stratigraphy and intersected the underlying Precambrian basement and about 600 of these wells have been cored (Burwash et al., 1994). Basement core from all areas in northern Alberta includes primarily high-grade metamorphic and/or plutonic rocks of a deep crustal level. The most abundant rock types in the northern Alberta basement are: quartzofeldspathic gneiss (58%), granitoid (16%), granulite (10%), metasedimentary rocks (5%), mylonite (5%) and amphibolite (4%), with all other types constituting less than 2% (Burwash et al., 2000). Existing P-T estimates suggest that most of the WCSB in northern Alberta is underlain by granulite grade rocks intruded by major batholitic complexes (e.g., Chacko, 1997; Grover et al., 1997; Ranger, 2000).

The crystalline basement rocks of northern Alberta represent the westernmost part of the Canadian Shield. U-Pb and Sm-Nd data are consistent with differentiation of sialic crust from the mantle during the Archean followed by reactivation of that crust by the Hudsonian tectonomagmatic events. Textural-mineralogical relationships in many basement rocks from northern Alberta are consistent with multiple phases of deformation and recrystallization (Burwash and Krupička, 1969; Burwash et al., 2000). Existing geological information on the sub-WCSB crystalline basement of northern Alberta has been variously assembled to support two different models of Proterozoic terrane accretion:

1) distinct continental slivers accreted to the composite Churchill province during the assembly of western Laurentia (~2.0 to 1.8 Ga; e.g., Hoffman, 1988; Ross et al., 1994), or
2) a more uniform continental fragment that separated from and then welded back to the Churchill province (Burwash et al., 1994, 2000).

Basement subdivisions beneath WCSB in northern Alberta have been inferred from aeromagnetic data, combined with geochronological data. Ross et al. (1994) proposed the basement was comprised of the Taltson, Buffalo Head, Chinchaga, Ksituan and Nova domains (Figure 2). The Great Slave Lake Shear Zone (GSLSZ) and the Snowbird Tectonic Zone (STZ) bound these domains to the northwest and southwest, respectively. The following domain descriptions are from a recent summary of the Alberta basement by Pana (2003).

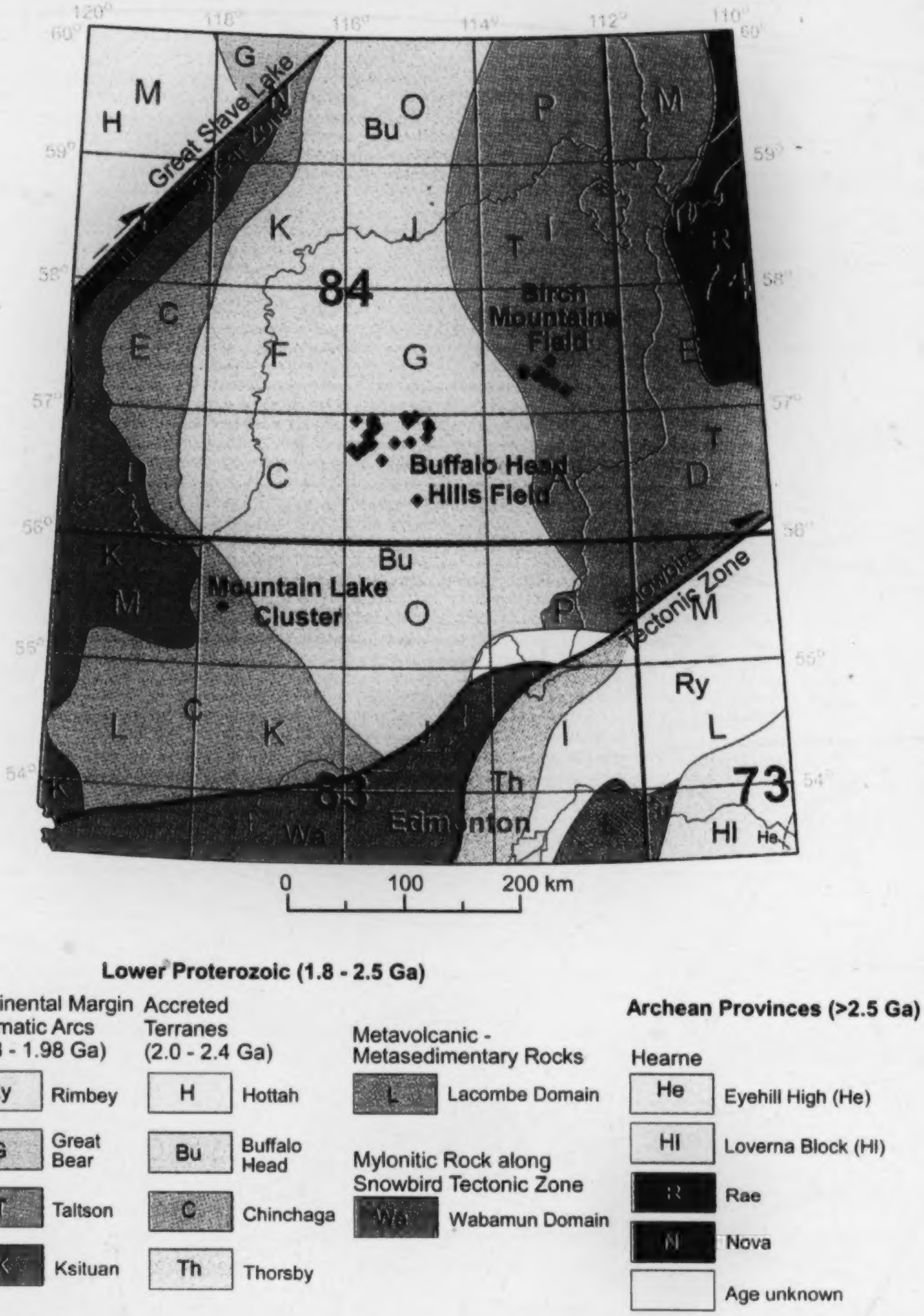
120°
118°
116°
114°
112°
110°
60°
59°
58°
57°
56°
55°
54°
Great Slave Lake Shear Zone
84
83
73
Birch Mountains Field
Buffalo Head Hills Field
Mountain Lake Cluster
Snowbird Tectonic Zone
Edmonton
0
100
200 km
Lower Proterozoic (1.8 - 2.5 Ga)
Continental Margin Magmatic Arcs (1.78 - 1.98 Ga)
Ry Rimbey
G Great Bear
T Taltson
K Ksituan
Accreted Terranes (2.0 - 2.4 Ga)
H Hottah
Bu Buffalo Head
C Chinchaga
Th Thorsby
Metavolcanic - Metasedimentary Rocks
L Lacombe Domain
Mylonitic Rock along Snowbird Tectonic Zone
Wa Wabamun Domain
Archean Provinces (>2.5 Ga)
Hearne
He Eyehill High (He)
Hl Loverna Block (Hl)
R Rae
N Nova
Age unknown

Figure 2. Inferred Precambrian basement terranes with kimberlitic rock occurrences in northern Alberta (basement terranes from Ross et al., 1994)

The Taltson Domain is a 150 to 200 km wide, north-trending belt of strike-parallel, tightly corrugated, positive aeromagnetic anomalies that are contained within broader aeromagnetic lows (Thériault and Ross, 1991). This is the southern continuation of the extensively exposed Taltson magmatic zone (TMZ). The exposed TMZ is dated at 1990 to 1910 Ma (McDonough et al., 1995). To the south, U-Pb dating of zircon and monazite from drill cores of the unexposed segment of the Taltson zone yielded ages in the 1975 to 1937 Ma range. Initial εNd values range from –3.7 to –9.7 and are in agreement with the range of values obtained for the exposed portion of the TMZ (Thériault and Bostock, 1989). Depleted mantle neodymium model ages (T_{DM}) vary from 2.57 to 2.68 Ga. The Nd isotopic signatures of the Taltson domain granitic rocks reflect recycling of material with a prolonged crustal history during the Early Proterozoic.

The Buffalo Head domain is defined as a 200 to 300 km wide, elongate region of internally complex, north-trending, convex-westward, moderately positive aeromagnetic anomalies containing aeromagnetically negative septa. Drillcore samples recovered from the Buffalo Head domain are mainly metaplutonic rocks ranging in composition from gabbro to leucogranite, with minor metavolcanic and high-grade gneissic rocks (Thériault and Ross, 1991; Burwash et al., 1994). U-Pb crystallization ages fall in the 2324 to 1993 Ma range, with four occurrences of plutonic rocks in the range 1.999 to 1.993 Ga. Epsilon Nd values scatter over the +0.2 to –6.3 range, whereas T_{DM} model ages vary from 2.83 to 2.51 Ga, with a preponderance of 2.8 to 2.7 Ga ages. There is no apparent correlation of rock type and εNd values. The scatter of initial εNd values may be a consequence of mixing various proportions of crust with evolved Nd isotopic composition with mantle-derived magmas of a more primitive signature.

The Chinchaga domain is a prominent, curvilinear, aeromagnetic low that wraps around the west-facing outline of the Buffalo Head high. Drilled basement in the Chinchaga low consists of thirteen occurrences of metasedimentary and metaplutonic rocks and one occurrence of massive porphyritic granitic rock (Ross et al., 1994; Pana, 2003). U-Pb crystallization ages range from 2.17 to 2.08 Ga. The three rock types from the Chinchaga domain yielded crustal residence ages of 2.57, 2.46 and 2.68 Ga, respectively. εNd values of +0.6, –0.4 and –1.8 suggest a greater proportion of juvenile material relative to the Taltson and Buffalo Head domains. The $^{147}Sm/^{144}Nd$ ratios fall in the 0.0943 to 0.1205 range, typical of light rare-earth element (LREE)–enriched crust.

The Ksituan domain is a prominent, north-trending aeromagnetic high that resembles the strong, positive aeromagnetic expression that is typical of calc-alkaline magmatic belts (Ross et al., 1991;

Thériault and Ross, 1991). The central to northern boundary between the Ksituan and Chinchaga domains has aeromagnetic signatures that are very sharp, suggesting a structural contact. To the south, the same boundary is irregular, suggesting that it may be magmatic in nature. Internally, the aeromagnetic fabric of the Ksituan high is characterized by moderately elongate, positive domains separated by narrow lows; based on this, Pana (2003) suggested that the basement rocks have undergone penetrative deformation. The drillcore samples from this domain are predominantly hornblende-biotite granitic gneiss. U-Pb crystallization ages in the range 1986 to 1900 Ma, do not overlap with crystallization ages obtained from rocks of the Chinchaga low immediately to the east (Ross et al., 1991), but do overlap with cooling ages from titanite grains in this region (Villeneuve et al., 1993). This suggests a younger tectonomagmatic event that resulted in granitoid emplacement and reactivation-metamorphism of the older basement to the east. Two samples yielded similar initial εNd values of -2.1 and -1.8, and indistinguishable T_{DM} ages of 2.63 and 2.62 Ga. Although this reflects the incorporation of Archean crust in the granitic rocks of the Ksituan domain, Pana (2003) suggested that the Archean component in these rocks is not as pronounced as in the Buffalo Head and Taltson domains to the east. The Ksituan high was interpreted to correspond to a magmatic arc dominated by metaplutonic rocks of largely calc-alkaline composition (e.g., Thériault and Ross, 1991).

The Nova domain is a 10 km wide, northeast-trending, positive aeromagnetic signature with little internal aeromagnetic fabric. This domain is bounded to the northwest by the subsurface extension of the GSLSZ (Figure 2) and to the southeast by a narrow (1–3 km wide) aeromagnetic low interpreted as a fault juxtaposing the Nova and Ksituan domains. A mylonitic mafic gneiss from the Nova domain has yielded a U-Pb zircon age of 2808 Ma. On this basis, Ross et al., (1991) postulated that the Nova domain may be a dislocated remnant of the Slave Province, the dominant lithotectonic entity north of the GSLSZ, whose southwestern region contains 3.9 to 2.8 Ga gneissic rocks. Archean crust, has however, been documented south of the GSLSZ (Henderson and Thériault, 1994).

2.2 Proterozoic Strata

The Athabasca Group, which is mostly in Saskatchewan, extends into northeastern Alberta south of Athabasca Lake and unconformably overlies a regolith-capped crystalline basement. In northeastern Alberta, the Athabasca Group consists of a nearly flat-lying sequence of non-metamorphosed Early Proterozoic clastic strata >1,255 m thick deposited in a series of northeast-southwest-oriented sub-basins of the intracratonic Athabasca Basin sometime between 1780 Ma and 1600 Ma (Wilson, 1986; Kyser et al., 2000). The basin-filling clastic strata, believed to have resulted from basement erosion, presently consist of ca. 95% detrital quartz (with minor heavy minerals) and 5% secondary minerals by volume (Wilson, 1986).

2.3 Paleozoic to Jurassic Platformal Succession

The Paleozoic to Jurassic platformal succession, which is dominated by carbonate rocks, can be summarized as two periods of continental margin sedimentation separated by cratonic indunations from the west, southeast and northwest (Kent, 1994).

During this period, marine inundation, sedimentation and erosion were strongly influenced by epeirogenic movements on various intracratonic arches (e.g., Peace River Arch in northwestern Alberta) that episodically differentiated the region into a complex array of sub-basins and uplifts (Mossop and Shetsen, 1994). As a result, much of the Paleozoic succession consists of unconformity-bounded, thin to thick sequences of carbonate rocks interlayered with predominantly fine- to medium-grained clastic marine sedimentary rocks.

In northeast Alberta, Middle and Upper Devonian marine shale, carbonate and evaporite comprise the exposed Paleozoic strata (Hamilton et al., 1999). To the west, platformal cover rocks were thrusted and folded as part of the Canadian Rocky Mountains and the Rocky Mountain Foothills. Emplacement of the imbricate thrust slices, progressively from west to east, produced thickening of the crust and downwarp of the foreland, forming an eastward-migrating foredeep that trapped clastic detritus shed from the developing mountains. Thick sequences of Paleozoic strata occur in the Inland Plains subsurface (up to 3,000 m thick) and range in age from Cambrian to Permian (Gabrielse and Yorath, 1992; Mossop and Shetsen, 1994).

2.4 Mid-Jurassic to Paleocene Foreland Basin Succession

The overlying mid-Jurassic to Paleocene foreland basin succession formed during active margin orogenic evolution of the Canadian Cordillera (Dawson et al., 1994). As a consequence of major episodes of compressional tectonism (e.g., Columbian and Late Cretaceous-Early Tertiary Laramide orogenies), erosion produced enormous volumes of clastic sediments that were progressively deposited eastward into the basin.

The Jurassic and lowest Cretaceous sedimentary rocks contain mineralogically mature, pre-orogenic strata derived from cratonic sediment sources in the east, and thick sequence of younger, less mature, foreland trough strata that were derived largely from orogenic uplifts to the west. The later assemblage contains an epicratonic record of the early phases of the Columbian Orogeny (Poulten et al., 1994).

Cretaceous rocks crop out or subcrop over more than two-thirds of northern Alberta (Figure 1) and provide a unique geological record of the final development of the basin, including its tectonic evolution, eustasy and climatic variations. In the northeastern Interior Plains, Lower Cretaceous marine to deltaic clastic sedimentary rocks unconformably overlie Paleozoic strata. The late Albian to early Turonian (about 100 to 92 Ma) Colorado Group marine shale is the thickest and most regionally extensive succession of Mesozoic rocks in Northern Alberta, exceeding 1,100 m thick in central-northwest Alberta and thinning to 250 m in central-northeast Alberta (Leckie et al., 1994). To the south and west, Upper Cretaceous marine to continental clastic sedimentary rocks conformably overlie the Lower Cretaceous strata. Upper Cretaceous sedimentary rocks are up to 900 m thick in northern Alberta and are often exposed in incised river valleys and on the edges of highlands.

Continental sedimentation continued through uppermost Cretaceous into Paleocene time in Alberta in response to continued uplift and erosion during Laramide orogenic activity (Yorath, 1992). The last major stage of uplift in the Eastern Rocky Mountains and Foothills of Alberta likely occurred during Eocene to Oligocene time (Shaw, 1963; Bally et al., 1966; Eisbacher et al., 1974). The final event during Late Cretaceous-Tertiary involved the uplift and erosion of greater than 1,000 m of post-Paleocene sediments from the basin, possibly related to regional tectonic uplift and isostatic rebound during Eocene to Pliocene time (~56 to 2 Ma; Dawson et al., 1994).

2.5 Late Tertiary to Quaternary Sand and Gravel Deposits

From Miocene to Quaternary, erosion of the Alberta Rocky Mountains and Interior Plains resulted in the removal of more than 1,000 m of stratigraphy, leaving scattered sand and gravel deposits at various elevations.

The three primary categories of sand and gravel deposits in Alberta are:

- Recent fluvial deposits, which are sourced by local bedrock, Laurentide and Cordilleran glacial deposits, and preglacial Tertiary and Quaternary fluvial deposits;
- Pleistocene glacial deposits, which may contain material derived from local bedrock, from up-ice bedrock or drift, and from preglacial Tertiary and Quaternary sand and gravel deposits; and

- preglacial Tertiary and Quaternary fluvial deposits, with the oldest typically being topographically highest and the youngest occurring in topographically low areas (e.g., within thalwegs of buried valleys).

Tertiary and early Quaternary erosion was extensive, leaving only small (metres to tens of metres thick), scattered patches of Oligocene to Pliocene fluvial sand and gravel deposits in isolated preglacial valleys and uplands (Yorath, 1992).

2.6 Quaternary

Quaternary deposits form the local landforms over virtually all of northern Alberta. The majority of the sediment is till (glacial diamicton), with glaciolacustrine and glaciofluvial sediment (Andriashek and Fenton, 1989; Klassen, 1989). The total thickness of the Late Tertiary to Quaternary sediments ranges from 300 m in a few preglacial valleys to zero on some of the interfluves and highlands. The surficial deposits in Alberta are primarily Late Wisconsin in age and were deposited by the Laurentide Continental and Cordilleran ice sheets between 23 000 and 11 000 years ago (Dyke et al., 2002). The nature of these deposits reflects broad aspects of the bedrock lithologies and patterns of glacial and glaciofluvial transport. Clay and silt till is mainly derived from the fine-grained Cretaceous bedrock with sand components from Cretaceous and Tertiary sandstones. Minor yet important components of the till come from lithologies of the Precambrian Shield, Paleozoic carbonates at the margin of the shield and quartzites and other clastic rocks from the Cordillera.

In general, glacial advances into Alberta originated from two directions: northeast or north from the Canadian Shield (Continental source), and west from interior Cordillera and Rocky Mountain sources. Late Wisconsin ice-flow directions in northern Alberta were dominantly southwestward as evidenced by the distribution and orientation of erratics, drumlins, and flutes (Gravenor and Bayrock, 1955; Gravenor and Meneley, 1958; Shilts et al., 1979; Dyke and Prest, 1987; Klassen, 1989).

2.7 Major Structures and Tectonic Features

A compilation of structural elements in northern Alberta was recently compiled by Pana et al. (2001) and is summarized here. The basement of Northern Alberta is roughly bound by two major northeast-trending dextral shear zones of Hudsonian age (approximately 1800 Ma): to the north, the Great Slave Lake Shear Zone (GSLSZ) and to the south by Snowbird Tectonic Zone (STZ).

The GSLSZ corresponds to a 25 km wide corridor of five mylonitic belts (Hanmer, 1988) and based on its aeromagnetic signature, can be traced as far west as the eastern edge of the Cordillera (Ross et al., 1994). The GSLSZ formed during the Hudsonian northeastward translation (up to 700 km) of the Slave Province relative to the Rae subdomain of the Churchill Province (Hoffman, 1987, 1988; Hanmer, 1988). Tectonic activity may have occurred along this structure until at least the late Middle Devonian (Skall, 1975), but the timing, kinematics and tectonic significance of this structure are still uncertain.

Across central Alberta, the STZ is a composite belt of northeasterly-trending, curvilinear aeromagnetic and gravity anomalies that can be traced from Hudson Bay, across the Shield and through Alberta as far west as the Foothills. To the northeast, in Saskatchewan, the STZ crops out as a broad zone of ductile mylonite (Hanmer, 1997), where it separates the Rae and Hearne subdomains of the Churchill Province (Ross et al., 1991; Ross et al., 1994). In Alberta, it truncates the northerly-trending geophysical fabrics of northern Alberta inferred to have been acquired in the Early Proterozoic. The timing, kinematics and tectonic significance of this structure are still uncertain.

The most prominent tectonic feature in northern Alberta is a roughly east-northeast-striking zone of long-lasting structural disturbance, which is known as the Peace River Arch (PRA). At present, it is an entirely subsurface structure, characterized by many sedimentological, structural and diagenetic aberrations (e.g., Sikabonyi and Rogers, 1959; Stott, 1982; Cant, 1988; O'Connell, 1994). The PRA recorded the longest history of tectonic activity and within the framework of the WCSB consists of three distinct phases of Phanerozoic evolution (e.g., Cant, 1988; O'Connell et al., 1990; O'Connell, 1994):

1) pre-Late Devonian development (or preservation) of the topographically high PRA on the WCSB passive margin of proto–North America (Figure 1). The PRA was an asymmetrical structure that reached a maximum width of 140 km at the sixth meridian (longitude 118°W) and a maximum elevation of about 1,000 m above the surrounding WCSB.
2) Early Carboniferous collapse and reversal of its topographic expression from a highland arch to an embayment (Peace River Embayment [PRE]), with enhanced subsidence relative to the WCSB as a whole persisting through the Triassic (e.g., Beaumont et al., 1993).

3) enhanced Mesozoic subsidence within the PRE, coeval with the initiation and evolution of thrust loading (Columbian and Laramide orogenies) in the Cordilleran orogen (O'Connell et al., 1990).

With respect to kimberlite emplacement, no obvious structural pattern can yet be confidently related to the NAKP. The Mountain Lake ultrabasic pipes appear to have been emplaced at the intersection of Jurassic to Cretaceous lineaments that is sub-parallel to the Cordilleran front, and a northeasterly fault zone bounding to the south the pre-Carboniferous PRA (Pana et al., 2001). The Buffalo Head Hills kimberlite field appear spatially related to an elongated, roughly northerly-trending zone of thickness and facies changes in the Devonian Duvernay, Woodbend, upper Leduc and Majeau Lake strata that may be structurally controlled (Eccles et al., 2001a; Paganelli et al., 2003). The Birch Mountains kimberlite field is located at the intersection of the Rimbey–Leduc–Meadowbrook reef chain, which is possibly related to a basement feature (Switzer et al., 1994), and to several inferred Devonian and Cretaceous lineaments within the Woodbend basin and Viking and Mannville strata, respectively (Pana et al., 2001).

3 Northern Alberta Kimberlite Province: Discoveries and General Geology

In this thesis, the kimberlitic rocks in northern Alberta are referred to as a new kimberlite province in western North America, the NAKP. The primary reason for this designation is that the northern Alberta pipes are removed both spatially and tectonically from other western North America kimberlite provinces (e.g., Montana alkaline province, southern Alberta and Montana; Fort à la Corne [FALC] kimberlite field, Saskatchewan; Slave province, Northwest Territories). For example, a distance of approximately 760 km separate the easternmost Alberta pipes from the nearest kimberlite field, the Saskatchewan FALC kimberlite field. It should be noted, however, that kimberlite exploration in western Canada, particularly Alberta and Saskatchewan, is still in its infancy, and future kimberlite discoveries might displace the idea of a NAKP in favour of a western Canada prairie kimberlite province.

A brief synopsis of the history of discovery and general geological characteristics of each field follows.

3.1 Mountain Lake Cluster

The geology of the ML cluster was recently summarized by Eccles (2003). The ML cluster is located northeast of Grande Prairie, Alberta and was discovered by Monopros Limited in 1989-1990 (Figure 3). The area was initially targeted because of a positive stream-sediment heavy-

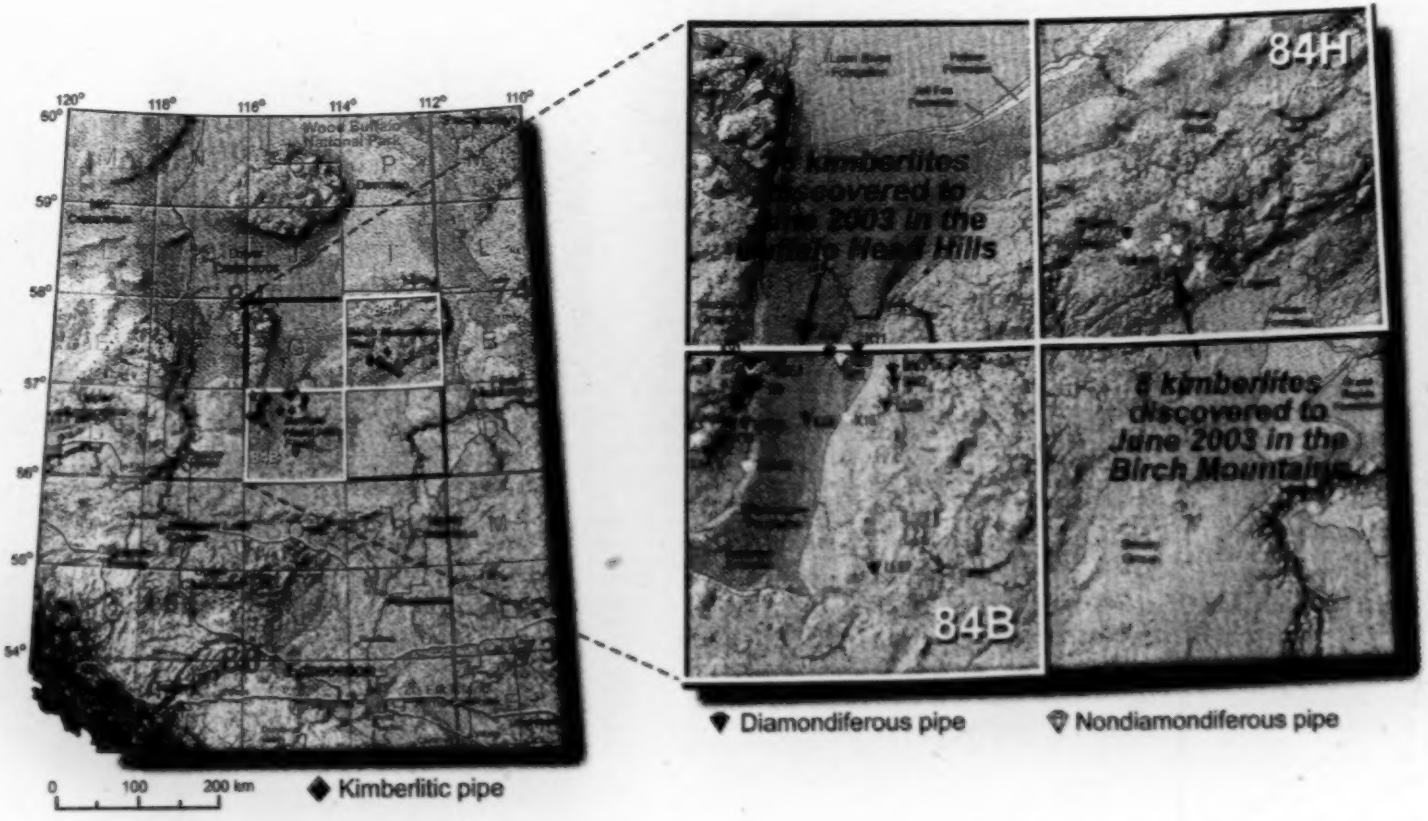
120°
118°
116°
114°
112°
110°
60°
59°
58°
57°
56°
55°
54°
Wood Buffalo National Park
0
100
200 km
◆ Kimberlitic pipe
kimberlites discovered to June 2003 in the Buffalo Head Hills
84H
8 kimberlites discovered to June 2003 in the Birch Mountains
84B
▼ Diamondiferous pipe
▽ Nondiamondiferous pipe

Figure 3. Distribution of kimberlitic rocks in Alberta. A) Mountain Lake, Buffalo Head Hills and Birch Mountains fields; B) distribution of diamondiferous and nondiamondiferous kimberlites in the Buffalo Head Hills and Birch Mountains fields.

mineral sample in Mountain Lake Creek, which occurs directly west of the intrusions. Volcanic rocks were discovered at two separate near-surface exposures, Mountain Lake South (MLS) and Mountain Lake North (MLN). The MLS pipe forms a pronounced topographic high and measures 400 by 650 m (29 ha), whereas MLN has no topographic expression and measures about 250 by 350 m (8.75 ha), as defined by the boundary of a weakly positive ground-magnetic signature.

The ML rocks were initially described as a "known kimberlite" (Wood and Williams, 1994). However, as various other petrologists examined rocks from the ML pipe it became apparent that the pipes were not archetypal kimberlite *sensu stricto*. Ensuing petrographic reports now seem to have established a basis for the classification of ML, which has been described as:

- alkaline ultrabasic volcanics (Leckie et al., 1997),
- similar to, but not totally characteristic of, kimberlites (Wood et al., 1998), and
- hybrid alkaline ultramafic rocks, with some petrologic affinities to alnoitic magmas (Skupinski and Langenberg, 2002).

During a joint 1995 drill program between the Alberta Geological Survey and Geological Survey of Canada, the MLS and MLN pipes were drilled with holes ML95-3 and ML95-1, respectively. The core was used to describe the petrology, indicator minerals, aeromagnetic signature, age, stratigraphic position and setting of the ML pipes by Leckie et al. (1997). Whole-rock and isotopic geochemistry was not included in the Leckie et al. (1997) study.

Palynology results were used by Wood et al. (1998) to infer an emplacement age of mid-Maastrichtian, probably ca. 68 Ma. Leckie et al. (1997) reported that *in situ* laminated sediments, which they interpreted to be interbedded with volcaniclastic deposits, and mudstone clasts, have a palynological assemblage that is similar to the Dinosaur Park Formation and are late Late Campanian in age (between ca. 75 and 76 Ma). Three samples of sandstone from MLN (drill core ML95-1) were processed for apatite fission track (AFT) dating. The central AFT ages range from 72±7 to 78±9 Ma (Leckie et al., 1997). To summarize, the existing data indicate the emplacement age for the ML pipes is late Late Cretaceous, or between about 76 and 68 Ma.

In hand specimen, the core is comprised of dark greenish-grey to black, brittle volcaniclastic juvenile material that consists dominantly of ash, olivine and juvenile lapilli. The majority of the juvenile lapilli and single grain olivine phenocrysts and macrocrysts are matrix supported and highly altered. The magmatic material is variably contaminated by clasts of sandstone (possibly Wapiti Formation) and shale (possibly Kaskapau Formation). In addition, there are variable amounts of contamination of the groundmass by quartz and feldspar xenocrysts, presumably from the Wapiti Formation.

Leckie et al. (1997), Wood et al. (1998), and Skupinski and Langenberg (2002) have published petrographic descriptions from ML rock samples. In summary, pyroclastic material is best observed in the MLS pipe where the rock consists mainly of olivine-rich tuff (>2 mm clast size) and coarse ash (<2 mm) with juvenile lapilli, and may be described simply as juvenile lapilli-rich olivine tuffs. Olivine phenocrysts occur as single crystals within the matrix and juvenile lapilli. They are euhedral to anhedral, up to 4 mm in size and are mostly altered to clay minerals (smectite), carbonate and/or serpentine. The juvenile lapilli have rounded to curvilinear boundaries and are comprised of altered olivine, serpentine, phlogopite-biotite mica, spinel, rutile, perovskite, apatite, calcite, clay and occasionally, fresh, euhedral clinopyroxene. The olivine pseudomorphs and lapilli are set in a fine-grained matrix that has been extensively altered to serpentine, carbonate and secondary smectite, which makes the original mineralogy and textures difficult to discern optically. Nonetheless, perovskite, spinel, phlogopite, apatite and pyrite are identifiable as individual crystals in the matrix.

The high volume of juvenile magmatic material in the MLS with only a minor component of xenocrystic quartz has led several authors (e.g., Field and Scott Smith, 1998; Leckie et al., 1997) to speculate that MLS is a pyroclastic deposit. In general, the MLN is similar in petrographic character to MLS, but with ash matrices that are highly contaminated by rounded quartz, plagioclase, alkali feldspar, hornblende and biotite, which have been interpreted to indicate a resedimented volcaniclastic rather than pyroclastic origin (Leckie et al., 1997).

Mantle xenoliths are extremely rare, and when observed are small (<1 cm) and highly altered. Basement xenoliths are rare, small (<4 cm) and typically are feldspathic gneisses. In general, there is a paucity of traditional 'kimberlite' indicator minerals (e.g., pyrope and eclogitic garnet, clinopyroxene, spinel and ilmenite), and when present, they are small, typically <1 mm.

Mineral separates of bulk rock samples were processed to obtain kimberlite indicator minerals. Chrome pyrope garnets, chrome diopside, orthopyroxene, chromite and picroilmenite were found. The heavy-mineral concentrates from pyroclastic units within the ML pipe include Ti-rich, Cr-poor Group 9, Group 11 and Group 12 pyrope garnets (G9, G11 and G12; Dawson and Stephens, 1975), and Mg-rich picroilmenites (Leckie et al., 1997).

Wood et al. (1998) reported "insignificant quantities of diamonds" were recovered from trench and drill core material from the ML pipe, and that the MLS and MLN were deemed uneconomic. The low abundances of mantle xenocrysts recovered by various authors and their overall chemistry (e.g., absence of G10 garnets and lack of diamond inclusion spinels), are consistent with these poor diamond results.

To date, no other pipes have been reported in the ML area, although exploration continued to at least 2003.

3.2 Buffalo Head Hills Kimberlite Field

In the mid 1990's, a geologist (Robert Pryde) with Alberta Energy Company (AEC), while exploring for hydrocarbons in the Red Earth Creek area along the east flank of the BHH, identified magnetic anomalies coincident with seismic disruptions and suggested they were potential kimberlite pipe(s). AEC then sought and formed a joint venture with Ashton Mining of Canada Inc. and Pure Gold Resources Ltd., with Ashton as operator. In 1997, Ashton discovered kimberlites on the southeast flank of the BHH, and to the end of June 2003, Ashton has discovered 38 kimberlitic pipes in this region (Figure 3).

The geological information in this section is summarized from Carlson et al. (1998, 1999) and Skelton et al. (2003). Inferred sizes of the pipes, based on aeromagnetic signatures and drilling, range from less than 1 ha to approximately 45 ha. Radiometric U-Pb dates of 86 ± 3 Ma to 88 ± 5 Ma on perovskite from three pipes are consistent with emplacement into sedimentary rocks of the Middle to Late Cretaceous (Cenomanian to Campanian) Smoky Group, the Dunvegan Formation and possibly the Shaftesbury Formation of the Western Canada Sedimentary Basin.

Petrographically, the kimberlites are mainly lapilli-bearing olivine crystal tuff, stratigraphically dominated by normally graded beds of coarse ash to coarse crystal tuff (Skelton and Bursey, 1998). Juvenile lapilli-rich beds have also been observed. Spherical or amoeboid lapilli, ovoid olivine macrocrysts up to 1 cm in length, and occasional laths of mica up to 5 mm in length occur in a groundmass that typically consists of a fine-grained, sometimes segregational assemblage of serpentine, dolomite, calcite and chlorite. Mica microphenocrysts show core-to-rim evolution from phlogopite toward aluminous phlogopite (Carlson et al., 1998), and plot along Mitchell's (1995) kimberlite trend in Al_2O_3-TiO_2 composition space. Carlson et al. (1998) also reported that the compositions of spinel microphenocrysts follow magmatic trend 1, which Mitchell (1995) associated with Group I kimberlites.

Crustal xenoliths consist of shale, predominately of the Shaftesbury Formation. Mantle-derived xenoliths include peridotitic (lherzolite, wehrlite and harzburgite), pyroxenitic, eclogitic, and corundum- and spinel-bearing rock types. Textures of the mantle xenoliths vary from coarse granular to coarse tabular and porphyroclastic sheared styles.

Xenocrysts include olivine, chrome pyrope and calcic knorringitic garnet, chrome diopside and augite, enstatite, and aluminous magnesium chromite. Kimberlites in the northern part of the BHH cluster contain subcalcic (G10) garnets with chromium contents of up to 17.8 wt. % Cr_2O_3, whereas the southern pipes contain only rare G10 garnets. Aluminous magnesium chromites generally contain between 30 and 62 wt. % Cr_2O_3, and the proportion of chromite grains with 'inclusion in diamond' chemistry (>60 wt. % Cr_2O_3 and 12–17 wt. % MgO; Carlson et al., 1999) is highly variable from one pipe to the next.

At least 26 of the 38 pipes in the BHH are diamondiferous and three pipes contain estimated grades at >11 carats per hundred tonnes (cpht). The 35th kimberlite discovered, kimberlite K252, provided the most encouraging results to date. A 22.8 tonne mini-bulk sample from the K252 kimberlite returned a total of 12.54 carats of diamonds for an estimated diamond content of 55.0 cpht (Ashton Mining of Canada Inc., 2001). In addition, a 0.94 carat stone indicates the potential for K252 to host commercial-sized stones.

3.3 Birch Mountains Field

The Legend property, which is located in the BM approximately 430 km north of Edmonton and 135 km northwest of Fort McMurray, was staked in a joint venture between Montello Resources Ltd. and Redwood Resources Ltd. in 1997. From March to June 1998, a 42,770 km fixed wing aeromagnetic survey was flown and processed. In August 1998, Kennecott Canada Exploration Inc. became the operator with Montello and Redwood. Thirty-five targets were selected based on the aeromagnetic survey.

During September to November 1998 and January to February 1999, ground and airborne (helicopter) geophysical surveys were completed on 27 of the 35 targets. Fourteen targets were tested with 19 drill holes totalling 2,713 m. The drilling delineated seven separate kimberlites, but the property was allowed to lapse because of poor diamond contents.

In 2000, New Blue Ribbon Resources (now Blue Diamond Mining Corporation) acquired the property and in December 2000 and reported a new kimberlite discovery in the BM, which brings the total number of known pipes in the BM area to eight (Figure 3).

The general geology presented here was compiled from Montello Resources Ltd. and New Blue Ribbon Resources Ltd. news releases, and from Aravanis (1999).

The approximate sizes of the pipes, which are inferred from magnetic anomalies (Montello Resources Ltd., 1998), are between 200 by 200 m (1 ha) and 1400 by 150 m (21 ha). The Phoenix, Dragon, Xena, Legend and Valkyrie pipes from the BM field have emplacement ages between ca. 70.3 and 77.6 Ma as determined by U-Pb from perovskite and Rb-Sr from phlogopite (Montello Resources Ltd., 1999).

In thin section, the kimberlite consists of a fine-grained serpentine-smectite-carbonate matrix that contains olivine microcrysts and macrocrysts (Aravanis, 1999). The olivine is fresh, partially serpentinized or totally replaced by dolomite and magnesite. The rock also contains rare macrocrystalline phlogopite and disseminated macrocrystalline and microcrystalline ilmenite. Some samples contain several generations of juvenile lapilli, possibly indicating that some of the pipes consist of resedimented pyroclastic material.

The country rock fragments are typically black angular clasts of shale and green, subangular to rounded clasts of argillite and rare carbonate. Macroscopic examination of the drillcore from the seven kimberlites discovered in 1998 and 1999 revealed few to no mantle xenoliths or xenocrysts in these samples. However, the Kendu kimberlite (discovered in December 2000) is characterized by an abundance of mantle xenocrysts and lherzolite and eclogite xenoliths (New Blue Ribbon Resources Ltd., 2001).

Reported heavy-mineral chemistry of the BM kimberlites indicates that they contain abundant olivine and ilmenite, and rare chromite. The compositions of the olivine grains (Fo_{88-92}) are typical of mantle peridotite and kimberlite. The ilmenite grains are Mg-rich, which Montello Resources Ltd. (1998) reported are favourable for the preservation of diamonds. According to New Blue Ribbon Resources Ltd. (2001), the Kendu kimberlite contains high-chrome pyrope, lherzolitic garnet, eclogitic garnet, high-Mg picroilmenite, chrome-rich clinopyroxene and spinel.

All eight pipes were sampled for diamond and only two pipes, Phoenix and Legend returned 3 micro- and 2 macro-diamonds (from two samples totaling 364.7 kg), and 4 micro-diamonds (from one 406.5 kg sample), respectively (Aravanis, 1999).

4 Sample Selection and Analytical Techniques

Eighty-three samples, including ten randomly picked duplicates, were sampled from 25 separate pipes and include material from pipes in all three kimberlitic areas (Table 1). The samples are numbered as sample ABK-01 to ABK-83, where the prefix ABK refers to 'Alberta kimberlite' and the number indicates the sample number provided. Sample selection from each field is summarized below.

Mountain Lake Field

Seventeen samples of core were collected from two drill holes completed during the 1995 drill program described previously. Of the 17 samples, eight samples, including two duplicates, were taken from core from drill hole ML95-1 (MLN) and nine samples, including two duplicates, were taken from core from drill hole ML95-3 (MLS).

Buffalo Head Hills Field

Thirty samples, including two duplicates, were collected from hand-sized core samples provided by Ashton Mining of Canada Inc. The sample set includes rock material from 16 individual pipes, although some pipes may be part of a single, larger complex (e.g., kimberlite complex K14 includes samples from targets K14, K14B and K14C). The low number of duplicate samples is due to an effort to conserve portions of the small-sized samples.

Birch Mountains Field

Thirty-six samples, including four duplicates, were collected from split drill core and one surface sample (kimberlitic rock clast discovered in glacial sediment directly over the Legend pipe). The samples are from seven separate pipes.

All 83 samples were analyzed for whole-rock geochemistry and based on these results, a subset of 10 samples from five pipes located in either the BHH and BM fields was selected for detailed petrographic and isotopic interpretation. The sample numbers and the basis for selection of a sample subset for detailed petrographic and isotopic interpretation are provided below in Sections 7 and 9.

The sample preparation and analytical techniques used for whole-rock geochemistry, petrography and radiogenic isotopes are discussed below.

Sample number	Original drill hole ID	Pipe name	Sample depth (m)	Location (UTM)			Whole-rock geochemistry	Whole-rock isotopes	U-Pb perovskite/ rutile	Rb-Sr phlogopite
				Easting	Northing	Zone				
Buffalo Head Hills: total of 30 samples (including 2 duplicates)										
ABK01	4A-02	K4A	49.15	578380	6301519	11	Yes	Yes		
ABK02	4B-01	K4B	140.65	578464	6300991	11	Yes	Yes		
ABK03	4C-01	K4C	63.00	578821	6301274	11	Yes			
ABK04	5A-02	K5	84.23	582687	6306035	11	Yes			
ABK05	6-02	K6	110.15	585550	6308383	11	Yes	Yes	Yes	
ABK06	7B-01	K7B	76.93	583131	6312089	11	Yes			
ABK07	7C-01	K7C	58.40	583052	6312455	11	Yes			
ABK08	11-01	K11	55.50	619724	6320041	11	Yes			
ABK09	11-01	K11	135.50	619724	6320041	11	Yes			
ABK10	14-01	K14	14.56	582883	6315050	11	Yes			
ABK11	14B-03	K14	30.17	582820	6315277	11	Yes			
ABK12	14C-06	K14	54.30	583030	6315357	11	Yes			
ABK13	**14C-06**	**K14**	**54.30**	**583030**	**6315357**	**11**	**Yes**			
ABK14	19-03	K19	19.85	575034	6289104	11	Yes			
ABK15	91-03	K91	84.93	581820	6317052	11	Yes			
ABK16	155-01	TQ155	102.50	581763	6293954	11	Yes			
ABK17	155-01	TQ155	148.60	581763	6293954	11	Yes			
ABK18	**155-01**	**TQ155**	**148.60**	**581763**	**6293954**	**11**	**Yes**			
ABK19	BM2-01	BM2	52.00	632349	6309823	11	Yes			
ABK20	BM2-01	BM2	79.50	632349	6309823	11	Yes			
ABK21	BM2-01	BM2	103.30	632349	6309823	11	Yes			
ABK22	BM2-01	BM2	113.80	632349	6309823	11	Yes			
ABK23	BM3-01	BM3	124.90	631219	6314208	11	Yes			
ABK24	BM3-01	BM3	144.90	631219	6314208	11	Yes			
ABK25	LL8-01	LL8	77.80	629936	6301692	11	Yes			
ABK26	LL8-01	LL8	121.50	629936	6301692	11	Yes			
ABK27	LL8-01	LL8	144.90	629936	6301692	11	Yes			
ABK28	K5 (surface)	K5	surface O/C	582432	6306145	11	Yes			
ABK29	K6 (surface)	K6	surface O/C	585317	6308651	11	Yes	Yes	Yes	
ABK30	K14 (surface)	K14	surface O/C	582894	6315185	11	Yes			
							Yes			
Mountain Lake Diatreme: total of 17 samples (including 4 duplicates)										
ABK31	ML95-1	MLN	7.22	454636	6145914	11	Yes			
ABK32	ML95-1	MLN	35.00	454636	6145914	11	Yes			
ABK33	**ML95-1**	**MLN**	**35.00**	**454636**	**6145914**	**11**	**Yes**			
ABK34	ML95-1	MLN	64.00	454636	6145914	11	Yes			
ABK35	ML95-1	MLN	95.00	454636	6145914	11	Yes			
ABK36	ML95-1	MLN	134.10	454636	6145914	11	Yes			
ABK37	**ML95-1**	**MLN**	**134.10**	**454636**	**6145914**	**11**	**Yes**			
ABK38	ML95-1	MLN	161.90	454636	6145914	11	Yes			
ABK39	ML95-3	MLS	7.45	454779	6145324	11	Yes			
ABK40	ML95-3	MLS	29.80	454779	6145324	11	Yes			
ABK41	ML95-3	MLS	60.00	454779	6145324	11	Yes			
ABK42	**ML95-3**	**MLS**	**60.00**	**454779**	**6145324**	**11**	**Yes**			
ABK43	ML95-3	MLS	88.80	454779	6145324	11	Yes			
ABK44	ML95-3	MLS	117.90	454779	6145324	11	Yes			
ABK45	ML95-3	MLS	133.90	454779	6145324	11	Yes			
ABK46	ML95-3	MLS	165.00	454779	6145324	11	Yes			
ABK47	**ML95-3**	**MLS**	**165.00**	**454779**	**6145324**	**11**	**Yes**			
Birch Mountains: total of 28 samples (4 duplicates)										
ABK48	98DH-XE01	Xena	87.70	376850	6347300	12	Yes			
ABK49	98DH-XE01	Xena	153.96	376850	6347300	12	Yes			
ABK50	**98DH-XE01**	**Xena**	**153.96**	**376850**	**6347300**	**12**	**Yes**			
ABK51	98DH-R001	Roc	123.00	365051	6357585	12	Yes			
ABK52	98DH-PH02	Phoenix	137.00	351550	6330493	12	Yes			
ABK53	98DH-PE01	Pegasus	100.00	374692	6368251	12	Yes			
ABK54	**98DH-PE01**	**Pegasus**	**100.00**	**374692**	**6368251**	**12**	**Yes**			
ABK55	98DH-PE01	Pegasus	128.00	374692	6368251	12	Yes			
ABK56	98DH-PE01	Pegasus	170.00	374692	6368251	12	Yes			
ABK57	98DH-LE01	Legend	12.20	386200	6340600	12	Yes			
ABK58	98DH-LE01	Legend	22.00	386200	6340600	12	Yes			
ABK59	98DH-LE01	Legend	44.00	386200	6340600	12	Yes	Yes	Yes	
ABK60	**98DH-LE01**	**Legend**	**44.00**	**386200**	**6340600**	**12**	**Yes**			
ABK61	98DH-LE01	Legend	58.00	386200	6340600	12	Yes			
ABK62	98DH-LE01	Legend	81.90	386200	6340600	12	Yes			
ABK63	98DH-LE01	Legend	104.20	386200	6340600	12	Yes			
ABK64	98DH-LE01	Legend	111.00	386200	6340600	12	Yes			
ABK65	98DH-LE01	Legend	120.00	386200	6340600	12	Yes			

Table 1. Sample summary with type of geochemical analyses performed.

Sample number	Original drill hole ID	Pipe name	Sample depth (m)	Location (UTM)			Whole-rock geochemistry	Whole-rock isotopes	U-Pb perovskite/ rutile	Rb-Sr phlogopite
				Easting	Northing	Zone				
ABK66	98DH-LE01	Legend	137.00	386200	6340600	12	Yes			
ABK67	98DH-LE01	Legend	159.00	386200	6340600	12	Yes			
ABK68	98DH-LE01	Legend	187.00	386200	6340600	12	Yes	Yes	Yes	
ABK69	98DH-LE01	Legend	203.65	386200	6340600	12	Yes			
ABK70	98DH-LE01	Legend	203.65	386200	6340600	12	Yes			
ABK71	98DH-VA01B	Valkryie	129.50	362350	6355490	12	Yes			
ABK72	98DH-VA02	Valkryie	136.00	362350	6355490	12	Yes			
ABK73	98DH-VA02	Valkryie	147.00	362350	6355490	12	Yes			
ABK74	98DH-VA02	Valkryie	160.00	362350	6355490	12	Yes			
ABK75	98DH-PH-01	Phoenix	105.00	351500	6330580	12	Yes	Yes	Yes	Yes
ABK76	98DH-PH-01	Phoenix	130.00	351500	6330580	12	Yes	Yes	Yes	Yes
ABK77	98DH-PH-01	Phoenix	159.00	351500	6330580	12	Yes			
ABK78	98DH-PH-01	Phoenix	175.00	351500	6330580	12	Yes			
ABK79	98DH-PH-01	Phoenix	218.00	351500	6330580	12	Yes			
ABK80	LE (surface)	Legend	Surface (till)	385924	6340845	12	Yes			
ABK81	Kendu	Kendu	102.00	368561	6353407	12	Yes	Yes	Yes	Yes
ABK82	Kendu	Kendu	127.25	368561	6353407	12	Yes	Yes	Yes	Yes
ABK83	Kendu	Kendu	154.04	368561	6353407	12	Yes			
				Total samples analyzed			**83**	**10**	**8**	**4**
▨	Shaded area denotes a sample duplicate of the previously listed sample in table									

Table 1. Sample summary with type of geochemical analyses performed.

4.1 Whole-Rock Geochemistry

The samples were sent to ACME Analytical Laboratories Ltd., Vancouver, British Columbia. The samples were crushed to less than 2 cm and large, visible, country-rock xenoliths (shale and carbonate) were removed to minimize contamination. The samples were dried at 60°C, pulverized to -150 mesh using a chrome-steel ring-and-puck pulverizer at ACME and analyzed by ACME using the following protocols:

- Group 4A total decomposition using $LiBO_2$ fusion followed by HNO_3 acid dissolution and analysis by inductively coupled plasma optical emission spectroscopy (ICP-OES)
- Carbon and sulphur by Leco carbon analyzer
- Group 4B total decomposition and analysis (same as above) for minor and trace elements, including rare-earth elements
- Base metals by aqua-regia digestion followed by inductively coupled plasma mass spectroscopy (ICP-MS).

The analytical precision quoted by ACME is ±5% and ±10% for Groups 4A and 4B, respectively. Nickel was analyzed by $LiBO_2$ in Group 4A and by aqua-regia digestion in Group 4B. The whole rock chemical analyses are presented in Appendices 1 and 2.

4.2 Petrography

Primary and secondary minerals from kimberlites selected for detailed petrographic interpretation are identified and described macroscopically and microscopically. These physical descriptions are coupled with electron microprobe elemental distribution maps and bulk-rock X-ray diffraction analysis. The X-ray diffraction analysis was completed at the University of Alberta using a Rigaku Geigerflex Power Diffractometer with a Co tube and a graphite monochromator.

The elemental distribution map combines backscattered electron and X-ray elemental images from the JEOL 8900 electron microprobe at the University of Alberta. The approximate size of each elemental distribution map area is 410 by 410 μm. Elemental distribution map areas were created for areas selected as representative of the sample. Each elemental distribution map area was stage scanned using the following specifications:

• Pixels:	1024 x 1024
• Pixel Size:	0.4 x 0.4 μm
• Dwell time:	10 milliseconds

- Electron Accelerating voltage: 15 kV
- Beam Current: 20 nA

Individual elemental distribution maps include two different types of back scattered images, which depict variations in average atomic number and sample topography, and ten X-ray elemental images: MgO, SiO_2, Al_2O_3, CaO, K_2O, P, TiO_2, Cr_2O_3, FeO and S.

With respect to grain-size nomenclature of matrix minerals, this report uses the convention that phenocrysts and microphenocrysts are <0.5 mm and macrocrysts are >0.5 mm. Some minerals (e.g., olivine, phlogopite and ilmenite) occur in both modes and because of similar morphologies it is not always possible to draw sharp distinctions between the different populations.

4.3 Isotope Geochemistry

A variety of radiometric methods was used to provide constraints on the source geochemistry and emplacement age of selected Alberta kimberlite pipes.

4.3.1 Whole-rock Sm-Nd, Rb-Sr and Pb-Pb

Kimberlite whole rock isotopic analyses can provide clues to the origin and contamination history of these mantle-dervied magmas:

- the Rb-Sr system is applicable because information on initial $^{87}Sr/^{86}Sr$ ratios is useful in constraining the magma's source region and in interpreting the history of the Earth's crust and mantle.
- the Sm-Nd system also is useful in constraining the magma's source region because the system is relatively resilient to geological disturbances such as metamorphism and weathering.
- the Pb-Pb system offers an opportunity to determine mantle isochron ages without the effects of parent daughter fractionation during partial melting, and is also sensitive to crustal contamination.

The analytical procedures for Rb-Sr, Sm-Nd and Pb-Pb follow those described by Holmden et al. (1996), Unterschutz et al. (2002) and Yamashita et al. (1999), respectively, and is summarized as follows:

- Pulverize sample to -150 mesh using a chrome-steel ring-and-puck pulverizer at ACME Analytical Laboratories Ltd., Vancouver, British Columbia.

- Samples were dissolved in Savillex PFA digestion vessels in $HF:HNO_3$, soaked in HCl and dried.
- Aliquots of the whole rock samples were weighed and spiked with mixed ^{149}Sm-^{145}Nd and ^{87}Rb-^{84}Sr tracers and placed on a hot plate (ca. 150° C) for five days. For Sm-Nd analysis, 10 ml of 6.2N HCl were added prior to additional heating for 24 hours.
- Rb and Sr were separated using standard cation exchange chromatography. Pb was extracted using standard anion chromatography. Sm and Nd were purified using hexyl diethyl hydrogen phosphate (HDEHP) chromatography.

Isotope ratios were measured on a VG 354 and S54 multi-collector thermal ionization mass spectrometers. Rb and Sr were loaded as chlorides on the side rhenium filament of a double filament bead assembly. Sm and Nd were loaded as nitrates on the side rhenium filament of a double filament bead. For measurement of Pb isotope ratios, the purified Pb was loaded with a phosphoric acid-silica gel mixture onto a single rhenium filament bead. All errors are reported at the 2σ level.

4.3.2 U-Pb Perovskite

Kimberlites can be dated by U-Pb analysis of perovskite (e.g., Heaman, 1989; Heaman and Kjarsgaard, 2000), which contains high-U contents and typically provides good precision and accuracy. However, the small grain size (often <50 um) of the mineral in many instances renders mineral separation extremely difficult.

The separation and analytical technique for U-Pb perovskite analysis may be summarized as follows.

- Perovskite was isolated from 0.1 to 1 kg samples by pulverizing rock samples using standard crushing (jaw crusher and Bico disk mill), standard heavy liquid separation (Methylene Iodide), and magnetic separation (Frantz).
- Perovskite was hand picked using a binocular microscope at high magnification to ensure that grains with inclusions, alteration or other imperfections were excluded.
- Each mineral fraction was weighed and washed in warm, 4N HNO_3 for one hour at ca. 50° C, given a one-minute rinse in an ultrasonic bath, and then triple rinsed with distilled H_2O followed by distilled acetone prior to dissolution in teflon bombs.
- The perovskite and rutile fractions were spiked using a mixed ^{205}Pb-^{235}U tracer solution and dissolved in a mixture of HF and 7N HNO_3 at 230° C for 5 days.

- Prior to column chemistry, the perovskite/rutile samples were equilibrated in 3.1N HCl for 12 hours.
- Uranium and lead were purified using an HBr procedure (Heaman, 1989).
- The purified uranium and lead were loaded onto outgassed Re filaments with a mixture of silica gel and phosphoric acid, and were analyzed on a VG 354 mass spectrometer in single Daly photomultiplier dector mode. All errors are reported at the 2σ level.

4.3.3 Rb-Sr Phlogopite

Rb-Sr analysis of phlogopite is a well-established dating technique for kimberlite (e.g., Smith et al., 1985a; Allsopp et al., 1989). Phlogopite mica is present in many kimberlites as fine-grained groundmass phlogopite and coarser-grained macrocrysts. The latter are easier to date by virtue of their larger size, ease of separation and lower common Sr content (i.e., a higher radiogenic Sr content). Limitations of the technique include contamination from inherited crustal micas, secondary alteration and presence of strontium-rich inclusions (e.g., apatite).

The separation and analytical technique for Rb-Sr phlogopite analysis may be summarized as follows.

- The samples were crushed in a jaw crusher to less than 2 cm.
- Phlogopite macrocrysts for Rb-Sr isotopic geochemistry were hand picked from the <2 cm fraction (immersed in ethanol) using a binocular microscope, and selected grains free of visible alteration were dried and weighed.
- The samples were leached in a 0.75N HCl ultrasonic bath for 30 minutes at room temperature to extract carbonate material following an adopted leaching method (Brown et al., 1989).
- The HCl supernatant was decanted and residue washed twice in H_2O prior to addition of a mixed ^{84}Sr-^{87}Rb spike.
- The leached fraction was dissolved in Savillex capsules in 24N HF and 16N HNO_3 at ca. 150° C for 12 hours, evaporated to dryness, and re-dissolved in 6N HCl at 80° C for 12 hours and dried.
- Prior to column chemistry, the dried samples were re-dissolved in oxalic and HCl acid. Rb and Sr were separated using conventional cation exchange chromatography.

Purified Rb and Sr aliquots were loaded onto single rhenium filaments and coated with H_3PO_4 and tantalum gel. The Rb and Sr aliquots were analysed on the VG 354 and S54 thermal ionization mass spectrometers. All errors are reported at the 2σ level.

5 Criteria Used for Classification of Alberta Kimberlitic rocks

5.1 Comparative Rock Descriptions for Geochemical Classification

Despite quite variable characteristics (e.g., mineralogy and whole-rock chemistry), a wide spectrum of magmas ranging from alkali basalt to kimberlite has been considered by Green (1971), Frey et al. (1978), Alibert et al. (1983), and Rogers et al. (1992) to be generated by a small degree of partial melting in the lithospheric to sublithospheric mantle. These magmas are considered to have developed at different source depths, under different physical conditions, and potentially from different source rock types. This variability corresponds to a variety of magma types within or near kimberlite clusters. For example, kimberlite and melilitite coexist at Namaqualand, South Africa (Rogers et al., 1992) and in the Bargydamalakh pipe, Anabar region, USSR (Ukhanov, 1963). In the Sarfartoq region of western Greenland, a continuum of rock composition from kimberlite through ultramafic lamprophyre to dolomitic carbonatite is present (Larsen and Rex, 1992; Dalton and Presnall, 1998a).

In addition to compositional variability produced in the generation of the primary magma, the chemistry of kimberlites can be altered by variable amounts and types of mantle and/or crustal fragments from the country rock into which they intrude, and alteration associated with late-stage degassing and/or groundwater circulation (e.g., Ilupin and Lutz, 1971; Clement, 1982; Mitchell, 1986). To minimize contamination issues, previous studies (e.g., Ilupin and Lutz, 1971) experimented with separating and analyzing the groundmass of kimberlite with relative success. Fesq et al. (1975) noted that the 'groundmass approach' does not overcome the effects of the presence of finely comminuted particles in the groundmass of kimberlites or the possibility of contamination by assimilation, where the assimilating material is incorporated by partial fusion.

To classify the kimberlitic rocks from Alberta, and to place these samples in a global context, the major-element geochemical data from Alberta pipe samples are compared to compositions of kimberlites and alkaline rocks worldwide. Mitchell (1986) cautioned that the 'representative' average composition of kimberlite is derived from global data sets that were not assessed for alteration and contamination. The same cautionary note applies to other rock types used for comparative purposes. Nevertheless, comparisons must be an integral part of any classification and, therefore, selected geochemical data for kimberlite, alkali olivine basalt/basanite, minette, alnöite and melilitite are included throughout this thesis. A brief description for each of these rock types follows.

Kimberlites exhibit a wide range in composition; minimally contaminated kimberlite is low in SiO_2 (25–30 wt. %), low in Al_2O_3 (usually <5 wt. %) and very low in Na_2O (usually < 1 wt. %). Kimberlites have been divided into Group I and Group II types (e.g., Smith et al., 1985b). Group I kimberlites in South Africa are Cretaceous (90–114 Ma) in age and have initial $^{87}Sr/^{86}Sr$ values of 0.7033-0.7049 and ε_{Nd} values ranging from –0.5 to +6.0 (Smith, 1983). In contrast, micaceous Group II kimberlites have higher $^{87}Sr/^{86}Sr$ ratios (0.7064-0.7109) and more negative ε_{Nd} (–7 to –12; Smith, 1983), which are interpreted to have been derived from ancient (>1 Ga), trace element–enriched, possibly mixed sources situated within the subcontinental lithosphere. Geochemical averages for Group I and Group II global kimberlite and average kimberlite in this report are taken from Dawson (1967), Ilupin and Lutz (1971), Gurney and Ebrahim (1973), Ilupin et al. (1974), Scott (1979), Muramatsu (1983), Zhang and Liu (1983), Smith et al. (1985b), Mitchell (1986), Taylor et al. (1994), Mitchell (1995), Berg and Carlson (1998), and Price et al. (2000).

Basanite (alkali olivine basalt) contains olivine and feldspathoid (nepheline/leucite) with or without clinopyroxene and plagioclase. In general, basanitic rocks contain 43.01–45.54 wt. % SiO_2, 7.57–10.74 wt. % MgO, 11.94–14.70 wt. % Al_2O_3 and 3.26–4.06 wt. % Na_2O. This report uses the geochemical averages for worldwide basanitic rocks (Le Maitre, 1976), basanite data compiled by Le Bas (1989) that includes examples from the USSR (Andreeva et al., 1983), Anjouan, Comores Island (Flower, 1973) and central Spain (Ancochea and Ibarrola, 1982), and basanite and alkali-olivine basalt from Frey et al. (1978).

The Sweet Grass Intrusives, located in the Milk River area of southern Alberta, comprise 48 Ma (K-Ar biotite; Currie, 1976) and 49 to 52 Ma (K-Ar; Hearn et al., 1978) potassic igneous rocks. Based on bulk-rock major- and trace-element geochemical characteristics, as well as zoning trends in mica phenocrysts, most of the rocks have been classified as minette (Kjarsgaard, 1994; Buhlmann et al., 2000). Geochemical data for Sweet Grass olivine minette used in this study are from Kjarsgaard (1994) and Buhlmann et al. (2000).

Mitchell and Bergman (1991) demonstrated that most minettes plot in the field for Roman Province type (RPT) lavas on Barton's (1979) plot of SiO_2 versus molar ($[K_2O+Na_2O]/Al_2O_3$) and that this diagram is useful to distinguish RPT-lavas from lamproites. Where applicable, RPT geochemical data summarized by Mitchell and Bergman (1991) and Mitchell (1995) are included in this study.

The 41 to 51 Ma alkalic ultramafic magmas in north-central Montana consist of a variety of rocks, including alnöite, monticellite peridotite, carbonate-rich mica peridotite, and kimberlite (Hearn, 1986). The rock types show a continuum of major- and trace-element compositions, and have overlapping ranges of MgO content (10–25, 19–30, 24–31 and 23–32 wt. %, respectively). Thus, the geochemical data from the Haystack Butte and Winnett Sill were selected and used in this study as representative alnöite (melilite-bearing, 10–25 wt. % MgO) from the Montana alkalic ultramafic suite (Hearn, 1986).

Melilitite has high Mg and contains ultramafic inclusions of high-pressure origin, and is therefore a likely candidate for a primary magma composition (Brey, 1978). Le Bas (1989) classified olivine melilitite as having <40 wt. % SiO_2 and <11 wt. % Al_2O_3, >14 wt. % MgO, >15 wt. % CaO and >22 wt. % TiO_2, and a Na_2O/K_2O ratio of 1.65–1.86. Melilitite is extremely enriched in incompatible elements, especially Nb and LREE. Geochemical data from Rogers et al. (1992) and Wilson et al. (1995) are used for comparisons in this report.

5.2 Petrographic Nomenclature and Terminology of Kimberlite

5.2.1 Nomenclature

Wagner (1914) published the first comprehensive summary on kimberlite diatreme occurrences in South Africa. Based on the mineralogical assemblage of primary minerals, he subdivided South African kimberlite into two groups: "basaltic" and "micaceous or lamprophyric" kimberlite.

More recently, detailed studies on South African kimberlites have demonstrated that basaltic and micaceous kimberlite groups are geochemically, mineralogically and petrogenetically separate rock types and have been termed Group I and Group II kimberlites, respectively (Smith, 1983; Smith et al., 1985b; Skinner, 1989). Group I (basaltic) kimberlites possess isotopic characteristics similar to many ocean island basalts (OIBs) and are believed to be derived from very small-degree partial melts that originate in comparatively 'fertile' asthenospheric sources. In contrast, Group II (micaceous) kimberlites have a more radiogenic $^{87}Sr/^{86}Sr$ signature and lower $^{206}Pb/^{204}Pb$ and $^{143}Nd/^{144}Nd$ compositions (Smith, 1983), often interpreted to represent partial melts from continental lithospheric mantle sources that were isolated for 1-2 billion years prior to the partial melting that produced the Group II magmas.

While petrologists actively studying kimberlites have concluded that there are significant petrological differences between the two groups, opinion is divided as to the extent of the revisions to their nomenclature. Some wish to retain the *status quo* (e.g., Skinner 1989), whereas others (e.g., Mitchell and Bergman 1991, Mitchell 1995) propose that the terminology should be completely revised and the nomenclature changed (see below).

Following a concept originally developed by Dawson (1980), kimberlite may be recognized as containing a characteristic assemblage of minerals. The following characterization of Group I kimberlites is after Mitchell (1995), which evolved from Mitchell (1986, 1994), and earlier definitions by Clement et al. (1984) and Mitchell (1979).

> "Kimberlites are a group of volatile-rich (dominately CO_2) potassic ultrabasic rocks commonly exhibiting a distinctive inequigranular texture resulting from the presence of macrocrysts (and in some instances megacrysts) set in a fine-grained matrix. The mega/macrocryst assemblage consists of anhedral crystals of olivine, magnesian ilmenite, Cr-poor titanian pyrope, diopside (commonly subcalcic), phlogopite, enstatite, and Ti-poor chromite. Olivine macrocrysts are a characteristic constituent in all but fractionated kimberlites. The matrix contains a second generation of primary euhedral-to-subhedral olivine which occurs together with one of more of the following primary minerals: monticellite, phlogopite, perovskite, spinel (magnesian ulvöspinel-Mg-chromite-ulvöspinel-magnetite solid solutions), apatite and serpentine. Many kimberlites contain late-stage poikilitic micas belonging to the barian phlogopite-kinoshitalite series. Nickeliferous sulfides and rutile are common accessory minerals. The replacement of earlier formed olivine, phlogopite, monticellite, and apatite by deuteric serpentine and calcite is common. Evolved members of the group may be poor in, or devoid of, macrocrysts and/or composed essentially of second-generation olivine, calcite, serpentinite and magnetite, together with minor phlogopite, apatite and perovskite".

Group-II kimberlite terminology is less clear, probably because their occurrence is limited to South Africa. Mitchell (1995) suggested that these rocks should be termed "orangeite", in recognition of their distinct character and Wagner's (1928) previous suggestion that the micaceous kimberlite rocks be renamed "orangite" *(sic).* The following characterization of the rocks currently described as Group-II kimberlites or orangeite follows that of Mitchell (1995).

> "Orangeites are a clan of ultrapotassic peralkaline volatile-rich (dominantly H_2O-rich) rocks, characterized by the presence of phlogopite macrocrysts and microphenocrysts,

> together with groundmass micas, which vary in composition from phlogopite to tetraferriphlogopite. Rounded olivine macrocrysts and euhedral primary olivines are common, but are not always major constituents. Characteristic primary groundmass phases include diopside, commonly zoned to, and mantled by, titanian aegirine, spinels ranging in composition from Mg-chromite to Ti-magnetite, Sr- and rare earth element (REE)-rich perovskite, Sr-rich apatite, REE-rich phosphates (monazite, daqingshanite), potassian barian titanates belonging to the hollandite group, potassium triskaidecatitanates, Nb-rutile, and Mn-ilmenite. These are set in a metostasis, which may contain calcite, dolomite, ancylite, and other rare earth carbonates, witherite, norsethite and serpentine. Evolved members of the group contain groundmass sanidine and potassium richterite. Zirconium silicates (wadeite, zircon, kimzeyitic garnets, Ca-Zr silicate) are common as late-stage groundmass minerals. Quartz may occur rarely as mesostasis mineral. Barite is a common secondary mineral."

Based on Mitchell's (1995) description, Group II kimberlites have a greater mineralogical affinity to lamproites than to Group I kimberlites. There are, however, significant differences in the compositions and overall assemblage of minerals as presented in Table 2, that permit their discrimination from lamproites.

Although the concept of a two-group classification system (Group I and Group II, or kimberlite and orangeite) seems relatively straightforward, the variable nature of a hybrid rock such as kimberlite tends to add controversy. At least two authors have described rocks that require further classification. For example, Smith et al. (1985b) further subdivided Group I South Africa kimberlites into Group IA (on craton) and Group IB (off craton) on the basis of their chemistry. Compared to Group IA, Group IB kimberlites have lower SiO_2 and higher CaO, $FeO+Fe_2O_3$ and volatile contents, as well as somewhat greater TiO_2, P_2O_5, Nb, Zr and Y. Furthermore, Skinner et al. (1994) proposed a "transitional" kimberlite group on the basis that rocks, which occur primarily in "domain V" of the Prieska region, South Africa, have isotopic signatures that are intermediate between those of Group I and Group II kimberlite. Skinner et al. (1994) reported that the transitional rocks have petrographic affinities to Group I kimberlite as they contain relatively abundant, coarse-grained, primary spinels and perovskite, but Mitchell (1995) also noted that the presence of amphibole and sanidine would suggest some kinship with orangeite.

To summarize, a single definition cannot be used to describe both kimberlite and orangeite rock types, because of the mineralogical complexity within both rock types.

	Kimberlites	**Orangeites**	**Lamproites**
Olivine Macrocrysts	Common	Common to rare	Rare
Phenocrysts	Common: subhedral/euhedral	Minor: subhedral to euhedral to dog's tooth	Common
Mica Macrocrysts	Minor: phlogopite	Common: phlogopite	Common: phlogopite to Ti-phlogopite
Phenocrysts	Rare: phlogopite	Common: phlogopite	Ti-phlogopite
Groundmass	Common: phlogopite - kinoshitalite	Common: phlogopite to tetraferriphlogopite	Common: Ti-tetraferriphlogopite
Spinels	Abundant: Mg- chromite to Mg-ulvospinel (Trend 1)	Rare: Mg-chromite to Ti-magnetite (Trend 2)	Rare: Mg-chromite to Ti-magnetite
Monticellite	Common	Absent	Absent
Diopside	Primary diopside absent	Common: Al- and Ti-poor	Common: Al- and Ti-poor
Perovskite	Common: Sr- and REE-poor	Rare: Sr- and REE-rich	Rare: Sr- and REE-rich
Apatite	Common to rare: Sr- and REE-poor	Abundant euhedral prisms: Sr- and REE-rich	Common: Sr- and REE-rich
Carbonate	Common calcite; minor dolomite	Common calcite; common Sr-Mn-Fe dolomite	Absent
Serpentine	Common primary and secondary	Common: secondary	Common: secondary
Sanidine	Absent	Rare: groundmass	Common: phenocrysts and groundmass
K-richterite	Absent	Rare: groundmass	Common: phenocrysts and groundmass
K-Ba-titanates	Very rare	Common	Common
Zr-silicates	Very rare	Common	Common
Mn-ilmenite	Rare	Common	Very rare
Leucite	Absent	Rare: pseudomorphs	Common: phenocrysts
Barite	Rare	Common	Common: late stage (?) hydrothermal veins and vesicle fillings

Table 2. Mineralogical comparisons between kimberlites, orangeites and lamproites (after Mitchell 1995; slightly modified).

5.2.2 Textural- and Mineraological-Genetic Classifications

In the mineralogical-genetic classification, rock names reflect the modal abundance of major phases present. The parental magma or clan (e.g., kimberlite, lamproite) is assigned the root, with subdivisions of the clan given as prefixes to the root in the order of increasing modal abundance (e.g., monticellite kimberlite, monticellite serpentine kimberlite). Skinner and Clement (1979) recommended including mineral prefixes for those that have two-thirds the volume of the dominant mineral.

Scott Smith (1995) noted, however, that caution should be exercised in the use of the mineralogical classification. That is, it should only be used for rocks that have been determined to be kimberlite *sensu stricto* and that the classification should mainly be restricted to fresh, non-contaminated, hypabyssal-facies rocks.

More commonly, a textural-genetic classification is employed, based on the assumption that differences in the emplacement processes have specific products with unique textures. A generally accepted textural-genetic classification of kimberlites was devised by Clement and Skinner (1979, 1985) and Clement (1982) and expanded by Mitchell (1995). The classification relies on the generally accepted composite kimberlite pipe model, which consists of three dominant zones: crater, diatreme and root (Hawthorne, 1975; Mitchell, 1986). Generally, specific textures define each zone, which are termed crater-, diateme- and hypabyssal-facies textures, respectively (Scott Smith, 1995).

Crater facies kimberlites include lava, pyroclastic and epiclastic rocks and form deposits that include: basal breccia, poorly stratified coarse pyroclastic, well-stratified tuff, and epiclastic lacustrine deposits. Underlying the crater facies kimberlite, the diatreme consists of a carrot-shaped body with steeply dipping margins typically composed of homogenous tuffisitic kimberlite breccia. The diatreme facies terminates at depth in a root zone, where the diatreme expands, contracts or splits up into an irregularly shaped multiphase intrusion of hypabyssal kimberlite. Hypabyssal facies kimberlites are macrocrystal to aphanitic kimberlite formed by the crystallization of volatile-rich kimberlitic magma, and occur predominantly as vertically dipping tabular dykes.

Further subdivisions of each facies may be required to describe textural-emplacement associations. For example, Field and Scott Smith (1998) divided crater-facies textures into the following sub-categories:

- VK – volcaniclastic kimberlite describes extrusively formed fragmental kimberlite deposits for which the mode of deposition is not known
- RVK – resedimented volcaniclastic kimberlite describes VK for which depositional mechanisms can be recognized and ascribed to 'normal' sedimentary processes
- PK – pyroclastic kimberlite describes VK for which *prima facie* evidence shows direct deposition by explosive volcanic processes.

6 Whole-Rock Geochemistry

The major- and trace-element analytical data are presented in Appendices 1 and 2, respectively.

The duplicate analysis of ten randomly selected samples from drillcore yielded low relative errors (Table 3), as defined by the standard deviation divided by the mean (Le Maitre, 1982). Relative errors for element groups are:

- <6.5% for the major elements,
- <2.3% for the compatible elements, with ranges from 0.6% for Sc to 3.5% for Co,
- <8.6% for alkaline earth elements and <5.7 % for the rare-earth elements, and
- <10% for alkali and volatile elements Mo, Pb, As, Cd, Cs and Ga, and between 13.7% and 21.7% for Sb, Bi, C, S, Sn and W.

The <6.5% relative error for major elements is biased because of the relatively large errors in Na_2O and K_2O, which have relative errors of 5.6% and 6.5%. The analytical reproducibility of the duplicate samples is less than 3.7% for the major-element oxides SiO_2, Al_2O_3, $Fe_2O_{3(T)}$, MgO, CaO, Na_2O, TiO_2, P_2O_5, MnO and Cr_2O_3. The high relative errors for oxides such as Na_2O are reflected by the wide range of Na_2O content. Samples with low Na_2O content, such as ABK59 (0.04%) and its duplicate sample ABK60 (0.4%), have a high relative error of 20%. Samples with high Na_2O content, such as ABK32 (2.31%) and its duplicate sample ABK33 (2.29%), have a much lower relative error (1%). These differences may reflect the precision of the analytical technique, particularly for elements, such as Na_2O, that measure close to the limit of detection.

6.1 Contamination and Alteration

Tests proposed by Clement (1982), Mitchell (1986), Taylor et al. (1994) and Berg (1998) are used below to determine the type and extent of contamination. Clement (1982) used the Contamination

Duplicate Pairs: Major Elements																		
	SiO_2	Al_2O_3	Fe_2O_3	MgO	CaO	Na_2O	K_2O	TiO_2	P_2O_5	MnO	Cr_2O_3	Ba	Ni	Sc	LOI	C_{tot}	S_{tot}	SUM
Sample No.	%	%	%	%	%	%	%	%	%	%	%	ppm	ppm	ppm	%	%	%	%
ABK12	28.89	1.63	7.66	29.11	11.78	0.08	0.15	0.80	0.47	0.11	0.14	535.00	1524.00	10.00	18.60	2.69	0.17	99.67
ABK13	28.92	1.62	7.77	29.34	11.48	0.08	0.14	0.84	0.51	0.10	0.15	550.00	1562.00	10.00	18.70	2.62	0.14	99.93
Relative error	0.00	0.00	0.01	0.01	0.02	0.00	0.06	0.03	0.06	0.07	0.05	0.03	0.02	0.00	0.00	0.02	0.14	0.00
ABK17	29.47	2.54	8.62	35.41	5.82	0.08	0.22	0.48	0.41	0.14	0.15	959.00	1298.00	10.00	15.90	5.89	0.32	99.72
ABK18	30.49	1.95	8.55	36.06	5.41	0.07	0.15	0.45	0.38	0.14	0.15	909.00	1429.00	10.00	13.60	5.58	0.31	99.66
Relative error	0.02	0.19	0.01	0.05	0.08	0.18	0.27	0.06	0.05	0.00	0.02	0.04	0.07	0.00	0.11	0.04	0.02	0.00
ABK32	59.21	11.15	5.82	7.42	2.65	2.31	2.93	0.76	0.23	0.09	0.06	982.00	204.00	12.50	6.80	0.87	0.37	99.89
ABK33	59.99	11.40	5.44	6.97	2.67	2.29	3.10	0.79	0.22	0.09	0.06	1044.00	271.00	13.60	6.70	0.01	2.91	99.95
Relative error	0.01	0.02	0.05	0.04	0.08	0.01	0.04	0.03	0.03	0.08	0.08	0.04	0.20	0.06	0.02	1.17	1.10	0.00
ABK36	61.24	11.23	5.25	6.46	2.95	2.68	2.16	0.75	0.22	0.09	0.06	911.00	204.00	13.00	6.20	0.82	0.12	99.42
ABK37	61.61	11.35	5.38	6.48	2.71	2.56	2.15	0.73	0.20	0.09	0.06	945.00	197.00	13.00	6.10	0.72	0.14	99.84
Relative error	0.00	0.01	0.02	0.00	0.06	0.03	0.00	0.02	0.07	0.00	0.02	0.03	0.02	0.00	0.01	0.09	0.11	0.00
ABK41	46.20	7.58	7.78	16.39	4.40	1.35	1.71	0.79	0.29	0.11	0.14	837.00	712.00	12.00	12.60	0.66	0.21	99.82
ABK42	47.14	7.89	7.16	15.75	4.72	1.39	2.16	0.85	0.31	0.11	0.14	915.00	721.00	13.00	11.90	0.66	0.24	99.73
Relative error	0.01	0.03	0.06	0.03	0.05	0.02	0.16	0.05	0.05	0.00	0.01	0.06	0.01	0.06	0.04	0.00	0.09	0.00
ABK46	51.37	9.29	6.43	13.71	3.24	1.82	2.44	0.89	0.30	0.10	0.12	956.00	507.00	14.00	9.80	0.80	0.22	99.58
ABK47	51.51	9.42	6.39	13.43	3.21	1.89	2.58	0.89	0.28	0.10	0.12	980.00	487.00	14.00	9.80	0.84	0.24	99.63
Relative error	0.00	0.01	0.00	0.01	0.01	0.03	0.04	0.00	0.05	0.00	0.02	0.02	0.03	0.00	0.00	0.05	0.08	0.00
ABK49	48.52	9.34	7.11	13.59	3.86	1.73	2.56	1.41	0.44	0.07	0.08	1344.00	356.00	14.00	11.00	1.48	0.46	99.84
ABK50	48.10	9.38	7.00	13.23	3.49	1.81	2.26	1.39	0.46	0.07	0.08	1114.00	337.00	14.00	11.40	1.42	0.50	99.82
Relative error	0.01	0.00	0.01	0.02	0.07	0.03	0.09	0.01	0.02	0.00	0.01	0.13	0.04	0.00	0.03	0.03	0.03	0.00
ABK53	31.87	3.50	9.79	23.41	8.86	0.19	0.61	2.08	0.43	0.17	0.20	811.00	834.00	16.00	18.70	2.69	0.18	99.99
ABK54	32.33	3.46	9.93	23.37	8.71	0.18	0.56	2.11	0.43	0.17	0.21	709.00	860.00	16.00	18.30	2.52	0.25	99.65
Relative error	0.01	0.01	0.01	0.00	0.01	0.04	0.06	0.01	0.00	0.00	0.05	0.10	0.02	0.00	0.02	0.05	0.23	0.00
ABK59	27.50	2.74	10.15	28.00	8.38	0.04	0.53	3.54	0.55	0.18	0.15	780.00	726.00	18.00	17.60	2.85	0.28	99.78
ABK60	27.42	2.74	10.25	28.04	8.54	0.03	0.58	3.53	0.54	0.18	0.15	769.00	712.00	18.00	17.80	2.91	0.30	99.76
Relative error	0.00	0.00	0.01	0.00	0.02	0.20	0.06	0.00	0.01	0.04	0.01	0.01	0.01	0.00	0.01	0.01	0.05	0.00
ABK69	13.07	2.82	7.83	10.14	16.02	0.18	0.19	3.15	0.46	0.19	0.13	632.00	551.00	15.00	38.40	10.38	1.06	99.51
ABK70	12.78	2.86	7.49	10.15	16.15	0.19	0.20	3.10	0.41	0.19	0.13	662.00	547.00	15.00	37.00	10.57	0.78	99.52
Relative error	0.02	0.01	0.03	0.00	0.01	0.04	0.04	0.01	0.08	0.00	0.00	0.03	0.01	0.00	0.01	0.01	0.21	0.00
Avg. relative error (%)	0.82	2.76	2.17	1.64	3.18	5.78	8.12	2.12	4.16	1.89	2.87	4.90	4.28	1.13	2.47	14.62	20.36	0.06

Duplicate Pairs: Trace Elements (INNA)																				
	Co	Cs	Ga	Hf	Nb	Rb	Sn	Sr	Ta	Th	Tl	U	V	W	Zr	Y	La	Ce	Pr	Nd
Sample No.	ppm	ppm	ppm	ppm	ppm	ppm	ppm	ppm	ppm	ppm	ppm	ppm	ppm	ppm	ppm	ppm	ppm	ppm	ppm	ppm
ABK12	87.30	0.30	2.60	4.10	158.30	6.60	1.00	737.30	11.30	20.50	< 1	4.70	51.00	< 1	162.20	10.40	163.70	312.50	30.96	105.80
ABK13	91.40	0.30	2.10	4.50	172.60	6.10	2.00	773.70	12.50	22.90	0.30	4.60	53.00	< 1	175.00	11.10	176.40	341.80	33.69	112.60
Relative error	0.03	0.00	0.15	0.07	0.06	0.06	0.47	0.03	0.07	0.08	BLLD*	0.02	0.03	BLLD	0.05	0.05	0.05	0.06	0.06	0.04
ABK17	87.20	0.50	3.90	2.00	121.20	10.00	1.00	891.20	8.20	22.40	< .1	3.00	75.00	< 1	87.50	6.90	128.20	229.60	20.11	58.00
ABK18	101.70	0.20	3.80	1.60	120.20	5.20	1.00	846.80	8.50	22.30	< 1	3.00	69.00	< 1	78.50	6.40	107.90	190.30	17.33	52.20
Relative error	0.11	0.61	0.02	0.16	0.01	0.45	0.00	0.05	0.03	0.00	BLLD	0.00	0.06	BLLD	0.08	0.05	0.12	0.13	0.11	0.07
ABK32	26.70	4.00	15.50	3.60	46.20	104.20	1.00	322.60	2.90	11.20	0.20	3.50	115.00	2.00	129.50	18.10	50.60	93.30	9.65	35.40
ABK33	27.70	4.30	15.00	3.70	46.90	104.80	1.00	319.00	3.00	11.00	0.30	3.50	109.00	3.00	128.80	18.10	50.20	92.80	9.41	35.60
Relative error	0.03	0.05	0.02	0.02	0.01	0.00	0.00	0.01	0.02	0.01	0.28	0.00	0.04	0.28	0.00	0.00	0.01	0.00	0.02	0.00
ABK36	26.20	3.60	13.30	3.70	45.40	62.90	1.00	365.70	2.90	10.80	0.20	3.40	108.00	2.00	142.20	16.40	48.80	90.20	9.28	35.20
ABK37	25.80	3.40	13.90	3.60	41.10	62.40	1.00	353.00	2.50	9.40	0.50	3.10	102.00	2.00	133.40	15.80	44.10	81.70	8.44	31.60
Relative error	0.01	0.04	0.03	0.02	0.07	0.00	0.00	0.02	0.10	0.08	0.61	0.07	0.03	0.00	0.05	0.03	0.07	0.07	0.07	0.08
ABK41	54.90	1.90	13.60	3.20	77.20	55.80	2.00	428.90	4.90	12.90	0.80	3.10	103.00	4.00	121.00	13.70	66.00	117.80	11.75	42.20
ABK42	55.60	1.90	12.70	2.90	83.20	64.60	1.00	456.70	5.20	13.30	0.80	3.00	106.00	3.00	118.30	13.90	70.10	127.10	12.71	45.60
Relative error	0.01	0.00	0.04	0.07	0.05	0.10	0.47	0.04	0.04	0.02	0.00	0.02	0.02	0.20	0.02	0.01	0.04	0.05	0.06	0.05
ABK46	44.10	3.70	12.10	3.60	79.20	79.20	1.00	432.40	4.80	13.00	0.20	3.60	117.00	2.00	133.10	15.40	68.90	126.10	12.74	45.50
ABK47	43.50	3.80	12.20	3.40	76.70	84.90	< 1	419.60	5.00	13.00	0.20	3.60	123.00	2.00	132.70	15.90	69.50	126.80	12.76	45.10
Relative error	0.01	0.02	0.01	0.04	0.00	0.05	BLLD	0.02	0.03	0.00	0.00	0.00	0.04	0.00	0.00	0.02	0.01	0.01	0.00	0.01
ABK49	40.20	4.20	14.10	5.00	104.80	92.50	2.00	687.30	6.40	16.20	0.50	4.70	150.00	2.00	199.90	19.40	84.30	171.60	17.56	64.30
ABK50	37.50	4.10	12.40	4.90	97.00	86.00	1.00	592.30	6.00	15.10	0.40	4.20	142.00	2.00	183.10	18.60	77.30	158.10	16.06	59.30
Relative error	0.05	0.02	0.09	0.01	0.05	0.05	0.47	0.10	0.05	0.05	0.16	0.08	0.04	0.00	0.06	0.03	0.06	0.07	0.06	0.06
ABK53	84.70	0.80	5.80	3.60	215.80	35.60	1.00	780.00	15.60	39.00	0.10	4.90	90.00	3.00	136.10	15.10	200.20	386.50	37.00	127.80
ABK54	91.80	0.90	6.50	3.90	210.80	33.30	2.00	778.60	16.80	38.60	0.20	5.00	90.00	3.00	137.40	15.26	207.60	391.50	37.76	131.20
Relative error	0.06	0.08	0.08	0.06	0.01	0.05	0.47	0.00	0.05	0.01	0.47	0.01	0.00	0.00	0.01	0.00	0.03	0.01	0.01	0.02
ABK59	89.40	1.00	7.40	5.50	253.60	34.80	2.00	736.60	23.40	37.70	< .1	6.00	145.00	2.00	202.20	13.10	187.30	322.80	30.08	98.20
ABK60	90.40	1.00	8.06	5.50	268.50	37.50	3.00	809.70	22.10	37.30	0.50	6.00	135.00	1.00	201.90	14.60	202.80	344.50	32.05	101.50
Relative error	0.01	0.00	0.06	0.00	0.04	0.05	0.28	0.07	0.04	0.01	BLLD	0.00	0.05	0.47	0.00	0.08	0.06	0.05	0.05	0.02
ABK69	72.00	0.70	5.80	4.40	223.90	14.20	2.00	775.30	13.90	31.30	< .1	3.90	104.00	< 1	172.70	9.90	133.60	230.30	21.80	72.50
ABK70	75.90	0.60	6.70	4.70	220.70	14.90	2.00	803.00	12.20	31.30	< .1	4.10	98.00	< 1	171.70	10.40	140.00	236.20	22.57	72.00
Relative error	0.04	0.09	0.10	0.05	0.01	0.03	0.00	0.02	0.09	0.00	BLLD	0.04	0.04	BLLD	0.00	0.03	0.03	0.02	0.02	0.00
Avg. relative error (%)	3.51	9.11	6.00	4.89	3.23	8.56	21.68	3.79	5.27	2.09	25.29	2.33	3.31	13.86	2.78	2.75	4.80	4.70	4.55	3.64

Duplicate Pairs: Trace Elements (INNA)						Duplicate Pairs: Trace Elements (ICP)													
	Sm	Eu	Gd	Tb	Dy	Ho	Er	Tm	Yb	Lu	Mo	Cu	Pb	Zn	Ni	As	Cd	Sb	Bi
Sample No.	ppm	ppm	ppm	ppm	ppm	ppm	ppm	ppm	ppm	ppm	ppm	ppm	ppm	ppm	ppm	ppm	ppm	ppm	ppm
ABK12	12.10	3.11	5.58	0.61	3.41	0.39	1.17	0.10	0.56	0.07	1.00	32.00	8.00	53.00	1279.00	< 2	< 2	< 5	< 5
ABK13	13.00	3.33	6.33	0.68	3.66	0.44	1.33	0.10	0.63	0.07	< 1	32.00	7.00	54.00	1280.00	< 2	< 2	< 5	< 5
Relative error	0.05	0.05	0.09	0.08	0.05	0.09	0.09	0.00	0.06	0.00	BLLD	0.00	0.09	0.01	0.00	BLLD	BLLD	BLLD	BLLD
ABK17	6.10	1.50	2.87	0.37	1.98	0.26	0.82	0.08	0.49	0.07	1.00	22.00	11.00	54.00	1077.00	< 2	0.20	< 5	0.70
ABK18	5.40	1.39	2.74	0.32	1.92	0.25	0.74	0.06	0.47	0.07	1.00	21.00	8.00	54.00	1191.00	< 2	< .2	< 5	1.10
Relative error	0.09	0.05	0.03	0.10	0.02	0.03	0.07	0.20	0.03	0.00	0.00	0.03	0.22	0.00	0.07	BLLD	BLLD	BLLD	0.31
ABK32	5.40	1.46	4.09	0.56	3.34	0.65	2.02	0.27	1.71	0.25	1.00	37.00	11.00	74.00	219.00	7.00	0.60	< .5	< .5
ABK33	5.50	1.40	4.12	0.55	3.32	0.67	2.01	0.26	1.74	0.27	1.00	38.00	11.00	75.00	222.00	8.00	0.60	< .5	0.50
Relative error	0.01	0.04	0.01	0.01	0.00	0.02	0.00	0.03	0.01	0.05	0.00	0.02	0.00	0.01	0.01	0.09	0.00	BLLD	BLLD
ABK36	5.30	1.18	3.88	0.50	3.09	0.59	1.65	0.23	1.60	0.26	1.00	36.00	9.00	72.00	223.00	5.00	0.60	< .5	< .5
ABK37	4.80	1.14	3.68	0.48	2.96	0.58	1.76	0.24	1.50	0.23	1.00	36.00	10.00	71.00	210.00	6.00	0.60	< .5	0.80
Relative error	0.07	0.02	0.04	0.03	0.03	0.01	0.04	0.03	0.05	0.09	0.00	0.00	0.07	0.01	0.04	0.13	0.00	BLLD	BLLD
ABK41	6.00	1.53	3.71	0.51	2.68	0.52	1.44	0.22	1.25	0.20	3.00	42.00	9.00	65.00	732.00	5.00	0.40	< .5	< .5
ABK42	6.00	1.55	4.08	0.51	3.02	0.52	1.59	0.19	1.27	0.17	4.00	43.00	9.00	66.00	730.00	5.00	0.50	< .5	< .5
Relative error	0.00	0.01	0.06	0.00	0.08	0.00	0.07	0.10	0.01	0.11	0.20	0.02	0.00	0.01	0.00	0.00	0.16	BLLD	BLLD
ABK46	6.20	1.60	4.04	0.56	3.17	0.54	1.80	0.22	1.43	0.20	1.00	46.00	11.00	70.00	510.00	6.00	0.70	< .5	< .5
ABK47	6.70	1.68	4.23	0.53	3.14	0.57	1.76	0.21	1.45	0.21	< 1	48.00	10.00	71.00	494.00	5.00	0.70	< .5	< .5
Relative error	0.05	0.03	0.03	0.04	0.01	0.04	0.02	0.03	0.01	0.03	BLLD	0.03	0.07	0.01	0.02	0.13	0.00	BLLD	BLLD
ABK49	9.20	2.30	5.60	0.75	4.11	0.75	2.15	0.25	1.69	0.23	1.00	52.00	13.00	77.00	350.00	6.00	0.60	< .5	0.50
ABK50	8.80	2.19	5.37	0.69	3.90	0.71	2.24	0.25	1.65	0.25	1.00	48.00	13.00	78.00	335.00	7.00	0.70	< .5	< .5
Relative error	0.03	0.03	0.03	0.06	0.04	0.04	0.03	0.00	0.02	0.06	0.00	0.06	0.00	0.01	0.03	0.11	0.11	BLLD	BLLD
ABK53	14.40	3.70	6.66	0.74	4.34	0.55	1.72	0.16	0.94	0.12	2.00	45.00	12.00	62.00	787.00	< 2	0.20	0.60	< .5
ABK54	14.80	3.76	7.09	0.83	4.35	0.58	1.74	0.15	0.99	0.13	2.00	45.00	11.00	65.00	844.00	< 2	< 2	< .5	< .5
Relative error	0.02	0.01	0.04	0.08	0.00	0.04	0.01	0.05	0.04	0.06	0.00	0.00	0.06	0.03	0.05	BLLD	BLLD	BLLD	BLLD
ABK59	11.70	2.83	4.86	0.63	3.95	0.53	1.33	0.12	0.88	0.12	2.00	65.00	11.00	73.00	636.00	2.00	< .2	< .5	< .5
ABK60	12.00	2.95	5.22	0.65	4.05	0.57	1.46	0.13	0.81	0.11	2.00	67.00	11.00	80.00	613.00	< 2	< .2	< .5	0.50
Relative error	0.02	0.03	0.05	0.02	0.02	0.05	0.07	0.06	0.06	0.06	0.00	0.02	0.00	0.06	0.03	BLLD	BLLD	BLLD	BLLD
ABK69	8.40	2.11	4.20	0.49	3.06	0.42	1.51	0.10	0.71	0.11	1.00	48.00	9.00	55.00	515.00	< 2	< 2	1.40	1.00
ABK70	8.70	2.08	4.04	0.52	2.90	0.42	1.57	0.09	0.71	0.10	1.00	47.00	8.00	55.00	513.00	< 2	< 2	1.70	1.00
Relative error	0.02	0.01	0.03	0.04	0.04	0.00	0.03	0.07	0.00	0.07	0.00	0.01	0.08	0.00	0.00	BLLD	BLLD	0.14	0.00
Avg. relative error (%)	3.68	2.95	4.10	4.64	2.92	3.12	4.17	5.72	2.79	5.34	2.53	1.91	6.04	1.61	2.57	9.20	5.32	13.69	15.71
	BLLD*	Below lower limit of detection																	
		Buffalo Head Hills																	
		Mountain Lake																	
		Birch Mountains																	

Table 3. Duplicate samples from northern Alberta kimberlitic rocks with geochemical data and relative error.

Index (C.I.) to measure the proportion of clay minerals and tectosilicates relative to olivine and phlogopite:

$$\text{C.I.} = \frac{SiO_2 + Al_2O_3 + Na_2O}{MgO + K_2O}$$

Clement (1982) found that uncontaminated Group I kimberlite has a C.I. near 1.0, but that some apparently fresh and contamination-free micaceous Group II kimberlite has a C.I. up to 1.5.

Of the samples analyzed during this study, all of the ML, 33% of the BM, and 7.5% of the BHH samples have a C.I. of greater than 1.5 (Figure 4; Appendix 1). Samples with a C.I. >1.5 include 1) ABK31 to ABK47 (all samples, ML); 2) ABK14, ABK19, ABK23 and ABK24 (BHH); and 3) ABK48, ABK49, ABK50, ABK51, ABK55, ABK81, ABK82 and ABK83 (BM). With the possible exception of the Xena pipe samples (ABK49 to ABK51) and MLS (ABK39 to ABK47), most of these samples contain macroscopically obvious sources of contamination, including shale, siltstone and sandstone, and/or oxidized, highly weathered material. The generalized physical observations of samples with a C.I. >1.5 is included on Figure 4.

Taylor et al. (1994) used the ilmenite index (Ilm.I.) to identify kimberlite that potentially contains accumulated xenocrystalline or megacrystalline ilmenite:

$$\text{Ilm.I.} = \frac{(FeO_t + TiO_2)}{(2K_2O + MgO)}$$

Taylor et al. (1994) suggested that the Ilm.I. of type Group IA kimberlite (South African) and Group II kimberlite (South African) should not exceed 0.52 and 0.47, respectively. They further suggested that the limit for Group IB kimberlite (South African) is difficult to judge due to its relatively high bulk-rock TiO_2 content. Of the samples analyzed during this study, 3% of the ML, 6.7% of the BHH, and 36% of the BM samples have an Ilm.I. of greater than 0.52 (Figure 4; Appendix 1).

The plot of C.I. versus of Ilm.I. in Figure 4 indicates that the compositions of Alberta pipes differ depending on their location:

- The BHH samples generally have low C.I. (<1.5) and Ilm.I. (<0.3), and 60% (19 samples) plot close to the primitive kimberlite magma from the Northwest Territories (Price et al., 2000; Berg and Carlson, 1998).
- The BM samples generally have relatively low C.I. (<1.5) and high Ilm.I. (>4.0), the latter consistent with the observed relatively high bulk-rock TiO_2 contents.

- The ML samples are characterized by two separate high C.I. groups. The MLS pipe has a lower C.I. value (0.34 to 0.39) than those from the MLN pipe (0.38 to 0.85).

Because the MLS pipe is comprised of juvenile magmatic material with only a minor component of xenocrystic quartz in comparison to the MLN pipe, the differences in composition between the ML pipe and the BHH and BM pipes are more likely a function of the ultramafic magma type rather than solely a result of more extensive crustal contamination in the ML pipe. This contention is supported when the C.I. versus Ilm. I. values from the Sweet Grass minette and worldwide basanite rock are plotted on Figure 4 and roughly coincide with the ML pipe rocks. The hypothesis that the major element compositions of the ML and Xena (BM) pipes are more compatible with a rock type other than kimberlite is discussed in Section 6.2.1 below.

Mitchell (1986) used a similar approach to distinguish between "contaminated" and "noncontaminated" kimberlite when he concluded that <35 wt. % SiO_2 and <5 wt. % Al_2O_3 are indicative of contamination-free kimberlite, and that mixing lines of various contaminants and weathering products could explain variations in kimberlite chemistry. Figure 5 (Al_2O_3 vs. SiO_2) shows that, in contrast to the ML samples, the majority of the BHH samples (90%) and BM samples (75%) plot in the contamination-free field. Berg (1998) proposed that 2.2% Al_2O_3 be used as a maximum cutoff for contamination-free Group I kimberlite. Berg's cutoff would limit contamination-free kimberlite in Alberta to the BHH.

Seven samples, including ABK01, ABK02, ABK03, ABK08, ABK11, ABK26 and ABK27, contain lower Al_2O_3 and higher SiO_2 than the Northwest Territories primitive kimberlite (e.g., Jericho aphanitic kimberlite; Price et al., 2000). The negative trend of these samples in Figure 5 corresponds to the serpentine alteration line of Mitchell (1986). The bleached, green-yellow appearance of some of these samples suggests serpentine alteration.

6.2 Major Element Geochemistry

The average major element compositions of the northern Alberta pipes are presented in Table 4 in comparison with Sweet Grass olivine minette (southern Alberta) and worldwide kimberlite, olivine/madupitic lamproite, melilitite and basanite.

6.2.1 Mountain Lake

The major-element chemistry of the ML samples is not consistent with either kimberlite (25 to 35 wt. % SiO_2; <5 wt. % Al_2O_3; Na_2O/K_2O ratio <0.5) or lamproite (peralkaline index >0.7, Niggli K

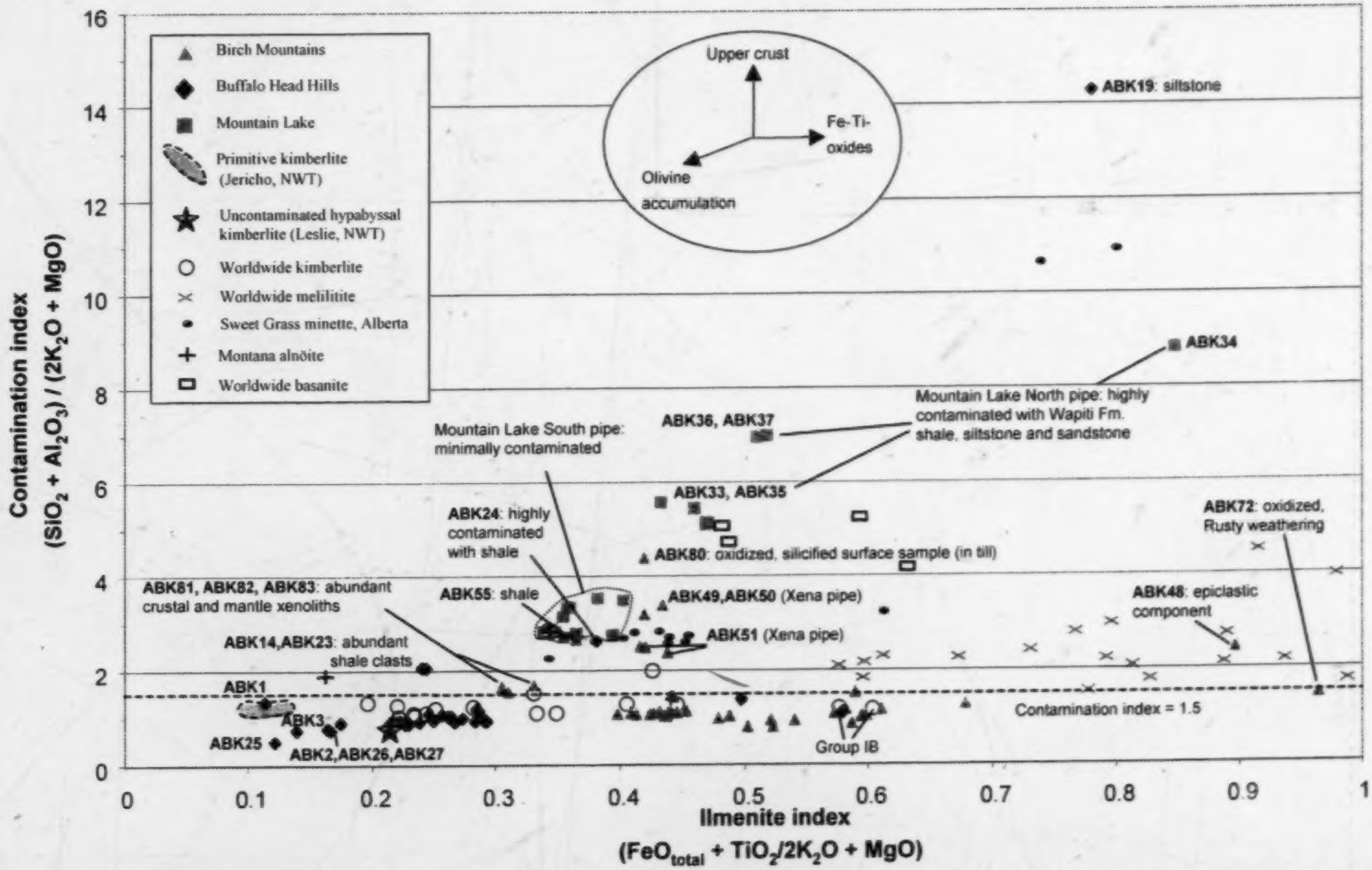

Figure 4. Plot of contamination index of Clement (1982) versus ilmenite index of Taylor et al. (1994) for northern Alberta kimberlitic whole-rock compositions. Contaminated rocks (C.I. >1.5) are labelled and include macroscopic observations. Dashed line represents a C.I. of 1.5; vectors show trends for kimberlite contamination by granitic and siliceous crustal rocks, Fe- and Ti-oxide (ilmenite) accumulation, and olivine accumulation (Taylor et al., 1994). See section 5.1 in text for sources of comparative data.

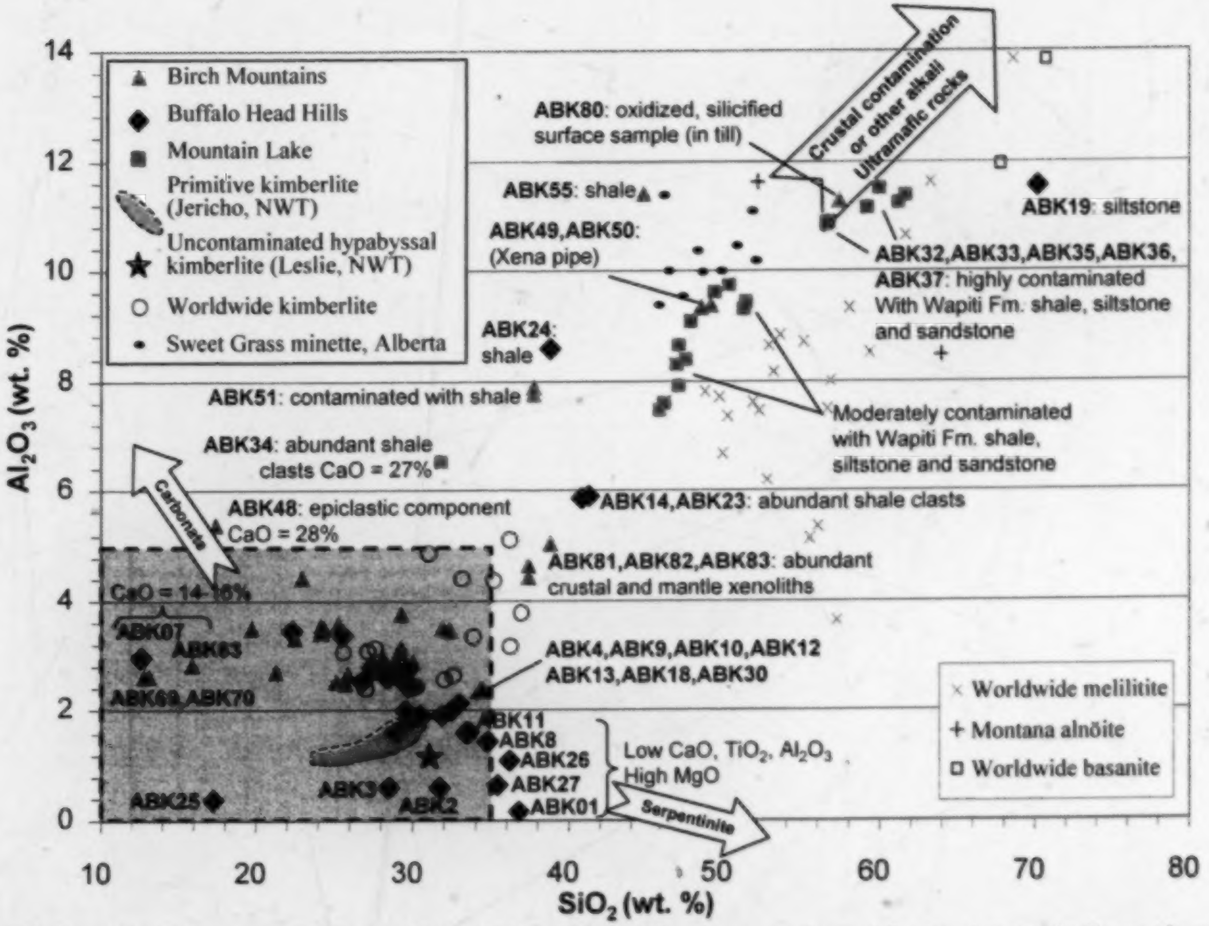

Figure 5. Whole-rock Al_2O_3 versus SiO_2 for kimberlitic rock samples from northern Alberta. Arrows indicate alteration (serpentinization and carbonate enrichment) and crustal contamination (shale, siltstone, sandstone and felsic rocks) vectors for northern Alberta. See section 5.1 in text for sources of comparative data.

	Average kimberlite[1]		Average lamproite[2]		Average	Average Sweet	Average	Mountain Lake			Buffalo Head Hills			Birch Mountains		
Element	Min.	Max.	Min.	Max	melilitite[3]	Grass minette[4]	Basanite[5]	Min.	Max.	Avg.	Min.	Max.	Avg.	Min.	Max.	Avg.
SiO_2	25.50	36.40	40.00	51.00	36.21	49.76	44.30	31.96	61.61	51.35	12.66	70.12	31.60	12.76	57.39	29.25
Al_2O_3	2.50	5.10	3.00	9.00	8.03	10.72	14.70	6.56	11.49	9.46	0.17	11.53	2.66	2.50	11.42	4.32
Fe_2O_3	3.90	6.78	1.85	8.78	14.50	8.71	3.94	3.62	7.78	6.21	3.47	9.51	7.66	3.62	14.98	8.92
MgO	17.00	28.60	12.00	28.00	15.18	9.91	8.54	2.45	16.74	11.51	1.90	44.94	30.34	4.51	29.60	22.46
CaO	7.60	21.37	4.00	13.00	14.40	7.70	10.19	2.67	27.55	5.09	0.75	23.09	7.38	1.78	27.97	9.82
Na_2O	0.12	0.48	0.29	1.42	2.25	1.68	3.55	0.92	2.66	1.84	0.01	2.38	0.19	0.03	3.00	0.33
K_2O	0.34	2.10	3.00	9.00	1.41	5.25	1.96	1.03	3.10	2.22	0.06	3.86	0.54	0.04	4.62	0.91
TiO_2	1.20	3.40	1.00	5.00	3.96	0.97	2.51	0.56	0.92	0.83	0.01	1.44	0.71	0.54	4.76	2.73
P_2O_5	0.70	1.10	1.00	3.00	1.12	1.00	0.74	0.20	0.44	0.29	0.12	0.96	0.47	0.27	0.91	0.54
MnO	0.10	0.19	0.10	0.13	0.22	0.14	0.16	0.08	0.22	0.11	0.03	0.19	0.13	0.05	0.32	0.16
Cr_2O_3	0.11	0.25	N/A*	N/A	N/A	N/A	N/A	0.05	0.14	0.01	0.01	0.22	0.14	0.02	0.21	0.12
Na_2O/K_2O	0.35	0.23	0.10	0.16	1.60	0.32	1.81	0.89	0.86	0.83	0.17	0.62	0.35	0.75	0.65	0.36
Peralkalinity index[6]	0.23	0.60	1.24	1.34	0.65	0.79	0.54	0.40	0.67	0.57	0.48	0.70	0.34	0.04	0.87	0.35
Niggli K[7]	0.65	0.74	0.87	0.81	0.29	0.67	0.27	0.42	0.43	0.44	0.80	0.52	0.65	0.47	0.50	0.64
Niggli mg[8]	0.85	0.85	0.89	0.81	0.58	0.60	0.74	0.47	0.74	0.71	0.42	0.86	0.84	0.62	0.72	0.77
Mg#[9]	89.62	89.31	92.78	86.33	67.46	69.26	81.11	57.27	80.99	78.59	52.02	90.35	88.69	71.16	79.65	83.30

1 Representative average composition of kimberlite (Mitchell, 1986)

2 Geochemical criteria for olivine/madupitic lamproite (Mitchell and Bergman (1991). Included are the:
- composition of Fe_2O_3, Na_2O and MnO for madupitic lamproite, Prairie Creek (Scott Smith and Skinner, 1984)
- composition of Fe_2O_3, Na_2O and MnO from average of 52 olivine lamproites (Scott, 1979)

3 Average worldwide composition for olivine melilitite (Wilson et al., 1995; Rogers et al., 1992)

4 Average composition of Sweet Grass, Alberta olivine minette (Kjarsgaard, 1994; Buhlmann et al., 2000)

5 Average worldwide basanite (Le Maitre, 1976)

6 Peralkalinity Index = molar $(K_2O+Na_2O)/Al_2O_3$

7 Niggli K = molar $K_2O/(K_2O+Na_2O)$

8 Niggli mg = molar $MgO/(MgO+FeO_{total}+Fe_2O_3+MnO)$

9 Mg# = $100^*MgO/(MgO+FeO_{total})$

* N/A = not available

Table 4. Comparison of selected major elements in northern Alberta kimberlitic rocks with average kimberlite, olivine/madupitic lamproite, olivine melilitite, olivine minette and basanite.

>0.8 and Niggli mg >0.8). This finding is consistent with that based on petrographic examination by Leckie et al. (1997) and Skupinski and Langenberg (2002), who concluded that the ML pipe was not archetypal kimberlite.

Accordingly, the ML pipe samples have very different major-element chemistries compared to the BHH and BM samples (Figure 6; Table 4). Generally, the ML samples contain high SiO_2 (average 51.4 wt. %), high MgO (average 11.5 wt.% with Mg# of 78.6), low Al_2O_3 (average 9.5 wt. %) and relatively low alkalis (average 2.2 wt. % K_2O and 1.8 wt. % Na_2O). The ML rocks have higher SiO_2, Al_2O_3, Na_2O, K_2O, Na_2O/K_2O ratio (0.83); higher peralkalinity index (average molar $[K_2O+Na_2O]/Al_2O_3 = 0.57$); and lower MgO, Niggli K (average molar $K_2O/[K_2O+Na_2O] = 0.44$) and Niggli mg (average molar $MgO/[MgO+FeO+ Fe_2O_3+MnO] = 0.71$) compared to the BHH and BM samples.

The major-element chemistry of the ML samples shows some similarity to those of the Sweet Grass minette and worldwide basanite (Table 4). There is a negative correlation in both the ML samples and the Sweet Grass minette for SiO_2 versus MgO and Al_2O_3 versus MgO, and a positive correlation for TiO_2 versus $Fe_2O_{3(T)}$. However, significant differences exist in K_2O, $Fe_2O_{3(T)}$ and P_2O_5. For example, average values for the ML pipe and the Sweet Grass minette are 2.22 versus 5.25 wt. % K_2O, 6.21 versus 8.71 wt. % $Fe_2O_{3(T)}$ and 0.29 versus 1.0 wt. % P_2O_5, respectively. Despite these differences, the two suites show parallel trends for K_2O versus MgO and K_2O versus $Fe_2O_{3(T)}$.

With high SiO_2 contents and peralkalinity indices, the ML samples ABK31 to ABK33 and ABK35 to ABK47 plot in the field of Roman Province type (RPT) potassic lavas (Figure 7), which Mitchell and Bergman (1991) have suggested characterize most minettes worldwide. The data from basanite, Sweet Grass minette and Montana alnöite (Hearn, 1986) also plot in the RPT field, suggesting a similar petrogenesis. Sample ABK34 has a lower SiO_2 content (31.96 wt. %) and plots below the RPT field near kimberlite and melilitite.

A K_2O versus Na_2O diagram (Figure 8A) discriminates clearly between kimberlite and the ML samples. The majority of the ML samples plot on the potassic side of the 1:1 discrimination line used by Le Bas (1989) to divide potassic rocks (e.g., lamprophyric) from nonpotassic rocks (e.g., melilitite, nephelinite). The lack of overlap between kimberlite and the more sodic ML pipe rocks

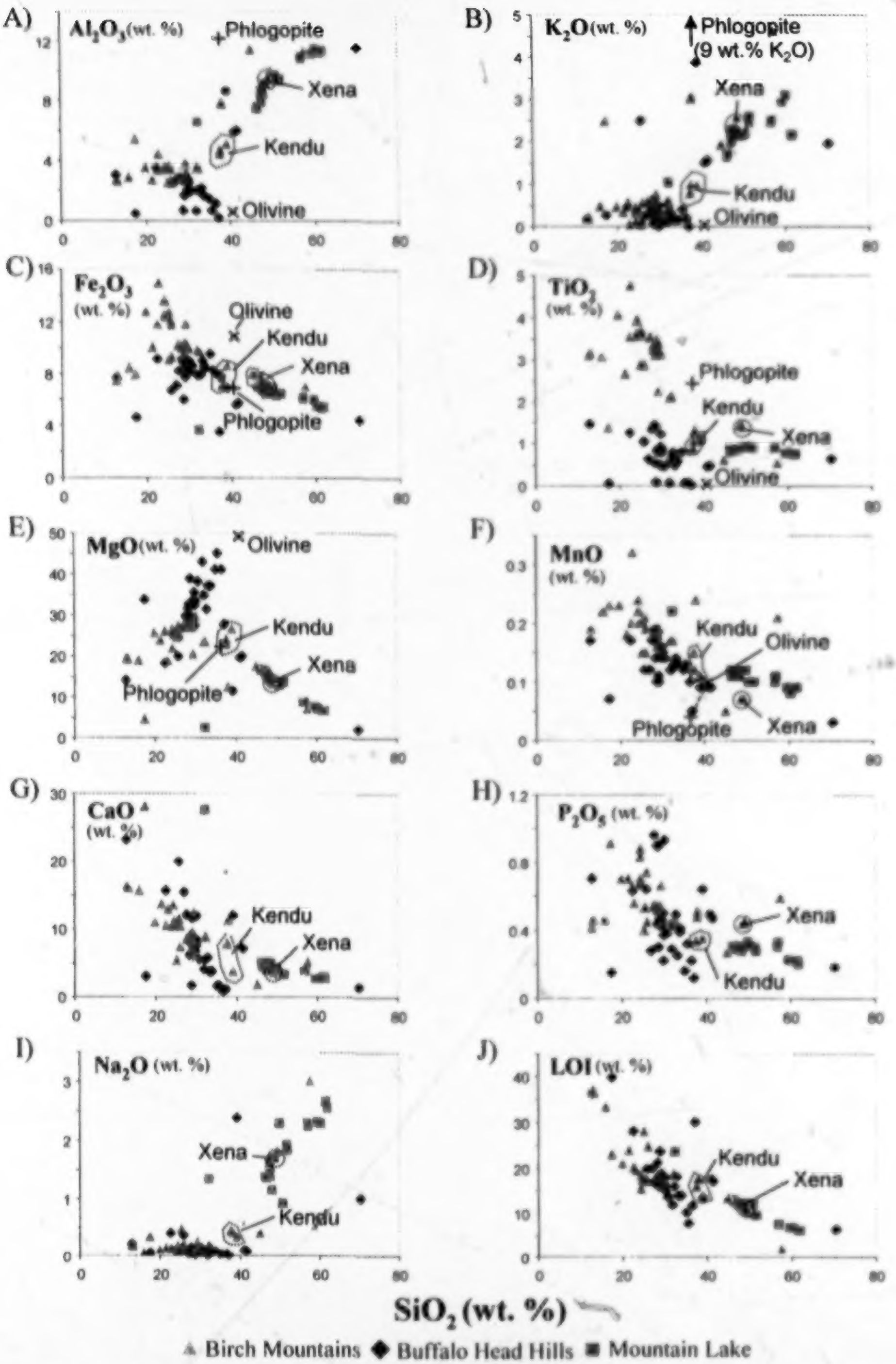

Figure 6. Major-element whole-rock variation diagrams with SiO$_2$ for kimberlitic rocks from northern Alberta. Olivine and phlogopite compositions from selected kimberlite pipes in the northern Alberta kimberlite province (Creighton and Eccles, 2003).

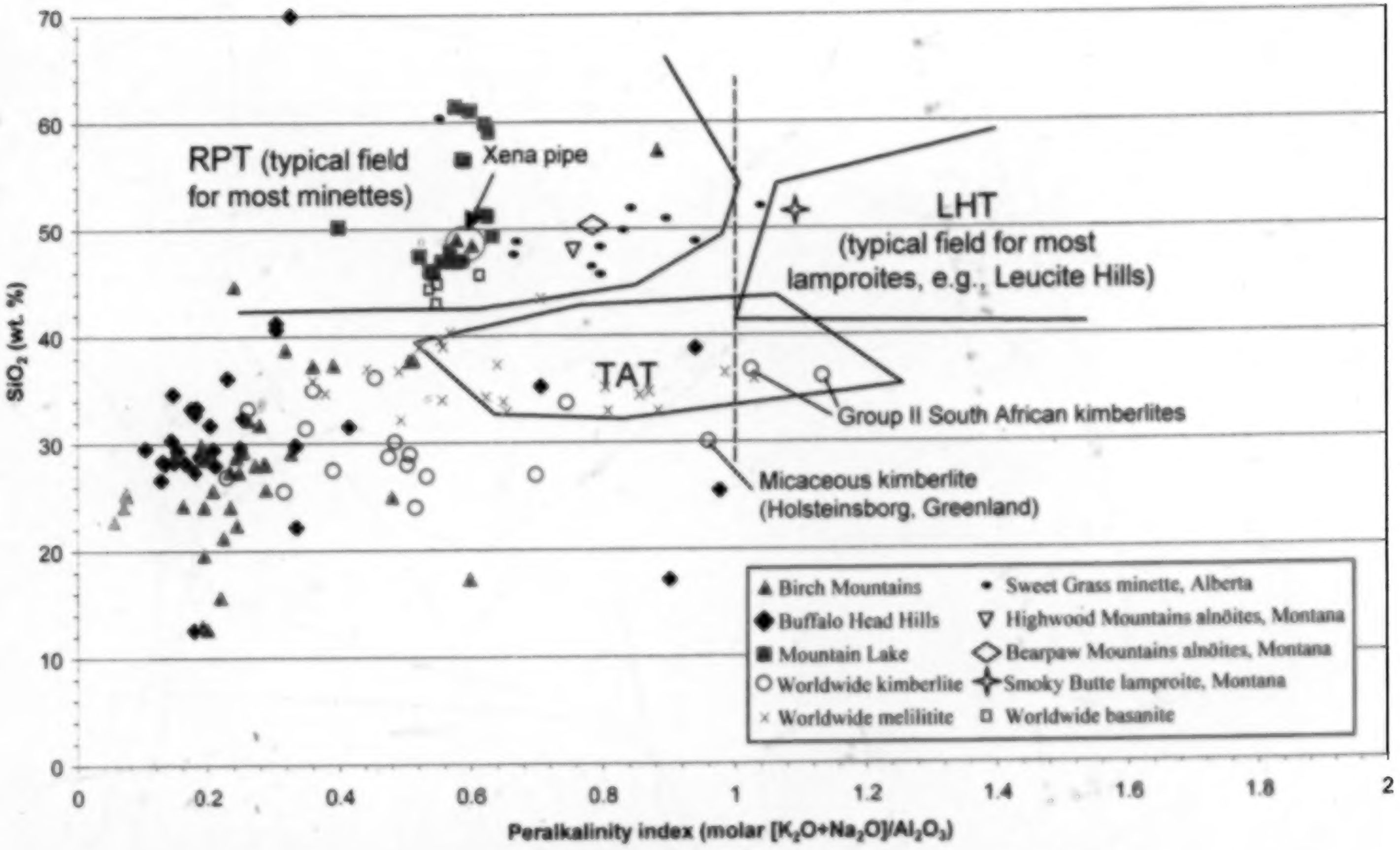

Figure 7. SiO$_2$ versus peralkalinity index (molar [K$_2$O+Na$_2$O]/Al$_2$O$_3$) for northern Alberta kimberlitic whole-rock compositions. Dashed line represents a peralkalinity value of 1.0. Solid vectors or polygons represent the three groups of potassic lavas recognized by Barton (1979): RPT, Roman Province type lavas; LHT, Leucite Hills type lavas; TAT, Toro-Ankole type lavas. See section 5.1 in text for sources of comparative data.

must reflect major mineralogical differences between their mantle sources, degree of melting or subsequent fractionation.

The ML samples were also plotted on the total alkalis versus SiO_2 diagram (TAS classification, Figure 8B) and on the $CaO+Na_2O+K_2O$ versus $SiO_2+Al_2O_3$ diagrams (Figure 8C) of Le Bas (1989) and Le Maitre (1989) to differentiate between similar potassic rocks. The ML samples plot in the field for basalt to andesite on Figure 8B and in the field for basanite on Figure 8C. These plots support a difference in genesis between the ML samples and those from the BHH and BM. Sample ABK34 from ML plots in the field of melilitite on Figure 8C. It is not presently known why sample ABK34 contains such a different chemistry (e.g., lower SiO_2 and MgO) than the rest of the ML samples, but the high CaO (27.6 wt. %) and LOI (23.6 wt. %) is consistent with a significant proportion of carbonate in this sample. Leckie et al. (1997) logged the portion of the drill core that contains sample ABK34 as being microfaulted and containing abundant quartz and feldspar xenocrysts in the matrix.

Ocean island basalts situated above smaller plumes and/or located on old and thick ocean lithosphere are characterized by a variety of basalt that has lower SiO_2, but higher Na_2O and K_2O contents than tholeiites (Figure 8B). Such basalts are termed alkaline olivine basalt or alkali basalt. The mineralogical variety of alkali basalt is considerable and is a result of both a reduction of SiO_2 and an increase in the alkali elements, particularly Na_2O, and other minor and trace elements. This trend toward increasing alkalinity also produces magma compositions outside the field of alkali basalts, which are generally known as basanites.

Possible contamination of the ML samples must be evaluated before any conclusions can be drawn regarding their original chemistry. The rocks are highly altered to smectitic minerals (montmorillonite) and the olivine is completely pseudomorphed by serpentine or carbonate. Formation of clay minerals, serpentinization of olivine and the entrainment of Cretaceous clastic sedimentary rocks will increase SiO_2 and Al_2O_3 contents. Berg (1998) proposed that a positive trend between Na_2O and SiO_2 is likely related to high sodium in shale, post-emplacement water circulation, or the presence of pectolite and Ti-rich acmite. The positive trends of Al_2O_3, K_2O and Na_2O versus SiO_2 (Figure 6A, B and I) and a high contamination index (>2.7) suggest that the ML samples may have been contaminated by Cretaceous Wapiti Formation shale, siltstone and sandstone. In addition, a negative correlation between MgO and SiO_2 was interpreted by Berg (1998) as being the result of contamination by country rock (Figure 6E). Finally, extensive

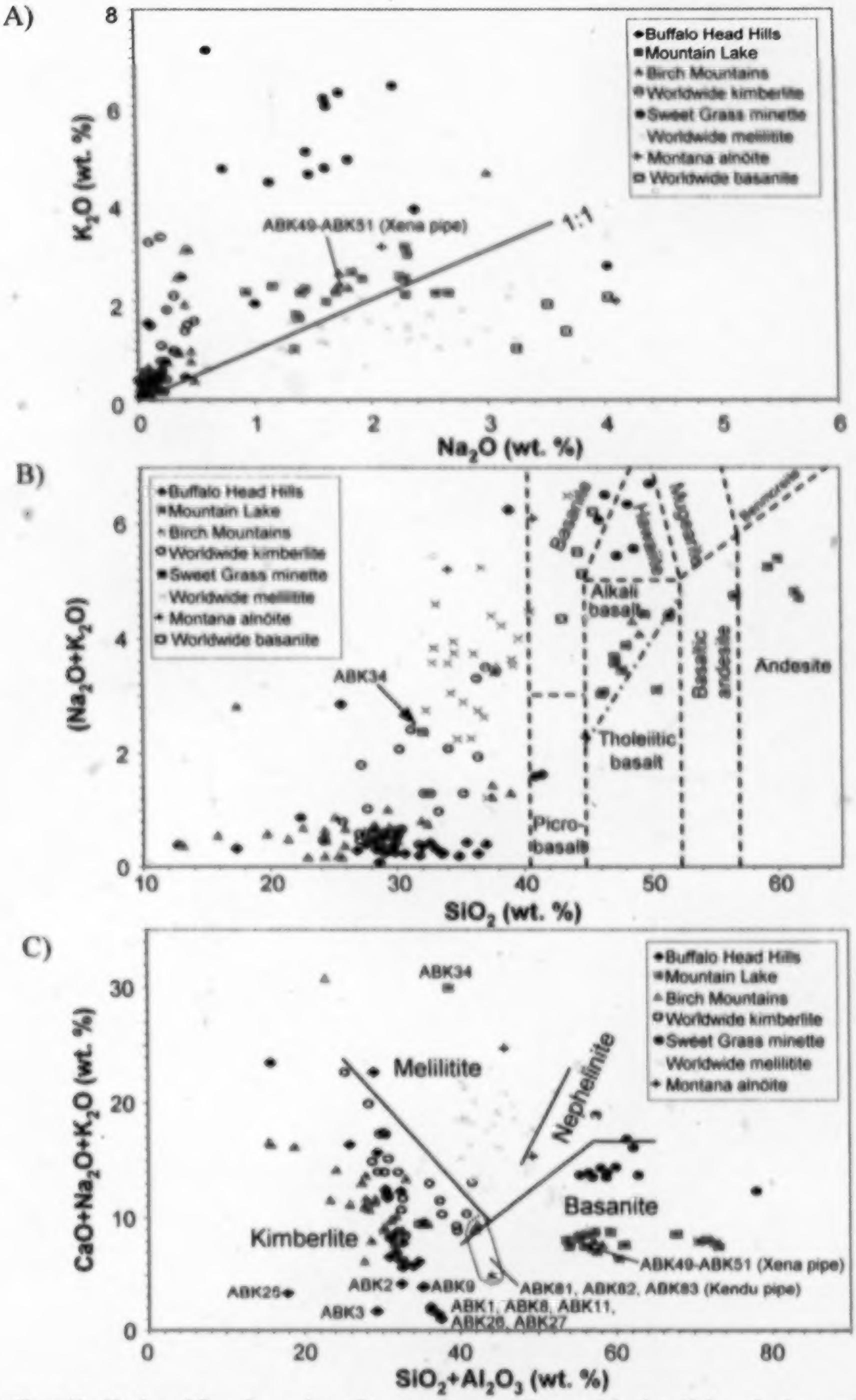

Figure 8. Alkali classification plots for northern Alberta kimberlitic whole-rock compositions: A) K$_2$O versus Na$_2$O; B) total alkalis versus SiO$_2$ (TAS classification); C) CaO+Na$_2$O+K$_2$O versus SiO$_2$+Al$_2$O$_3$. See section 5.1 in text for sources of comparative data.

contamination might be expected, since Leckie et al. (1997) reported that the ML pipe was syndepositionally emplaced with the mid-Cretaceous Wapiti Formation sedimentary rocks and is therefore, contaminated by variable amounts of quartz and feldspathic minerals. This resedimentation is most noticeable in MLN, which has higher average SiO_2 (53.8 wt. %) and Al_2O_3 (10.4 wt. %) compared to MLS. Addition of quartz would clearly affect the classification of the ML pipe rocks. Thus, if the rocks were not contaminated by quartz, the samples might plot to the left of basalt on the TAS diagram (Figure 8B) and more likely resemble a basanite.

To reiterate, the MLS pipe has the higher proportion of juvenile magmatic material, and therefore, is the closest to the true representative composition of the pipe. The freshest, least contaminated samples from MLS are characterized by: 47.6 wt. % SiO_2, 8.4 wt. % Al_2O_3, 15.4 wt.% MgO with Mg# of 82 mol. %, 2.1 wt. % K_2O, 1.5 wt. % Na_2O, and peralkalinity index of 0.56). Even the major-element chemistry of the least-contaminated MLS rocks is not consistent with this rock type being kimberlite. Depending on the combination of major elements used for interpretation, the ML rocks have affinities that are similar to alkaline olivine basalt rock types (e.g., basanite).

6.2.2 Buffalo Head Hills

In comparison to samples from ML and BM, the BHH samples have low SiO_2 (average 31.6 wt. %), high MgO (average 30.3 wt. %; Mg# averages 88.7 and is up to 90.4), very low Al_2O_3 (average 2.7 wt. %) and a low Na_2O/K_2O ratio (0.35). When compared to worldwide kimberlite averages (Table 4), the pipes in the BHH region may be described as archetypal Group I kimberlite.

A steep, positive MgO versus SiO_2 correlation (Figure 6E) characterizes the BHH samples. Berg (1998) observed, from the bulk geochemistry and petrography of 70 South African kimberlites, that a positive correlation between SiO_2 and MgO is typically associated with hypabyssal, primitive kimberlite. A primitive nature for the BHH samples is supported by their geochemical similarity to primitive kimberlite from the Northwest Territories.

A small group of between six and eight samples (samples ABK01, ABK02, ABK03, ABK08, ABK11, ABK25, ABK26 and ABK27) cluster together on several bivariate plots (e.g., Figures 4, 5 and 8C). These samples contain the lowest values of Al_2O_3 (1.11 wt. %), TiO_2 (0.08 wt. %) and CaO (3.97 wt. %), and the highest values of MgO (up to 44.9 wt. %) and Cr_2O_3 (up to 0.22 wt. %) of the northern Alberta samples. In Figure 4, they plot close to the most primitive samples from the Jericho kimberlite (Northwest Territories) and a sample from the Leslie kimberlite (Northwest Territories) that are considered by Price et al. (2000) and Berg and Carlson (1998), respectively, to represent hypabyssal kimberlite that is either minimally contaminated or uncontaminated. Conversely, a negative trend for samples ABK01, ABK02, ABK03, ABK26 and ABK27 on the plot of Al_2O_3 versus SiO_2 (Figure 5) suggests that these samples are moderately to highly serpentinized (e.g., Mitchell, 1986) and, instead, samples ABK04, ABK09, ABK10, ABK12, ABK13, ABK18 and ABK30 plot close to Northwest Territories primitive kimberlite.

In summary, the BHH represent the most primitive Group I kimberlite phase in this dataset based on their:

- major-element chemistry (low SiO_2, high MgO and Mg#, and very low Al_2O_3);
- similarity between the BHH kimberlites and primitive kimberlite from the Jericho and Leslie pipes (Northwest Territories); and
- positive correlation between MgO and SiO_2.

6.2.3 Birch Mountains

Major-element geochemistry from the BM pipes (Table 4) indicates that they have low SiO_2 (average 29.3 wt. %), low Al_2O_3 (average 4.3 wt. %) and low Na_2O/K_2O ratios (0.36).

Mitchell (1986) suggested that differentiation of kimberlite magma by fractionational crystallization of olivine would lead to a residual melt depleted in MgO and SiO_2, but enriched in CaO, TiO_2 and volatiles. Figure 6 shows plots of various oxides versus SiO_2. Compared to samples from the BHH, most of the samples from the BM have lower contents of MgO and SiO_2 and higher contents of $Fe_2O_{3(T)}$, MnO, CaO, P_2O_5 and TiO_2. In addition, high Ilm.I. and TiO_2 (typically >2 wt. % and averaging 2.73 wt. %) may reflect the effect of late-stage accumulation of minerals such as ilmenite on the whole rock geochemistry. Therefore, the major-element geochemistry of the BM pipes is consistent with that of kimberlite that has experienced fractional crystallization (i.e., evolved kimberlite).

Samples ABK81, ABK82 and ABK83 from the Kendu kimberlite have the highest SiO_2 content from non-crustally contaminated samples in the BM field and on some plots (e.g., Figure 8C; $CaO+Na_2O+K_2O$ versus $SiO_2+Al_2O_3$) show geochemical affinities that plot between kimberlite and basanite. Figure 6 shows that the Kendu samples (ABK81, ABK82 and ABK83) consistently plot between the majority of the BHH and BM kimberlite samples and the ML alkaline ultrabasic rocks suggestive of a greater degree of evolution from primitive kimberlite. The BM Xena pipe has major element compositions that contrast with the majority of the BM pipes, but are more similar to the MLS pipe.

6.2.4 Major-Element Comparisons of the Buffalo Head Hills and Birch Mountains with Kimberlites Worldwide

In general, the BHH and BM samples have higher concentrations of $Fe_2O_{3(T)}$ and slightly lower concentrations of Cr_2O_3 than worldwide kimberlite averages (Table 4). The BM samples contain significantly higher TiO_2 concentrations. With the exception of higher $Fe_2O_{3(T)}$ and lower P_2O_5, the major-element chemistry of samples from the BM pipes falls within the field of average kimberlite (Table 4). Compared to average kimberlite (Table 4), samples from the BHH contain slightly higher $Fe_2O_{3(T)}$ and MgO, and slightly lower CaO, TiO_2 and P_2O_5.

In Figures 4 and 5, the BHH and BM samples coincide with other kimberlites. Some of the BM rocks with higher Ilm.I coincide with previously reported compositions for Group IB South Africa kimberlites. The majority of the BHH samples coincide with a grouping of worldwide kimberlite (low C.I. and Ilm.I. between 0.2 and 0.3). A large number of BHH samples (e.g., ABK01 to ABK04, ABK08 to ABK13, ABK18, ABK25 to ABK27 and ABK30) plot close to primitive kimberlites from Northwest Territories.

On plots of Mg# versus SiO_2, K_2O and TiO_2 (Figure 9), the BHH, ML and BM samples are compared to representative fields for South African Group I and Group II kimberlites (Clement, 1982; Smith et al., 1985b). Although there is significant overlap between the two South African groups, the high-Mg# BHH samples and high-TiO_2 BM samples plot in the Group I kimberlite field. The BHH samples plot close to the primitive kimberlite magma from the Jericho pipe (Northwest Territories).

Mountain Lake samples with high Mg# plot in the field of Group I kimberlite on the diagram of Mg# versus K_2O (Figure 9B) and outside the kimberlite fields for Mg# versus SiO_2 and TiO_2 (Figures 9A and 9C, respectively). As discussed previously, the ML pipe rocks are not kimberlite but more similar in composition to an olivine-rich basanite/alkali basalt. ML pipe samples with lower Mg# plot close to the Sweet Grass minette and basanite for Mg# versus SiO_2 and, in particular, close to the Sweet Grass minette for Mg# versus TiO_2.

Compared to Group IA, Group IB kimberlites have lower SiO_2 and higher CaO, $FeO+Fe_2O_{3(T)}$ and volatile contents, as well as somewhat greater TiO_2, P_2O_5, Nb, Zr and Y (e.g., Smith et al.,

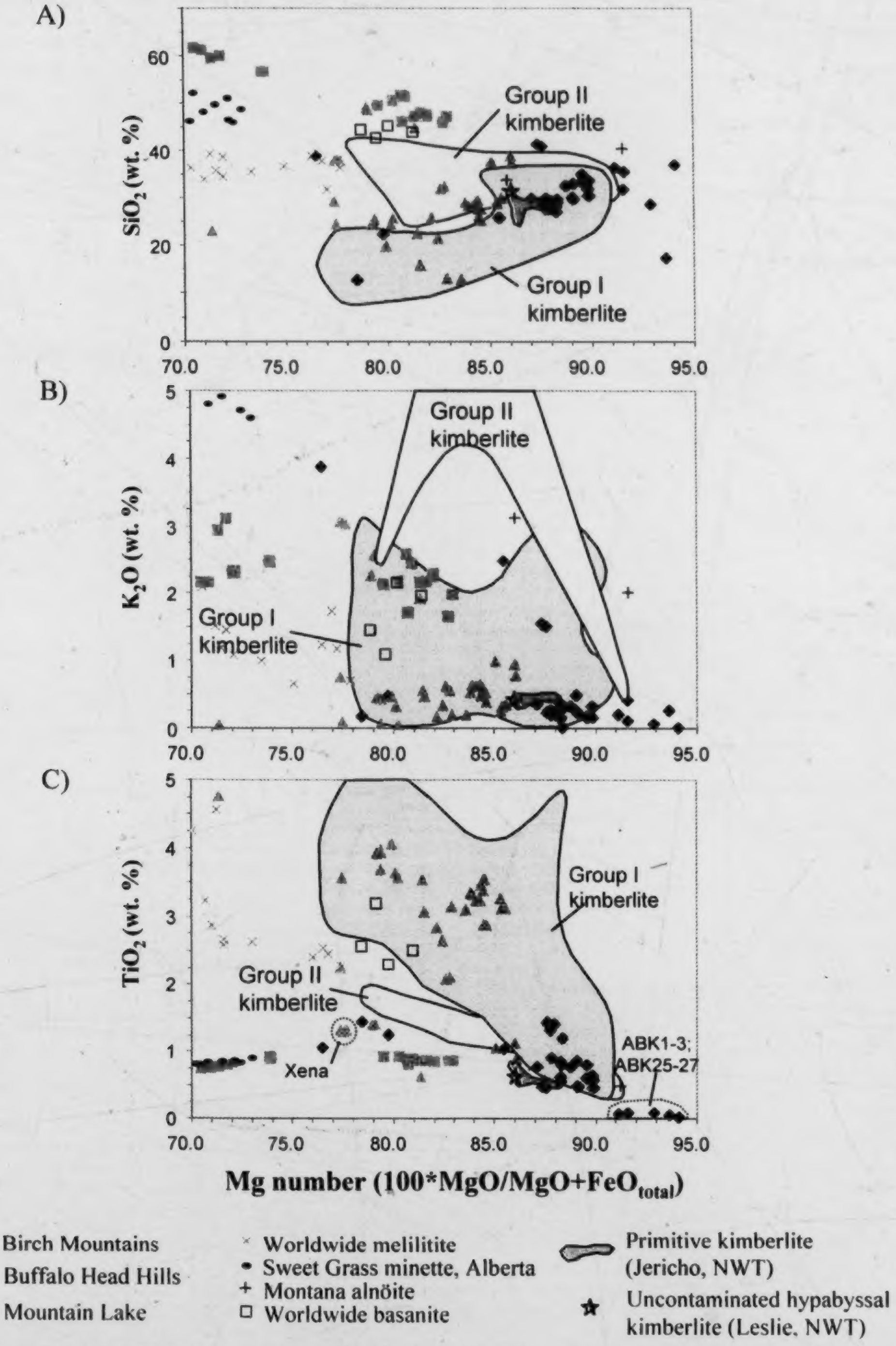

Figure 9. Plot of Mg# versus SiO$_2$, K$_2$O and TiO$_2$ for northern Alberta kimberlitic whole-rock compositions. Fields for South African Group I and II kimberlites are from Clement (1982) and Smith et al. (1985). See section 5.1 in text for sources of comparative data.

1985b). The TiO_2 and K_2O contents of the Alberta samples (Figure 10) are compared with the fields defined by Taylor et al. (1994). Except for six samples from the BM (ABK53, ABK54, ABK56, ABK81, ABK82 and ABK83), the plot of TiO_2 versus K_2O places the BHH and BM samples into Subgroup 1A and Subgroup 1B fields, respectively. Because the basement geology is still not well constrained, on-craton and off-craton terminology may not be appropriate for the BHH and BM. In addition, ML, Xena and contaminated or resedimented volcaniclastic kimberlite plot in the Taylor et al (1994) Group II kimberlite field, which may require revision to better classify NAKP rock types (*see* Figure 10).

Buffalo Head Hills samples (ABK01, ABK02, ABK03, ABK25, ABK26 and ABK27) have a TiO_2 content of less than 0.08 wt. %, and therefore, do not plot in the field of Subgroup 1A kimberlite on Figure 10.

6.3 Compatible- and Incompatible-Trace Element Geochemistry

The trace-element geochemistry of kimberlites has been discussed by various authors (e.g., Dawson, 1962, 1967, 1971, 1980; Wedepohl and Muramatsu, 1979; Muramatsu, 1983; Smith et al., 1985b; Mitchell, 1986, 1995; Taylor et al., 1994). In general, kimberlites are characterized by concentrations of first-period transition elements (Sc, V, Cr, Ni, Co, Cu and Zn) similar to ultramafic rocks such as dunite and peridotite, and concentrations of incompatible elements (e.g., Nb, Zr, Ta, Hf, U, Th, REE) similar to alkaline rocks such as melilitite, carbonatite, and potassic lavas.

6.3.1 Compatible-Trace Element Variation Between Magmas

Average values of Ni and Cr are lowest in samples from ML (433 ppm Ni and 685 ppm Cr) and highest in samples from the BHH (1241 ppm Ni and 937 ppm Cr). Concentrations of Ni and Cr in samples from the ML pipe are well below those of worldwide kimberlite (Table 5) but comparable to the worldwide averages for melilitite (416 ppm Ni and 565 ppm Cr) and to the Sweet Grass minette (512 ppm Ni and 591 ppm Cr).

Concentrations of Ni and Cr from the BHH and Cr from the BM are similar to those of Group I South African kimberlites. Average Ni values in samples from the BM (618 ppm) are slightly lower than Group IB Ni values (800 ppm). Price et al. (2000) noted that Cr and Ni concentrations were higher in their hybabyssal samples from the Jericho kimberlite and that high Ni concentrations (ranging from 600 to 1400 ppm) were associated with primitive mantle melts.

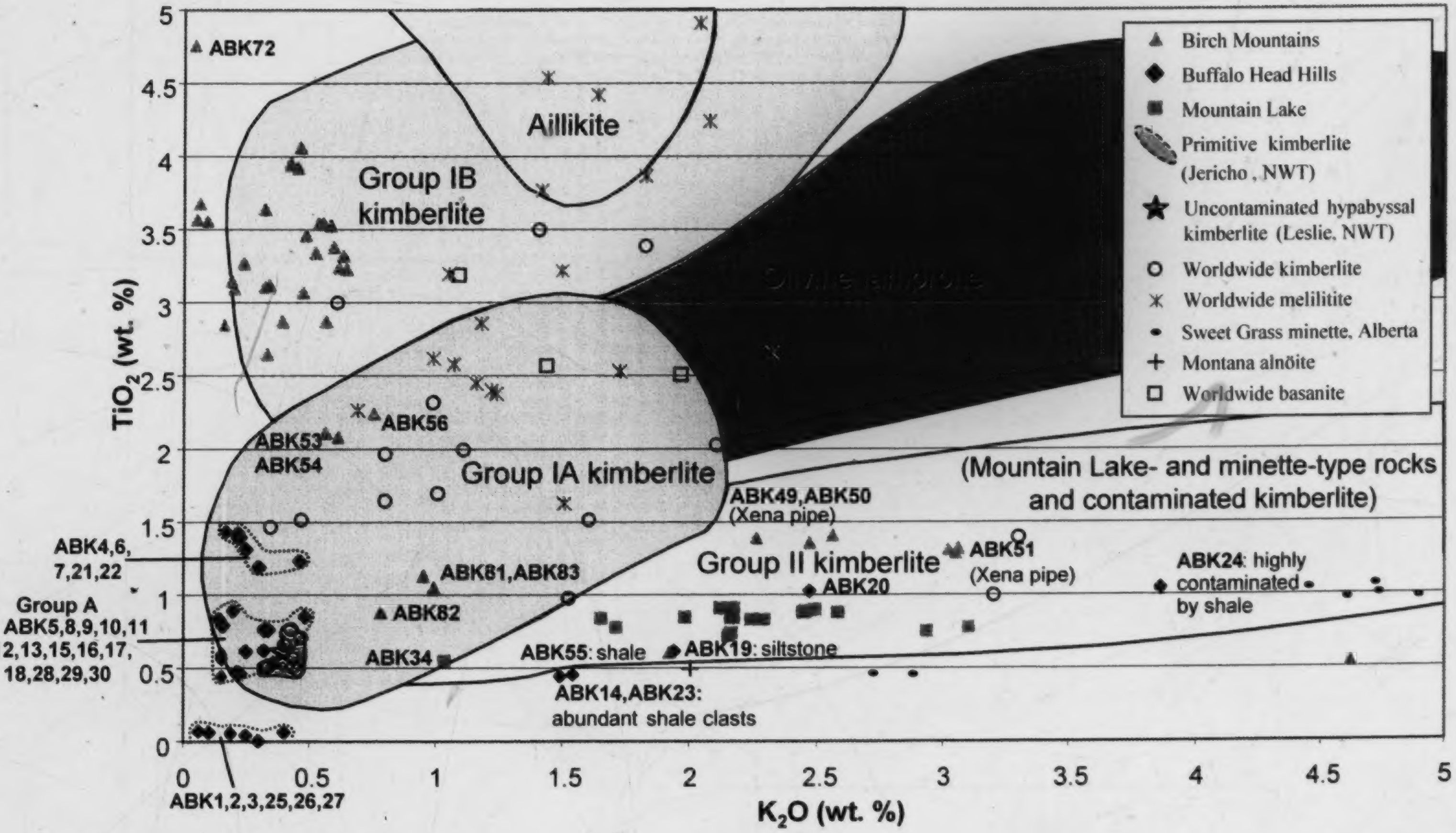

Figure 10. Plot of TiO$_2$ versus K$_2$O for northern Alberta kimberlitic whole-rock compositions. Fields for kimberlite and related rock types are from Taylor et al. (1994). See section 5.1 in text for sources of comparative data.

Element	South Africa kimberlite[1]			Global kimberlite[2]		Average	Average	Average Sweet	Mountain Lake			Buffalo Head Hills			Birch Mountains		
or ratio	Group IA	Group IB	Group II	Group I	Group II	kimberlite[3]	melilitite[4]	Grass minette[5]	Min.	Max.	Avg.	Min.	Max.	Avg.	Min.	Max.	Avg.
Ni	1360.00	800.00	1400.00	NA**	NA	965.00	415.52	512.42	197.00	721.00	433.26	45.00	2171.00	1240.47	31.00	1165.00	618.36
Cr	1400.00	1000.00	1800.00	NA	NA	893.00	565.36	591.42	362.68	944.33	685.11	95.80	1512.30	937.26	123.17	1443.87	893.77
Co	83.00	79.00	85.00	NA	NA	65.00	NA	44.17	21.20	55.80	39.89	10.40	115.50	77.98	10.90	105.30	76.89
Cu	54.00	79.00	30.00	NA	NA	93.00	NA	70.00	29.00	49.00	42.65	3.00	63.00	28.17	26.00	78.00	54.03
Zn	56.00	75.00	60.00	NA	NA	69.00	NA	93.50	43.00	75.00	68.59	20.00	94.00	53.20	23.00	92.00	66.22
V	75.00	170.00	85.00	NA	NA	100.00	270.52	170.25	68.00	138.00	111.12	17.00	173.00	73.67	66.00	180.00	120.19
Sc	13.00	20.00	20.00	NA	NA	14.00	25.89	19.29	11.00	15.00	13.32	2.00	17.00	10.06	10.00	26.00	17.38
Nb	165.00	210.00	120.00	NA	NA	141.00	144.32	13.08	41.10	87.50	69.74	11.00	284.20	134.36	13.00	508.50	240.45
Zr	200.00	385.00	290.00	NA	NA	184.00	405.44	247.00	88.70	146.60	126.79	35.80	323.50	136.69	99.80	324.30	192.76
Y	13.00	30.00	16.00	NA	NA	22.00	26.48	17.17	13.50	21.70	16.16	0.70	21.60	9.95	9.00	22.30	14.92
Sr	825.00	1020.00	1140.00	NA	NA	851.00	1279.96	1316.75	319.00	544.30	421.65	123.50	1581.80	645.32	174.50	1408.70	743.32
Rb	50.00	30.00	135.00	NA	NA	73.00	48.15	167.83	41.50	104.80	74.79	1.10	135.90	25.38	3.70	195.40	39.91
Th	18.00	27.00	30.00	NA	NA	17.00	11.57	8.72	8.30	15.60	12.39	5.50	37.10	19.43	8.40	97.30	38.92
Ba	1000.00	850.00	3000.00	NA	NA	1100.00	919.13	2979.92	829.00	2641.00	1033.26	77.00	2704.00	971.91	471.00	3932.00	1287.31
La	90.00	125.00	200.00	NA	NA	150.00	98.89	42.04	44.10	80.70	64.72	13.10	320.70	127.19	43.00	487.60	204.48
Ce	140.00	220.00	350.00	NA	NA	200.00	191.48	89.68	81.70	147.10	117.99	25.20	596.20	237.94	84.00	882.50	363.19
Nd	90.00	100.00	145.00	NA	NA	85.00	83.75	42.92	31.60	52.90	42.80	6.90	197.90	76.45	34.90	281.90	118.04
Ga	4.00	8.00	6.00	NA	NA	5.70	NA	11.00	7.80	15.50	12.40	0.80	15.10	4.39	5.80	15.70	8.08
U	4.00	6.00	5.00	NA	NA	3.10	3.87	2.56	2.30	3.80	3.29	1.30	7.60	4.13	2.00	10.30	5.89
Pb	7.00	10.00	30.00	NA	NA	15.30	10.46	22.78	7.00	11.00	9.71	3.00	17.00	8.61	7.00	23.00	11.28
Hf	NA	NA	NA	NA	NA	5.60	12.81	6.16	2.80	3.80	3.34	0.80	7.80	3.40	2.50	9.10	5.17
P_2O_5/Ce*	78.57	50.00	31.40	58.00	33.00	NA	59.52	115.18	22.08	43.91	24.79	5.60	47.62	21.25	7.93	23.39	15.55
Nb/Zr	0.83	0.55	0.41	1.10	0.48	0.77	0.44	0.06	0.31	0.77	0.56	0.14	1.79	1.14	0.75	1.67	1.35
Nb/U	41.25	35.00	24.00	42.00	25.00	45.48	43.99	5.21	13.20	28.13	21.24	17.77	57.15	34.69	31.64	57.43	43.78
Nb/La	1.83	1.68	0.60	1.80	0.70	0.93	1.50	0.32	0.72	1.19	1.06	0.89	1.83	1.16	0.94	1.68	1.25
Nb/Ta	NA	NA	NA	NA	NA	12.80	12.63	20.26	14.67	16.67	15.94	10.60	20.13	14.31	10.52	37.02	15.82
TiO_2/Nb*	121.21	142.86	83.30	NA	NA	NA	290.45	753.92	97.48	177.62	123.90	4.33	89.89	42.26	75.88	145.28	116.62
La/Yb	NA	NA	NA	NA	NA	125.00	54.13	32.01	28.85	61.49	44.97	13.24	311.36	213.99	22.05	435.36	212.54
Ce/Sr	0.17	0.22	0.31	0.24	0.32	0.24	0.16	0.07	0.23	0.31	0.28	0.11	2.85	0.49	0.24	0.95	0.52
Ce/Y	10.77	7.33	21.88	NA	NA	9.09	7.20	5.25	4.62	10.11	7.45	17.95	40.23	29.21	15.68	43.47	26.71
Ba/Rb	20.00	28.33	22.22	26.00	19.00	15.07	21.07	17.92	9.52	36.23	14.69	8.83	727.27	88.83	15.95	339.55	63.31
Sc/Al_2O_3	5.00	6.45	6.25	7.20	6.00	NA	3.00	1.88	1.08	1.74	1.45	2.82	11.76	5.64	2.15	7.56	5.54
U/Th	0.22	0.22	0.17	0.21	0.17	0.18	0.41	0.30	0.22	0.33	0.27	0.11	0.32	0.20	0.09	0.23	0.15
Zr/Hf	NA	NA	NA	NA	NA	32.86	42.49	40.34	34.08	41.78	38.09	31.49	54.88	41.10	33.52	41.49	37.19
Ni/MgO	47.72	33.61	47.14	40.00	49.00	NA	27.10	50.06	27.49	96.33	39.87	22.15	53.24	40.25	20.04	48.74	28.58

[1] Smith et al. (1985b) [2] Taylor et al. (1994) [3] Mitchell (1986); Muramatsu (1983)

[4] Rogers et al. (1992); Wilson et al. (1995) [5] Kjarsgaard (1994); Buhlmann et al. (2000) * Ratio x 104 NA = not available

Table 5. Selected trace and major elements and element ratios from northern Alberta kimberlitic rocks and, for comparison, worldwide kimberlite, olivine melilitite and Sweet Grass minette.

Samples ABK08, ABK26 and ABK27 have the highest Ni values (1702, 2091 and 2171 ppm, respectively) of all Alberta samples. Cobalt shows a good correlation with Ni, and Co values are highest in samples ABK08 (116 ppm), ABK26 (103 ppm) and ABK27 (112 ppm). The high Ni and Co can be directly correlated with the accumulation of olivine in these samples.

The compatible elements from Alberta samples and various ultramafic rock types are plotted on a compatible-element distribution diagram (Figure 11), which has been normalized to the pyrolite abundance of Jagoutz et al. (1979). The ML samples have higher V and slightly lower Cr, Co and Ni in comparison to average worldwide kimberlite (Figure 11A). The MLN pipe has higher V and lower Cr, Co and Ni than MLS, possibly related to Wapiti Formation sedimentary rock contamination. Samples from the BHH have the lowest concentrations of Sc, V, Cu and Zn, and the BM samples have the highest values of Sc, V, and Cu. In the BHH (Figure 11B), samples ABK19 to ABK24 (BM2 and BM3 pipes) have high V, Cu and Zn with low Cr, So and Ni, while samples ABK1, ABK2, ABK3, ABK25, ABK26 and ABK27 (K4 and LL8 pipes) have low Sc, V, Cu and Zn, and high Co and Ni. In the Birch Mountains (Figure 11C), samples ABK48, ABK49 and ABK50 (Xena pipe) have high V and low Cr, Co and Ni. Samples ABK81, ABK82 and ABK83 (Kendu pipe) have low Sc, V, Cu and Zn. Based on these compatible element patterns, the Xena (BM), BM2 and BM3 (BHH) pipes have similar compatible elements to ML; their high V and low Cr, Co and Ni suggest country rock contamination or a source similar to olivine-rich basanite/alkali basalt (Figure 11D). Kendu (BM), K4 and LL8 (BHH) also have similar compatible element patterns, although the low Sc and V, and high Cr, Co and Ni is more representative of the compatible element pattern for kimberlite (Figure 11D).

6.3.2 Incompatible-Trace Element Variation Between Magmas

The data for the incompatible elements are summarized on Table 5. In general, the incompatible-element patterns in the Alberta samples are similar to those of worldwide kimberlite, in the case of BHH and BM, and to potassic alkali rocks, in the case of ML. Moderate to good positive correlations exist between bivariate pairs from any selected elements withing the following groups of elements:

- Rb, Ga, SiO_2, K_2O, Al_2O_3 and Na_2O;
- Sc, Zr, Y, Nb, La, Ce, Th, TiO_2, $Fe_2O_{3(T)}$, MnO and P_2O_5;
- Pb, Ba and V; and
- MgO, Ni, Cr and Co.

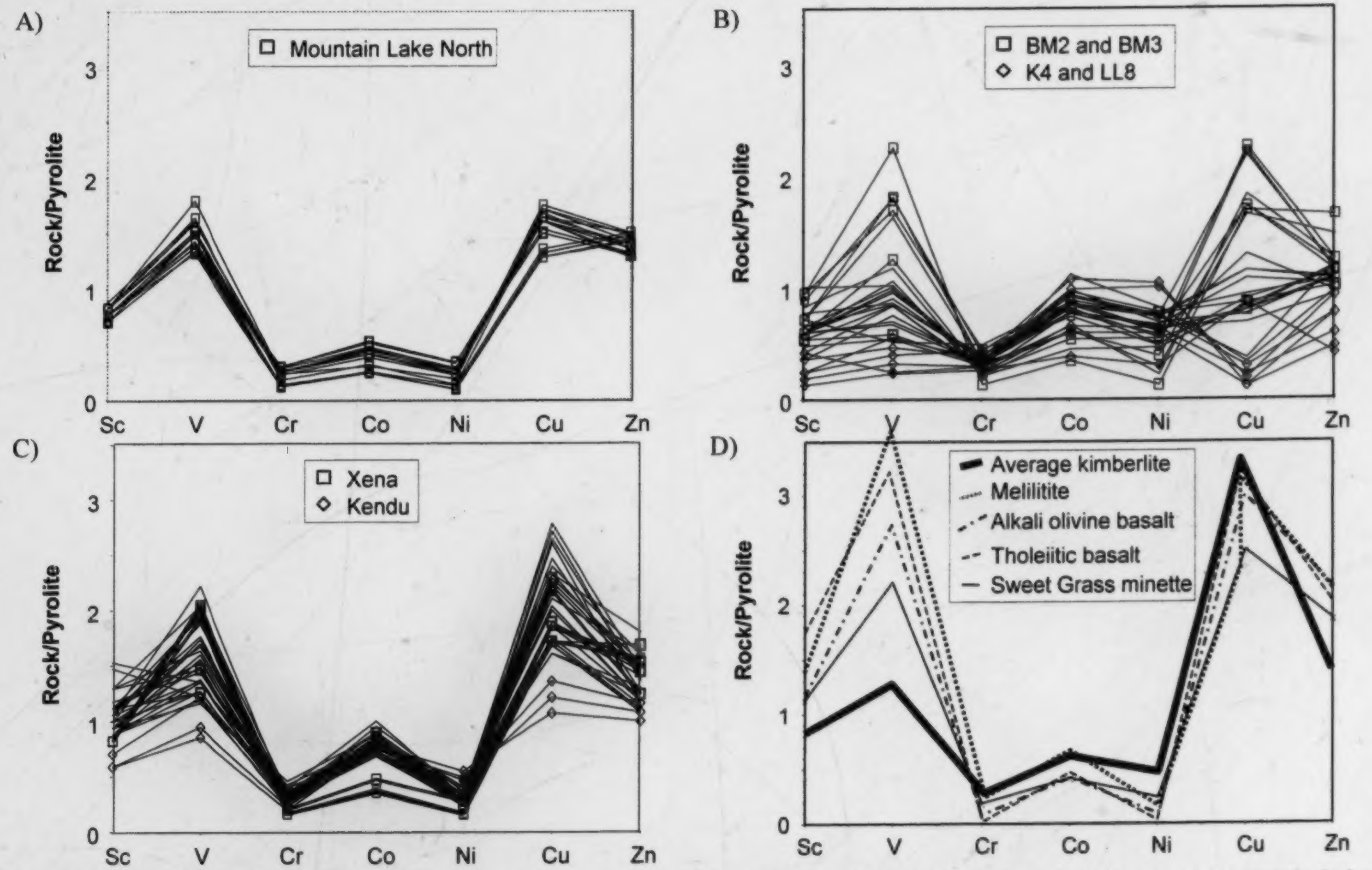

Figure 11. Compatible-element distribution diagram for northern Alberta kimberlitic whole-rock compositions. A) Mountain Lake; B) Buffalo Head Hills; C) Birch Mountains; and D) Average kimberlite, melilitite, alkali olivine basalt and tholeiitic basalt compiled from Mitchell (1986) shown for comparison. Pyrolite abundance from Jagoutz et al. (1979).

The following sections describe major differences between the NAKP fields and comparisons with worldwide ultramafic rock types.

6.3.3 Mountain Lake

Compared to the BHH and BM areas, the ML pipe is characterized by low Nb (70 ppm), REE and particularly LREE (e.g., Ce 118 ppm), Sr (422 ppm) and high Ga (12.4 ppm), Rb (75 ppm). The incompatible trace element abundances normalized to the composition of primitive mantle (McDonough and Sun, 1995) are illustrated on Figure 12 for comparative purposes with other rock types.

Normalized to primitive mantle, the ML rocks are characterized by lower Rb relative to Cs and Ba, lower K, Sr, P and (slight) Ti relative to LREE, and higher Ta-Nb-La, Nd and Sm relative to MREE and Zr (Figure 12A). Barium, Th, U, Ta, Nb and La are >100 times primitive mantle. The MLN samples generally can be distinguished from the MLS samples by their lower Ta, Nb, La, Ce, Sr, Nd and P compositions, probably related to Wapiti Formation sedimentary rock contamination.

The ML samples have a similar primitive mantle-normalized distribution pattern in comparison to kimberlite, but with higher K and lower overall trace element abundances (Figure 12B). Although the major-oxide data showed some trends similar to the Sweet Grass minette, the trace-element data highlight significant differences (Figure 12B). For example, the ML pipe contains lower average values than the Sweet Grass minette of Sr (422 vs. 1317 ppm), Zr (127 vs. 247), Rb (75 vs. 168 ppm), V (111 vs. 170), Ba (1033 vs. 2980 ppm), and higher average values of Th (12 vs. 9 ppm) and Nb (70 vs. 13 ppm). The ML rocks have a significantly more positive Ta-Nb distribution pattern in comparison to the minette, Roman Province–type (RPT) and alnöite rocks, which are typically characterized by low Nb values.

To test whether entrainment of Wapiti Formation sedimentary rocks influences the incompatible-element distribution of the ML samples, Figure 12B compares the average trace-element values from four Wapiti Formation samples, which were collected from Cretaceous bedrock located directly adjacent to the pipe by Dufresne et al. (2001) with the ML samples. The Wapiti Formation samples generally have lower incompatible element compostions in comparison to the MLS, particularly for Th, Ta, Nb, La, Ce, Sr, Nd and P. These elements can, therefore, be used to distinguish Wapiti Formation contaminated MLN samples from MLS, which have Ta-Nb-La compositions of <100 and >100 times primitive mantle, respectively (Figure 12A).

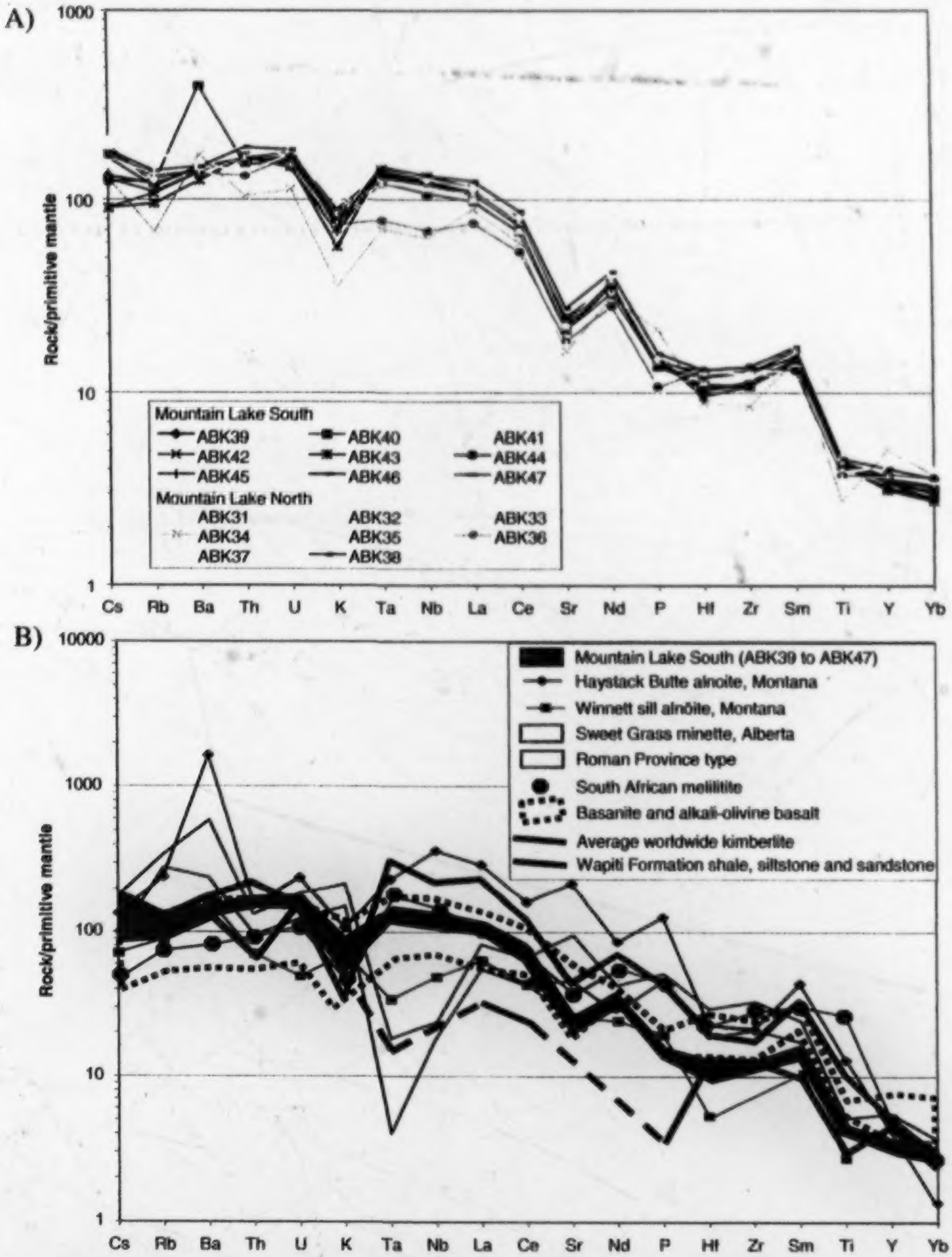

Figure 12. Incompatible-element distribution diagram for whole-rock compositions from the Mountain Lake pipes. A) Mountain Lake samples; and B) Mountain Lake field with average kimberlite (Mitchell, 1986; Muramatsu, 1983), Montana alnöite (Hearn, 1986), Sweet Grass minette (Buhlmann et al., 2000), Roman Province–type lavas from Mount Ernici and Mount Vulsini (*from* Mitchell, 1995; *after* Peccerillo et al., 1988), South African melilitite (Rogers et al., 1992), basanite and alkali-olivine basalt (Frey et al., 1978), and Wapiti Formation sedimentary rocks sampled adjacent to the Mountain Lake pipes (Dufresne et al., 2001) shown for comparison. Primitive mantle values from McDonough and Sun (1995).

In comparison to other NAKP pipes, the REE abundances from the ML pipe are the lowest of all the samples except the contaminated rocks from the BHH and BM (Figure 13). The sum of yttrium and the lanthanides ($\Sigma_{Y,\ La\text{-}Lu}$) from ML is 273, compared with values of 496 for the BHH and 770 for BM. The ML pipe also exhibits a flatter chondrite-normalized REE profile relative to the majority of the samples from BHH and BM (Figure 13A). Light rare-earth element enrichment (90 to 210 times chondrite abundance for La) and the average La/Yb ratio (44) are lower than for average kimberlite (Table 5). Such a profile may reflect either crustal contamination of the ML samples, a non-kimberlitic original REE pattern, or both.

The REE patterns from the Sweet Grass olivine minette, Montana alnöite and melilitite are included on Figure 13A for comparison. Total REEs from the ML pipe are considerably lower than RPT lavas and melilitite. The REE profile from the ML pipe can be distinguished from those of the Sweet Grass olivine minette and the Montana alnöite by the slight concave down trough between Sm and Ho, and high HREE.

Alibert et al. (1983) suggested that Ce/Yb_{norm}, or $(Ce/Yb_{sample})/(Ce/Yb_{chondrite})$, ratios are distinctive for alkali basalt, melilitite and kimberlite, with enrichment relative to chondrite of 40 to 100 for kimberlite, 20 to 30 for melilitite; and 8 to 15 for alkali basalt. The BHH and BM kimberlites exhibit average Ce/Yb_{norm} ratios of 104 and 97, respectively. However, the ML pipe has a very low Ce/Yb_{norm} ratio, between 14 and 29, and averaging 21. Using the criteria of Alibert et al. (1983), the ML pipe is not kimberlite, but more likely a rock type hybrid between alkali basalt and melilitite. There is no petrographic or major element geochemical evidence, however, to support a melilitite rock type.

6.3.4 Buffalo Head Hills

High Ni (up to 2171 ppm) and low V (average 74 ppm), Y (average 10 ppm), Pb (average 9 ppm), Sr (average 645 ppm) and Ga (average 4 ppm) characterize the BHH samples, compared to those from ML and BM. The Cr content, which averages 937 ppm in the BHH, is comparable with worldwide kimberlite and only slightly higher than that of the BM (average 894 ppm Cr).

The majority of the BHH samples form a tight grouping on the incompatible-element distribution diagram; this group exhibits a pattern similar to that of Group I kimberlite (Figure 14) with depleted Rb, K, Sr, Hf and Ti relative to enriched Ba-Th-U, Ta-Nb-LREE, Nd and Sm. A smaller group of samples (ABK01, ABK02, ABK03, ABK04, ABK08, ABK11, ABK25, ABK26 and ABK27) has lower overall incompatible element abundance compared to the rest of the BHH

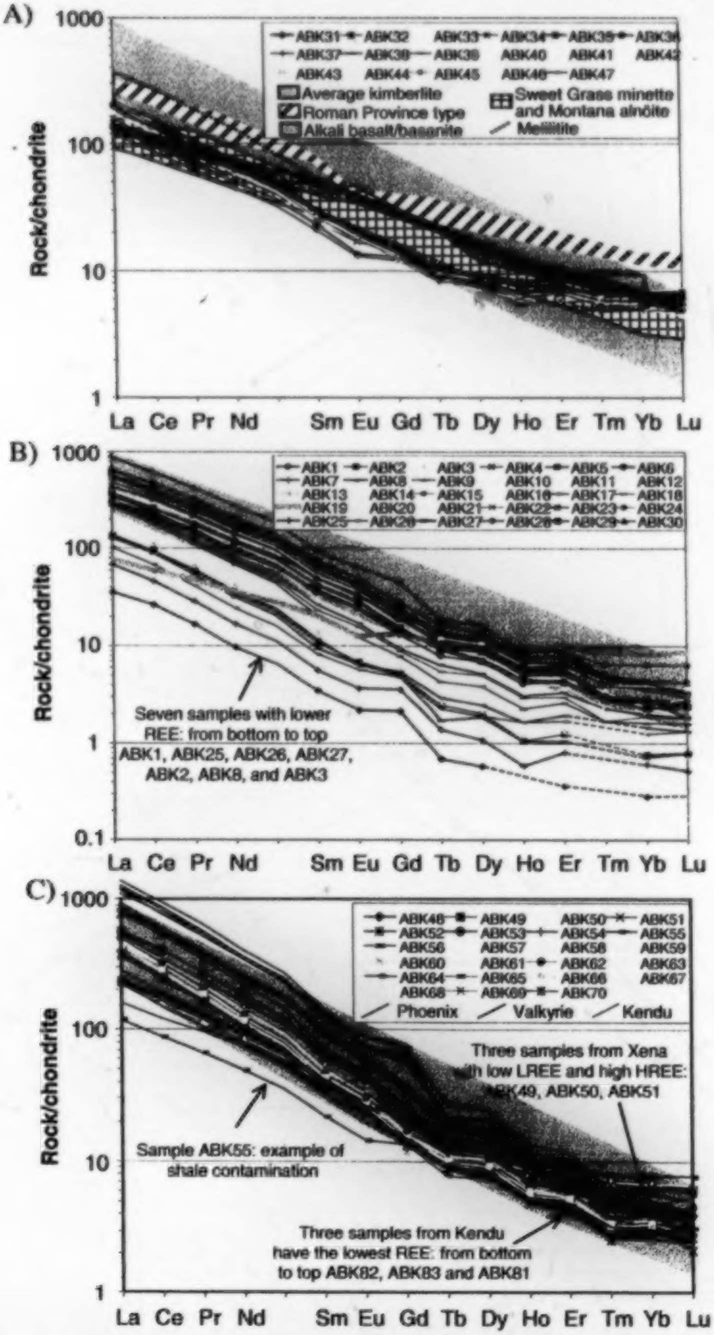

Figure 13. Chondrite-normalized rare-earth element patterns for northern Alberta kimberlitic whole-rock compositions: A) Mountain Lake; B) Buffalo Head Hills; and C) Birch Mountains. Shaded pattern represents average worldwide kimberlite (Mitchell 1986). Roman Province–type lavas from Ernici, Italy (Civetta et al., 1981); alkali-olivine basalt and basanite from Frey et al. (1978); olivine minette from Sweet Grass Hills, Alberta (Kjarsgaard, 1994; Buhlmann et al., 2000); and alnöite from Montana (Hearn, 1986). Chondrite values from Taylor and McLennan (1985).

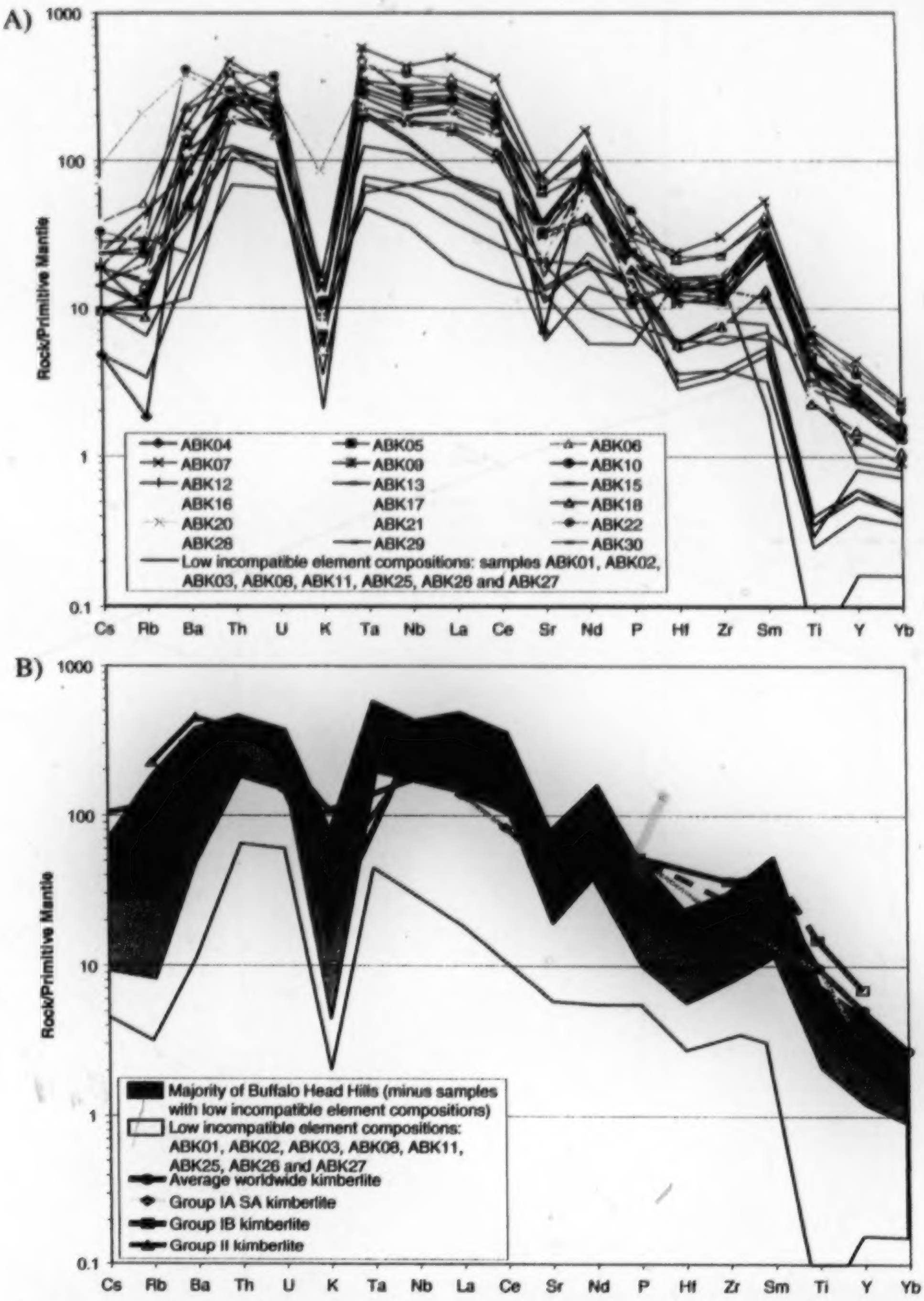

Figure 14. Incompatible-element distribution diagram for whole-rock compositions from the Buffalo Head Hills. A) Buffalo Head Hills samples; and B) Selected Buffalo Head Hills groups with average kimberlite (Mitchell, 1986; Muramatsu, 1983) and Group I and Group II kimberlite (Smith et al., 1985) shown for comparison. Primitive mantle values from McDonough and Sun (1995).

samples, and therefore, are either contaminated by country rock, have a lower degree of olivine fractionation than the majority of the BHH samples, or both.

The chondrite-normalized REE plots (Figure 13B) show two distinct groups with differing REE abundances but similar LREE-enriched patterns. Most of the BHH samples plot within the shaded REE pattern for worldwide kimberlite. Accordingly, they exhibit high LREE enrichment (300 to 870 times chondrite abundance for La) with La/Yb ratios of 214. Samples ABK06, ABK07 and ABK22 have the highest abundance of REE in the BHH.

A less fractionated group of samples, including ABK01, ABK02, ABK03, ABK08, ABK19, ABK25, ABK26 and ABK27, have lower LREE (35 to 145 times chondrite abundance for La versus an average of 435 for the rest of the BHH samples), total REE abundance ($\Sigma_{Y, La\text{-}Lu}$ of 142 versus 610), and slightly lower La/Yb ratios (196 versus 225). This is consistent with the incompatible trace elements, where this group of samples is characterized by the lowest degree of olivine fractionation.

6.3.5 Birch Mountains

Compared to the BHH and average worldwide kimberlite, the BM pipes are characterized by high concentrations of Nb (average 240 ppm and up to 509 ppm). The BM pipes contain comparable amounts of Cr to the BHH pipes, but appreciably lower values of Ni (average 618 ppm vs. average 1240 ppm). The BM generally contain higher average values of trace elements than the BHH, including V (120 ppm), Sc (17.4 ppm), Zr (193 ppm), Hf (5.2 ppm), Y (14.9 ppm), Ba (1287 ppm), Rb (40 ppm), LREE (e.g., 204 ppm La), Ga (8.1 ppm) and Pb (11.3 ppm).

The primitive mantle- normalized incompatible element signature of the majority of BM samples is similar to kimberlite (Figure 15), and is characterized by high overall incompatible element compositions, with negative Rb, K, Sr and Hf relative to positive Ba-Th-U, Ta-Nb-La, Nd and Sm.

The BM incompatible element compositions can be used to distinguish between individual BM pipes, and thus, suspected different magma batches. Incompatible-element distributions for samples from the Legend pipe (ABK57 to ABK70) have higher Ta-Nb-La than in the rest of the BM pipes, which have a broad, flat Ta-Nb-La profile and a noticeably more negative K. Samples from the Kendu pipe (ABK81, ABK82 and ABK83) are characterized by their low overall incompatible element values. Samples from the Phoenix pipe (samples ABK75 to ABK79) exhibit the highest abundance of incompatible elements, particularly for Th, Ta to Ce, Nd and Sr.

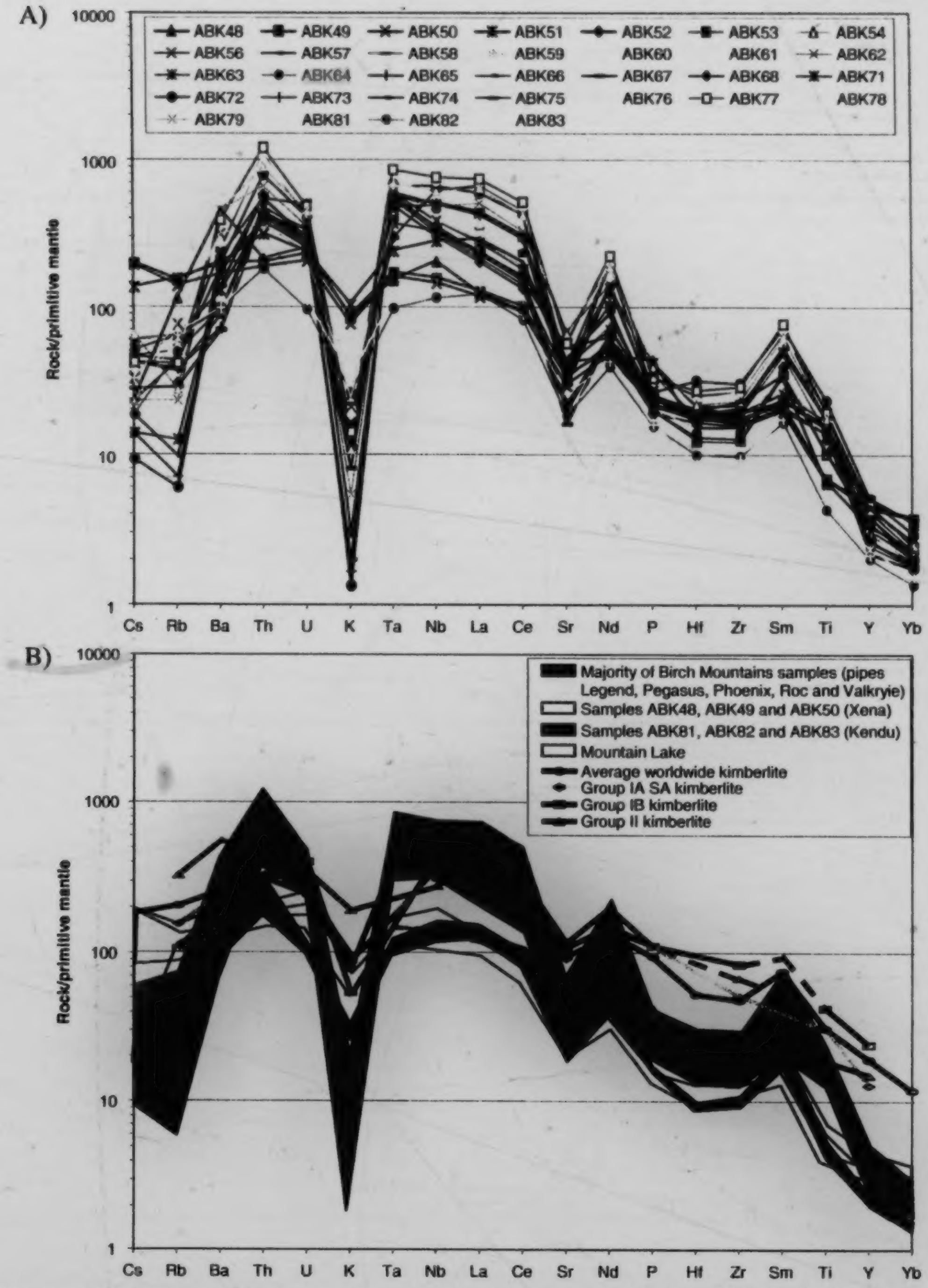

Figure 15. Incompatible-element distribution diagram for whole-rock compositions from the Birch Mountains. A) Birch Mountains; and B) Selected Birch Mountains groups with average kimberlite (Mitchell, 1986; Muramatsu, 1983) and Group I and Group II kimberlite (Smith et al., 1985) shown for comparison. Primitive mantle values from McDonough and Sun (1995).

Finally, the Xena pipe has a much flatter incompatible element distribution pattern in comparison to the rest of the BM samples. Figure 15B shows that Xena has a similar incompatible element signature to ML, albeit having a slightly higher overall incompatible element abundance.

Most of the chondrite-normalized REE patterns for the BM samples coincide with the REE pattern for average kimberlite (Figure 13C). Generally, the majority of the BM samples are LREE-enriched (390 to 1,340 times chondrite abundance for La) with La/Yb ratios of 213. Samples with flatter patterns are attributed to a different magma type or sample contamination. Samples with La/Yb ratios between 22 and 50 include: ABK49 to ABK51 from the Xena pipe, which has similar major and trace element compositions as the MLS pipe, and ABK55 and ABK80, which have macroscopic evidence for crustal contamination.

Samples from the Kendu kimberlite (ABK81, ABK82 and ABK83; Figure 13C) are less LREE-enriched, or have a less steep chondrite-normalized pattern with a $\Sigma_{Y, La\text{-}Lu}$ of between 305 and 381 versus an average $\Sigma_{Y, La\text{-}Lu}$ of 810 for the rest of the BM samples. The Kendu REE distribution profile has a shallower slope, with an La/Yb ratio of between 130 and 144 versus 225 for the rest of the BM samples, and lower LREE (220 to 275 times chondrite abundance for La). Thus, the REE indicate a significant geochemical difference between the Kendu pipe and the rest of the BM samples that may be related to differences in their sources.

6.4 Linear Relationships Using Multi-Element Principal-Component Analysis

6.4.1 Introduction to Principal Component Analysis

Principal component analysis (PCA), or *Karhunen-Loeve transform*, summarizes the variation in correlated multi-attribute data to a set of uncorrelated components, each of which is a particular linear combination of the original variables. A simple three-step process for forming principal components of any data set is that for any *n* x *m* data matrix (*n* = the number of samples and *m* = the number of variables measured on each sample):

- Form the *m x m* covariance matrix from the *n x m* data matrix.
- Extract the eigenvectors and eigenvalues from the covariance matrix.
- The eigenvectors are the principal components and the eigenvalues are their magnitudes.

The extracted uncorrelated components are called principal components (PC) and are estimated from the eigenvectors of the covariance matrix of the original variables. Thus, the fundamental characteristic of PCA is that it allows for a study of the structure of variance within your data set.

Eigenvalues measure the amount of the variation explained by each PC and will be largest for the first PC and smaller for the subsequent PCs. An eigenvalue greater than 1 indicates that PCs account for more variance than accounted by one of the original variables in standardized data. This is commonly used as a cutoff point for which PCs are retained. Eigenvectors provide the weights to compute the uncorrelated PC, which are the linear combination of the centered standardized or centered un-standardized original variables. Eigenanalysis, as summarized by Cliff (1987) is generally defined as follows:

> "Let **A** be a *p* by *p* matrix and **w** a *p-element* vector. If it is true that **Aw** = l **w** for some scalar l , then **w** is an *eigenvector* of **A** and l is the corresponding *eigenvalue*. That is, an *eigenvector* of a matrix is a vector such that when we multiply the matrix by the vector we get the vector back again except that it has been multiplied by a particular constant, called the *eigenvalue*."

Plotting the eigenvalues against the corresponding PC produces a scree plot that illustrates the rate of change in the magnitude of the eigenvalues for the PC. Figure 16 illustrates an example scree plot based on selected major and trace elements from northern Alberta kimberlitic whole-rock compositions. The rate of decline tends to be fast first then levels off. In PCA, uncorrelated PC's are extracted by linear transformations of the original variables so that the first few PC's contain most of the variations in the original dataset. The 'elbow', or the point at which the curve bends, is considered to indicate the maximum number of PC to extract for interpretation.

The scaling constants used to reconstruct the eigenvectors are generally known as scores. *PC scores* are the derived composite scores computed for each observation based on the eigenvectors for each PC. *PC loadings* are correlation coefficients between the PC scores and the original variables. PC loadings measure the importance of each variable in accounting for the variability in the PC.

6.4.2 Results of Principal Component Analysis Results

Principal component analysis was carried out using whole-rock geochemical data from the ML, BHH and BM samples. In addition, data were included from the Jericho kimberlite, NWT (Price et al., 2000) and Group IA, IB and II South African kimberlites (Smith et al., 1985b). The objective of the PCA was to to reduce the dimension of the data and evaluate multivariate Alberta pipe data for any linear relationships. The analysis was completed using the S-PLUS program of

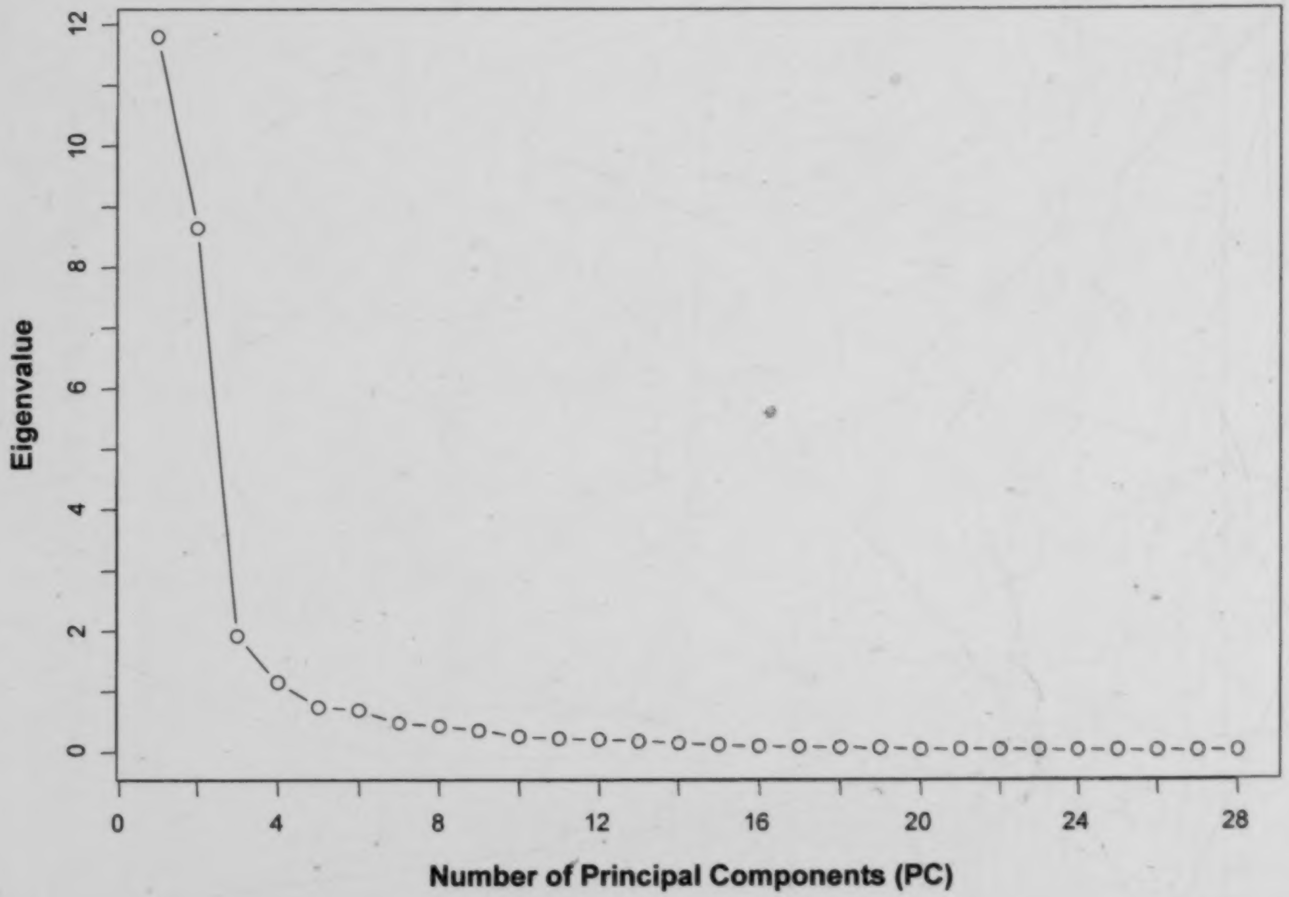

Figure 16. Screeplot showing the fraction of total variance in the data as represented by each Principal Component. Based on selected major and trace elements from northern Alberta kimberlitic whole-rock compositions.

Grunsky (2001). The program allows for the computation and same-figure plotting of principal component factor loadings for solutions of the scores of both the variables and the samples.

Major elements SiO_2, Al_2O_3, $Fe_2O_{3(T)}$, MgO, CaO, K_2O, Na_2O, MnO, TiO_2, P_2O_5 and Cr_2O_3, and trace elements Ba, Ni, Ga, Nb, Rb, Sr, Th, V, Zr, Y and Pb were selected for the PCA. Components 1, 2, 3, 4 and 5 account for 71.2%, 19.5%, 9.1%, 1.0% and 0.1% of the total variance, respectively. Because PC's 1 and 2 account for 90.7% of the variance, these were choosen for bi-plot display to visualize the inter-relationships between the observations and variables in multivariate data (Figure 17).

To understand which elements contributed to which axes, relative contributions of selected major and trace elements to PCs 1 to 5 are presented in Table 6. For example, the value of an element along PC 1 is 0.8820 times the standardized abundance of SiO_2, 0.9292 Al_2O_3, –0.6806 Fe_2O_3, and so on. Thus, PC 1 is interpreted as being positively related to, and therefore, correlated with the abundance of SiO_2, Al_2O_3, Na_2O, K_2O, Ga and Rb. Principal component axis 2 is positively related to the abundance of Fe_2O_3, CaO, TiO_2, P_2O_5, MnO, Ba, Nb, Sr, Th, V, Zr, Y and Pb.

The PC 1 versus PC 2 plot (Figure 17) illustrates two distinct trends, a kimberlite trend and a trend of crustal contamination or, more commonly, a trend associated with potassic alkali rocks such as the ML pipe.

6.4.3 Kimberlite Trend

The left side of Figure 17 shows a vertical trend of samples associated with non-contaminated kimberlite samples from the BHH and BM. This trend is interpreted to represent a magma evolution line from primitive to evolved kimberlite. A low PC 2 score (negative load) is related to high MgO, Ni and Cr_2O_3, or 'primitive' kimberlite ('P' in Figure 17). The primitive end of the line is dominated by BHH samples and supports previous conclusions that samples from the BHH represent the most primitive kimberlite magma in the current data set. A cluster of geochemically similar samples (Group A in Figure 17) is interpreted to represent the most primitive samples in this dataset because the samples coincide with pipes that have elevated diamond content and primitive kimberlite from the Jericho kimberlite in the Northwest Territories. The geochemical characteristics of the Group A samples relative to diamond content are discussed below. The average values for Group IA South African kimberlite plot above the primitve Group A towards the middle of the kimberlite trend.

A)

	Principal Component				
	1	2	3	4	5
SiO_2	***0.8820***	-0.1613	***0.2041***	-0.2506	***0.0625***
Al_2O_3	***0.9292***	***0.2666***	***0.1342***	-0.0265	-0.0359
Fe_2O_3	-0.6806	***0.4963***	***0.3472***	-0.2388	-0.1406
MgO	-0.7598	-0.4949	***0.0618***	-0.3273	***0.0279***
CaO	-0.3518	***0.5222***	-0.4982	***0.5147***	-0.1925
Na_2O	***0.8814***	***0.1225***	***0.0320***	-0.0846	-0.0883
K_2O	***0.9008***	***0.2308***	-0.1556	-0.1473	-0.0866
TiO_2	-0.4822	***0.6805***	***0.4425***	***0.1138***	-0.0712
P_2O_5	-0.4563	***0.6874***	-0.3679	-0.1571	-0.0281
MnO	-0.5693	***0.6065***	-0.0072	***0.1062***	-0.3854
Cr_2O_3	-0.7804	-0.0848	***0.1067***	-0.3196	-0.2091
Ba	***0.1109***	***0.6855***	-0.4345	-0.3890	-0.1043
Ni	-0.5678	-0.6594	-0.1936	-0.2893	-0.0382
Ga	***0.7959***	***0.4739***	***0.3027***	-0.0271	-0.0451
Nb	-0.6883	***0.6628***	***0.1969***	-0.0505	***0.0738***
Rb	***0.8624***	***0.3065***	-0.1492	-0.1622	-0.0616
Sr	-0.3636	***0.6142***	-0.4629	-0.0487	***0.3345***
Th	-0.5868	***0.6507***	***0.2551***	-0.1419	***0.1234***
V	***0.3290***	***0.7139***	***0.2004***	***0.0426***	-0.1494
Zr	-0.2265	***0.7925***	***0.1796***	***0.0978***	***0.4011***
Y	***0.3866***	***0.8279***	***0.0915***	***0.0550***	***0.0306***
Pb	***0.3142***	***0.7602***	-0.2476	-0.2914	***0.0445***

B)

	Principal Component				
	1	2	3	4	5
SiO_2	***79.1179***	2.3174	4.2102	6.4208	0.7315
Al_2O_3	***87.1912***	7.7323	1.6873	0.0941	0.0525
Fe_2O_3	***47.1832***	24.9005	12.1307	6.0205	1.9897
MgO	***57.8113***	25.2250	0.5029	10.9472	0.0163
CaO	12.7799	27.3350	26.6048	24.7460	3.8013
Na_2O	***78.5737***	1.7271	0.0747	0.7266	0.1004
K_2O	***81.7254***	5.6741	2.4534	2.2037	0.5528
TiO_2	23.9976	***46.5137***	19.5685	1.5216	0.7914
P_2O_5	21.5830	***47.2931***	13.8469	2.7259	0.0314
MnO	33.2325	***36.9876***	0.0212	0.8799	13.6147
Cr_2O_3	***61.4032***	0.7854	1.1822	10.7245	2.9109
Ba	1.1000	***47.1809***	18.8076	14.8462	0.2032
Ni	31.8677	***43.9147***	3.7285	9.7642	0.1178
Ga	***63.0389***	24.0196	8.8260	0.1074	0.2527
Nb	***48.6357***	***43.8179***	3.8953	0.1812	0.7833
Rb	***74.8006***	9.8797	2.2340	2.6670	0.4253
Sr	13.8104	***37.4814***	21.6299	0.2046	11.3245
Th	***35.4716***	***42.1817***	6.7531	1.6108	2.2413
V	10.6659	***52.3563***	3.8097	0.1324	4.3217
Zr	5.5192	***62.8429***	3.2295	1.4479	17.3736
Y	14.7223	***70.3521***	0.6869	0.2595	0.2900
Pb	8.3191	***60.0027***	4.4590	10.0140	0.1655

Table 6. Relative contributions of selected major and trace elements to principal components 1 to 5: A) Component scores with positive values in bold; and B) relative contribution expressed as percentages with values greater than 35% in bold. Because only principal components 1 to 5 are presented the percentages for individual elements do not add up to 100.

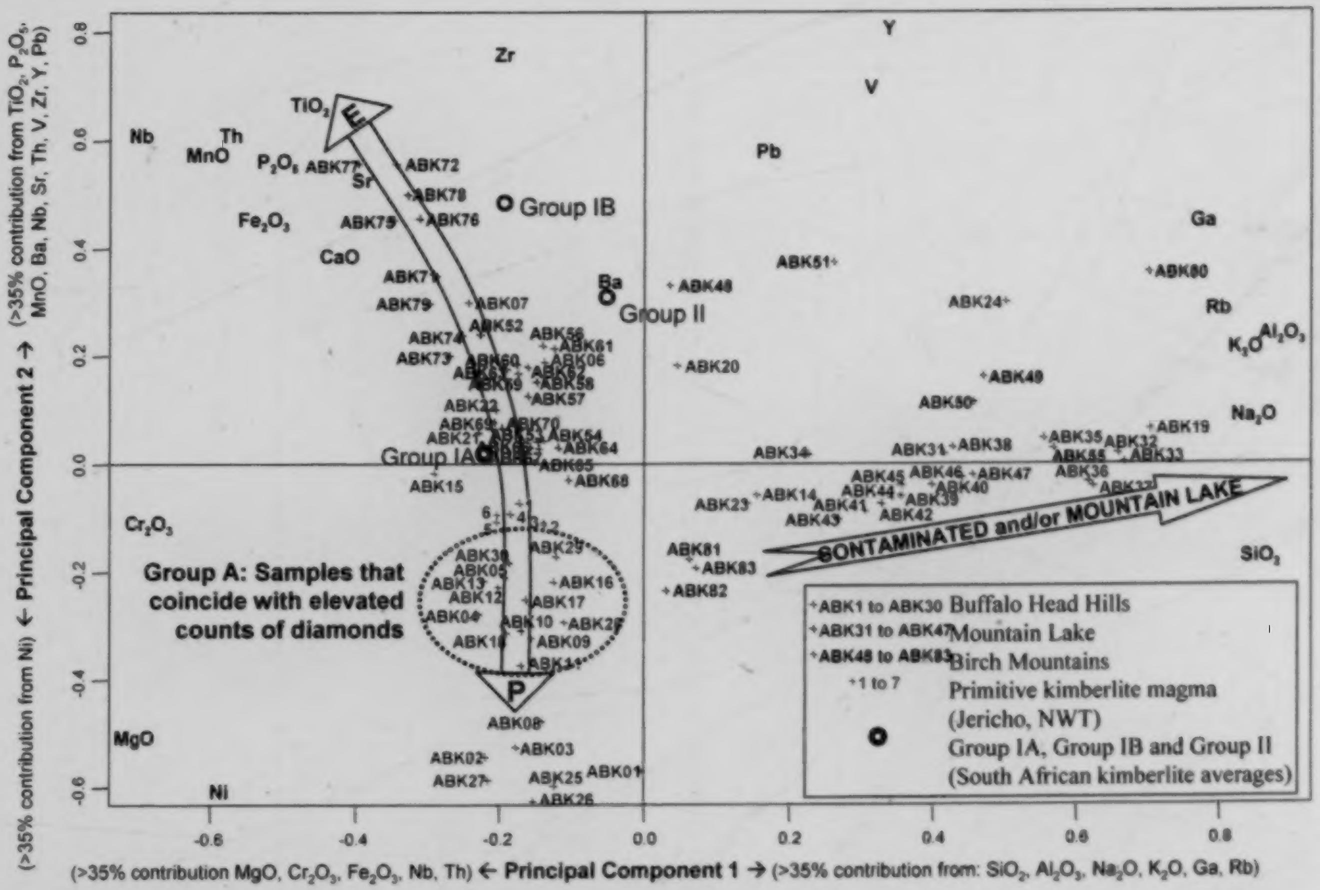

Figure 17. Principal-component analysis of selected major and trace elements from northern Alberta kimberlitic whole-rock compositions. Arrows indicate line of descent directions for primitive (P) to metasomatically enriched (E) kimberlite, and the direction for kimberlite contamination and/or Mountain Lake hybrid-type rocks. Kimberlite values from Jericho, Northwest Territories (Price et al., 2000) and South Africa (Smith et al., 1985).

A group of samples, which include ABK01, ABK02, ABK03 (K4), ABK08 (K11) and ABK25, ABK26 and ABK27 (LL8), plot below the primitive Group A endmember (Figure 17). These samples are not interpreted to represent the most primitive NAKP kimberlite, but rather, their low incompatible element (*see* Figure 14) and REE (e.g., $\Sigma_{Y,\ La\text{-}Lu}$ <217; *see* Figure 13) abundance, and high Ni and Mg# (e.g., Mg# >91; *see* Figure 9) and MgO/SiO_2 ratios (>1.4) are directly related to olivine accumulation.

The high PC 2 score (positive load) is related to high TiO_2, P_2O_5, MnO, $Fe_2O_{3(T)}$, Nb, Th and Zr. This end of the mixing line is interpreted to represent the most evolved kimberlite in the current data set ('E' in Figure 17). The high PC 2 loadings (i.e., high TiO_2, Nb, etc.) are characteristic of the BM. The Phoenix kimberlite (samples ABK75, ABK76, ABK77 and ABK78), which was shown earlier as having the highest abundance of incompatible elements, plots as the most evolved kimberlite in the current data set. The average values for Group IB South African kimberlite plot close to those of the Phoenix pipe, closer to the evolved end of the trend.

6.4.4 Mountain Lake Trend

The right side of Figure 17 shows a horizontal trend of samples associated with potassic alkali rocks from the ML pipe and contaminated BHH and BM kimberlite. Medium PC 1 scores associated with SiO_2, Na_2O, Al_2O_3, K_2O, Rb and Ga characterize the ML trend. As was the case for most of the bivariate plots, samples from the ML pipe are divided into two groups on Figure 17. Samples from drillhole ML95-1 (MLN; samples ABK31 to ABK38) have been characterized as resedimented volcaniclastic rocks (i.e., highly contaminated rocks). These plot close to ABK19 from the BHH, which is highly contaminated by siltstone and shale. Samples from drillhole ML95-3 (MLS; samples ABK39 to ABK48), which in comparison is interpreted to represent juvenile magma, plot toward the low PC 1 score and are characterized by higher MgO, Ni and Cr_2O_3. Samples from the Xena pipe, particularly samples ABK49 and ABK50, also plot along the ML trend. Contaminated samples, including ABK55 and ABK80 from the BM and ABK19 and ABK24 from the BHH, are close to the ML trend, as PC 2 consists of high loads from SiO_2, Na_2O, K_2O, Al_2O_3, Rb and Ga.

6.5 Geochemistry and Diamond Content

Previous authors have tried to relate bulk kimberlite chemistry to diamond potential. For example, Ilupin et al. (1974) suggested that average Rb content of diamondiferous kimberlites (23 ppm) from Yakutia, USSR is less than that of barren kimberlites (64 ppm). Akimov and Semenov

(1970), Lutts and Mineyeva (1973) and Marshintsev and Lapin (1976) demonstrated that diamondiferous kimberlites from the Siberian platform have lower U (1.2 ppm) and Th (6.7 ppm) contents than barren kimberlite (2.5 ppm U and 17.5 ppm Th). Mitchell (1986) noted that these correlations are not present in data for South African kimberlites.

Kimberlites in northern Alberta that contain known elevated concentrations of diamonds are restricted to the BHH. To date, Ashton has 'mini-bulk' sampled six kimberlite pipes on the basis of elevated micro- and macrodiamond contents discovered during preliminary evaluation of samples from drillcore and trenches (Ashton Mining of Canada Inc., 1998, 1999a, 2000). These pipes, with corresponding sample numbers from this study, include kimberlites: K5 (sample ABK04), K6 (sample ABK05), K11 (samples ABK08 and ABK09), K14 (samples ABK10 to ABK13 and ABK30), K91 (sample ABK15) and K252 (not included in this study).

Most of the BHH pipes with elevated diamond contents (K5, K6, K11 and K14 kimberlites) have similar geochemistry. Samples ABK04, ABK05, ABK09, ABK10, ABK11, ABK12, ABK13, ABK28, ABK29 and ABK30 form a tight cluster labelled Group A on Figures 10 and 17. Samples ABK16, ABK17 and ABK18, which also plot in the Group A field, are from kimberlite TQ155, which was not bulk sampled, but contained 30 microdiamonds (<0.05 mm) from a 275 kg sample (Ashton Mining of Canada Inc., 1999b). Only two samples from pipes with elevated diamond content exhibit different geochemistry: kimberlite K91 (sample ABK15) and one sample from kimberlite K11 (sample ABK08) although samples ABK09 and ABK10, which are also from kimberlite K11, did plot within Group A.

In general, the Group A samples plot at the primitive end of the kimberlite trend line and contain low TiO_2 (0.45–1.2 wt. %), P_2O_5 (0.22–0.51 wt. %) and Nb (108–189 ppm), and high MgO (26.7–38.1 wt. %), Mg# (87–90), Cr_2O_3 (0.11–0.22 wt. %) and Ni (1007–1621 ppm). The samples also have low SiO_2 (26.8–33.5 wt. %) and very low Al_2O_3 (1.61–2.77 wt. %). The presence of diamonds in pipes that exhibit a primitive magma geochemical signature is not surprising. The high Mg#, Cr and Ni, low Al_2O_3 and SiO_2, together with the presence of diamonds in pipes from the BHH suggest that these kimberlites are the most 'primitive' magma in the NAKP implying that they have not undergone as much differentiation as ML or BM.

It should be recognized, therefore, that the majority of the samples collected from pipes that contain higher diamond contents have similar major and trace element contents. Subject to minimal contamination, these data may be used as an evaluation tool for future discoveries in the BHH area and possibly elsewhere in Alberta.

7 Selection of Pipes for Detailed Petrography and Isotopic Analysis

Results of the whole-rock geochemistry were used as a basis for the selection of pipes for detailed petrographic examination and isotopic analysis. The samples were separated into five 'groups' based on similar whole-rock geochemical distributions (Figure 18).

A pipe from each geochemical 'group' was selected for detailed study to develop a better understanding of the spectrum from primitive to evolved kimberlite magma. Pipes selected were the K4 and K6 from the BHH field and the Legend, Phoenix and Kendu pipes from the BM field. Two samples were collected at various depths from the K6, Legend, Phoenix and Kendu pipes, and three samples were collected from three pipes that make up the K4 complex for 11 samples total (Table 7; Figure 18).

The amount of sample material available for study varied. Sample descriptions from the K4A, K4B and K4C pipes (samples ABK01, ABK02 and ABK03) in the BHH field are based on single, hand-sized samples. Because a single sample may not be characteristic of the whole pipe, and examination of a suite of rocks or complete drill core was not accessible, it is possible that the K4 samples are not representative of the intrusion at that locale. Sample ABK29 was collected from an exposed outcrop of K6 on the southeastern flanks of the BHH and subsequently, a suite of samples was collected for interpretation with the permission of Ashton Mining of Canada Inc. Complete drill core intersections were available for all of the BM pipes.

8 Textural-Genetic Classification and Petrographic Summary

An overview of the textural and mineralogical highlights of each selected pipe is presented in Table 8. In general, the dominant minerals include: olivine, serpentine (lizardite-1M, lizardite-6T1 and chrysotile), calcite, dolomite, phlogopite and magnesite. Because the pipes are volumetrically dominated by olivine, serpentine and variable proportions of carbonate they are classified as serpentine kimberlite to carbonate-bearing or calcite-serpentine kimberlite.

Pyroclastic kimberlitic (PK) rocks are by far the dominant textural rock type in the NAKP followed by less common resedimented pyroclastic kimberlitic (RVK) rocks. The PK rocks are juvenile lapilli-bearing olivine (crystal) tuff. The macrocryst suite of minerals includes rounded, <1 cm, forsteritic olivine and a minor component of phlogopite and ilmenite, which are thought to originate from the disaggregation of mantle-derived peridotite xenoliths. No megacrysts were observed. The groundmass is dominated by mostly subhedral olivine microphenocrysts

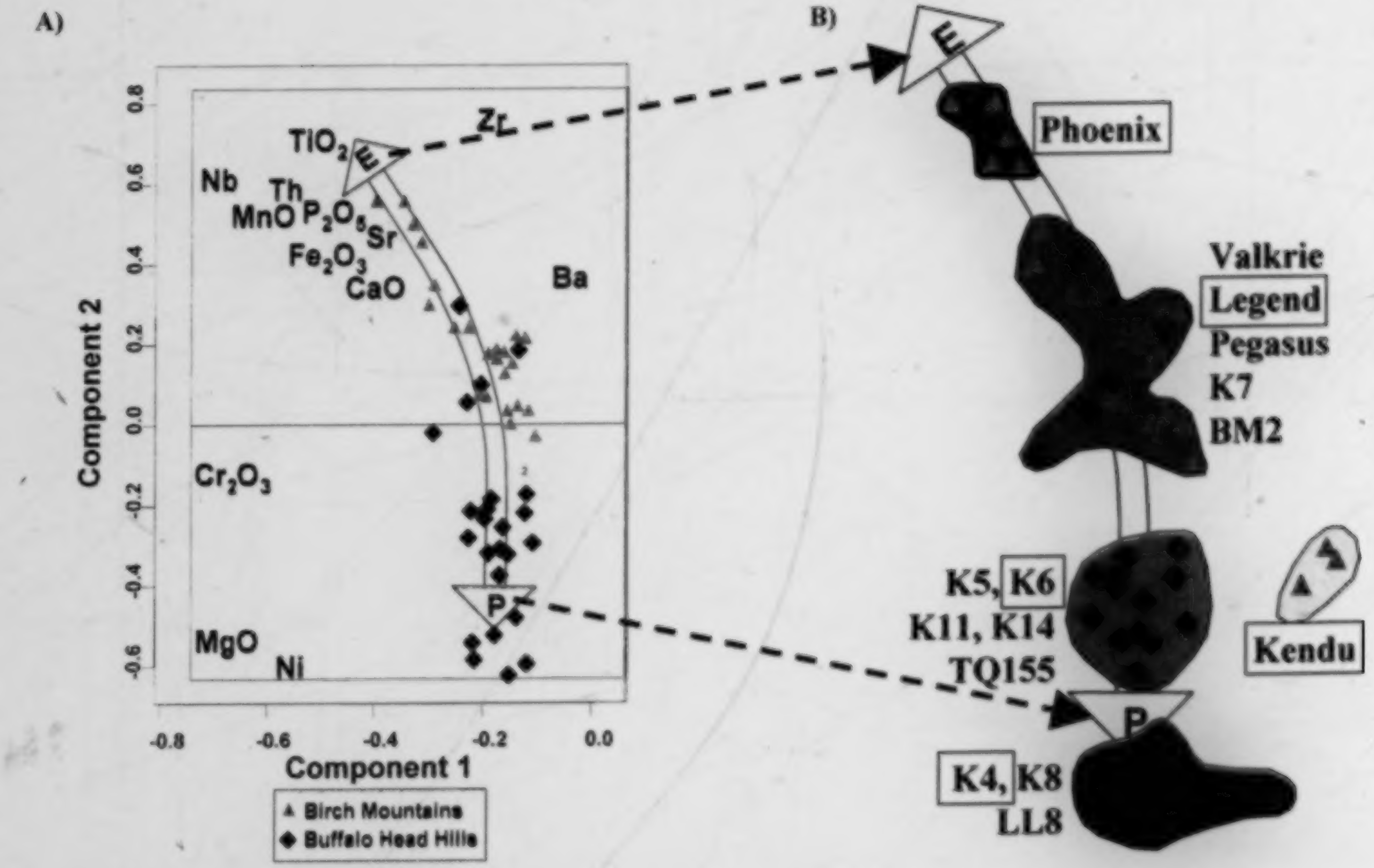

Figure 18. Whole-rock geochemical groups used for selection of pipes for detailed petrography and isotopic analysis. A) magma evolution line from primitive to metasomatically enriched kimberlite (from Figure 16) and B) five selected geochemical groups. Pipes selected for detailed petrography and isotopic analysis are highlighted in B (K4, K6, Kendu, Legend and Phoenix).

Sample number	Pipe name (general area)*	Drill hole number	Depth (m)	Easting (m)	Northing (m)	Zone
ABK-01	K4A (BHH)	4A-02	49.15	578380	6301519	11
ABK-02	K4B (BHH)	4B-01	140.65	578464	6300991	11
ABK-03	K4C (BHH)	4C-01	63.00	578821	6301274	11
ABK-05	K6 (BHH)	6-02	110.15	585550	6308383	11
ABK-29	K6 (BHH)	Outcrop	0 - surface	585317	6308651	11
ABK-59	Legend (BM)	98DH-LE01	44.00	386200	6340600	12
ABK-68	Legend (BM)	98DH-LE01	187.00	386200	6340600	12
ABK-75	Phoenix (BM)	98DH-PH01	105.00	351500	6330580	12
ABK-76	Phoenix (BM)	98DH-PH01	130.00	351500	6330580	12
ABK-81	Kendu (BM)	Kendu	102.00	368567	6353618	12
ABK-82	Kendu (BM)	Kendu	127.25	368567	6353618	12

* BHH – Buffalo Head Hills, north-central Alberta; BM – Birch Mountains, northeastern Alberta

Table 7. Samples selected for detailed petrography and whole-rock isotope analysis.

Pipe Name	Unique properties	Mantle xenoliths	Primary (accessory) minerals	Infilling*	Mineralogical-genetic classification
K4A, K4B, K4C	K4A – carbonate and silica alteration; K4B – abundant, fresh, olivine tuff; K4C – secondary hydrous vermiform serpentine	Rare	Olivine; serpentine (dolomite; quartz; pyrite; Ni-sulphide; phlogopite; magnesite)	Juvenile lapilli-bearing, olivine tuff; PK	Serpentine kimberlite
K6	Ash- to lapilli-sized juvenile pyroclasts; abundant, fresh olivine macrocrysts (>0.5 mm) and phenocrysts (<0.5 mm); calcite-rich and calcite veining	Rare to moderate	Olivine; serpentine; calcite (chromite; perovskite; apatite; magnetite; ilmenite)	Juvenile lapilli-bearing, olivine tuff; VK, where PK is greater than RVK	Calcite serpentine kimberlite
Legend	Carbonate-rich; abundant ilmenite	Rare	Serpentine; ankerite; ilmenite (olivine; calcite; magnesite; apatite; Ni-sulphide; chromite)	Juvenile lapilli-bearing, olivine tuff; PK	Carbonate-bearing serpentine kimberlite
Phoenix	Carbonate-rich; abundant perovskite (up to 0.12 mm) and phlogopite	Rare	Serpentine; ankerite (olivine; phlogopite; perovskite; atoll-textured spinel; magnesite)	Juvenile lapilli-bearing, olivine tuff; PK	Carbonate-bearing serpentine kimberlite
Kendu	Abundant phlogopite-rich lapilli and country rock xenoliths (mainly anorthite); minor component of pelletal lapilli; secondary hydrous vermiform serpentine	Abundant xenoliths and xenocrysts	Serpentine; phlogopite; calcite; garnet (omphacite; rutile; chromite; ilmenite; apatite)	Heterolithic VK	Phlogopite, carbonate-bearing kimberlite

* Infilling definitions from Field and Scott-Smith (1998): VK – volcaniclastic kimberlite; RVK – resedimented volcaniclastic kimberlite; PK – pyroclastic kimberlite

Table 8. Summary of the properties, infilling and classification of selected northern Alberta kimberlitic pipes.

(<0.25 mm) set in a fine-grained, serpentine- and sometimes carbonate-rich groundmass, and occur together with one or more of the following primary minerals: phlogopite, perovskite, spinel, ilmenite and apatite. Spherical and amoeboid juvenile lapilli are either isolated in the olivine crystal tuff, or occur together with ash- to lapilli-sized juvenile pyroclasts; their coexistence may result from multiple eruptions that have subsequently been mixed together.

Microscopically, the samples are crater-facies volcaniclastic rocks because they:

- contain irregular (spherical and amoeboid), extrusively-formed juvenile lapilli (Clement and Skinner, 1985).
- quenched acicular microlites of diopside (clinopyroxene) in the rims of the lapilli and their interclast matrix are absent (Scott Smith, 1995).
- The interclast matrix is composed primarily of serpentine and primary microcrystalline (quenched) carbonate.

Megascopic (i.e., drillcore) properties that support this contention include the following:

- The Birch Mountain cores show bedding and graded layers, particularly stratified tuff with alternating layers of coarse lapilli-sized (2–64 mm) and laminae of finer ash-sized (<2 mm) tuff (Aravanis, 1999).
- Drillholes K6-7, K6-8 and K6-10 from the K6 pipe penetrated cycles of kimberlite interlayered with mudstone, with gradational lower contacts between the kimberlite and the underlying mudstone (Skelton and Bursey, 1998).
- The Legend and Phoenix holes bottom out in 'kimberlite tuff' (Aravanis, 1999).

The fragile lapilli (often curvilinear) and shale clasts (often angular and unaltered), lack of breakage on fresh olivine grains, lack of sedimentary rocks in the matrix, lack of sorting and sedimentary structures, loosely packed and clast-supported textures, and nature of bedding (or lack or it) are all strong indicators that the selected pipes should be classified as PK deposits. The coexistence of variably sized lapilli, some with different groundmass mineralogies, may result from different eruptions or variations in the conditions during eruptions, with the tephra having been subsequently mixed together in their current host. Multi-generation lapilli, or lapilli that formed cores for later generations of lapillus development support this interpretation.

There is, however, some evidence for RVK, particularly in the Buffalo Head Hills pipes, where the boundaries of some lapilli are curvilinear on one side and fragmented on the other, and the lapilli are 'somewhat' horizontally oriented. In addition, some olivine grains are broken and fractured. Many of the lapilli, however, are more or less preserved and the presence of highly irregular amoeboid lapilli suggests that transport of clasts has not been extensive. In addition, little to no sedimentary rock material occurs in the matrix. Thus, it is concluded that the PK component is greater than the RVK component and these pipes should therefore be classified as PK.

The detailed petrographic descriptions of individual samples selected in this study are presented in Apppendix 3, and brief petrographic overviews are presented here. The K6 pipe in the Buffalo Head Hills exhibits a distinctive inequigranular texture resulting from the presence of macrocrysts set in a fine-grained matrix and of the samples studied, best fits the petrographic definition of kimberlite. Ash- to lapilli-sized juvenile pyroclasts (i.e., variably-sized single crystal olivine coated by juvenile material), which are diagnostic of the east side of the K6 pipe surface exposure, may be related to a near-vent environment. That is, the abundance and pristine preservation of the K6 pyroclasts would indicate that these lapilli have not travelled far in comparison to PK or RVK rocks with rare and/or broken lapilli.

Single hand-sized samples ABK01, ABK02 and ABK03 from the pipes K4A, K4B and K4C, respectively, have different petrographic characteristics ranging from unaltered olivine tuff PK (K4B) to extremely altered carbonate- and silica-rich kimberlite (K4A) to widespread hydrous replacement of original material by vermiform-textured serpentine (K4C). Kimberlite K4B is comprised of an abnormal amount (up to 65 vol. %) of single olivine crystals suggestive of olivine addition.

In contrast to the Buffalo Head Hills samples, the Legend and Phoenix kimberlites are carbonate-rich, relatively devoid of olivine macrocrysts, and have much higher concentrations of the late-stage minerals ilmenite, phlogopite, apatite, perovskite, and sulphides, all of which are suggestive of evolved or fractionated kimberlite magma.

The Kendu pipe has a unique petrographic appearance in the NAKP, but overall displays features consistent with volcaniclastic kimberlite. Juvenile lapilli and an abundance of basement and mantle xenoliths occur within a non-uniform, segregated matrix. The juvenile lapilli and xenoliths occur together with pelletal-textured lapilli, which commonly have a rim of tangentially aligned, extremely fine grained (<0.01 mm long) phlogopite- and vermiform serpentine-rich (lizardite) microlitic material surrounding olivine pseudomorphs. The pelletal lapilli flow-alignment textures are similar, but lack the diopside microlites described by Scott Smith (1995) and Mitchell (1995) as a 'hallmark' texture of diatreme-facies kimberlite. The microlitic material also form 'haloes' around pre-existing constituents that include metasomatized basement-rock xenoliths with irregular, diffuse boundaries. The lapilli and mantle and basement xenoliths occur in a matrix that has a nonuniform distribution with isolated 'pools' of groundmass minerals.

9 Mineralogical Summary

The detailed petrographic descriptions of individual samples selected in this study are presented in Appendix 3. Electron microprobe backscatter, X-ray elemental images and bulk-rock X-ray diffractograms, which complement the detailed descriptions, are presented in Appendices 4 and 5, respectively. The intent of this section is to summarize Appendices 3, 4 and 5, and describe aspects of minerals specific to selected Alberta kimberlites, particularly those that have significant paragenetic implications.

9.1 Olivine

Olivine is abundant in the northern Alberta pipes, forming up to 65 vol. % (e.g., K4 pipe) of the total mineral content. Measurements of olivine in thin section show that approximately 90% of the grains occur as microphenocrysts measuring 0.5 mm or less, and commonly less than 0.25 mm (Figure 19). These olivine crystals are usually subhedral, although euhedral and anhedral varieties occur in any given pipe.

The relative proportion of primary microphenocrystalline to macrocrystalline olivine varies. For example, the K4 pipe is composed primarily of ash-sized olivine crystals, whereas the K6 pipe contains abundant large, ovoid olivine macrocrysts. When present, the olivine macrocrysts are typically ovoid in shape and range in size from 0.5 to 10 mm. Figure 19 shows a general lack of olivine macrocrysts in the BM samples.

The degree of alteration of olivine to serpentine, calcite and magnesite varies; therefore, the colour of the olivine grains ranges from dark green to pale green to pale greenish white. Fresh, unaltered olivine is rare, but was observed in the K4B and K6 pipes with the latter having fresh olivine present in surface exposure. Partial pseudomorphs are common, for both the microphenocrystal and macrocrysts, where the outer portion of the grain is replaced, but the cores are preserved. Finally, complete pseudomorphing by serpentine is typical of many of the smaller crystals. Despite serpentinization and/or carbonate enrichment, the morphology of the olivine phenocrysts is generally well preserved.

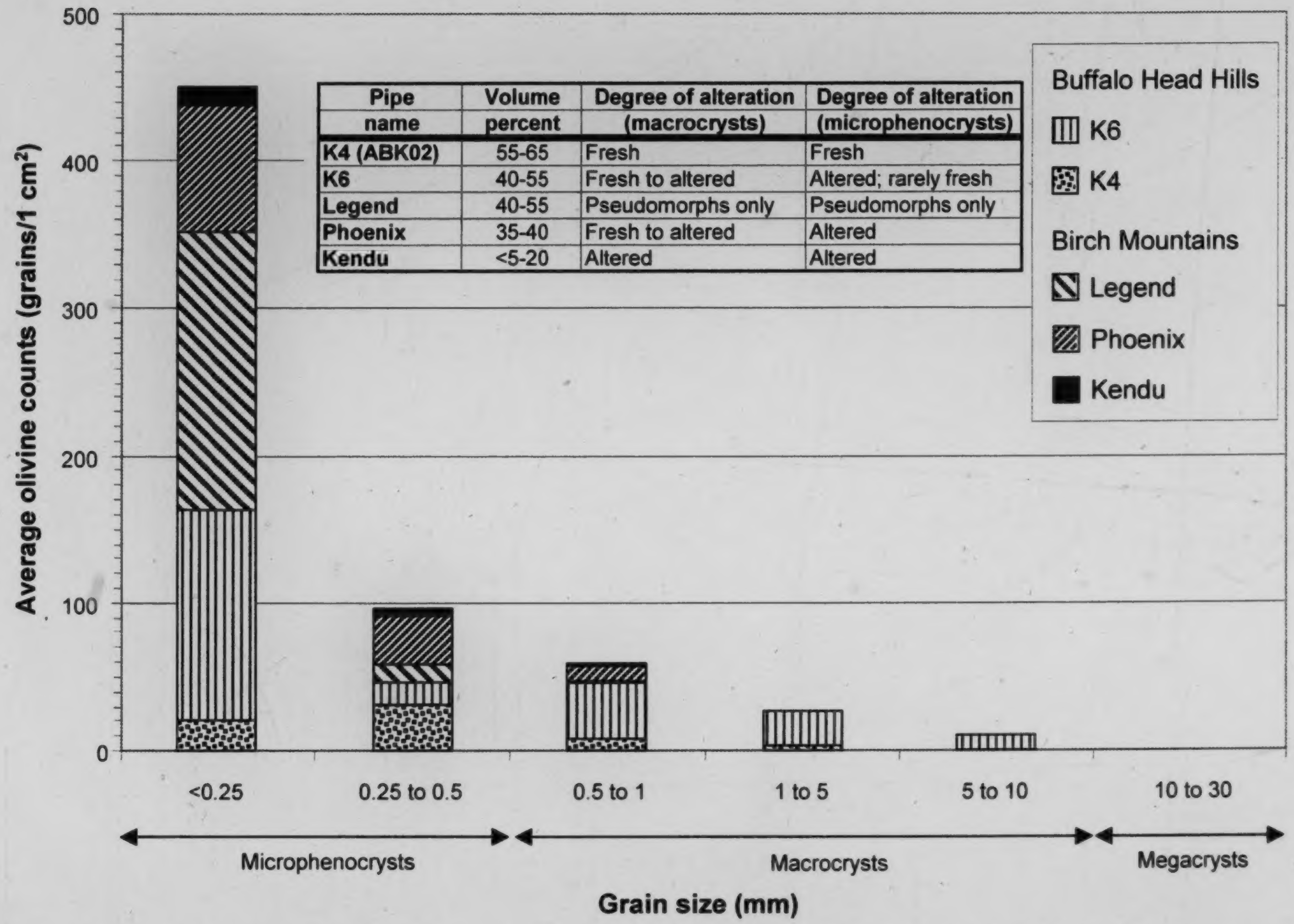

Pipe name	Volume percent	Degree of alteration (macrocrysts)	Degree of alteration (microphenocrysts)
K4 (ABK02)	55-65	Fresh	Fresh
K6	40-55	Fresh to altered	Altered; rarely fresh
Legend	40-55	Pseudomorphs only	Pseudomorphs only
Phoenix	35-40	Fresh to altered	Altered
Kendu	<5-20	Altered	Altered

Figure 19. Modal distribution of olivine, as determined in thin section, from selected northern Alberta kimberlitic pipes.

9.2 Serpentine

Next to olivine, serpentine is the most abundant mineral, followed by carbonate (calcite and/or dolomite). Although intimately associated with carbonate, serpentine dominates the groundmass and is the primary replacement mineral of olivine xenocrysts. There are several generations of serpentine, as determined by their different textural variations, from pseudomorphs to relatively coarse platy varieties.

The predominant serpentine is pseudomorphic lizardite. Based on degradation and preservation of various primary minerals, the serpentine typically pseudomorphs olivine phenocrysts and forms the groundmass along with other late-stage minerals (e.g., perovskite, apatite, phlogopite). This serpentine is oxidized and stained brown to dark brown, likely by iron oxyhydroxide.

Whole-rock powder X-ray diffraction shows at least three types of serpentine to be present: 1M, 1T and 6T lizardite and chrysotile (see Appendix 3). Jago and Mitchell (1985) suggested that X-ray diffraction techniques could be used to distinguish between primary groundmass serpentine (1T lizardite) and nonpseudomorphic prograde (terminology of Wicks and Plant, 1979; 6H lizardite) replacement of pre-existing pseudomorphic serpentine, in which case both types are present in the northern Alberta pipes.

From the few X-ray maps obtained, serpentine in the olivine margins has higher Al_2O_3 and FeO contents, probably related to alteration and/or separate serpentinitization events (e.g., K6, Legend, Phoenix; Appendix 4). In some cases, serpentine-rich pseudomorphs are accompanied by extensive development of magnetite, particularly in the Legend and Phoenix pipes. It should be noted, however, that the development of any additional groundmass minerals (e.g., phlogopite, apatite) appears to be preceded by an initial stage of serpentinization.

A specific serpentine morphology, which is apparently restricted to the K4 and Kendu pipes, is characterized by elongated (up to 3.5 mm long), randomly orientated, vermiform serpentine. The genesis of this serpentine is unknown, although it may be similar to antigorite/clinochrysotile observed in the Sturgeon Lake kimberlite block and Fort à la Corne kimberlites, Saskatchewan (Scott Smith, 1995; B. Kjarsgaard, pers. comm., 2003). The serpentine is interpreted to result from the hydrothermal or retrograde metamorphism of minerals such as olivine, pyroxene or amphibole, and occurs in varying amounts of local concentrations of up to 20% (e.g., Kendu pipe) to widespread replacement (e.g., K4B pipe).

9.3 Carbonate

In the NAKP, carbonate typically occurs in the groundmass together with serpentine as fine-grained (often <0.1 mm), discontinuous aggregates in the groundmass with magnetite and phlogopite, and/or as pseudomorphs of earlier formed olivine (Appendices 3 and 4). As such, the relationship and ratio between serpentine and carbonate varies considerably from one pipe to another, with up to about 25% carbonate in calcite serpentine kimberlite.

The most common carbonate mineral identified in this study is calcite, followed by dolomite and ankerite. Calcite occurs to some extent in all of the pipes investigated, particularly K6, Legend, Phoenix and Kendu. Dolomite is the predominant carbonate in the K4 pipe.

Pipe-specific examples of carbonate distribution include:

- concentrations of carbonate at the margins of partially serpentinized olivine grains (dolomite in K4, calcite in Legend);
- calcite filling the cores, or possibly vugs, in altered olivine grains (K6, Legend and Phoenix);
- pool-like segregations of carbonate-rich serpentinized matrix (calcite and/or ankerite in Kendu); and
- intimate intergrowths evenly distributed throughout the serpentinized matrix (all pipes).

Later, clearly secondary addition of carbonate, probably resulting from circulation of groundwater and/or hydrothermal solutions, is evidenced by vein calcite and infilling of small pores and cavities in the K6, Legend and Phoenix pipes. In addition, fibrous, 1 to 3 mm calcite veinlets occur in outcrop at kimberlite K6.

9.4 Phlogopite

Phlogopite is a minor constituent of the BHH pipes, generally forming <5 vol. % of the mineral assemblage with dispersed macrocrysts up to 10 mm in length. The modal amount of phlogopite in the BM pipes varies from nonexistent (Legend pipe) to moderate (up to 8 vol. % in the Phoenix pipe) to high, with local concentrations of up to 40 vol. % (Kendu pipe).

Phlogopite typically occurs as small groundmass crystals characterized by subhedral to euhedral laths that range in length from 0.05 to 0.1 mm with a length-breadth ratio of 2.5 to 3.5. With the exception of the Kendu pipe, the grains are typically isolated and randomly oriented. In Kendu, phlogopite occurs within lapilli, or is aligned by flow, forming haloes around pre-existing country rock and mantle xenoliths, which give a superficial similarity in appearance to Group II kimberlite.

Phlogopite typically displays normal pleochroism and none of the phlogopites identified display reverse pelochroism characteristic of tetraferriphlogopite (Farmer and Boettcher, 1981). Back-scattered images show that some of the phlogopites have sharply defined euhedral to irregularly shaped core-to-rim boundaries, which may represent Fe-rich phlogopite xenocrysts that have been mantled by primary kimberlite phlogopite overgrowths. Some overgrowth zones, however, appear erratic or random so that a clear distinction between the core and mantle is not always possible. Inclusions of pyrite and apatite in phlogopite from the Phoenix pipe demonstrate the late-crystallizing nature of some BM phlogopite. The phlogopite is modified by varied degrees of corrosion and/or chloritization at margins and along cleavage planes.

9.5 Apatite

Apatite is a late-crystallizing groundmass phase, ranging in modal abundance from trace amounts (≤1 vol. %) in the BHH pipes (K4 and K6) up to about 5 vol. % in the BM pipes. The apatite is relatively unaltered, and usually forms as euhedral, prismatic crystals with distinct hexagonal base sections. Apatite is larger (up to 0.9 mm in diameter in the Phoenix pipe) and better formed in carbonate-rich portions of the BM pipes compared to those in the BHH, where the apatite is predominantly small (about 0.01 mm) and forms as anhedral grains.

9.6 Perovskite

Perovskite was identified in thin sections of samples of the K6, Phoenix and Kendu pipes. Perovskite grains typically occur as isolated pinkish-brown subhedral, rounded crystals, but also occur as mantles on xenocrystic ilmenite. The size of perovskite crystals varies appreciably between pipes. In kimberlite K6, perovskite occurs as very small (typically <3 μm), rounded crystals that, in some locales, dominate the opaque mineral suite. Abundant (up to 5 vol. %), unusually large perovskite, in comparison to perovskite from other NAKP pipes and kimberlite perovskite worldwide, occurs in the Phoenix pipe, where it averages 0.08 mm in diameter and ranges up to 0.12 mm. Mineral separates of perovskite from the Phoenix pipe are coated by a whitish, carbonate-rich alteration material that is present with ilmenite to give a salt-and-pepper appearance. Perovskite in the Phoenix pipe represent the best perovskite observed in the selected samples in terms of abundance, size and preservation. The very small perovskite crystals in the K6 and Kendu pipes may be altered, possibly to a titanium phase (e.g., rutile, anatase or ilmenite).

9.7 Opaque Minerals

Spinel is ubiquitous and occurs in all samples. It often forms euhedral to anhedral, cubic to corroded grains that range in size from 0.01 to 0.1 mm, and varies in abundance from 1 to 5 vol. %. Spinel, in conjunction with perovskite and ilmenite, may form 'necklaces' around discrete olivine crystals or around pseudomorphed, subhedral olivine. Spinel is typically altered, particularly in the BM pipes, where 'cloudy fringes' of iron hydroxide/oxide characterize the crystals. Atoll-textured spinel (e.g., Mitchell and Clarke, 1976) is common in the Phoenix pipe, where chromite cores are surrounded by multiple atolls of resorbed spinel (dominantly magnetite).

Ilmenite is present in all of the pipes, particularly the Legend pipe, where Mg-ilmenite macrocrysts constitute up to 5 vol. % and range up to 9 mm in diameter. Ilmenite more typically occurs as intergrowths with groundmass spinel and perovskite, or as disseminated single crystal and polycrystalline macrocrysts.

Sulphide minerals are present as a minor component in all of the pipes investigated. Minor (1–3 vol. %) to moderate (up to 7 vol. %) quantities of sulphide minerals occur in the K4 (BHH) and Legend and Kendu pipes (BM). Sulphide minerals, which include dominantly pyrite, but also Ni-sulphide minerals (e.g., millerite), typically occur as acicular to anhedral disseminations and clusters in the groundmass, or as replacements of various biota associated with sedimentary clasts. In the matrix, sulphide minerals are commonly intimately associated with carbonate (typically dolomite). Carlson et al. (1999) reported that, in addition to pyrite, chalcopyrite, sphalerite and millerite, and an unidentified Ca-REE phosphate mineral have been identified in trace amounts in the BHH pipes. Aravanis (1999) identified the sulphide mineral greigite [$Fe^{2+}Fe_2^{3+}S_4$] from either the Jason target (magnetic anomaly with no kimberlitic rocks intersected) or the Legend pipe in the BM area.

10 Radiogenic Isotopes

Ten samples from five pipes (K4, K6, Legend, Phoenix and Kendu) were analyzed for whole-rock Sm-Nd, Rb-Sr and Pb-Pb isotopes. Their initial isotopic ratios were calculated using ages of 86 and 76 Ma for samples from the BHH and BM fields, respectively. The results, which are presented in Table 9, have wide initial isotopic ranges: $^{87}Sr/^{86}Sr$ between 0.704 to 0.709, ε_{Nd} between –7.4 to +2.7, $^{206}Pb/^{204}Pb$ between 18.2 to 19.8, $^{207}Pb/^{204}Pb$ between 15.49 to 15.58 and

Table 9A. Rb-Sr whole-rock isotopic data for selected Alberta kimberlites.

Sample	Pipe name	Rb (ppm)	Sr (ppm)	$^{87}Rb/^{86}Sr$	$^{87}Sr/^{86}Sr$ corrected*	Uncertainty +/- 2sm	Initial $^{87}Sr/^{86}Sr$
ABK01	K4A	2.14	295.72	0.0210	0.70673	0.00001	0.70671
ABK02	K4B	6.81	452.42	0.0436	0.70626	0.00001	0.70621
ABK05	K6	9.56	515.33	0.0537	0.70406	0.00002	0.70400
ABK29	K6	29.78	928.65	0.0928	0.70434	0.00001	0.70423
ABK59	Legend	37.53	878.38	0.1236	0.70521	0.00001	0.70508
ABK68	Legend	30.27	543.40	0.1612	0.70645	0.00001	0.70628
ABK75	Phoenix	36.99	1273.17	0.0841	0.70585	0.00001	0.70576
ABK76	Phoenix	3.67	118.69	0.0896	0.70565	0.00001	0.70556
ABK81	Kendu	4.11	42.72	0.2786	0.70778	0.00001	0.70749
ABK82	Kendu	32.38	407.46	0.2300	0.70879	0.00001	0.70856

* Sr correction S54 Multi Dynamic

Table 9B. Sm-Nd whole-rock isotopic data for selected Alberta kimberlites.

Sample	Sm (ppm)	Nd (ppm)	$^{147}Sm/^{144}Nd$	$^{143}Nd/^{144}Nd$ corrected*	Uncertainty +/- 2sm	TDM	Epsilon NdT
ABK01	0.74	6.55	0.0683	0.51221	0.00001	1.00	-7.0
ABK02	2.54	25.26	0.0607	0.51218	0.00001	0.97	-7.3
ABK 05	11.11	94.21	0.0713	0.51270	0.00001	0.50	2.5
ABK 29	8.90	74.93	0.0719	0.51271	0.00001	0.49	2.7
ABK 59	10.79	92.43	0.0706	0.51259	0.00001	0.61	0.2
ABK 68	8.42	71.63	0.0710	0.51258	0.00001	0.62	0.0
ABK 75	26.66	242.18	0.0666	0.51267	0.00001	0.51	1.8
ABK 76	27.02	245.83	0.0665	0.51267	0.00001	0.51	1.8
ABK 81	8.43	62.02	0.0822	0.51226	0.00001	1.05	-6.3
ABK 82	6.81	49.39	0.0833	0.51238	0.00001	0.91	-4.0

* Nd correction S54 Multi Dynamic

Table 9C. Pb-Pb whole-rock isotopic data for selected Alberta kimberlites.

Sample	U	Th	Pb	206/204 corrected	207/204 corrected	208/204 corrected	206/204 initial	207/204 initial	208/204 initial
ABK 01	1.3	5.5	<3	19.135	15.566	39.447	19.130	15.565	39.440
ABK 02	2	9.5	4	19.123	15.486	39.757	19.119	15.486	39.750
ABK 05	3.9	23.2	8	19.530	15.550	39.886	19.526	15.550	39.877
ABK 29	3.1	18.1	5	19.418	15.544	39.685	19.412	15.544	39.675
ABK 59	6	37.7	11	19.673	15.578	40.249	19.669	15.578	40.241
ABK 68	5.3	31.1	8	19.724	15.576	40.248	19.719	15.576	40.238
ABK 75	8.5	88	12	19.828	15.577	41.077	19.822	15.577	41.059
ABK 76	8.9	85.9	11	19.764	15.578	40.866	19.758	15.578	40.847
ABK 81	2.4	26.6	9	18.238	15.500	39.602	18.236	15.500	39.595
ABK 82	2	14.7	8	18.203	15.490	38.616	18.201	15.490	38.611

Table 9. Results of northern Alberta kimberlitic whole-rock isotopic analysis.

^{208}Pb/^{204}Pb between 38.61 to 41.06. The ^{87}Sr/^{86}Sr versus ^{143}Nd/^{144}Nd and isotopic Pb ratios diagrams are presented in Figures 20 and 21, respectively.

Before the results of the whole-rock isotopic analyses are used to make inferences on mantle source composition in the NAKP, the degree and type of contamination must be considered. Two preliminary lines of isotopic evidence that indicate a possibility for contamination of at least some of the NAKP pipes include:

- Figure 20 shows that the isotopic composition of samples from the K4, K6 and Phoenix pipes have similar isotopic ratios, and thus, indicate that the whole-rock isotopic values obtained for these pipes are reproducible. However, Figure 20 also shows that there is a significant difference in the Sr-Nd isotopic compositions of samples from the Legend and Kendu pipes, and
- Independent Sr isotope analysis on perovskite from the Phoenix pipe (sample ABK76) has a significantly lower ^{87}Sr/^{86}Sr ratio (0.70479±0.00002) compared to Phoenix whole rock, which has initial ^{87}Sr/^{86}Sr ratios of between 0.70576 and 0.70556. This suggests that there was addition of radiogenic Sr following perovskite crystallization or that the perovskite is xenocrystic.

10.1 Considerations for Country Rock Contamination

Composite mixing diagrams (1/Sr concentration versus ^{87}Sr/^{86}Sr isotopic composition; Faure, 1977) are presented in Figures 22 and 23, and test mixing relations between isotope sample 'pairs' from the K4, K6, Kendu, Legend and Phoenix pipes, with potential sources of contamination in northern Alberta, which could infiltrate the kimberlite during magma transport and eruption and/or post depositional disturbances. Country rock and water end members selected for the mixing diagrams include continental pluton, Devonian carbonate and clastic sediment rock, and Cretaceous-Tertiary aquifer water. End member Sr concentration and ^{87}Sr/^{86}Sr ratio values used in Figures 22 and 23 are from Alberta-based compilations of basement rock (D. Pana, personal communication, 2003), Devonian and Cretaceous sedimentary rock (Dufresne et al., 2001; Eccles et al., 2001b; Eccles and Panu, in preparation) and ground/formation water (Connolly, 1990; Lemay, 2002).

Figures 22 and 23 show that a possible source of contamination in the NAKP pipes is from Devonian carbonate and Cretaceous-Tertiary aquifers, particularly for the K4, Kendu and

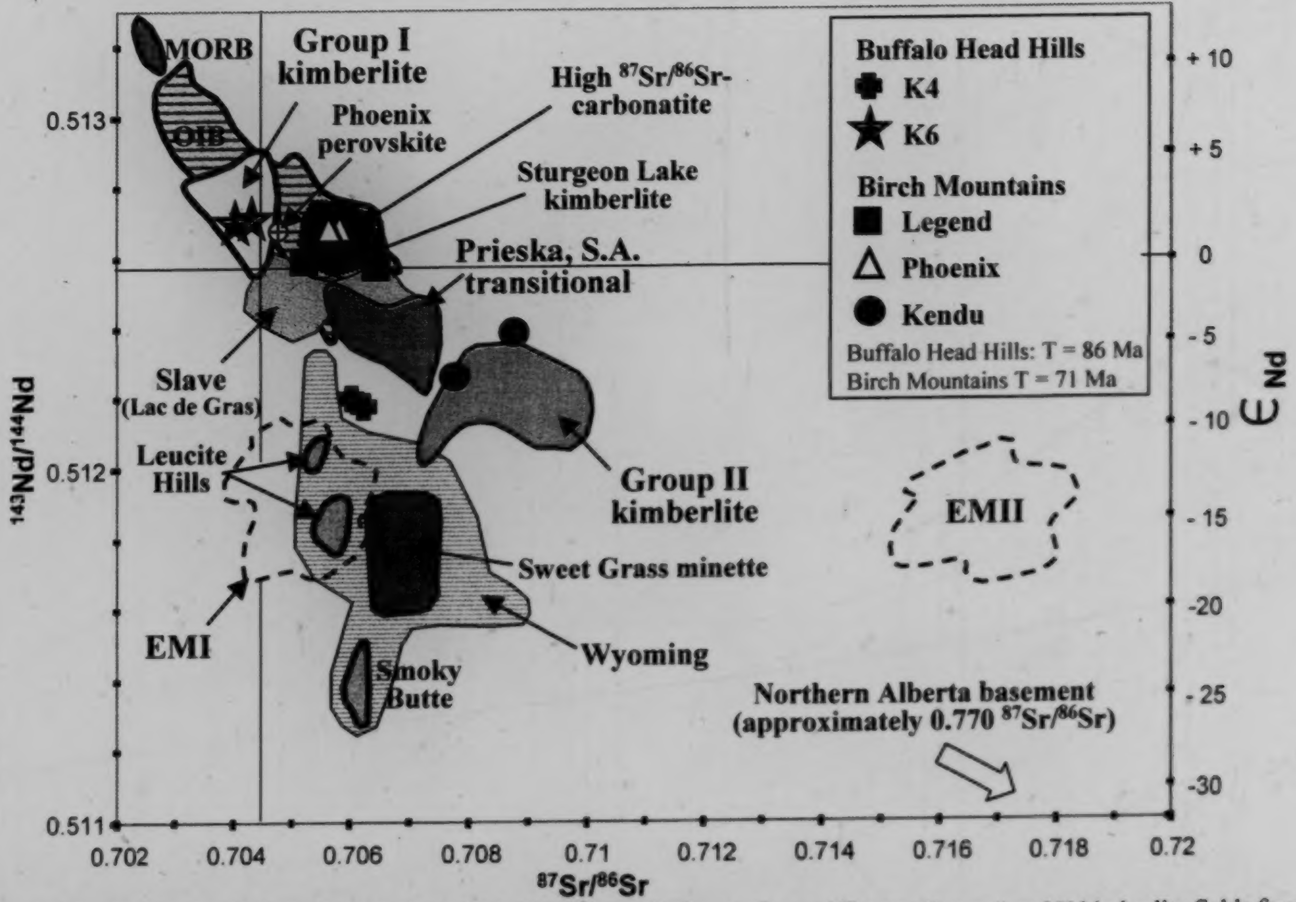

Figure 20. Nd-Sr isotope variations from selected kimberlitic rocks in northern Alberta. Group I and II kimberlite fields from Mitchell (1986); Prieska transitional kimberlite field from Skinner et al. (1994); Slave Lake de Gras field from Dowall et al. (2000); Sturgeon Lake kimberlite from Hegner et al. (1995); Wyoming ultrapotassic fields from Vollmer et al. (1984) and O'Brien et al. (1995); Sweet Grass minette from Buhlmann (1996); high $^{87}Sr/^{86}Sr$ carbonatite from Harmer and Gittins (1998); and mid-oceanic ridges (MORB), oceanic islands (OIB) and EM-II mantle reservoir from Zindler and Hart (1986).

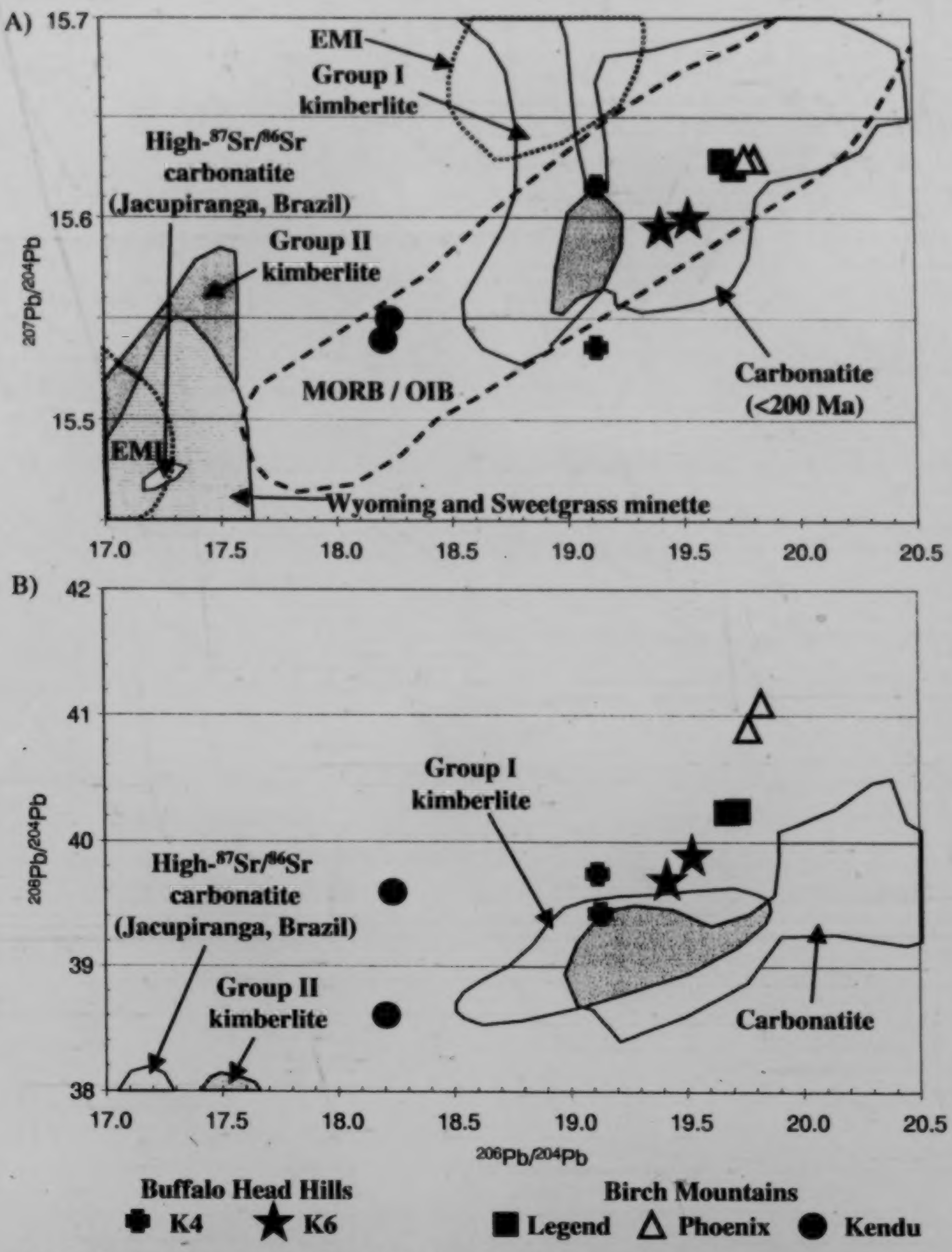

Figure 21. Isotopic composition of Pb from kimberlitic rocks in northern Alberta. A) $^{207}Pb/^{204}Pb$ versus $^{206}Pb/^{204}Pb$, B) $^{208}Pb/^{204}Pb$ versus $^{207}Pb/^{204}Pb$. Kimberlite fields from Mitchell (1995); Wyoming and Sweetgrass field from O'Brien et al. (1995) and Buhlmann (1996); carbonatite from Harmer and Gittins (1998); and mid-oceanic ridges (MORB) and oceanic island basalts (OIB) from Zindler and Hart (1986).

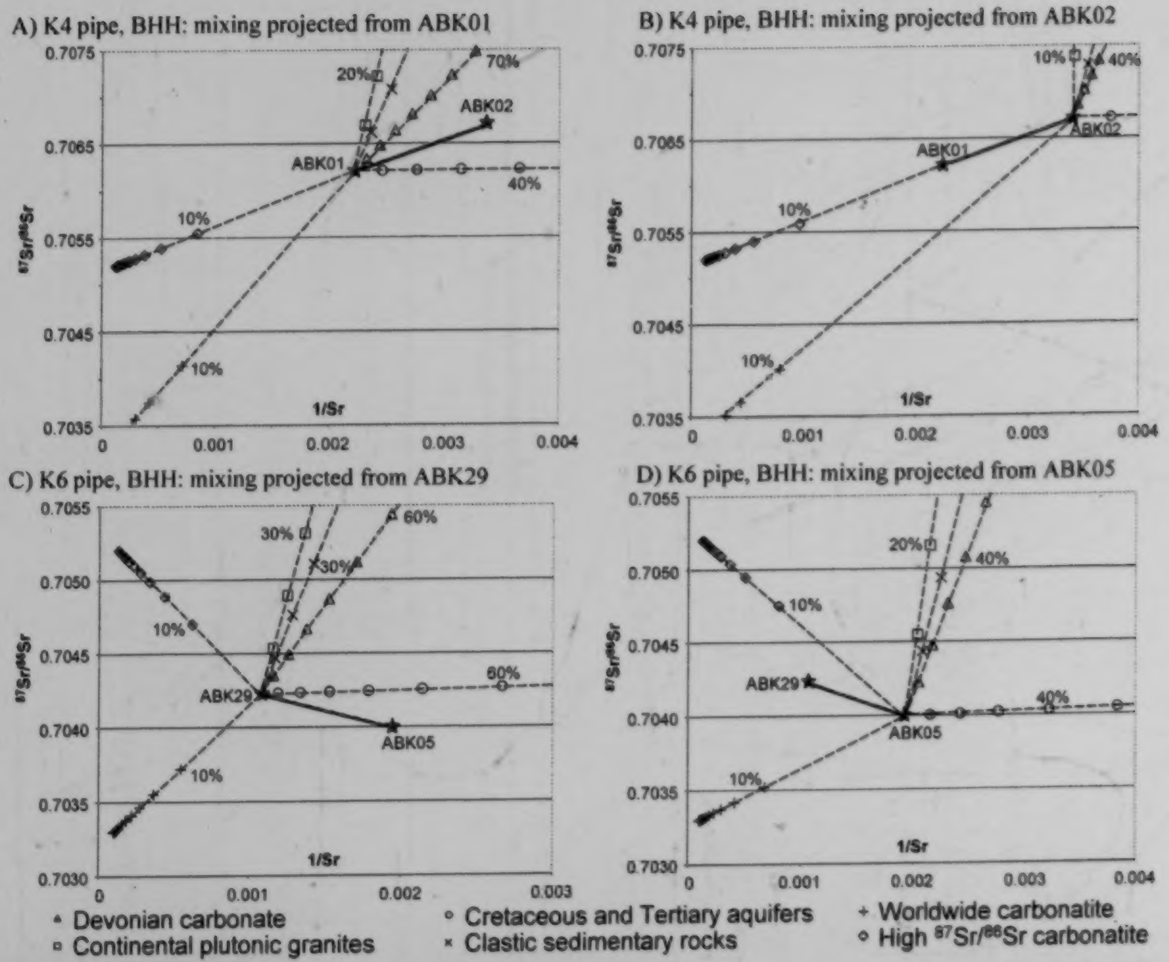

Figure 22. Composite isotope-mixing diagrams for Buffalo Head Hills kimberlites with selected Sr (ppm) and initial $^{87}Sr/^{86}Sr$ values for continental plutonic rock (270, 0.7140), Devonian carbonate (245, 0.7085), clastic sediment (170, 0.7165), Cretaceous-Tertiary aquifers (6.4, 0.7080), worldwide carbonatites (10 000, 0.7032) and high-$^{87}Sr/^{86}Sr$ carbonatite (7 750, 0.7052). See text for references. Stars represent kimberlite samples.

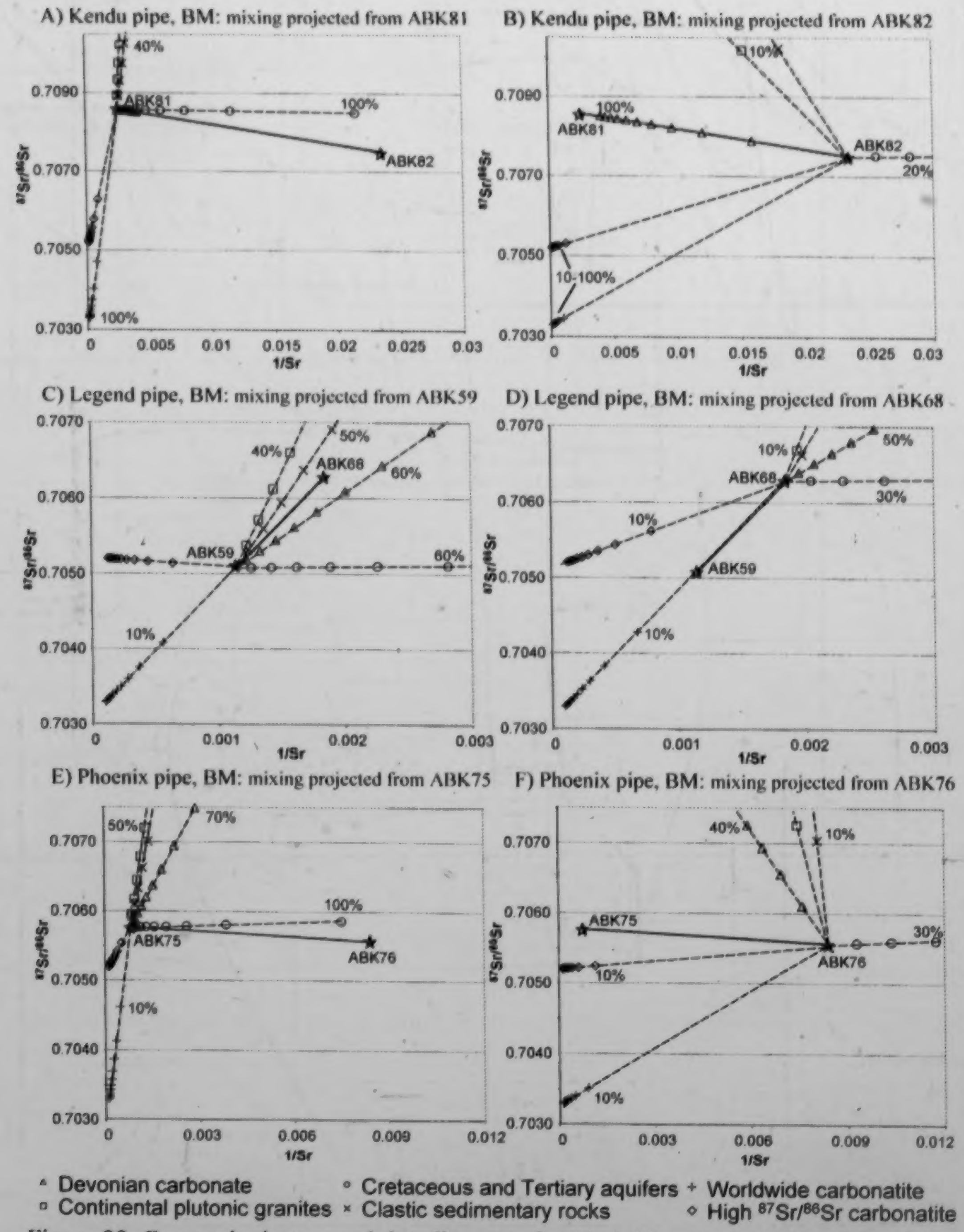
A) Kendu pipe, BM: mixing projected from ABK81

B) Kendu pipe, BM: mixing projected from ABK82

C) Legend pipe, BM: mixing projected from ABK59

D) Legend pipe, BM: mixing projected from ABK68

E) Phoenix pipe, BM: mixing projected from ABK75

F) Phoenix pipe, BM: mixing projected from ABK76

Figure 23. Composite isotope-mixing diagrams for Birch Mountains kimberlites with selected Sr (ppm) and initial $^{87}Sr/^{86}Sr$ values for continental plutonic rock (270, 0.7140), Devonian carbonate (245, 0.7085), clastic sediment (170, 0.7165), Cretaceous-Tertiary aquifers (6.4, 0.7080), worldwide carbonatites (10 000, 0.7032) and high $^{87}Sr/^{86}Sr$ carbonatite (7 750, 0.7052). See text for references. Stars represent kimberlite samples.

Phoenix pipes. Other possible sources of contamination include a combination of continental pluton and clastic sediment rock, and aquifer water in the Legend pipe. However, the relative proportions of country rock and ground/formation water contamination is too high, and is therefore, not an accurate assessment of potential sources of contamination in these kimberlite samples. Specific examples include:

- the K4 pipe would have contamination from some combination of up to about 55% Devonian carbonate and 35% Cretaceous-Tertiary aquifer water (Figure 22A);
- the K6 pipe would have contamination from approximately 45% Cretaceous-Tertiary aquifer water (Figure 22C);
- the Kendu pipe would have >100% contamination from Devonian carbonate (Figure 23A);
- the Legend pipe would have some combination of approximately 58% Devonian carbonate, 42% clastic sediment and 38% basement plutonic rocks (Figure 23 C);
- the Phoenix pipe would have >100% contamination from Cretaceous-Tertiary aquifer water (Figure 23E).

Based on these mixing ratios, the K4, K6, Kendu, Legend and Phoenix pipes would have 40% to impossible (>100%) levels of contamination from Alberta country rock, ground/formation water, or a mixture of both. With the exception of the Kendu pipe, country rock contamination is generally considered negligible because there is no petrographic evidence to support a substantial component of country rock in the samples analyzed and the contamination index (C.I.) for these kimberlites is generally low. Thus, there is no evidence to support such a substantial influx of country rock in the samples analyzed. In fact, <10% country rock was observed, and a substantial proporation of foreign xenoliths were removed during sample preparation (i.e., visible country xenoliths were removed after crushing the sample to <2 cm). It is acknowledged, however, that it is very difficult to evaluate the content of very finely comminuted crustal material.

With respect to ground/formation water, the influence of waters on NAKP kimberlite seems likely – the exposure of crater-facies volcaniclastic rocks to waters in a basin environment can be envisaged as being subject to prolonged alteration. The mixing line diagrams show a dependency towards Devonian carbonate contamination and this could be related to gravity-driven, carbonate-rich meteoric water subsequent to the Laramide Orogeny. Although the exact influence of ground/formation water on the geochemical and isotopic compositon of NAKP volcaniclastic rocks is unknown at this time, it seems unlikely that the kimberlite would be contaminated by carbonate-rich waters to the extent of that required by the mixing diagrams to explain the variability of isotopic compositions within individual pipes.

In summary, given the enriched incompatible element compositions these kimberlites and their low Contamination Index ratios, the whole rock isotopic compositions of the northern Alberta kimberlite province kimberlitic rocks obtained in this study are interpreted to generally reflect the isotopic nature of their mantle source region(s).

10.2 Considerations for Mantle Metasomatism

Because the NAKP rocks lack Devonian carbonate country rock xenoliths and cross-cutting carbonate veins, have high MgO/SiO_2 ratios (typically between 0.6 and 1.5), and a matrix composed pervasively of serpentine-carbonate, the potential for CO_2-rich fluids, such as carbonatitic melts, warrant investigation. Especially because petrographic and geochemical evidence presented in this study shows that the modal volume of matrix carbonate can be used as important criteria to distinguish between the BHH and the BM kimberlite fields with the latter being more carbonate-rich. Geochemical similarities of the BHH and BM samples to carbonatite, include:

- enrichment in Th, U, Sr, Ti, Zn, Nb, Y, Mo, Cu, V, P, Mn, S, La, Ce, Sm, Eu, Pb, Zr and Ba (Tables 4 and 5; Appendices 1 and 2), and
- pronounced Cs, Rb, Hf and Ti depletions and Th-U, Ta-Nb enrichment relative to REE (Figures 14 and 15)
- a wide range of CaO contents (e.g.: 1 to 28 wt. %) related to wide variations of contained carbonate minerals (dolomite and calcite).

In order to test what influence carbonic-rich fluids may have had on the NAKP, Figures 22 and 23, include 1/Sr and $^{87}Sr/^{86}Sr$ from the BHH and BM in mixing relationships with worldwide average carbonatite and high-$^{87}Sr/^{86}Sr$ carbonatite end members (end member values averaged from Nelson et al., 1988; Bell and Blenkinsop, 1989; Harmer and Gittins, 1998). The mixing distributions between the NAKP and carbonatite show that a more plausible explanation for isotopic enrichment in the NAKP is by metasomatism of the lithospheric upper mantle by carbonic-rich magmas and/or fluids. For example,

- K4 would require 5% mixing with high-$^{87}Sr/^{86}Sr$ carbonatite melt (Figure 22B);

- K6 would require approximately 6% mixing with worldwide carbonatite and high-$^{87}Sr/^{86}Sr$ carbonatite melt, or a carbonic-rich melt with about 0.7045 $^{87}Sr/^{86}Sr$ (Figure 22D);
- Kendu would require about 8.5% mixing with high-$^{87}Sr/^{86}Sr$ carbonatite (Figure 23B);
- A simple two-component mixing line between Legend and worldwide carbonatite is shown in Figure 23D with about 6% mixing from carbonatite
- Phoenix would require between 15 and 18% mixing with high-$^{87}Sr/^{86}Sr$ carbonatite (Figure 23F).

Based on this observation, the NAKP kimberlite samples are influenced by 5 to 18% carbonic-rich melts/fluids that have $^{87}Sr/^{86}Sr$ values of between 0.7035 and 0.7050. The BHH pipes have 5 to 6% mixing and the BM have a higher carbonate component with between 6 and 18% mixing.

10.3 Whole-Rock Isotopic Tracing

On the Nd-Sr (Figure 20) and Pb-Pb (Figure 21) plots, the isotopic data obtained for NAKP kimberlite display a large range in composition. With respect to Bulk Earth, samples from the K6 kimberlite are characterized by low $^{87}Sr/^{86}Sr$ (0.70400 to 0.70423), positive ε_{Nd} (+2.5 to +2.7), and plot within the field for South African Group I kimberlite in Figure 20. The K6 pipe has slightly more radiogenic Pb isotope compositions (19.41 to 19.53 $^{206}Pb/^{204}Pb$ and 39.68 to 39.88 $^{208}Pb/^{204}Pb$) compared to Group I kimberlite (Figure 21). The Legend and Phoenix pipes have similar ε_{Nd} (0.0 to +1.8), but more radiogenic $^{87}Sr/^{86}Sr$ compositions (0.70508 to 0.70628) and Pb isotope ratios (e.g., 40.24 to 41.06 $^{208}Pb/^{204}Pb$) in comparison to the K6 pipe and the field for Group I kimberlite. The K4 and Kendu pipes have higher $^{87}Sr/^{86}Sr$ (0.70778 to 0.70879) and lower ε_{Nd} (-4.0 to –6.3) than the Bulk Earth and plot within the enriched, bottom right quadrant of the Nd-Sr diagram. In Pb-Pb space, K4 and Kendu pipes are characterized by less radiogenic Pb-isotope ratios in comparison to the K6, Legend and Phoenix pipes with K4 plotting closest to the field for Group I kimberlite.

With the exception of K4 in Nd-Sr space, the NAKP has a more primitive OIB-type signature in comparison to the Wyoming Craton ultrapotassic rocks, which underlies southernmost Alberta, providing evidence for a separate protolith. Based on isotopic evidence, the diamondiferous K6 pipe (BHH) has the most primitive depleted upper mantle (MORB-like) source.

One of the interesting features of the Sr-Nd isotopic data is that the Legend, Phoenix and K6 pipes have similar positive ε_{Nd} (+1.8 to +2.7), but have variable strontium isotopic compositions.

The $^{87}Sr/^{86}Sr$ ratio of the Legend and Phoenix samples are more radiogenic than those of K6, but are not atypical isotopic compositions for worldwide kimberlite. Figure 20 shows that Legend and Phoenix have comparable Sr-Nd to the diamondiferous kimberlites of the Slave province, Northwest Territories, Sturgeon Lake kimberlite, Saskatchewan, and Kaapvaal 'transitional' kimberlites, as well as high-$^{87}Sr/^{86}Sr$ carbonatite (e.g., Jacupiranga, Brazil; Walloway, South Australia; Amba Dongar, India). The Legend and Phoenix samples also have similar Sr-Nd isotopic ratios to kimberlite from Finland (O'Brien and Tyni, 1999), Brazil (Bizzi et al., 1994), Siberian Platform (Agashev et al., 2000) and Arkhangelsk regions in Russia (Mahotkin et al., 2000) and China (Tompkins et al., 1999). In addition, Legend and Phoenix have similar isotopic compositions to worldwide carbonatite in $^{207}Pb/^{204}Pb$-$^{206}Pb/^{204}Pb$ space.

Perovskite from the Phoenix pipe has a less radiogenic $^{87}Sr/^{86}Sr$ (0.7048) in comparison to its whole-rock isotopic ratio (0.7058 to 0.7063). If the analysed perovskite represents a primary crystallizing phase (i.e., is not xenocrystic) in the Phoenix kimberlite magma then the more radiogenic whole rock strontium isotopic composition must reflect $^{87}Sr/^{86}Sr$ contribution after perovskite crystallization. Potential sources for strontium enrichment could include contamination by crustal or enriched mantle (e.g. EMII) and/or by interaction of hydrothermal- or groundwater-related fluids. Further work that includes age determinations and geochemical analyses via the electron microprobe on the same primary mineral grains (e.g., perovskite) are required to resolve this problem.

The K4 and Kendu pipes have the most negative ε_{Nd} and radiogenic $^{87}Sr/^{86}Sr$ in this dataset. Although contamination cannot be ruled out, their isotopic signature is interpreted to be the result of a subcontinental lithosphere component in the mantle source region for these pipes. Evidence for minimal contamination by country rock or supporting criteria for a subcontinental lithospheric source, includes:

- K4 and Kendu: both pipes are reportedly barren of diamond, and therefore, may not have originated at depths deep enough to sample diamonds
- K4 and Kendu: samples from both pipes, including samples (e.g., ABK02, K4 pipe) with no petrographic evidence for country rock contamination, exhibit the 'flattest' chondrite-normalized REE profiles in their respective fields. The flat REE profiles suggests these pipes have the largest degree of partial melting, which would correspond to a sub-continental lithospheric component

- K4: samples ABK01and ABK02 have Contamination Index ratios of 1.3 with suspected hydrothermal silica alteration, and 0.75 with up to 65 vol. % olivine, respectively. Despite having different mineralogical and geochemical compositions, the two K4 pipe samples have similar whole rock isotopic compositions (e.g., initial $^{87}Sr/^{86}Sr$ compositions of 0.70671 and 0.70621). This suggests that penecontemporaneous and/or post emplacement hydrothermal silica-enrichment events have not influenced the isotopic composition of K4.

The Sr-Nd isotopic composition of the K4 pipe trends towards the Wyoming craton and enriched mantle I (EM I), and therefore, is representative of a metasomatized sub-continental lithosphere (e.g., Zindler and Hart, 1986). High initial $^{87}Sr/^{86}Sr$ in Kendu indicate a source composition similar to that of Society OIB (EM II) mantle component, which has been attributed to recycling of continental crust, sediments, delaminated lithosphere into the mantle and/or mantle metasomatism (e.g., Menzies, 1983; White, 1985; Zindler and Hart, 1986). Because there is petrographic (anorthosite basement xenoliths) and geochemical evidence (Contamination Index ratio of 1.7) for country rock contamination in the Kendu pipe, its whole rock isotopic composition may be influenced by crustal contamination, which would explain an isotopic signature that trends towards northern Alberta basement rocks (Figure 20).

10.4 Emplacement Age Results

The sample location and description of the mineral separates selected for U-Pb and Rb-Sr isotopic analysis are presented in Table 10. Nine perovskite and four rutile fractions were selected from four different pipes (K6, Legend, Phoenix and Kendu) for U-Pb analysis. Six phlogopite samples were selected from the Phoenix and Kendu pipes for Rb-Sr analysis. Fresh rutile picked from the Kendu pipe is characterized by two different morphological and colour populations: dark brown to black subhedral grains and amber to light orange angular fragments.

The results of isotopic analysis on mineral separates from this study are presented in Table 11. Problems encountered during emplacement age dating in this study are generally attributed to:

- the current lack of rock available from the BHH for mineral processing and minerals separation, which resulted in low initial fraction weights,
- not having the right mineral constituents available in the rock, or in the case of perovskite, the mineral being too small to properly identify, and/or isolate

Table 10A. Samples selected for U-Pb perovskite and rutile isotopic analysis.

Sample number	Pipe name (general	Drill hole number	Depth (m)	Easting (m)	Northing (m)	Zone	Mineral separate	Paramagnetic fraction (A)	Number of grains	Description
ABK-29-1	K6 (BHH)	Outcrop	0-outcrop	585317	6308651	11	Perovskite	0.4	35	Dark black, irregular grains with whitish alteration (possibly carbonate-coating on spinels)
ABK-29-2	K6 (BHH)	Outcrop	0-outcrop	585317	6308651	11	Perovskite?	0.3	150	Very small (<10 um), cubic, black grains; some with whitish alteration
ABK-59-1	Legend (BM)	98DH-LE01	44	386200	6340600	12	Perovskite?	0.45	100	Small (<20 um), cubic, black grains; some with whitish alteration
ABK-75-1	Phoenix (BM)	98DH-PH01	105	351500	6330580	12	Perovskite	0.6	25	Large, brown, broken and 'scorched' grains; no alteration
ABK-75-2	Phoenix (BM)	98DH-PH01	105	351500	6330580	12	Perovskite	0.6	50	Smaller, cubic to sub-rounded cubic, altered perovskite (salt [Ca-rich] and pepper [ilmenite] texture)
ABK-76-1	Phoenix (BM)	98DH-PH01	130	351500	6330580	12	Perovskite	0.45	40	Fresher than ABK-75; Large, black, cubic, lustrous grains with slight whitish alteration
ABK-76-2	Phoenix (BM)	98DH-PH01	130	351500	6330580	12	Perovskite	0.45	200	Smaller, cubic to sub-rounded, brown to black cubes
ABK-76-3	Phoenix (BM)	98DH-PH01	130	351500	6330580	12	Perovskite		50	Fresher than ABK-75; Large, brown, cubic grains with slight whitish alteration
ABK-81-1	Kendu (BM)	Kendu	102	368567	6353618	12	Perovskite	0.45	67	Large, sub-rounded to rounded, brownish-black, altered
ABK-82-1	Kendu (BM)	Kendu	127.25	368567	6353618	12	Rutile	0.6	27	Brown, semi-transparent and angular
ABK82-2	Kendu (BM)	Kendu	127.25	368567	6353618	12	Rutile	0.6	30	Light brown-orange (amber), semi-transparent, and angular
ABK82-3	Kendu (BM)	Kendu	127.25	368567	6353618	12	Rutile	0.6	50	Light brown-orange (amber), semi-transparent, and angular
ABK82-4	Kendu (BM)	Kendu	127.25	368567	6353618	12	Rutile	0.6	50	Brown, semi-transparent and angular

Table 10B. Samples selected for Rb-Sr phlogopite isotopic analysis.

Sample number	Pipe name (general	Drill hole number	Depth (m)	Easting (m)	Northing (m)	Zone	Mineral separate	Description
ABK-75-1	Phoenix (BM)	98DH-PH01	105	351500	6330580	12	Phlogopite	Single, subhedral macrocrysts; sulfide and apatite inclusions
ABK-76-1	Phoenix (BM)	98DH-PH01	130	351500	6330580	12	Phlogopite	Single, subhedral macrocrysts; sulfide and apatite inclusions
ABK-81-1	Kendu (BM)	Kendu	102	368567	6353618	12	Phlogopite	Single, subhedral macrocrysts; minor chloritization
ABK-82-1	Kendu (BM)	Kendu	127.25	368567	6353618	12	Phlogopite	Single, subhedral macrocrysts; minor chloritization

* BHH – Buffalo Head Hills, north-central Alberta; BM – Birch Mountains, northeastern Alberta

Table 10. Sample location and description of isotopic analysis on mineral separates from kimberlitic rocks in northern Alberta.

Table 11A. U-Pb perovskite and rutile.

Sample	Weight (ug)	U (ppm)	Th (ppm)	Pb (ppm)	Th/U	Total common Pb (pg)	Radiogenic Pb (pg)	^{206}Pb/ ^{204}Pb	Initial ^{206}Pb/ ^{204}Pb	^{206}Pb/ ^{238}U	^{238}U/ ^{204}Pb	^{207}Pb/ ^{206}Pb	^{207}Pb/ ^{235}U	^{206}Pb/ ^{238}U	Age ^{207}Pb/ ^{235}U	Age ^{206}Pb/ ^{238}U
K6 - perovskite																
ABK-29-1	78	19.9	1548.3	7.5	77.87	169.5	417.1	27	20.2±0.27	0.01436±3.1	601.9±15	0.0393±96	0.0779±190	0.01436±31	76.1±17.8	91.9±2.0
ABK-29-2	12	28.6	450.9	2.8	15.76	32.3	0.7	21	17.4±2.7	0.00324±13	886.1±597	0.0455±612	0.0203±286	0.00324±130	20.4±28.1	20.8±8.3
Legend - perovskite																
ABK-59-1	13	32.9	51.4	2.1	1.57	30.9	\	27	20.1±0.7	0.00897±3.7	1199.6±261	0.0399±163	0.0494±206	0.00897±37	48.9±19.7	57.6±2.4
Phoenix -perovskite																
ABK-75-1	432	122.5	8305.5	37.0	67.80	3405.4	12581.1	31	19.3±0.4	0.01242±1.9	974.9±2.6	0.0385±67	0.0660±115	0.01242±19	64.9±10.9	79.6±1.2
ABK-75-2	235	112.5	2987.7	19.0	26.56	1822.8	2636.5	29	18.6±0.4	0.01170±2.6	911.2±8.8	0.0344±119	0.0556±195	0.01170±26	54.9±18.3	75.0±1.6
Phoenix - perovskite																
ABK-76-1	80	122.0	2301.1	16.4	18.86	585.7	723.8	31	18.9±0.4	0.01203±1.8	1043.8±2.7	0.0378±63	0.0627±104	0.01203±18	61.7±9.9	77.1±1.1
ABK-76-2	325	119.7	2076.5	15.4	17.37	2435.1	2565.5	31	19.8±0.4	0.01213±2.1	1002.79±6.5	0.0420±83	0.0702±142	0.01213±21	68.9±13.4	77.7±1.3
ABK-76-3	128	131.0	3017.6	18.5	23.04	974.4	1394.2	32	19.9±0.4	0.01211±1.7	1087.8±6.2	0.0433±62	0.0724±104	0.01211±17	71.0±9.8	77.6±1.1
Kendu - rutile																
ABK-82-1*	334	8.8	\	0.3	\	55.0	31.8	67	17.3±2.1	0.01453±5	3900.8±366	0.0509±19	0.1019±39	0.01453±5	98.6±3.6	93.0±0.3
ABK-82-2**	530	9.0	\	0.3	\	104.0	55.0	56	8.9±1.7	0.01240±12	2999.9±78.3	0.4819±23	0.0822±39	0.01239±13	80.2±3.7	79.4±0.8
ABK-82-3**	441	8.4	\	0.2	\	35.0	53.2	131	31.1±3.8	0.01440±6	7803.4±726.5	0.0532±12	0.1057±25	0.01440±6	101.9±2.3	92.2±0.4
ABK-82-4*	945	8.6	\	0.3	\	166.0	117.5	61	20.5±1.3	0.01354±12	3150.8±50.7	0.0528±20	0.0986±37	0.01354±12	95.5±3.4	86.7±0.8
* Brown rutile; ** Light brown-orange rutile																

Table 11B. Rb-Sr phlogopite

Sample	Rb (ppm)	Sr (ppm)	^{87}Rb/^{86}Sr	^{87}Sr/^{86}Sr corrected	Initial ^{87}Sr/^{86}Sr	+-2sm	T Ma (0.7025)	T Ma (0.705)	T Ma (0.710)
Phoenix									
ABK-75-PHL3	383.19	80.10	13.8603	0.719431	0.705446	0.000040		73.29	
ABK 75 RG*	381.07	230.14	4.7932	0.710495	0.705658	0.000019	117.36	80.68	7.27
ABK76-PH1-1	378.25	67.51	16.2325	0.718192	0.701813	0.000036		57.21	
ABK 76 RG	367.85	61.30	17.3882	0.719067	0.701522	0.000016	67.06	56.95	36.71
Kendu									
ABK 81 phl-1	170.06	27.56	17.8834	0.723870	0.705826	0.000016	84.10	74.27	54.60
ABK 82 phl-1	310.31	93.86	9.5778	0.718440	0.708776	0.000096	117.10	98.75	62.03
* RG = re-ground phlogopite									

Table 11C. Sr perovskite.

Sample	^{87}Sr/^{86}Sr corrected	+-2sm
Phoenix		
ABK-75 Perov	0.704786	0.000019

▨ Robust model age

▣ Recommended model age

Table 11. Results of U-Pb perovskite, U-Pb rutile, Rb-Sr phlogopite and Sr perovskite isotopic analysis for northern Alberta kimberlitic rocks. All errors reported to 1 sigma.

- alteration associated with the mineral separates (e.g., incipient chloritization of phlogopite macrocrsyts).

Sample ABK29-1 from the K6 pipe has an initial sample weight of 78 μg, Th/U ratio of 77.9, which is typical of perovskite, and 417 and 169 pg of radiogenic and common lead, respectively. Therefore, the recommended emplacement age for the K6 pipe is a $^{206}Pb/^{238}U$ date of 91.9±2.0 Ma (Table 11, Figure 24A). This age is similar to, but slightly older, than the 88±5 to 86±3 Ma U-Pb perovskite emplacement dates for the BHH K5, K7A and K14 pipes reported by Skelton et al. (2003). In order to verify and improve upon the robustness of this age, it is recommended that this analysis be duplicated with follow up age dating because perovskite ABK29-1 contains low U (19.9 ppm) and a fairly low $^{238}U/^{204}Pb$ ratio (603; see explanation below) compared to typical kimberlite perovskite (e.g., Heaman et al., 2003).

From the selected NAKP pipes, perovskite fractions ABK29-2 and ABK59-1 are examples of U-Pb analyses that are the most sensitive to the choice of initial common Pb correction. The magnitude of this correction is largest for perovskite fractions with small fraction weights (<50 μg), low U and hence low radiogenic Pb concentrations (i.e., <30 ppm U) and young crystallization ages (i.e., <200 m.y.). For example, Heaman (1989) has shown that changing the initial $^{206}Pb/^{204}Pb$ isotopic composition by 5% can shift the calculated $^{206}Pb/^{238}U$ age by up to 16 Ma in young, low radiogenic Pb perovskite. Sample ABK29-2, which is also from the K6 pipe, has a low initial sample weight (12 μg), low U (28.6 ppm), and very low radiogenic Pb (0.7 pg), and therefore, yielded an erroneous emplacement age of 20.8±8.3 Ma. In addition, sample ABK29-2 perovskite grains were very small (<10 μm), making it difficult to ensure that 100% of the selected grains were in fact perovskite. Sample ABK59-1 from the Legend pipe yielded an emplacement age of 57.6±2.4 Ma, which is significantly lower than the 77.6±0.8 Ma Rb-Sr phlogopite date reported by Aravanis (1999). The 57.6±2.4 Ma date obtained for sample ABK59-1 is also suspect as it has a low initial sample weight of 13 μg, very little radiogenic Pb, low U (32.9 ppm), and there is some uncertainty whether all the selected grains were in fact perovskite.

As a measure of reproducibility of the U-Pb perovskite procedure in cases where there is abundant relatively large crystals (>30 μm) present, three perovskite fractions (ABK76-1, ABK76-2 and ABK76-3) from the Phoenix kimberlite yielded identical $^{206}Pb/^{238}U$ dates of 77.1±1.1, 77.7±1.3 and 77.6±1.1 Ma (2σ level), respectively (Figure 24B). In addition, two

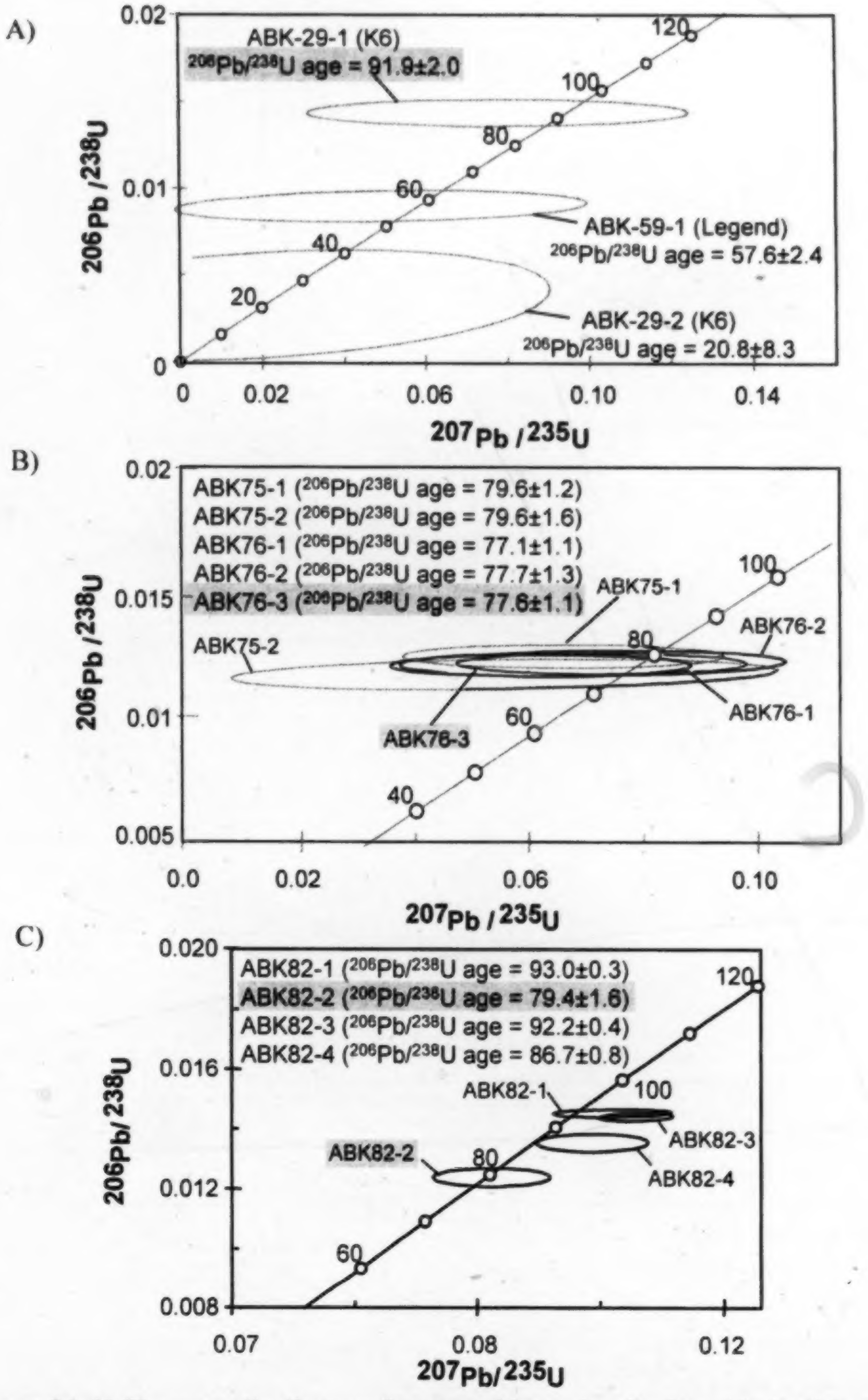

Figure 24. U-Pb concordia diagram for perovskite and rutile from kimberlitic rocks in northern Alberta. A) perovskite from the K6 and Legend pipes; B) perovskite from the Phoenix pipe; and C) rutile from the Kendu pipe. Shaded samples are recommended model age for K6 and Phoenix, and best estimate upper emplacement age for Kendu.

perovskite fractions (ABK75-1 and ABK75-2) yielded ages of 79.6±1.2 and 75.0±1.6 Ma and at 2σ, are within error of the 77 Ma date. Thus, a robust weighted average $^{206}Pb/^{238}U$ date of 77.6±1.1 Ma is suggested for the emplacement age for the Phoenix pipe. This date is older than previously reported ages of 70.3±1.6 and 70.9±0.4 Ma by U-Pb perovskite and Rb-Sr phlogopite, respectively (Aravanis, 1999). This is possibly the result of separate eruption events, which have subsequently mixed in the crater environment, and further analyses are needed to resolve the disparity in these age determinations.

Rutile was analyzed on the premise that rutile has a low closure temperature to Pb diffusion (approximately 400° C), and xenocrystic rutile formed under normal mantle conditions should be reset to the time of kimberlite entrainment. To our knowledge, this is the first attempt to apply U-Pb mantle rutile age determinations to estimate the emplacement age of a kimberlite. The best "estimate" for the emplacement age of the Kendu pipe is from the light brown-orange rutile fraction ABK82-2, which yielded a $^{206}Pb/^{238}U$ date of 79.4±1.6 Ma (2 sigma). This age should be considered as an upper limit on the emplacement age because other Kendu rutile fractions yielded older U-Pb isotope ages (up to 93.0±0.3 Ma for sample ABK82-1; Figure 24C), suggestive of an 'older' rutile component. This supposition is supported by the preliminary investigation of eclogitic xenoliths from the Kendu pipe by Eccles (unpublished data, 2003), which indicate that the proportion of xenoliths are 20% garnet websterite, 70% transitional Group B and C eclogite and 10% metamorphic eclogite. Therefore, it is likely that the rutile fractions analyzed have multiple origins, which may include mantle and upper crust rutile components. The results of this first attempt to determine U-Pb mantle rutile ages are encouraging and future studies should combine U-Pb age determinations with geochemical analyses on the same rutile grain(s) in an effort to distinguish between crustal and mantle-derived rutile.

The Rb and Sr concentrations of the phlogopite did not yield sufficiently high Rb/Sr ratios to be considered ideal for robust ages determinations because model age calculations for low Rb/Sr phlogopite are quite sensitive to the initial Sr composition used. The Rb concentrations are typical for kimberlite phlogopite (between 170 and 383 ppm), but the Sr content is very high (up to 230 ppm) relative to Sr levels from successfully dated phlogopites (generally <50 ppm; Brown et al., 1989; R. Creaser, personal communication). As a result, the phlogopite Rb-Sr results yielded ambiguous dates for the Phoenix and Kendu pipes. Four phlogopite Rb-Sr analyses from the Phoenix pipe yielded emplacement age dates of between 57 and 81 Ma. Because samples ABK75 and ABK76 are sampled at close intervals, 105 and 130 m, respectively, the variation in emplacement ages seem unlikely. In an attempt to reduce the Sr content, two samples (ABK75-

RG and ABK76-RG) from the Phoenix pipe were reanalyzed after grinding the phlogopite and subjecting the pulverized phlogopite to a longer (4 hour) 0.75N HCl leach. The experiment did not work as anticipated. The Sr content of the ABK76-RG sample is slightly lower, however the Sr content in ABK75-RG is significantly higher (230 ppm) versus the initial ABK75 analysis (80 ppm). The high Sr contents of Phoenix and Kendu phlogopite is likely due to incorporation of carbonate and/or other Ca-bearing minerals as inclusions in phlogopite that are not easily removed during sample preparation. A similar conclusion was proposed for high Sr content in late-crystallizing groundmass phlogopite by Smith et al. (1985a). Finally, Schmidt et al. (1999) reported that phlogopite is able to store significant amounts of Rb, Cs and Ba in the lithospheric mantle resulting in the radiogenic evolution of Sr.

When the combined phlogopite and whole-rock isotopic data from the Phoenix and Kendu pipes are plotted on the Rb-Sr isochron diagram (Figure 25), a three-point isochron for sample ABK75 yielded the 'best' model age of 69.4±0.1 Ma with an mean square of weighted deviates (MSWD) of 0.105. This age is relatively close to the U-Pb perovskite dates for the Phoenix pipe (between 70 and 79 Ma; Aravanis, 1999; this study), and as such, the use of phlogopite in determining age dates for the northern Alberta pipes should be further explored.

A compatible Rb-Sr phlogopite-whole rock versus U-Pb perovskite date could not be substantiated for ABK76, which has a Rb-Sr three-point isochron of 55±1 Ma with an unsatisfactory MSWD of 5.8. The shallower slope associated with sample ABK76 may be related to the narrow range of ^{87}Rb/^{86}Sr relative to sample ABK75 (Figure 25A). Perovskite from ABK76 has a lower ^{87}Sr/^{86}Sr ratio (0.7048) than the whole rock. When the ABK76 perovskite ratio is substituted for the whole rock ^{87}Sr/^{86}Sr ratio, sample ABK76 yielded a slightly older age of 57.9±3.5 Ma with an MSWD of 14. The whole rock ^{87}Sr/^{86}Sr may therefore, be too high and results in anomalously younger isochron dates.

With respect to the relative younger ages obtained by the phlogopite, there is a danger in the use of macrocryst phlogopite because the origins of such mica are enigmatic as to whether they are cognate inclusions or xenocrysts of variable origins (e.g., Clement, 1982; Dawson and Smith, 1975). Creighton and Eccles (2003) observed that some of the Phoenix kimberlite phlogopite macrocrysts show a zoning relationship from Fe- and, relatively, Al-rich cores (approximately 2 and 2.8 cations per structural formula, respectively) to Fe- and, relatively, Al-poor phlogopite mantles. If these complexly mantled phlogopites represent Fe-rich phlogopite xenocrysts mantled by primary kimberlite phlogopite overgrowths, then the phlogopite age of a composite macrocryst

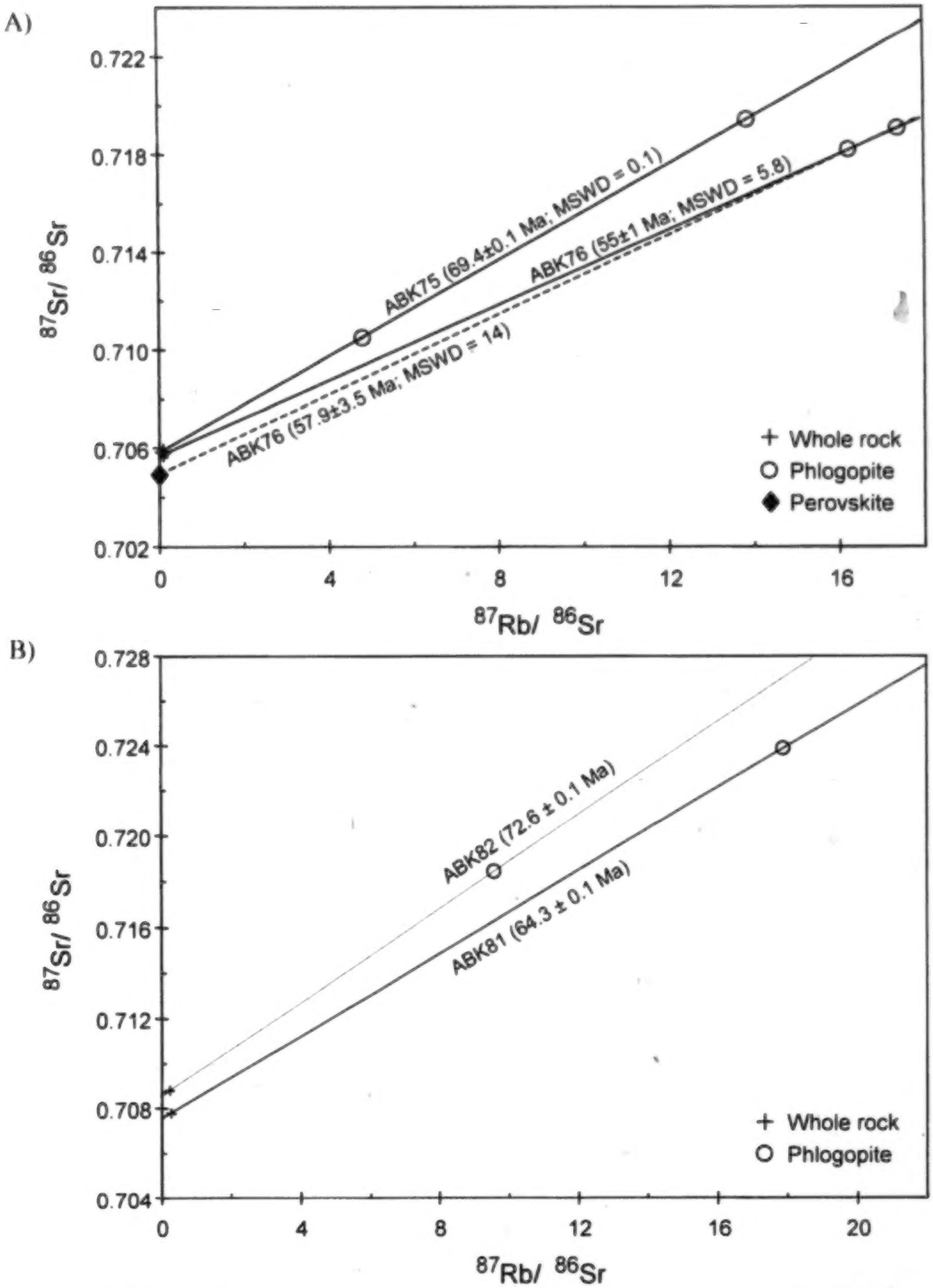

Figure 25. Rb-Sr isochron diagram for whole-rock and phlogopite macrocrysts from selected kimberlitic rocks in northern Alberta. A) three-point isochrons for samples ABK75 and ABK76 from the Phoenix pipe; and B) two-point tie line for samples ABK81 and ABK82 from the Kendu pipe. Regression method from Ludwig (2000).

should be between the age of kimberlite growth and the older age of the xenocryst phlogopite (i.e., older than the age of the kimberlite emplacement as determined by repeatable and robust U-Pb perovskite ages). It is concluded, therefore, that the young Rb-Sr phlogopite ages require post kimberlite emplacement alteration of phlogopite.

Two-point whole-rock and phlogopite isochrons from Kendu samples ABK81 and ABK82 yielded ages of 64.3±0.1 Ma and 72.7±0.1 Ma, respectively. The latter age is slightly younger than the estimated upper emplacement age constraint based upon the U-Pb rutile age of 79.4±1.6 Ma and thus, cannot eliminate the possibility that the Rb-Sr phlogopite whole rock ages are slightly too young for the same arguments used to explain the relatively young Rb-Sr phlogopite ages obtained for the Phoenix kimberlite (discussed above). Therefore, the best estimate for the emplacement age of the Kendu pipe should be constrained between 64.3±0.1 and 79.4±1.6 Ma.

10.5 Temporal and Spatial Associations between Western North America Kimberlite Fields

Table 12 is a compilation of northern Alberta kimberlitic pipe emplacement ages, available to date. The emplacement age of the NAKP is Late Cretaceous (Coniacian to Maastrichtian). The K5, K7A and K14 kimberlites from the Buffalo Head Hills field have reported emplacement ages of between 86±3 to 88±5 Ma by U-Pb perovskite (Carlson et al., 1998; Skelton et al., 2003; Heaman et al., 2003). The Birch Mountains pipes are younger: the Phoenix, Dragon, Xena, Legend, Valkyrie and Kendu pipes have emplacement ages of between 70.3±1.6 to 79.4±1.6 Ma as determined by U-Pb perovskite/rutile and Rb-Sr phlogopite (Aravanis, 1999; this study). Palynological results are consistent with emplacement ages for the Mountain Lake pipes of 75-76 and 68 Ma from *in situ* laminated sediments (Leckie et al., 1997) and from non-marine sedimentary clasts (Wood et al., 1998), respectively. Therefore, the Mountain Lake pipes are similar in emplacement age to the Birch Mountains.

The compilation of NAKP emplacement ages allows for the comparison with other North American kimberlite fields. Based on the distribution of the three fields and emplacement ages, which range between 92-68 Ma, the NAKP can be classified as a Type 2 province, defined by Mitchell (1986) as a province consisting of several kimberlite fields of similar age. Because the northern Alberta diamond play is young (<15 years old), the NAKP may change into a Type 3 province, or a province with multiple fields and ages, pending the discovery of kimberlites of differing age.

Area	Pipe	Depth (m)	Age (Ma)	Method	Reference
Mountain Lake	Mountain Lake	N/A	68	Palynology	Wood et al. (1998)
Mountain Lake	Mountain Lake North	Various depths	75 to 76	Palynology	Leckie et al. (1997)
Mountain Lake	Mountain Lake South	N/A	74±7 to 78±9	Apatite fission track (central age)	Leckie et al. (1997)
Mountain Lake	Mountain Lake North	N/A	72±7	Apatite fission track (central age)	Leckie et al. (1997)
Birch Mountain	Phoenix	113.9	70.3±1.6	U-Pb perovskite	Aravanis (1999)
Birch Mountain	Phoenix	113.9	70.9±0.4	Rb-Sr phlogopite	Aravanis (1999)
Birch Mountain	Phoenix	130.0	77.6±1.1	U-Pb perovskite	This study
Birch Mountain	Dragon	142.5	72.4±0.9	Rb-Sr phlogopite	Aravanis (1999)
Birch Mountain	Xena	157.4	72.6±2.1	Rb-Sr phlogopite	Aravanis (1999)
Birch Mountain	Valkyrie	158.2	75.8±2.7	U-Pb perovskite	Aravanis (1999)
Birch Mountain	Legend	29.8	77.6±0.8	Rb-Sr phlogopite	Aravanis (1999)
Birch Mountain	Kendu	127.3	79.4±1.6	U-Pb rutile	Best, not absolute, age from this study
Buffalo Head Hills	K7A	N/A	86±3	U-Pb perovskite	Skelton et al. (2003); Heaman et al. (in press)
Buffalo Head Hills	K14	N/A	88±5	U-Pb perovskite	Skelton et al. (2003); Heaman et al. (in press)
Buffalo Head Hills	K5	N/A	87±3	U-Pb perovskite	Skelton et al. (2003); Heaman et al. (in press)
Buffalo Head Hills	K6	0	91.9±2	U-Pb perovskite	This study

N/A – Not available

Table 12. Age compilation for northern Alberta kimberlitic rocks.

Heaman and Kjarsgaard (2000) and Heaman et al. (2003) compiled emplacement ages for kimberlite and associated rock types throughout North America. Based on the distribution of fields and emplacement histories, Heaman et al. (2003) separated North America Phanerozoic kimberlite magmatism into three physiographic regions:

1. Eastern province: Jurassic (140-180 Ma) magmatism in Ontario (176-180 Ma Attawapiskat, 146-166 Ma Kirkland Lake and 134-155 Ma Timiskaming) and New York (145-176 Ma Finger Lake);
2. Central province: Cretaceous magmatism in Saskatchewan (95-101 Ma Fort à la Corne) and the Northwest Territories (94-103 Ma Somerset Island); and
3. Western province: defined as multiple kimberlite fields with a variety of emplacement ages, including Eocene, Cretaceous, Jurassic, Silurian and Cambrian emplacement between approximately 50 and 540 Ma in the Slave craton, Northwest Territories, and Tertiary (48 Ma), Devonian (386-400 Ma) and Neoproterzoic (615 and 780 Ma) emplacement in the Wyoming craton, Colorado, Wyoming and Montana.

With respect to the kimberlite emplacement regions of Heaman et al. (2003), the 92-68 Ma NAKP classifies as either: 1) an isolated field of Cretaceous-aged magmatism within the Type 3 'western province', or 2) is a western extension of the Cretaceous 'central corridor, albeit with an extension into the Late Cretaceous (i.e., from 103-94 Ma to 103-75 Ma). Combining the NAKP with the Cretaceous central-region may fit better with worldwide kimberlite events. For example, Heaman et al. (2003) reported that 69 of 95 dated South African kimberlites have emplacement ages in the range of 116-70 Ma, with a noticeable hiatus between 100-95 Ma.

11 Discussion: Petrogenetic Considerations for the Northern Alberta Kimberlite Province

11.1 Evolution of Kimberlitic Magma

Petrographic and geochemical evidence presented in this study leads to the general conclusion that the BHH and BM fields are composed of primitive and evolved kimberlite, respectively, and the ML pipes are not archetypal kimberlite, but their geochemistry is similar to alkali olivine basalt/basanite. The simplest way to interpret a volcanic province containing fields that exhibit a distinctive style of potassic magmatism is to postulate that the different fields are derived from different sources. The following section uses the data and interpretations presented in this study, together with current theories for kimberlite generation, to discuss the roles of source composition, mantle metasomatism and magmatic differentiation in the generation and evolution of the NAKP magmas.

11.1.1 Source Composition

Kimberlite magmas, which must be derived from depths of at least 100 to 200 km in order to incorporate diamond and garnet peridotite, provide an unparalleled opportunity to investigate the formation and evolution of deep-seated magmas. Experiments to determine the phase equilibra involving incipient melting of upper mantle are difficult because it is hard to maintain equilibrium and the melts generated are invariably modified upon quenching. However, reducing the number of components (e.g., CaO-MgO-SiO_2-CO_2 system, Wyllie and Huang, 1975; CaO-MgO-Al_2O_3-SiO_2-CO_2 system, Dalton and Presnall, 1998a,b) and hence the variance of the system, has allowed for the more accurate determination of melt compositions, including those melting paths where very small amounts of liquid are present.

These experiments provide useful information of how melt compositions, in those modal systems, change with pressure and temperature, and have shown that the presence of CO_2 and H_2O in peridotitic systems profoundly affects melting temperatures, phase relations (e.g., Wyllie, 1979), and the compositions of the partial melt produced (Eggler and Wendlandt, 1979). In general, the effect of dissolved H_2O is to shift partial melts toward more silica-rich compositions that favor generation of tholeiitic basalt- and andesite-type partial melts. In contrast, dissolved CO_2 shifts phase boundaries toward more silica-poor compositions typical for high-pressure, low-degree mantle melts. High pressure partial melting of carbonated peridotite, therefore, seems a prerequisite for the generation of kimberlite.

11.1.2 Magmatic Differentiation

In the NAKP, it is proposed that: 1) partial melting has occurred in diverse asthenospheric and/or lithospheric assemblages, and 2) kimberlite magma in the sub-continental mantle has been subjected to magmatic differentiation in the source regions during generation and mobilization. Geochemical data, particularly isotopic compositions, presented in this study support the contention that magmatism in the NAKP is derived from both asthenospheric and lithospheric sources. For example, the K6 (BHH), Legend and Phoenix (BM) pipes have positive ε_{Nd} (0 to +2.7), while the K4 (BHH) and Kendu (BM) pipes have negative ε_{Nd} (-4.0 to –6.3), which have been ascribed to asthenospheric and lithospheric sources, respectively (e.g., Smith, 1983). Because the ML pipes are geochemically similar to olivine alkaline basalt/basanite, it is assumed that the ML magmas were also derived from a shallower lithospheric source. In order to explain the diversity of the kimberlitic magmas in the NAKP, changes in the mantle source region or magma compositions must now be considered.

Magmatic differentiation may be defined simply as any process by which magma is able to diversify and produce a magma or rock of different composition. Various processes have been suggested to explain the variation of magma compositions observed within small regions. Among these processes are:

- Differences in mineralogy and composition of the source region
- Differences in degree of partial melting of a uniform source
- Mantle metasomatism, which would influence the two previous processes
- Mixing of two or more magmas
- Crystal fractionation
- Assimilation/contamination
- Liquid immiscibility

With respect to processes responsible for the formation of the NAKP kimberlite magmas, any single, or combination, of these processes could act to produce chemical diversity, but the following discussion will focus on partial melting, mantle metasomatism and crystal fractionation.

11.1.2.1 Partial Melting

Rare earth element profiles (Figure 13) show that the majority of the BHH and BM kimberlites are products of either very low degree partial melting or larger degrees of partial melting of an enriched source, as defined by their LREE enriched patterns in comparison to the HREE. Based on the REE, the Phoenix (BM) pipe has the highest La (1400 times chondrite abundance) and La/Yb ratio (435) in this dataset, and therefore, the lowest degree of partial melting in the NAKP. In contrast, ML, K4 (BHH), and Xena and Kendu (BM) have a much flatter REE profile and therefore, may be products of a higher degree of partial melt. However, LREE enrichment to values >200 times chondrite abundance cannot be produced by low degress of partial melting of a primitive peridotitic source alone, as unreasonably low degrees of partial melting (<0.1 %) would be required (e.g., Dawson, 1984; Mitchell, 1986). An additional factor is required, which most likely is partial melting of sources that were affected by variable degrees of metasomatic enrichment.

Finally, the chondrite-normalized REE patterns show that varying degrees of intra-field partial melting may only be relevant to the BM. The BHH samples have a uniform or parallel REE pattern suggestive of fractional crystallization processes, where the distribution or spread of the LREE ($La_{max-min}$) is approximately proportional to the spread of HREE ($Lu_{max-min}$; Figure 13B). In contrast, the BM samples have a larger LREE ($La_{max-min}$) spread than their HREE ($Lu_{max-min}$; Figure 13C). This suggests varying degrees of partial melting for kimberlites in the BM with the Phoenix pipe having the smallest degree of partial melting, followed by Valkyrie, Pegasus, Legend, and finally, the Kendu pipe, which represents the highest degree of partial melting in the BM.

11.1.2.2 Mantle Metasomatism

The unusually high enrichment of incompatible elements in kimberlite is not wholly satisfied by differentiation mechanisms or by very small degrees of partial melting of mantle peridotite. Because increased degrees of partial melting would dilute the incompatible element compositions by dissolution of silicate components, the degree of partial melting in kimberlite magmas must be very small (a few percent, at most). Mantle metasomatism, where sub-continental mantle has been subjected to various enrichment events before or penecontemporaneous to kimberlite formation, provides a conventional means to explain incompatible element-, H_2O- and carbonate-enrichment in kimberlite. Subsequent partial melting could then produce silica-undersaturated and incompatible element-enriched alkaline liquids.

Petrographic and geochemical interpretations presented earlier, such as the isotopic mixing lines between kimberlite and carbonatite (Section 10.2), show that carbonate enrichment is greater in the BM than the BHH. Infiltration of incompatible-rich fluids or melts into refractory peridotite, followed by partial melting of diverse lithospheric metasomatic assemblages, will result in kimberlite fields that exhibit an evolved style of potassic magmatism. Carbonate enrichment in the BM can be explained, therefore, by metasomatism involving carbonic-rich magmas and/or fluids in the upper mantle just prior to, or penecontemporaneous with, kimberlite magmatism. Variations in the metasomatizing fluids and/or the degree of partial melting would create geochemically and petrographically distinctive kimberlites, and help to explain intra-field kimberlite heterogeneity in the BM.

On a cautionary note, Girnis et al. (1995) argue that primary kimberlite magmas originate beneath the lithospheric mantle (possible as deep as the transition zone), but that these magmas have to interact with carbonated peridotite at the base of the cratonic lithosphere to obtain a carbonate fluid saturated character. During subsequent ascent through the lithosphere, these kimberlite magmas experience a massive decrease in the solubility of CO_2 (Brey and Ryabchikov, 1994) and may release in the order of 10-20 wt. % CO_2, with further degassing occurring en route, in particular at near surface conditions. A direct association between carbonate content and mantle metasomatism to explain mineralogical differences between the BHH and BM, may therefore, be misleading as it may only reflect more efficient carbonate loss during ascent for BHH, whereas some of the carbonate was retained for BM (i.e. originally the magmas for both BHH and BM formed under fluid saturated conditions).

11.1.2.3 Crystal Fractionation

The dominant process of magmatic differentiation in igneous systems is often assumed to result from the physical separation of crystals and melt. This process of differentiation is called crystal fractionation and occurs when crystals that form from the melt are separated, which in turn, results in a change in the bulk composition of the remaining melt.

Elements that are removed from the liquid at the expense of crystallization should have their concentrations decrease in the remaining fractionated magma. For example, decreases in MgO and SiO_2 (with Ni and Co) are a good measure of olivine fractionation from kimberlite melts. Figure 26 shows that the majority of the BHH and BM samples fall on an olivine control line in a plot of MgO-SiO_2. This trend suggests that variable degrees of olivine accumulation and fractionation act as the main differentiation process between primitive and evolved kimberlite in the NAKP. This contention is supported by parallel trending intra-field chondrite-normalized REE patterns, particularly for BHH, which indicate crystal fractionation plays a prominent role in the evolution of Group I-type kimberlites in the NAKP. Based on the chondrite-normalized REE patterns (Figure 13) and plot of MgO-SiO_2 (Figure 26),

- BHH samples ABK06 (K7B pipe) and ABK20 (BM2 pipe), and the BM Phoenix pipe samples represent NAKP pipes from their respective fields with the highest degree of olivine fractionation,
- BHH samples with elevated diamond contents, which have been classified previously as the most primitive NAKP kimberlite, are assumed to be the least affected by olivine fractionation/accumulation; these samples are labelled Group A on Figure 26 and correspond to Group A on Figures 10 and 17,
- BHH samples that are affected by olivine accumulation, include: ABK02 (K4B pipe), ABK08 (K11 pipe), and ABK26 and ABK27 (LL8 pipe).

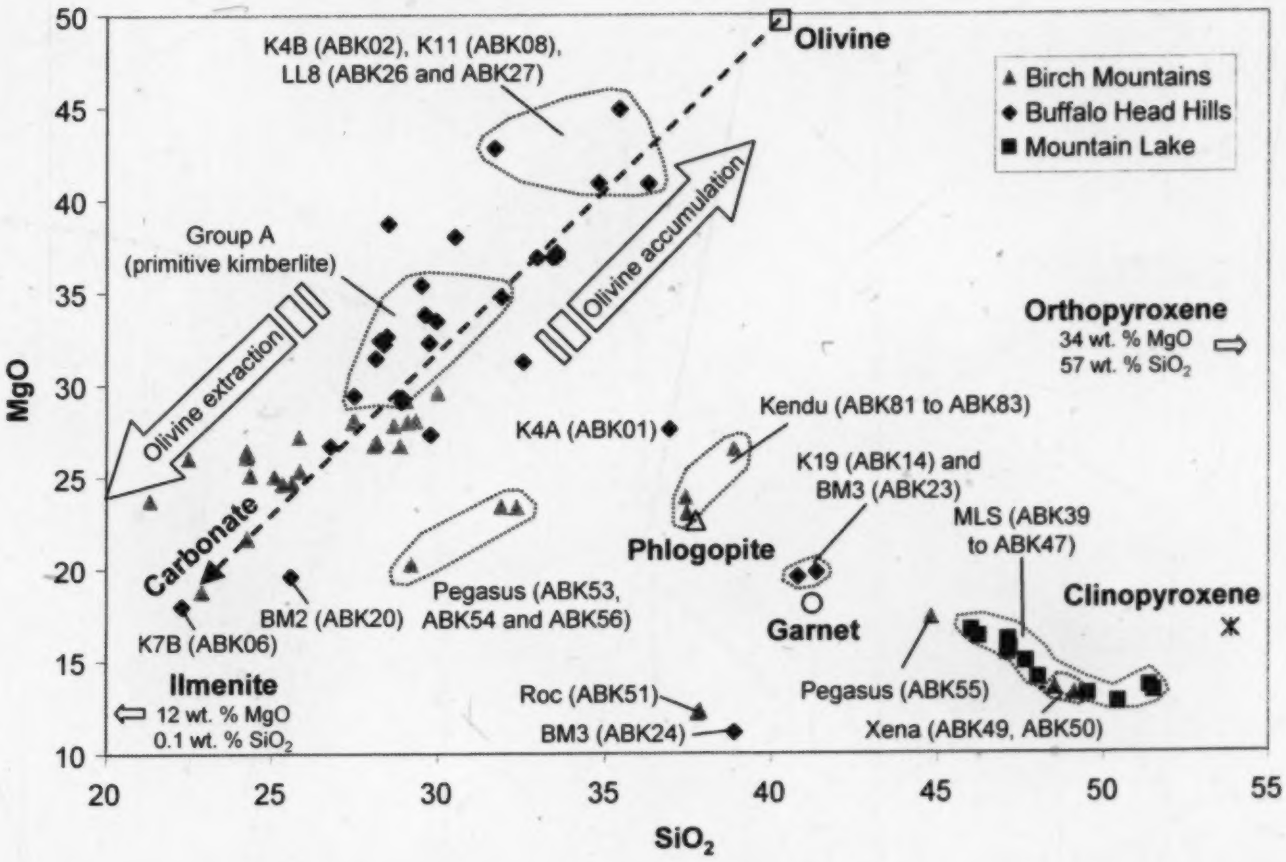

Figure 26. Whole-rock MgO versus SiO_2 for kimberlitic rock samples from northern Alberta. Average olivine, phlogopite, garnet and clinopyroxene are from a variety of northern Alberta pipes (Creighton and Eccles, 2003; Eccles, unpublished data).

Figure 26 shows that Kendu, and the Xena and ML samples do not plot on the kimberlite olivine control-line, but rather as individual outliers with higher SiO_2. Kendu has similar MgO-SiO_2 compositions as phlogopite, which is not surprising given Kendu's high phlogopite content. Mountain Lake and Xena have similar MgO-SiO_2 compositions to clinopyroxene, but this is not supported in macroscopic/microscopic observations. Interestingly, Kendu, ML and Xena exhibit similar trends on the plots of SiO_2 versus various oxide compositions (Figure 6), whereas Kendu plots between the Group 1 NAKP kimberlites, and ML and Xena. This is not interpreted to result from any fractionation control lines between kimberlite, Kendu, ML and Xena, but rather a function of their different source compositions. In addition, any apparent fractionation trends in ML are directly related to increased amounts of country rock contamination shown by increases in Al_2O_3, Na_2O and K_2O, and decreases in Fe_2O_3 and MgO with increasing SiO_2 (Figure 6).

11.2 Geodynamic Controls for Kimberlite Emplacement

A number of contradictory hypothesis have been used to explain the origin of kimberlite. These theories are often specific to a particular region, and therefore, none satisfy a global model for the location of kimberlite provinces in cratonized regions (e.g., Mitchell, 1986). Perhaps this is because each kimberlite province has its own individual or set of controls responsible for the onset of kimberlite magmatism in that specific region.

Knowledge about the geological setting of northern Alberta and information obtained as part of this study can collectively be used to make inferences on emplacement patterns in western North America and possible models that account for their generation. Three models considered in this study include: magmatism formed during the passage of one or more mantle plume hotspot tracks, subduction-related magmatism and deep-seated structures.

11.2.1 Mantle Plume Hotspot Tracks

Heaman et al. (2003) suggested that the majority of Mesozoic and Cenozoic kimberlite magmatism on Earth could be linked to sublithospheric mantle plume hotspot tracks. In eastern North America, Heaman and Kjarsgaard (2000) made genetic links between the Great Meteor Hotspot Track, the relative direction and rate of North American plate motion during the Mesozoic opening of the North Atlantic Ocean, and the age progression of five kimberlite fields that extend for more than 2000 km.

To date, no one has linked hotspot tracks with the northeastward spatial trend of the NAKP or with associated kimberlite fields in western North America. Regionally, the Late Cretaceous

NAKP does not match the location and timing of current predicted continental hotspot tracks, and locally, the NAKP intrafield ages do not support any age progression. The NAKP is located within a few hundred kilometres of the westerly-trending Labrador hotspot track (Morgan, 1983). The timing of the Labrador hotspot under north-central Saskatchewan is similar to the emplacement of the Fort à la Corne kimberlite field (approximately 100 Ma), however, the proposed timing for the Labrador hotspot track under northern Alberta was at approximately 110 Ma (Morgan, 1983), which is significantly older than the oldest known event in the NAKP (92 Ma; this study). To the south of the NAKP, the Yellowstone-Snake River Park (YSRP) hotspot track, which is centrally located in southern Idaho, is significantly younger than the NAKP and has not produced kimberlitic rocks. The YSRP produced 10 to 20 eruptions/Ma between 15.2 and 8.5 Ma and only 2.5 eruptions/Ma during the past 8.5 Ma (Smith and Braile, 1994).

The observation of mantle plume originated structures at the surface is constrained by the fact that the plume signature must penetrate the lithosphere and have persistent mantle support to result in a surficial hotspot expression. It is possible that a hotspot expression has not been established in northern Alberta because the underlying plume is smaller than the large plumes related to continental flood basalts, and therefore, comparable to deep (200-400 km) irregular regions of hot, perhaps partially molten mantle, termed "hot cells" or "hot regions" by Anderson et al. (1992). At this time, however, there is insufficient evidence to evaluate whether there is any temporal-spatial pattern of Cretaceous NAKP magmatism with mantle plume hotspot or hot cell tracks.

11.2.2 Subduction

Bunge and Grand (2000) suggested Mesozoic plate-motion below the northeast Pacific Ocean resulted in low-angle subduction of the Farallon plate under North America, and that its timing is coincident with the landward migration of tectonic activity far inland from the plate boundary. Subduction underneath thick cratonic regions, such as the predominantly Archean craton that underlies most of North America, may influence kimberlite magmatism. This led McCandless (1999) to suggest that the eastward-dipping Farallon plate subduction zone might be accountable for temporal-spatial kimberlitic emplacement patterns observed in North America because a regional southwest-younging trend of kimberlitic magmatism occurs during convergence between the Farallon, Kula and North American plates. At approximately 125 Ma, convergence shifted from east-southeast to northeast causing the onset of Upper Cretaceous to Late Eocene Laramide orogeny (between approximately 90 to 40 Ma), which was responsible for rejuvenated mountain-belt development and affected much of the western edge of North America (Douglas et al., 1969). Several episodes of ultramafic volcanism in western North America formed during, or close to, the Laramide orogeny. From Heaman et al. (2003) and this study, these include,

- 94-101 Ma Fort à la Corne, Saskatchewan;
- 92-68 Ma NAKP;
- 55-48 Ma Lac de Gras area, Northwest Territories;
- 50-54 Ma Bearpaw Mountains, Montana;
- 50-49 Ma Sweet Grass Intrusion.

Thus, it is possible that changes in slab direction during plate motion shifts coincident with the onset of the Laramide orogeny created suitable pathways for influx of enriched sub-slab peridotite. One mechanism that might explain this is the formation of a slab window, or a slab-free region beneath the convergent margin of an overriding plate (Thorkelson, 1996).

11.2.3 Structure

Lineaments interpreted to be continental manifestations of offshore fracture zones (e.g., West Africa; Sykes, 1978), and older continental shear zones (e.g., western Australia; Deakin and White, 1991; White et al., 1995) are important to kimberlite and lamproite location. Despite a Phanerozoic cover that masks most of northern Alberta basement, both of these fault/fracture types are believed to occur in northern Alberta.

- Continental extension of an oceanic transform fault: various mechanisms have been proposed for the origin and development of the Peace River Arch. O'Connell et al. (1990) felt that it is unlikely the arch is a failed rift or a flexural uplift, but formed as the result of the continental extension of an oceanic transform fault. They suggested that the PRA appears to have been uplifted along a single fault trend, "the northern boundary fault", and subsidence along this fault zone controlled the development of the basin to the north of the Arch. The exact location of the northern boundary fault is unknown. Nevertheless, it is interesting that the NAKP fields comprise a northeastward trending belt through northern Alberta, more or less along the eastward projection of the axis of the Devonian Peace River Arch (*see* Figure 1). If the transform fault is extended into northeastern Alberta, then its recognition as a deep-seated fault is supported by its independence to current basement terrane boundaries.

- Continental fault zones: An accretionary model proposed by Ross and Eaton (2002) assumes a style of crustal growth for northern Alberta that involved both tectonic accretion as well as magmatic contributions from the mantle. They proposed that the Buffalo Head and Chinchaga domains were assembled as rifted slivers of the western margin of the Rae Province and were bounded by outward-dipping subduction (Figure 27). Asthenosphere-lithosphere interaction and reworking during terrane accretion might develop deep suture zones between older continental blocks (e.g., Rae; Taltson) and younger accreted, or reattached, terranes (e.g., Buffalo Head) that make up the eastern and western parts of the northern Alberta basement, respectively.

With respect to extensional events, tectonic implications between the Laramide orogeny, the Peace River Arch (PRA) and the age of the NAKP have some merit for kimberlite genesis. This observation, in conjunction with the location, orientation and longevity of the Peace River Arch (PRA), has led several authors (e.g., Eccles et al., 2001a; Pana et al., 2001; Pana and Eccles, 2003) to suggest that successive episodes of Late Cretaceous stress accumulation and release resulted in the development of pathways for kimberlite emplacement.

These tectonic adjustments could enact depressurization of deep-seated faults and fractures during extensional periods, induce partial melting and result in the manifestation of kimberlite magmatism. A simplified explanation of the process follows,

- tectonic stress develops due to extensional forces related to major orogenic belts and/or in areas of terrane accretion;
- movement of the blocks along a curved preexisting deep-seated fault, which may be related to the continental extension of oceanic transform faults or continental intraplate stress fields, causes deep material gaps (i.e., a pull-apart void; Dooley and McClay, 1997) that might localize magmatic ascent;
- magmatism occurs as a result of any combination of the following conditions: 1) thermally induced melting as ambient temperatures exceed those of the solidus, 2) adiabatic decompressional melt production resulting from uplift, and 3) addition of volatiles, especially H_2O, from tensional downthrusting of oceanic lithosphere or ancient subducted material which lower the solidus; and

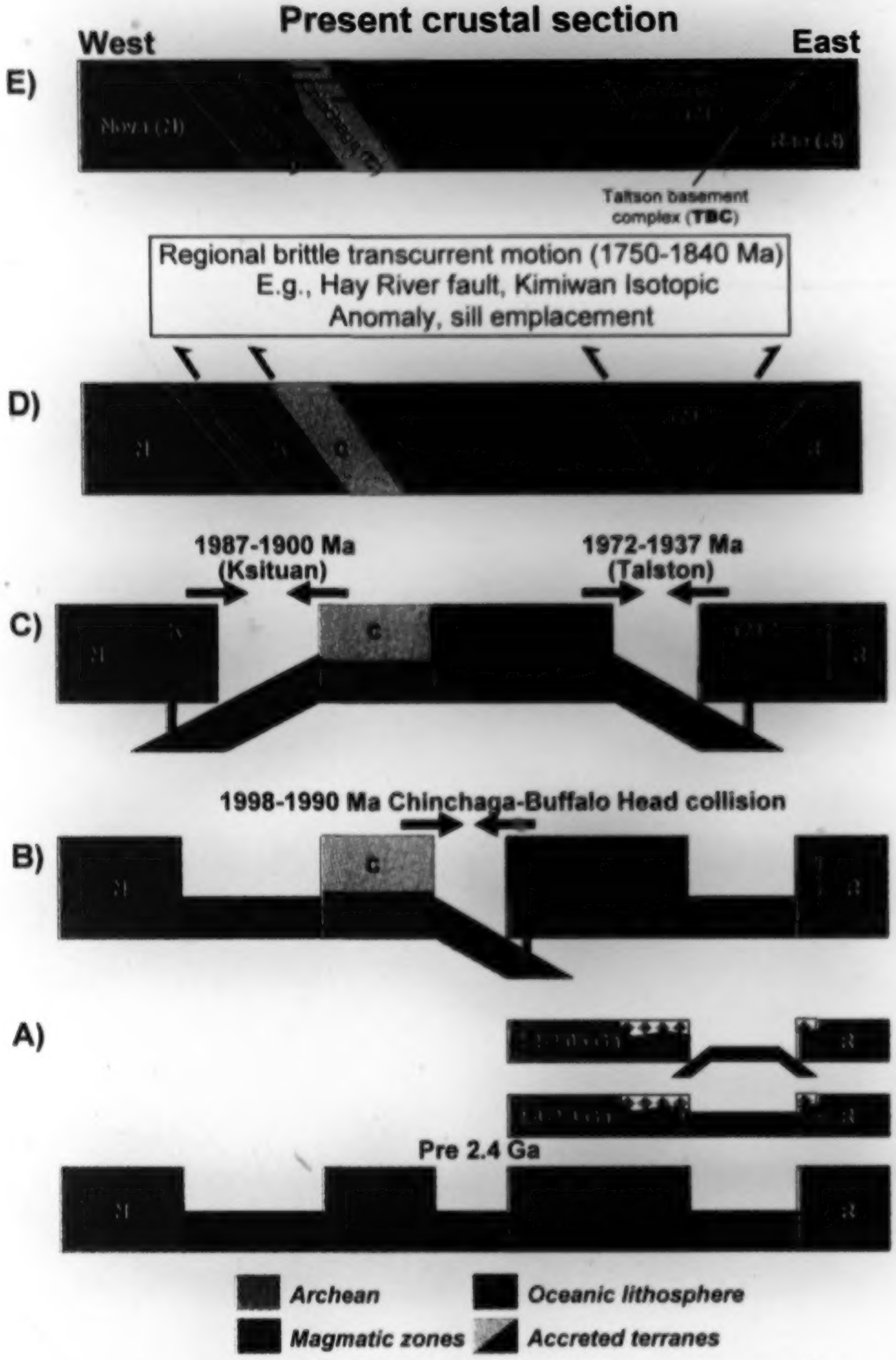
Present crustal section
West
East
E)
Taltson basement complex (TBC)
Regional brittle transcurrent motion (1750-1840 Ma) E.g., Hay River fault, Kimiwan Isotopic Anomaly, sill emplacement
D)
C
1987-1900 Ma (Ksituan)
1972-1937 Ma (Talston)
C)
C
1998-1990 Ma Chinchaga-Buffalo Head collision
B)
C
A)
Pre 2.4 Ga
Archean
Oceanic lithosphere
Magmatic zones
Accreted terranes

Figure 27. Hypothetical evolution of the crust in northern Alberta (Ross and Eaton, 2002; reproduced with permission from the Canadian Journal of Earth Sciences).

- kimberlitic magmas would then be transported through the lithosphere by a magma fracture-conduit flow mechanism if magma temperatures remain high enough to prevent significant amounts of crystallization and magma pressure at any depth exceeds the local lithostatic value (e.g., Spera, 1987). Possible mechanisms include gas fluxion (gas boiling out of kimberlite magma), crack propagation due to volumetric increases during partial melting, diapiric pressures attributed to pressure differences between the top and base of the magma chamber, and/or addition of groundwater to the magma (phreatomagmatic eruption).

Because of the extent of the Phanerozoic sedimentary cover in northern Alberta, any attempt to directly relate structure and the generation of kimberlite magma is at best, speculative. For example, Eccles et al. (2001a) proposed that a deep-seated structure may have initiated kimberlite magmatism in the BHH field, but the only evidence of this is a spatial association between a large (approximately 200 by 180 km) zone of retrograded granulite known as the Red Earth Granulite Domain (REGD; Burwash and Krupicka, 1969, 1970; Burwash and Power, 1990; Burwash et al., 2000) and a dominant, north-trending gravity low. While the REGD facies metamorphism is believed to have occurred ca. 1950 to 1900 Ma (I. Ranger, personal communication, 2003), Eccles et al. (2001a) speculated that subsequent tectonic adjustments associated with the Laramide orogeny might have reactivated deep-seated features in the BHH area. To reiterate, the role of deep-seated structures would then act as pathways for kimberlite emplacement.

12 Final Observations and Conclusions

12.1 General

- Forty-eight ultramafic pipes have been discovered to date in the NAKP: 2 at ML, 38 at BHH and 8 at BM. The best diamond content results to date are from the BHH, where at least 26 of the 38 pipes in the BHH are diamondiferous and three pipes contain estimated grades at >11 carats per hundred tonnes (cpht). The best BHH diamond content result is from kimberlite K252, where a 22.8 tonne mini-bulk sample returned a total of 12.54 carats of diamonds for an estimated 55.0 cpht.

- The size of the pipes, as inferred from geophysical surveys, varies between <1 to 45 ha. The pipes are covered by up to 130 m of bedrock and Quaternary surficial deposits, although several pipes are known to crop out, including the ML south pipe and BHH K5 and K6 pipes.

- The emplacement age of the NAKP is Late Cretaceous (Coniacian to Maastrichtian) between 92-68 Ma based on 11 pipes dated by palynology and/or radiometric techniques (U-Pb perovskite/rutile and Rb-Sr phlogopite). The NAKP can therefore, be classified as a Type 2 province, defined by Mitchell (1986) as a province consisting of several kimberlite fields of similar age. The age of the NAKP is intermediate between neighboring ultramafic fields, which include the 94-101 Ma Fort à la Corne field, Saskatchewan and several fields that range in age from 55-48 Ma (55-48 Ma Lac de Gras area, Northwest Territories; 50-54 Ma Bearpaw Mountains, Montana; and 50-49 Ma Sweet Grass Intrusives, Montana-southern Alberta).

- The oldest NAKP field is the BHH at 92-86 Ma, however, only three of 38 pipes have robust emplacement ages. More age dates are required in the BHH to determine whether modest diamond grades are restricted to a specific period of NAKP magmatism.

- Analysis in this study yielded a weighted average $^{206}Pb/^{238}U$ perovskite date of 77.6±1.1 Ma for the Phoenix pipe. This date is older than previously reported ages of 70.3±1.6 and 70.9±0.4 Ma by U-Pb perovskite and Rb-Sr phlogopite, respectively (Aravanis, 1999). This is possibly the result of separate eruption events, which have subsequently mixed in the crater environment, or that the perovskite fractions analyzed have multiple origins.

- A two-point Rb-Sr phlogopite-whole rock isochron and U-Pb rutile yielded estimated maximum emplacement ages of between 64.3±0.1 and 79.4±1.6 Ma, respectively, for the Kendu pipe. The younger Rb-Sr phlogopite-whole rock age may be suspect because of post kimberlite emplacement alteration of phlogopite. Older U-Pb rutile ages (up to 93.0±0.3 Ma) obtained on morphologically different rutile fractions suggest rutile contributions from multiple sources (i.e., mantle and crustal components). This is the first known attempt to apply U-Pb mantle rutile age determinations to estimate the emplacement age of a kimberlite.

- Analysis in this study yielded a weighted average $^{206}Pb/^{238}U$ perovskite date of 91.9±2.0 Ma for the emplacment age of the K6 pipe. This is the first publicly released date for the K6 pipe, which is similar, but slightly older, than the 88±5 to 86±3 Ma U-Pb perovskite emplacement dates for the BHH K5, K7A and K14 pipes reported by Skelton et al.

(2003). This analysis should be duplicated with follow up age dating because the analyzed perovskite contains low U (20 ppm) and a low $^{238}U/^{204}Pb$ ratio (602).

12.2 Petrological Characteristics

- Pyroclastic kimberlitic (PK) rocks, or juvenile lapilli-bearing olivine tuff, are by far the dominant textural rock type in the NAKP followed by less common resedimented pyroclastic kimberlitic (RVK) rocks. The pipes are volumetrically dominated by olivine, serpentine and carbonate, and are therefore, described as serpentine kimberlite and carbonate-bearing or calcite-serpentine kimberlite.

- The integration of petrography and geochemistry of minimally contaminated volcaniclastic rocks has been used to compare and aid in the classification of ultramafic rocks in three separate areas of the NAKP. The ML, BHH and BM fields can be distinguished from one another by a non-archetypal kimberlite signature (ML) or, in the case of kimberlite fields, primitive (BHH) to evolved (BM) magmatic signatures.

- The lack of whole-rock geochemical overlap between BHH, BM and worldwide kimberlite and the freshest, least contaminated ML rocks reflect significant mineralogical differences and ML is similar geochemically to olivine alkali basalt/basanite. The Xena pipe from the BM also has geochemical affinities similar to the ML pipes.

- The BHH and BM kimberlites have close geochemical affinities with Group I South African kimberlite. Petrographically, the BHH samples are distinct from the BM samples in that they contain less carbonate, have a smaller modal abundance of late-stage minerals such as phlogopite and ilmenite, and have a higher amount of fresh, coarse macrocrystal (>0.5 mm) olivine. Consequently, samples from the BHH have the lowest concentrations of SiO_2, Al_2O_3, V, Y, Pb, Sr and Ga, and the highest values of MgO, Mg#, Cr and Ni, and hence, have similar geochemical properties to primitive kimberlite from the Northwest Territories.

- In contrast to the BHH, the BM pipes are carbonate-rich, relatively devoid of olivine macrocrysts, have higher concentrations of late-stage minerals: ilmenite, rutile, phlogopite and sulphide, and higher high field strength elements (HFSE), all of which are consistent with evolved kimberlite. In comparison to the BHH, the BM pipes have lower SiO_2 and Ni and higher $Fe_2O_{3(T)}$, TiO_2, Nb, V, Sc, Zr, Hf, Y, Ba, Rb, LREE, Ga and Pb. Samples from the Phoenix kimberlite contain the highest concentrations of high field-strength elements (HFSEs) and are interpreted to represent the most evolved kimberlite in this dataset.

- Based on whole-rock isotopic data, the BHH K6 kimberlite has $^{87}Sr/^{86}Sr$ versus ε_{Nd} values similar to those of South African Group I kimberlites. The BM Legend and Phoenix kimberlites have similar ε_{Nd} values (between 0 to +1.9), but distinctly higher $^{87}Sr/^{86}Sr$ values (0.7051 to 0.7063) in comparison to K6. If Phoenix perovskite, which has lower $^{87}Sr/^{86}Sr$ (0.7048), represents a primary crystallizing phase (i.e, not xenocrystic), then Phoenix's more radiogenic whole rock strontium isotopic composition must reflect strontium contribution after perovskite crystallization.

- The K4 (BHH) and Kendu (BM) pipes have a distinctive depletion in compatible elements, lower overall incompatible element abundances, enriched Nd and Sr isotopic signatures relative to bulk Earth, and vermiform-textured antigorite (serpentine) in comparison to the majority of the NAKP pipes. Their isotopic signature is interpreted to be the result of a subcontinental lithosphere component in the mantle source region for these pipes although contamination cannot be ruled out. This is particularly evident for the Kendu pipe, which has a crustal component (anorthosite) and isotopic signature trending towards the isotopic composition of northern Alberta basement rocks.

- Pipes in the BHH with elevated contents of diamonds generally have similar chemistry and contain low TiO_2 (0.45–1.2 wt. %), P_2O_5 (0.22–0.51 wt. %) and Nb (108–189 ppm), and high MgO (26.7–38.1 wt. %), Mg# (87–90), Cr_2O_3 (0.11–0.22 wt. %) and Ni (1007–1621 ppm). These kimberlites are designated the most 'primitive' magma in the NAKP. These data may be used as an evaluation tool for future discoveries in the BHH area and possibly elsewhere in Alberta, if the discovery material is subject to minimal contamination.

12.3 Petrogenesis

- The majority of the selected NAKP pipes have similar isotopic and trace element compositions to an OIB-type source mantle. Kimberlites in the BHH and BM fields are very low degree partial melts. The ML and Xena (BM) pipes originated from shallower subcontinental lithosphere with higher degrees of partial melting relative to the BHH and BM kimberlites. Based on whole rock isotopic compositions of five separate pipes, the diamondiferous K6 pipe (BHH) has the most primitive depleted upper mantle (MORB-like) source.

- The dominant process of magmatic differentiation in the NAKP is crystal fractionation and accumulation of olivine, which acts as the main differentiation process between primitive and evolved Group I-type kimberlite in the NAKP. The BM pipes are further differentiated by varying degrees of partial melting, variable degrees of source enrichment (i.e., mantle metasomatism and/or less efficient carbonate loss during ascent than the BHH) in the sub-continental lithosphere.

- Regionally, the Late Cretaceous NAKP does not match the location and timing of current predicted continental hotspot tracks, and locally, the NAKP intrafield ages do not support any age progression.

- Magma generation in the NAKP could have been influenced by several tectonic events and some combination of involvement of mantle hot cells, subduction and deep-seated structure cannot be ruled out. Current evidence, however, suggests that the correlation between ultramafic magmatism, Laramide Orogeny, Peace River Arch, deep-seated structures and periods of extension are collectively dominant factors for the emplacement of kimberlite in the NAKP. That is, local and regional tectonic features could act in concert with larger-scale orogenic events (e.g., subduction), as controls of the generation and emplacement of NAKP kimberlite magmas. Future studies of mantle xenoliths and potential field data, such as deep seismic, will provide more convincing evidence for an association between kimberlite genesis and tectonic structures in northern Alberta.

13 References

Agashev, A.M., Orihashi, Y., Watanabe, T., Pokhilenko, N.P. and Serenko, V.P. (2000): Isotope-geochemical features of the Siberian Platform kimberlites in connection with the problem of their origin. Russian Geology and Geophysics, v. 41, p. 97-97.

Akimov, A.P. and Semenov, G.S. (1970): Radioelement contents of kimberlites from the Siberian Platform; Doklady Akademii Nauk SSSR, v. 190, p. 947–950.

Alibert, C., Michard, A. and Albarède, F. (1983): The transition from alkali basalts to kimberlites: isotope and trace element evidence from melilitites; Contributions to Mineralogy and Petrology, v. 82, p. 176–186.

Allsopp, H.L., Bristow, J.W., Smith, C.B., Brown, R., Gleadow, A.J.W., Kramers, J.D. and Garvie, O.G. (1989): A summary of radiogenic dating methods applicable to kimberlites and related rocks. *In*: Kimberlites and Related Rocks, Volume 1: Their Composition, Occurrence, Origin, and Emplacement. Proceedings of the 4th International Kimberlite Conference, Geological Society of Australia, Special Publication, No. 14, p. 343-357.

Anderson, D.L., Zhang, Y-S. and Tanimoto, T. (1992): Plume heads, continental lithosphere, flood basalts and tomography. In: Magmatism and the Causes of Continental Break-up, B.C. Storey, T. Alabaster and R.J. Pankhurst (eds.), Geological Society Special Publication, no. 68, p. 99-124.

Andreeva, E.D., Baskina, V.A., Boagatikov, O.A., Borodeavskaja, M.B., Gonshackova, V.I., Egorov, L.S., Efremova, S.V, Kovalenko, V.I., Lazko, E.E., Markovskii, B.A., Masaitis, V.L., Michailov, N.P., Nasedkin, V.V., Negrei, E.V., Petrova, M.A., Polunina, L.A., Rotman, V.K., Rumjantseva, N.A., Siminiva, L.L., Sobolev, R.N., Filippova, T.P., Frolova, T.I. and Jashina, R.M. (1983): Magmaticheskie Gornye Porody: klassifikatziva, nomenklatura, petrographiva, [Translated title: Magmatic rocks: classification, nomenclature, petrography]; Izd. Nauka. Moskow, USSR (in Russian), 2 v., 368 p.

Andriashek, L.D. and Fenton, M.M. (1989): Quaternary stratigraphy and surficial geology of the Sand River area 73L. Alberta Research Council, Alberta Geological Survey, Bulletin 57, 154 p.

Ancochea, E. and Ibarrola, E. (1982): Characterization geoquimica del vulcanismo de la region central Espanola; Boletin Real Sociedad Espanola de Historia Natural, v. 80, p. 57–88.

Aravanis, T. (1999): Legend property assessment report, Birch Mountains area, Alberta; Alberta Energy and Utilities Board, Alberta Geological Survey, Assessment File Report 20000003, 23 p.

Ashton Mining of Canada, Inc. (1998): 1998 Annual Report; Ashton Mining of Canada Inc., 36 p.

Ashton Mining of Canada, Inc. (1999a): Ashton reports diamond analysis for kimberlite K11; news release transmitted by Canadian Corporate News, January 15, 1999 (available 17-Jul-01 at http://www.ashton.ca/news/newsrelease.html).

Ashton Mining of Canada, Inc. (1999b): Ashton reports microdiamond results from kimberlites in Alberta; news release transmitted by Canadian Corporate News, April 28, 1999 (available 17-Jul-01 at http://www.ashton.ca/news/newsrelease.html).

Ashton Mining of Canada, Inc. (2000): Ashton to collect mini-bulk sample from K252; news release transmitted by Canadian Corporate News, September 11, 2000 (available 17-Jul-01 at http://www.ashton.ca/news/newsrelease.html).

Ashton Mining of Canada, Inc. (2001): K252 mini-bulk sample returns 55.0 cpht; news release transmitted by Canadian Corporate News, May 24, 2001 (available 17-Jul-01 at http://www.ashton.ca/news/newsrelease.html).

Bally, A.W., Gordey, P.L. and Stewart, G.A., (1966): Structure seismic data and orogenic evolution of southern Canadian Rocky Mountains. Canadian Journal of Earth Sciences, v 22. p. 384-398.

Barton, M. (1979): A comparative study of some minerals occurring in the potassium-rich alkaline rocks of the Leucite Hills, Wyoming, the Vico Volcano, western Italy, and the Toro–Ankole region, Uganda; Neues Jahrbuch fuer Mineralogie Abhandlungen, v. 137, p. 113–134.

Beaumont, C., Quinlan, G. and Stockmal, G.S. (1993); The evolution of the western interior basin: causes, consequences and unsolved problems. *In:* Geodynamic Evolution of the Western Interior Basin, W.G.E. Caldwell and E.G. Kauffman, (editors), Geological Association of Canada, Special Paper 39, p. 97-117.

Bell, K. and Blenkinsop, J. (1989): Neodymium and strontium isotope geochemistry of carbonatites. Geochemical et Cosmochimica Acta, v. 51, p. 291-298.

Berg, G.W. (1998): Geochemical relations which reflect the history of kimberlites from the type area of Kimberley, South Africa; *in* Seventh International Kimberlite Conference, Cape Town, South Africa, 1998, Extended Abstracts, p. 76–78.

Berg, G.W. and Carlson, J.A. (1998): The Leslie Kimberlite Pipe of Lac de Gras, Northwest Territories, Canada: evidence for near surface hypabyssal emplacement; *in* Seventh International Kimberlite Conference, Cape Town, South Africa, 1998, Extended Abstracts, p. 81–83.

Bizzi, L.A., Smith, C.B., de Wit, M.J., Armstrong, R.A., Meyer, H.O.A. (1994): Mesozoic kimberlites and related alkalic rocks in the southwestern São Francisco craton, Brazil: a case for local mantle reservoirs and their interaction. Proceedings 5th International Kimberlite Conference, v. 1, CPRM, Rio de Janeiro, Brazil, p. 158-171.

Brey, G. (1978): Origin of olivine melilitites: chemical and experimental constraints; Journal of Volcanology and Geothermal Research, v. 3, p. 61–88.

Brey, G.P. and Ryabchikov, I.D. (1994): Carbon dioxide in strongly silica undersaturated melts and origin of kimberlite magmas, Neues Jahrb. Mineral. Montash, v. 10, p. 449-463.

Brown, R.B., Allsop, H.L., Bristow, J.W. and Smith, C.B. (1989): Improved precision of Rb-Sr dating of kimberlite micas: an assessment of a leaching technique. Chemical Geology, v. 79, p. 125-136.

Buhlmann, A.L. (1996): Eocene minettes and their mica-clinopyroxenite inclusions in the Milk River area, southern Alberta; nature and origin. M.Sc Thesis, University of Alberta, Edmonton, Alberta, Canada, 139 p.

Buhlmann, A.L., Cavell, P., Burwash, R.A., Creaser, R.A. and Luth, R.W. (2000): Minette bodies and cognate mica-clinopyroxenite xenoliths from the Milk River area, southern Alberta: records of a complex history of the northernmost part of the Archean Wyoming craton; Canadian Journal of Earth Sciences, v. 37, p. 1629–1650.

Bunge, H-P. and Grand, S.P. (2000): Mesozoic plate-motion history below the northeast Pacific Ocean from seismic images of the subducted Farallon slab. Nature, v. 405, p. 337-340.

Burwash, R.A. and Krupicka, J. (1969): Cratonic reactivation in the Precambrian basement of western Canada, I. Deformation and chemistry. Canadian Journal of Earth Sciences, v. 6, p. 1381-1396.

Burwash, R.A. and Krupicka, J. (1970): Cratonic reactivation in the Precambrian basement of western Canada, II. Metasomatism and isotacy. Canadian Journal of Earth Sciences, v. 7, p. 1275-1295.

Burwash, R.A. and Power, M.A. (1990): Trout Mountain Anomaly, northern Alberta: its role in the Northwest Foreland of the Trans-Hudson Orogen. *In:* The Early Proterozoic Trans-Hudson Orogen of North America, J.F. Lewry and M.R. Stauffer (eds.). Geological Association of Canada, Special Paper 37, p. 301-311.

Burwash, R.A., McGregor, C.R. and Wilson, J.A. (1994): Precambrian basement beneath the Western Canada Sedimentary Basin. *In* G.D. Mossop and I. Shetsen, editors, Geological Atlas of the Western Canada Sedimentary Basin, Published Jointly by the Canadain Society Of Petroleum Geologists and the Alberta Research Council, p. 49-56.

Burwash, R.A., Kupricka, J. and Wijbrans, J.R. (2000): Metamorphic evolution of the Precambrian basement of Alberta. Canadian Mineralogoist, v 38, p. 423-434.

Cant, D.J. (1988): Regional structure and development of the Peace River Arch, Alberta: a Paleozoic failed-rift system? Bulletin of Canadian Petroleum Geology, v 36, p. 284-295.

Carlson, S.M., Hillier, W.D., Hood, C.T., Pryde, R.P. and Skelton, D.N. (1998): The Buffalo Hills kimberlite province, north-central Alberta, Canada; *in* Seventh International Kimberlite Conference, Cape Town, South Africa, 1998, Extended Abstracts, p. 138–140.

Carlson, S.M., Hillier, W.D., Hood, C.T., Pryde, R.P. and Skelton, D.N. (1999): The Buffalo Hills kimberlites: a newly-discovered diamondiferous kimberlite province in north-central Alberta, Canada; *in* Proceedings of the Seventh International Kimberlite Conference, Cape Town, South Africa, 1998, J.J. Gurney, J.L. Gurney, M.D. Pascoe and S.H. Richardson (ed.); Red Roof Design cc, South Africa, v. 1, p. 109–116.

Chacko, T. (1997): Ultra-high temperature metamorphism at Pelican Rapids, Taltson Magmatic Zone, northeast Alberta: possible implications for early Proterozoic collisional orogens. Geological Association of Canada–Mineralogical Association of Canada, Annual Meeting, Abstracts 22, p. A24.

Civetta, L., Innocenti, F., Manetti, P., Peccerillo, A. and Poli, G. (1981): Geochemical characteristics of potassic volcanics from Mt. Ernici (southern Latium, Italy); Contributions to Mineralogy and Petrology, v. 78, p. 37–47.

Clement, C.R. (1982): A comparative geological study of some major kimberlite pipes in the Northern Cape and Orange Free State, Ph.D. thesis (2 vols), University of Cape Town, South Africa.

Clement, C.R. and Skinner, E.M.W. (1979): A textural-genetic classification of kimberlite rocks. *In:* Proceedings of the Second International Kimberlite Conference. Volume 1. Kimberlite, Diatremes and Diamonds: Their Geology, Petrology and Geochemistry, F.R. Boyd Jr. and H.O.A. Meyer (editors), American Geophysical Union, Washington, D.C., Extended Abstracts.

Clement, C.R. and Skinner, E.M.W. (1985): A textural-genetic classification of kimberlites. Transactions Geological Society South Africa, v. 88, p. 403-409.

Clement, C.R., Skinner, E.M.W. & Scott Smith, B.H. (1984): Kimberlite redefined. Journal of Geology, v. 92, p. 223-228.

Cliff, N. (1987): Analyzing multivariate data. Harcourt Brace Jovanovich, Sand Diego.

Connolly, C.A. (1990): Geochemical and isotopic tracing of water/rock interactions in the western Canada sedimentary basin. Ph.D. thesis, University of Alberta, Canada, 300 p.

Creighton, S. and Eccles, D.R. (2003): A preliminary study of the mineral chemistry of selected Alberta kimberlites. Proceedings of the 8th International Kimberlite Conference, Extended Abstracts.

Currie, K.L. (1976): The alkaline rocks of Canada; Geological Survey of Canada, Bulletin 239, 228 p.

Dalton, J.A. and Presnall, D.C. (1998a): Carbonatitic melts along the solidus of model lherzolite in the system $CaO-MgO-Al_2O_3-SiO_2-CO_2$ from 3 to 7 GPa. Contributions to Mineralogy and Petrology, v. 131, p. 123-135.

Dalton, J.A. and Presnall, D.C. (1998b): the continuum of primary carbonatitic-kimberlitic melt compositions in equilibrium with lherzolite: Data from the system $CaO-MgO-Al_2O_3-SiO_2-CO_2$ at 6 GPa. Journal of Petrology, v. 39, p. 1953-1964.

Dawson, J.B. (1962): Basutoland kimberlites; Geological Society of America Bulletin, v. 73, p. 545–560.

Dawson, J.B. (1967): Geochemistry and origin of kimberlite; *in* Ultramafic and Related Rocks, P.J. Wyllie (ed.); John Wiley & Sons, New York, p. 269–278.

Dawson, J.B. (1971): Advances in kimberlite geology. Earth Science Reviews, v. 7, p. 187-214.

Dawson, J.B. (1980): Kimberlites and their xenoliths; Springer-Verlag, New York, 252 p.

Dawson, J.B. (1984): Contrasting types of upper mantle metasomatism. *In:* Proceedings of the Third International Kimberlite Conference, Volume 2. Kimberlites: Kimberlites and Related Rocks, J. Kornprobst (ed.), Elsevier Press, New York, 1984, p. 289-294.

Dawson, J.B. and Smith, J.V. (1975): Chemistry and origin of phlogopite megacrysts in kimberlite, Nature, v. 253, p. 336-338.

Dawson, J. B. and Stephens, W. E. (1975): Statistical classification of garnets from kimberlite and associated xenoliths; Journal of Geology, v. 83, p. 589–607.

Dawson, F.M., Evans, C.G., Marsh, R., and Richardson, R. (1994): Uppermost Cretaceous and Tertiary strata of the Western Canada Sedimentary Basin. *In:* Geological Atlas of the Western Canada Sedimentary Basin. G.D. Mossop and I. Shetsen (comps.). Calgary, Canadian Society of Petroleum Geologists and Alberta Research Council, p. 387-406.

Deakin, A.S. and White, S.H. (1991): In: 5th Internation Kimberlite Conference, Brazil. Extended Abstracts, p. 71-73.

Dooley, T. and McClay, K.R. (1997): Analog modelling of pull-apart basins. American Association of Petroleum Geologists Bulletin, v. 81, no. 11, p. 1804-1826.

Douglas, R.J.W., Gabrielse, H., Wheeler, J.O., Stott, D.F., and Belyea, H.R. (1969): Geology of Western Canada. *In:* Geology and Economic Minerals of Canada, R.J.W. Douglas (ed.). Geological Survey of Canada, Economic Geology Report No. 1, p. 365-488.

Dowall, D., Nowell, G., Pearson, D.G., and Kjarsgaard, B. (2000): The nature of kimberlite source regions: A Hf-Nd isotopic study of Slave craton kimberlites. Goldschmidt 2000, September 3rd-8th, 2000, Journal of Conference Abstracts, v. 5(2), p. 357.

Dufresne, M.B., Eccles, D.R. and Leckie, D.A. (2001): Geological and geochemical setting of the mid-Cretaceous Shaftesbury Formation and other Colorado Group sedimentary units; Alberta Energy and Utilities Board, Alberta Geological Survey, Special Report 9, 46 p.

Dyke A.S and Prest V.K. (1987): Late Wisconsinan and Holocene history of the Laurentide Ice Sheet. Géographie Physique et Quaternaire, v. 41, p. 237-263.

Dyke, A.S., Andrews, J.T., Clark, P.U., England, J.H., Miller, G.H., Shaw, J. and Veillette, J.J. (2002): The Laurentide and Innuitian ice sheets during the Last Glacial Maximum. Quaternary Science Reviews, v. 21, p. 9-31.

Eccles, D.R. (2003): Mountain Lake cluster, northern Alberta kimberlite province. *In*: Slave Province and Northern Alberta Field Trip Guidebook, B.A. Kjarsgaard (ed.). Guidebook prepared for the 8th International Kimberlite Conference, June, p. 21-30.

Eccles, D.R., Grunsky, E.C., Grobe, M., and Weiss, J. (2001a): Structural emplacement model for kimberlitic diatremes in northern Alberta. Alberta Energy and Utilities Board, Alberta Geological Survey, Earth Science Report 2000-01, 116 p.

Eccles, D.R., Bietting, M. and Skupinski, A. (2001b): Bedrock and stream sediment geochemical analysis and field observations of the sub-Cretaceous unconformity, northeast Alberta (NTS 74E and North half 74D). Alberta Energy and Utilities Board, Alberta Geological Survey, Geo-Note 2001-01, 42 p.

Eccles, D.R., Pana, D.I., Paulen, R.C. and Olson, R.A. (2003): Discovery and geological setting of the northern Alberta kimberlite province. *In*: Slave Province and Northern Alberta Field Trip Guidebook, B.A. Kjarsgaard (ed.). Guidebook prepared for the 8th International Kimberlite Conference, June, p. 1-10.

Eccles, D.R. and Pana, D.I. (In Preparation): Metallogenic considerations for Devonian carbonates in the Fort McMurray and Fort Vermillion areas, Alberta. Alberta Energy and Utilities Board, Alberta Geological Survey, Geo-Note 2002-20.

Eggler, D. and Wendlandt, R. (1979): Experimental studies on the relationships between kimberlite magmas and partial melting of peridotite. *In:* Kimberlites, diatremes and diamonds: their geology, petrology and geochemistry 1, F.R. Boyd and H.O. Meyer (eds.). AGU Washington DC, p. 330-338.

Eisbacher, G.H., Carrigy, M.A. and Campbell, R.B. (1974): Paleodrainage pattern and late-orogenic basins of the Canadian Cordillera. *In:* Tectonics and Sedimentation, Dickinson W.R. (ed.), Society of Economic Paleontologists and Mineralogists, Special Publication No. 22, p. 143-166.

Farmer, G.L. and Boettcher, A.L. (1981): Petrologic and crystal-chemical significance of some deep-seated phlogopites. American Mineralogist, v. 66, p. 1154-1163.

Faure, G. (1977): Principles of isotope geology. John Wiley & Sons, New York, 589 p.

Fesq, H.W., Kable, E.J.D. and Gurney, J.J. (1975): Aspects of geochemistry of kimberlites from the Premier Mine, and other selected South African occurrences with particular reference to the rare earth elements; Physics and Chemistry of the Earth, v. 9, p. 868–707.

Field, M. and Scott Smith, B.H. (1998): Contrasting geology and near-surface emplacement of kimbelrite pipes in Southern Africa and Canada. *In:* Proceedings of the Seventh International Kimberlite Conference, Cape Town, South Africa, 1998, J.J. Gurney, J.L. Gurney, M.D. Pascoe and S.H. Richardson (ed.); Red Roof Design cc, South Africa, v. 1, p. 214-237.

Flower, M.F.J. (1973): Evolution of basaltic and differentiated lavas from Anjouan, Comores Archipelago; Contributions to Mineralogy and Petrology, v. 38, p. 237–260.

Frey, F.A., Green, D.H. and Roy, S.D. (1978): Integrated models of basalt petrogenesis: a study of quartz tholeiites to olivine melilitites from South Eastern Australia utilizing geochemical and experimental petrological data; Journal of Petrology, v. 19, p. 463–513.

Gabrielse, H. and Yorath, C.J. (1992): Tectonic Synthesis. *In:* Gabrielse, H. and C.J. Yorath, editors, Geology of the Cordilleran Orogen in Canada, Geology of Canada, No. 4. Decade of North American Geology (DNAG) Vol. G-2. Geological Survey of Canada, p. 679-705.

Girnis, A.V., Brey, G.P. and Ryabchikov, I.D. (1995): Origin of Group IA kimberlites: Fluid-saturated melting experiments at 45-55 kbar. Earth and Planetary Science Letters, v. 134, p. 283-296.

Gravenor, C.P. and Bayrock, L.A. (1955): Use of indicators in the determination of ice-movement directions in Alberta. Bulletin of the Geological Society of America. v. 66, p. 1325-1328.

Gravenor, C.P. and Meneley, W.A. (1958): Glacial flutings in central and northern Alberta. American Journal of Science, v. 256, p. 715-728.

Green, D.H. (1971): Composition of basaltic magmas as indicators of conditions of origin: application to oceanic volcanism; Royal Society of London, Philosophical Transactions, v. 268A, p. 707–725.

Grover, T.W., Pattison, D.R.M., McDonough, M.R. and McNIcoll, V. (1997): Tectonometamorphic evolution of the southern Taltson Magmatic zone and associated shear zones, northeastern Alberta, The Canadian Mineralogist, v. 35, p. 1051-1067.

Grunsky, E.C. (2001): A program for computing RQ-mode principal components analysis for S-PLUS and R; Computers and Geosciences, v. 27, p. 229–235.

Gurney, J.J. and Ebrahim, S. (1973): Chemical composition of Lesotho kimberlites; *in* Lesotho Kimberlites, P.H. Nixon (ed.); p. 280–294.

Hamilton, W.N., Price, M.C. and Langenberg, C.W. (comp.) (1999): Geological Map of Alberta; Alberta Energy and Utilitites Board, Alberta Geological Survey, Map 236, scale 1:1 000 000.

Harmer, R.E. and Gittings, J. (1998): The case for primary, mantle-derived carbonatite magma. Journal of Petrology, v. 39, p. 1895-1903.

Hanmer, S.K. (1988): Great Slave Lake Shear Zone, Canadian Shield: reconstructed vertical profile of a crustal-scale fault zone. Tectonophysics, v. 149, p. 245-264.

Hanmer, S.K. (1997): Geology of the striding-Athabasca Mylonite Zone, northern Saskatchewan and southeastern District of Mackenzie, Northwest Territories. Geological Survey of Canada, Bulletin 501, 92 p.

Hawthorne, J.B. (1975): Model of a kimberlite pipe. Physics and Chemistry of the Earth, v. 9, p. 1-15.

Heaman, L.M. (1989): The nature of the subcontinental mantle from Sr-Nd-Pb isotopic studies on kimberlitic perovskite. Earth and Planetary Science Letters, v. 92, p. 323-334.

Heaman, L.M. and Kjarsgaard, B.A. (2000): Timing of eastern North American kimberlite magmatism: continental extension of the Great Meteor hotspot track? Earth and Planetary Science Letters, v. 178, p. 253-268.

Heaman, L.M., Kjarsgaard, B.A. and Creaser, R.A. (2003): The timing of kimberlite magmatism and implications for diamond exploration: A global perspective. Lithos, v. 71, p. 153-184.

Hearn, B.C., Jr. (1986): Alkalic ultramafic magmas in north-central Montana, USA: genetic connections of alnöite, kimberlite, and carbonatite; *in* Proceedings of the Fourth International Kimberlite Conference, Perth, Australia, 1986, J. Ross et al. (ed.); p. 109–119.

Hearn, B.C., Jr., Marvin, R.F., Zartman, R.E. and Naeser, C.W. (1978): Ages of alkalic activity in north-central Montana; United States Geological Survey, Professional Paper 1100, p. 60.

Hegner, E., Roddick, J.C., Fortier, S.M. and Hulbert, L. (1995): Nd, Sr, Pb, Ar and O isotopic systematics of Sturgeon Lake kimberlite, Saskatchewan, Canada: constraints on emplacement age alteration and source composition. Contribution to Mineralogy and Petrology, v. 120, p. 212-222.

Henderson, J.B. and Thériault, R.J. (1994): U-Pb zircon evidence for circa 3.1 Ga crust south of the McDonald Fault, northwestern Canadian Shield, Northwest Territories. *In:* Radiogenic Age and Isotopic Studies: Report 8, Geological Survey of Canada, Current Research 1994-F, p. 43-47.

Hoffman, P.F. (1987): Continental transform tectonics: Great Slave Lake shear zone (ca. 1.9 Ga), northwest Canada. Geology, v. 15, p. 785-788.

Hoffman, P.F. (1988): United Plates of America: the birth of a craton. Annual Review of Earth and Planetary Sciences, v 16, p. 543-604.

Holmden, C., Creaser, R.A., Muehlenbachs, K., Leslie, S.A., Bergstrom, S.M. (1996): Isotopic and elemental systematics of Sr and Nd in 454 Ma biogenic apatites: implications for paleoseawater studies. Earth and Planetary Science Letters, v. 142, p. 425-437.

Ilupin, I.P. and Lutz, B.G. (1971): The chemical composition of kimberlite, and questions on the origin of kimberlite magma; Sovetskaya Geologiya, v. 6, p. 61–73.

Ilupin, I.P., Sobolev, S.F., Zolotarev, B.P. and Lebedev-Zinovyev, A.A. (1974): Geochemical specialization of kimberlites from various parts of Yakutia; Geochemical International, v. 11, p. 357–370.

Jagoutz, E., Palme, H, Baddenhausen, H., Blum, K., Cendales, M., Dreibus, G., Spettel, B., Lorenz, V. and Wanke, H. (1979): The abundances of major, minor and trace elements in the earth's upper mantle as derived from primitive ultramafic nodules; *in* Proceedings from the 10th Lunar and Planetary Science Conference, p. 2031–2050.

Jago, B.C. and Mitchell, R.H. (1985): Mineralogy and petrology of the Ham kimberlite, Somerset Island, Northwest Territories, Canada. Canadian Mineralogist, v. 23, p. 619-634.

Jaques, A.L., Lewis, J.D., and Smith, C.B. (1986): The kimberlites and lamproites of Western Australia: Geological Survey of Western Australia, Bulletin 132, 268 p.

Kent, D.M. (1994): Paleogeographic evolution of the cratonic platform – Cambrian to Triassic. *In:* Geological Atlas of the Western Canadian Sedimentary Basin, G.D. Mossop and I. Shetson (comps). Canadian Society of Petroleum Geologists and Alberta Research Council, Calgary, Alberta, p. 69-86.

Kjarsgaard, B.A. (1994): Potassic magmatism in the Milk River area, southern Alberta: petrology and economic potential; Geological Survey of Canada, Current Research 1994-B, p. 59–68.

Klassen, R.W. (1989): Quaternary geology of the southern Canadian Interior Plains. *In:* Quaternary Geology of Canada and Greenland, R.J. Fulton (editors). Geological Survey of

Canada, Geology of Canada, no. 1 (also Geological Society of America, The Geology of North America, v. K-1), p. 138-174.

Kyser, K., Hiatt, E., Renac, C., Durocher, K., Holk, G. and Deckart, K. (2000): Diagenetic fluids in paleo- and meso-proterozoic sedimentary basins and their implications for long protracted fluid histories. In: Fluids and Basin Evolution, K. Kyser (editor), Mineralogical Association of Canada, Short Course Series, v. 28, p. 225-262.

Langenberg, C.W. and Nielson, P.A. (1982): Polyphase metamorphism in the Canadian Shield of northeastern Alberta. Alberta Research Council, Alberta Geological Survey, Bulletin 42, 80 p.

Larsen, L.M. and Rex, D.C. (1992): A review of the 2500 Ma span of alkaline-ultramafic, potassic and carbonatitic magmatism in West Greenland; Lithos, v. 28, p. 367–402.

Le Bas, M.J. (1989): Nephelinitic and basanitic rocks; Journal of Petrology, v. 30, p. 1299–1312.

Leckie, D.A., Battacharya, J.P., Bloch, J., Gilboy, C.F. and Norris, B. (1994): Cretaceous Colorado / Alberta Group of the Western Canada Sedimentary Basin. *In:* Geological Atlas of the Western Canadian Sedimentary Basin, G.D. Mossop and I. Shetson (comps). Canadian Society of Petroleum Geologists and Alberta Research Council, Calgary, Alberta, p. 335-352.

Leckie, D.A., Kjarsgaard, B.A., Peirce, J.W., Grist, A.M., Collins, M., Sweet, A., Stasiuk, L., Tomica, M.A., Eccles, D.R., Dufresne, M.B., Fenton, M.M., Pawlowicz, J.G., Balzer, S.A., McIntyre, D.J. and McNeil, D.H. (1997): Geology of a Late Cretaceous possible kimberlite at Mountain Lake, Alberta – chemistry, petrology, indicator minerals, aeromagnetic signature, age, stratigraphic position and setting; Geological Survey of Canada, Open File Report 3441, 202 p.

Le Maitre, R.W. (1976): The chemical variability of some common igneous rocks; Clarendon Press, Oxford, United Kingdom, v. 17, p. 589–637.

Le Maitre, R.W. (1982): Numerical petrology: statistical interpretation of geochemical data; Elsevier Scientific Publishing Company, New York, p. 19–20.

Le Maitre, R.W., (ed.). (1989): A classification of Igneous Rocks and Glossary of Terms, Blackwell, Oxford, 193 p.

Lemay, T.G. (2002): Geochemical and isotope data for formation water from selected wells, Cretaceous to Quaternary succession, Athabasca Oil Sands (in situ) Area, Alberta; Alberta Energy and Utilities Board, Alberta Geological Survey, Geo-Note 2002-02, 31 p.

Le Roex, A.P. (1986): Geochemical correlation between southern African kimberlites and South Atlantic hotspots. Nature, v. 324. p. 243-245.

Ludwig, K.R. (2000): User's manual for Isoplot/Ex version 2.2: a geochronological toolkit for Microsoft Excel. Berkeley Geochronology Center, Special Publication No. 1a, Berkeley, California.

Lutts, B.G. and Mineyeva, I.S. (1973): Uranium and thorium in Siberian kimberlites; Geochemistry International, p. 1278–1281.

Mahotkin, I.L., Gibson, S.A., Thompson, R.N., Zhuravlev, D.Z., Zherdev, P.U. (2000): Late Devonian diamondiferous kimberlite and alkaline picrite (proto-kimberlite?) magmatism in the Arkhangelsk region, NW Russia. Journal of Petrology, v. 41, p. 201-227.

Marshintsev, V.K. and Lapin, A.V. (1976): Geochemical heterogeneity of kimberlite; Doklady Akademii Nauk SSSR, v. 226, p. 200–203.

McCandless, T.E. (1999): Kimberlite: Mantle expressions of deep-seated subduction. *In:* Proceedings of the 7th International Kimberlite Conference (J.J. Gurney, J.L. Gurney, M.D. Pascoe and S.H. Richardson, eds.), v. 2, p. 545-549.

McDonough, W.F. and Sun, S.-S. (1995): Composition of the Earth; Chemical Geology, v. 120, p. 223–253.

McDonough, M.R., McNicoll, V.J., and Schetselaar, E.M. (1995): Age and kinematics of crustal shortening and escape in a two-sided oblique-slip collisional and slip orogen, Paleoproterozoic Taltson magmatic zone, northeastern Alberta. *In:* 1995 Alberta Basement Transects Workshop, G.M. Ross (ed.). Lithoprobe Secretariat, University of British Columbia., Lithoprobe Report No. 47, p. 264-308.

Menzies, M. (1983): Mantle ultramafic xenoliths in alkaline magmas: evidence for mantle heterogeneity modified by magmatic activity. *In:* Continental Basalts and Mantle Xenoliths, C.J. Hawkesworth and M.J. Norry (eds.), Cheshire, England, Shiva, p. 92-110.

Mitchell, R.H. (1979): The alleged kimberlite-carbonatite relationship: additional contrary mineralogical evidence. American Journal of Science, v. 279, p. 570-589.

Mitchell, R.H. (1986): Kimberlites: Mineralogy, Geochemistry and Petrology. Plenum Press, New York, 442 p.

Mitchell, R.H. (1994): Suggestions for revisions to the terminology of kimberlites and lamprophyres from a genetic viewpoint. *In*: Proceedings of the Fifth International Kimberlite Conference 1. Kimberlites and Related Rocks and Mantle Xenoliths, H.O.A. Meyer and O.H. Leonardos (editors). Companhia de Pesquisa de Recursos Minerais (Brasilia), Special Publication 1/A, p. 15-26.

Mitchell, R.H. (1995): Kimberlites, Orangeites and Related Rocks. Plenum Press, New York, 410 p.

Mitchell, R.H. and Clarke, D.B. (1976): Oxide and sulphide mineralogy of the Peuyuk kimberlite, Somerset Island, N.W.T., Contributions to Mineralogy and Petrology, v. 56, p. 157-172.

Mitchell, R.H. and Bergman, S.C. (1991): Petrology of Lamproites. Plenum Press, New York. 447 p.

Montello Resources Ltd. (1998): Third kimberlite pipe discovered; news release, October 20, 1998 (available 17-Jul-01 at http://www.montello.com/s/NewsReleases.asp).

Montello Resources Ltd. (1999): Report from Kennecott Canada Exploration Inc.; news release, March 12, 1999 (available 17-Jul-01 at http://www.montello.com/s/NewsReleases.asp).

Morgan, W.J. (1983): Hotspot tracks and the early rifting of the Atlantic. Tectonphysics, v. 94, p. 123-129.

Mossop, G.D. and Shetsen, I. (1994): Introduction to the Geological Atlas Of The Western Canada Sedimentary Basin. *In:* Geological Atlas of the Western Canadian Sedimentary Basin, G.D. Mossop and I. Shetson (comps). Canadian Society of Petroleum Geologists and Alberta Research Council, Calgary, Alberta, p. 1-12.

Muramatsu, Y. (1983): Geochemical investigations of kimberlites from the Kimberley area, South Africa; Geochemical Journal, v. 17, p. 71–86.

Nelson, D.R., Chivas, A.R., Chappell, B.W. and McCulloch, M.T. (1988): Geochemical and isotopic systematics in carbonatites and implications for the evolution of ocean-island sources. Geochimica et Cosmochimica Acta, v. 52, p. 1-17.

New Blue Ribbon Resources Ltd. (2001): Exploration update; news release, January 15, 2001 (available 17-Jul-01 at http://www.newblueribbon.com/s/NewsReleases.asp).

O'Brien, H.E., Irving, A.J., McCallum, I.S., Thirwall, M.F. (1995): Sr, Nd and Pb isotopic evidence fo interaction of post-subduction asthenospheric potassic mafic magmas of the Highwood Mountains, Montana with ancient Wyoming Craton lithospheric mantle. Geochimica et Comochimica Acta, v. 59, p. 4539-4556.

O'Brien, H.E. and Tyni, M. (1999): Mineralogy and geochemistry of kimberlites and related rocks from Finland. Proc. 7th International Kimberlite Conference, v. 2, Red Roof Design, Cape Town, South Africa, p. 625-636.

O'Connell, S.C. (1994): Geological History of the Peace River Arch. *In:* Geological Atlas of the Western Canadian Sedimentary Basin, G.D. Mossop and I. Shetson (comps). Canadian Society of Petroleum Geologists and Alberta Research Council, Calgary, Alberta, p. 431-438.

O'Connell, S.C., Dix, G.R., and Barclay, J.E. (1990): The origin, history and regional structural development of the Peace River Arch, Western Canada. Bulletin of Canadian Petroleum Geology, v 38A, p. 4-24.

Paganelli, F., Grunsky, E.C. and Richards, J.P. (2003): Structural interpretation of RADARSAT 1 principal components imagery and Its Potential Application to kimberlite exploration in the Buffalo Head Hills area, north central Alberta. Alberta Energy and Utilities Board, Alberta Geological Survey, Special Report 21, 49 p.

Pana, D. (2003): Precambrian Basement of the Western Canada Sedimentary Basin in Northern Alberta. Alberta Energy and Utilities Board, Alberta Geological Survey, Earth Science Report 2002-02, 32 p.

Pana, D., Waters, J. and Grobe, M. (2001): GIS Compilation of Structural Elements in Northern Alberta, Release 1.0. Alberta Energy and Utilities Board, Alberta Geological Survey, Earth Science Report 2001-01, 53 p.

Pana, D. and Eccles, D.R. (2003): Structural controls of kimberlites in the Buffalo Head Hills-Loon River lowlands area: evidence versus conventional wisdom. Calgary Mineral Exploration Group Forum, Abstracts, Calgary, April, 2003.

Peccerillo, A., Poli, G. and Serri, G. (1988): Petrogenesis of orenditic and kamafugitic rocks from central Italy; Canadian Mineralogist, v. 26, p. 45–65.

Poulton, T.P., Christopher, J.E., Hayes, B.J.R., Losert, J., Tittemore, J. and Gilchrist, R.D. (1994): Jurassic and Lowermost Cretaceous Strata of the Western Canada Sedimentary Basin. *In:* Geological Atlas of the Western Canadian Sedimentary Basin, G.D. Mossop and I. Shetson (comps). Canadian Society of Petroleum Geologists and Alberta Research Council, Calgary, Alberta, p. 297-316.

Price, S.E., Russell, J.K. and Kopylova, M.G. (2000): Primitive magma from the Jericho Pipe, N.W.T., Canada: constraints on primary kimberlite melt chemistry; Journal of Petrology, v. 41, no. 6, p. 789–808.

Ranger, I. (2000): Two-feldspar geothermometry applied to the Red Earth granulite domain in Alberta, Canada; B.Sc. thesis, Department of Earth and Atmospheric Sciences, University of Alberta, 46 p.

Rogers, N.W., Hawkesworth, C.J. and Palacz, Z.A. (1992): Phlogopite in the generation of melilitites from Namaqualand, South Africa and implications for element fractionation processes in the upper mantle; Lithos, v. 28, p. 347–365.

Ross, G.M., Parrish, R.R., Villeneuve, M.E., and Bowring, S.A. (1991): Geophysics and geochronology of the crystalline basement of the Alberta Basin, western Canada. Canadian Journal of Earth Sciences, v. 28, p. 512-522.

Ross, G.M., Broome, J. and Miles, W. (1994): Potential Fields and Basement Structure - Western Canada Sedimentary Basin. *In:* Geological Atlas of the Western Canadian Sedimentary Basin, G.D. Mossop and I. Shetson (comps). Canadian Society of Petroleum Geologists and Alberta Research Council, Calgary, Alberta, p. 41-48.

Ross, G.M. and Eaton, D.W. (2002): Proterozoic tectonic accretion and growth of western Laurentia: results from Lithoprobe studies in northern Alberta. Canadian Journal of Earth Sciences, v. 39, p. 313-329.

Schmidt, K.H., Bottazzi, P., Vannucci, R. and Mengel, K. (1999): Trace element partitioning between phlogopite, clinopyroxene and leucite lamproite melt. Earth and Planetary Science Letters, v. 168, p. 287-300.

Scott, B.H. (1979): Petrogenesis of kimberlites and associated potassic lamprophyres from Central West Greenland; *in* Second International Kimberlite Conference, 1979, F.R. Boyd and H.A.A. Neyer (ed.); p. 190–205.

Scott Smith, B.H. (1992): Contrasting kimberlites and lamproites. Exploration and Mining Geology, v. 4, p. 127-140.

Scott Smith, B.H. (1995): Kimberlites. *In*: Undersaturated Alkaline Rocks: Mineralogy, Petrogenesis and Economic Potential, R.H. Mitchell, editor, Mineralogical Association of Canada, Short Course Series, v. 24, p. 217-243.

Scott Smith, B.H. and Skinner, E.M.W. 1984. A new look at Prairie Creek, Arkansas. In: Kornprobst (1984), Vol. 1, p. 255-284.

Shaw, E.W. (1963): Canadian Rockies - orientation in time and space. *In:* Childs, O.E., editor, Backbone of the Americas, American Association of Petroleum Geologists, Memoir 2, p. 231-242.

Shilts, W.W., Cunningham, C.M., and Kaszycki, C.A. (1979): Keewatin Ice Sheet - Re-evaluation of the traditional concept of the Laurentide Ice Sheet. Geology, v. 7, p. 537-541.

Sikabonyi, L.A. and Rodgers, W.J. (1959): Paleozoic tectonics and sedimentation in the northern half of the west Canadian Basin. Journal of the Alberta Society of Petroleum Geologists, v. 7. p. 193-216.

Skall, H. (1975): The paleoenvironment of the Pine Point lead-zinc district. Economic Geology, v. 70, p. 22-47.

Skelton, D. and Bursey, T. (1998): Assessment report: Buffalo Head Hills property (AL01), Ashton Mining of Canada Inc. Assessment File 19980015, Alberta Geological Survey, 19 p.

Skelton, D., Clements, B., McCandless, T.E., Hood, C., Aulbach, S., Davies, R. and Boyer, L.P. (2003): The Buffalo Head Hills kimberlite province, Alberta. *In*: Slave Province and Northern Alberta Field Trip Guidebook, B.A. Kjarsgaard (ed.). Guidebook prepared for the 8th International Kimberlite Conference, June, p. 11-20.

Skinner, E.M.W. (1989): Contrasting group-1 and group-2 kimberlite petrology: towards a genetic model for kimberlites. *In:* Proceedings of the Fourth International Kimberlite Conference (Perth). Geological Society of Australia, GSA Special Publication, no. 14, p. 528-544.

Skinner, E.M.W. & Clement, C.R. (1979): Mineralogical classification of southern African kimberlites. *In*: Proc. Second Int. Kimberlite Conf. 1. Kimberlites, Diatremes and Diamonds: their Geology, Petrology and Geochemistry, F.R. Boyd & H.O.A. Meyer, editors, American Geophysical Union, Washington, D.C., p. 129-139.

Skinner, E.M.W., Viljoen, K.S., Clark, T.C., Smith, C.B. (1994): The petrography, tectonic setting and emplacement ages of kimberlites in the southwestern border region of the Kaapvaal craton, Prieska area. *In:* Proceedings of the 5th International Kimberlite Conference, Volume 1: Kimberlites and related rocks, H.O.A. Meyer and O.H. Leonardos (editors), p. 80-97

Skupinski, A. and Langenberg, C.W. (2002): Petrography of the Mountain Lake Pipe; Alberta Energy and Utilities Board, Alberta Geological Survey, Earth Sciences Report 2000-13.

Smith, C.B. (1983): Pb, Sr and Nd isotopic evidence for sources of southern African Cretaceous kimberlites. Nature, v. 304, p. 51-54.

Smith, C.B., Allsopp, H.L., Kramers, J.D., Jutchinson, G. and Roddick, J.C. (1985a): Emplacement ages of Jurassic-Cretaceous South African kimberlites by the Rb-Sr Method on phlogopite and whole-rock samples. Transactions Geological Society South Africa, v. 88, p. 249-266.

Smith, C.B., Gurney, J.J., Skinner, E.M.W., Clement, C.R. and Ebrahim, N. (1985b): Geochemical character of Southern African kimberlites: a new approach based on isotopic constraints; Transactions Geological Society South Africa, v. 88, p. 267–281.

Smith, R.B. and Braile, L.W. (1994): The Yellowstone hotspot. Journal of Volcanology and Geothermal Research, v. 61, p. 121-187.

Spera, F.J. (1987): Dynamics of translithospheric migration of metasomatic fluid and alkaline magma. *In*: Mantle Metasomatism, M.A. Menzies and C.J. Hawkesworth (eds). Academic Press Inc., p. 1-18.

Stott, D.F. (1982): Lower Cretaceous Fort St. John Group and Upper Cretaceous Dunvegan Formation of the Foothills and Plains of Alberta, British Columbia and Yukon Territory; Geological Survey of Canada, Bulletin 328, 124 p.

Switzer, S.B., Holland, W.G. Christie, D.S., Graf, G.C., Hedinger, A.D., McAuley, R.J., Wierzbicki, R.A., and Packard, J.J. 1994. Devonian Woodbend-Winterburn strata of the Western Canada Sedimentary Basin. *In:* Geological Atlas of the Western Canada Sedimentary Basin, G.D. Mossop and I. Shetsen (comps.). Canadian Society of Petroleum Geologists and Alberta Research Council, Alberta Geological Survey, Calgary, Alberta, p. 165-202.

Sykes, L.B. (1978): Reviews of Geophysics and Space Physics, v. 16, p. 621-629.

Taylor, S. R. and McLennan, S. M. (1985): The Continental Crust: Its Composition and Evolution; Blackwell and Son Ltd., Oxford, United Kingdom, 312 p.

Taylor, W.R., Tompkins, L.A. and Haggerty, S.E. (1994) Comparative geochemistry of West African kimberlites: evidence for a micaceous kimberlite end-member of sublithospheric origin; Geochimica et Comochimica Acta, v. 58, no. 19, p. 4017–4037.

Thériault, R.J. and Bostock, H.H. (1989): Nd isotopic studies in the ~1.9 Ga Taltson Magmatic Zone, NWT; Geological Association of Canada-Mineralogical Association of Canada, Program with Abstracts, v. 14, p. A10.

Thériault, R.J. and Ross, G.M. (1991): Nd isotopic evidence for crustal recycling in the ca.2.0 Ga subsurface of western Canada. Canadian Journal of Earth Sciences, Vol. 28, p. 1140-1147.

Thorkelson, D.J. (1996): Subduction of diverging plates and the principles of slab window formation. Tectonophysics, v. 255, p. 47-63.

Tompkins, L.A., Meyer, S.P., Han. Z., Hu, S., Armstrong, R., Taylor, W.R. (1999): Petrology and geochemistry of kimberlites from Shandong and Liaoning provinces, China. Proceedings of the 7th International Kimberlite Conference, v. 2, Red Roof Design, Cape Town, South Africa, p. 872-887.

Ukhanov, A.V. (1963): Olivine melilitite from the diamond-bearing diatremes on Anabar; Doklady Akademii Nauk SSSR, v. 153, p. 923–925.

Unterschutz, J.L.E., Creaser, R.A., Erdmer, P., Thompson R.I., and Daughtry, K.L. (2002): North American margin origin of Quesnel terrane strata in the southern Canadian Cordillera: Inferences from geochemical and Nd isotopic characteristics of Triassic metasedimentary rocks. Geological Society of America Bulletin, v. 114, p. 462-475.

Villeneuve, M.E., Ross, G.M., Theriault, R.J., Miles, W., Parrish, R.R. and Broome, J., (1993): Tectonic subdivision and U-Pb geochronology of the crystalline basement of the Alberta Basin, western Canada. Geological Survey of Canada, Bulletin 447, 93 p.

Vollmer, R., Ogden, P., Schilling, J.G., Kingsley, R.H. and Waggoner, D.G. (1984): Nd and Sr isotopes in ultrapotassic volcanic rocks from the Leucite Hills, Wyoming. Contributions to Mineralogy and Petrology, v. 87, p. 359-368.

Wagner, P.A. (1914): The Diamond Fields of Southern Africa. Transvaal Leader, Johannesburg, South Africa.

Wagner, P.A. (1928): The evidence of kimberlite pipes on the constitution of the outer part of the Earth. S. A,fr. J. Sci., v. 25, p. 127-148.

Wedepohl, K.H. and Muramatsu, Y. (1979): The chemical composition of kimberlites compared with the average composition of three basaltic magma types; *In:* Second International Kimberlite Conference, 1979, F.R. Boyd and H.A.A. Neyer (ed.); p. 300–312.

White, W.M. (1985): Sources of oceanic basalts: radiogenic isotopic evidence, Geology, v. 13, p. 115-118.

White, S.H., de Boorder, H., and Smith, C.B. (1995): Structural controls of kimberlite and lamproite emplacement. Journal of Geochemical Exploration, v. 53. p. 245-264.

Wicks, F.J. and Plant, A.G. (1979): Electron-microprobe and x-ray-microbeam studies of serpentine textures. Canadian Mineralogist, v. 17, p. 785-830.

Wilson, J.A. (1986): Geology of the basement beneath the Athabasca Basin in Alberta; Alberta Research Council, Alberta Geological Survey, Bulletin 55, 61 p.

Wilson, M., Rosenbaum, J.M. and Dunworth, E.A. (1995): Melilitites: partial melts of the thermal boundary layer? Contributions to Mineralogy and Petrology, v. 119, p. 181–196.

Wood, B.D., Scott Smith, B.H. and de Gasparis, S. (1998): The Mountain Lake kimberlitic pipes of northwest Alberta: exploration, geology and emplacement model; *in* Seventh International Kimberlite Conference, Extended Abstracts, Cape Town, South Africa, 1998, J.J. Gurney, J.L. Gurney, M.D. Pascoe and S.H. Richardson (ed.); Red Roof Design cc, South Africa, p. 960–962.

Wood, B.D. and Williams, A.C. (1994): Mountain Lake Prospect, Alberta. Monopros Ltd. Metallic and Industrial Permits 9390080014, 9390080019 and 9390080020. Alberta Geological Survey, Assessment File Report 19940001, 5 p.

Wyllie, P.J. (1997): Petrogenesis and the physics of the Earth. *In:* The Evolution of Igneous Rocks: Fiftieth Anniversary Perspectives, H.S. Yoder, Jr. (ed.). Princeton, Princeton University Press, p. 483-520.

Wyllie, P.J. and Huang, W.-L. (1975): Peridotite, kimberlite and carbonatite explained in the system CaO-MgO-SiO_2-CO_2. Geology, v. 3, p. 621-624.

Yamashita, K., Creaser, R.A., Stemler, J. and Zimaro, A. (1999): Geochemical and Nd-Pb isotopic systematics of late Archean granitoids, SW Slave province: Constraints for granitoid origin and crustal isotopic structure. Canadian Journal of Earth Sciences, v. 36, p. 1131-1147.

Yorath, C.J. (1992): Upper Jurassic to Paleogene Assemblages. *In:* Gabrielse, H. and C.J. Yorath, editors, Geology of the Cordilleran Orogen in Canada, Geology of Canada, No. 4. Decade of North American Geology (DNAG) Vol. G-2, Geological Survey of Canada, p. 329-371.

Zhang, R. and Liu, B. (1983): Kimberlites from North China; Geochemical Journal, v. 17, p. 209–221.

Zindler, A. and Hart, S. (1986): Chemical Geodynamics. Annual Review Earth and Planetary Science, v. 14, p. 493-571.

Sample	Drillhole/	Sample	UTM	UTM	UTM	SiO_2	Al_2O_3	Fe_2O_3	MgO	CaO	Na_2O	K_2O	TiO_2	P_2O_5	MnO	Cr_2O_3	Ba	Ni	Sc	LOI
No.	surface sample	depth	Easting	Northing	Zone	(%)	(%)	(%)	(%)	(%)	(%)	(%)	(%)	(%)	(%)	(%)	(ppm)	(ppm)	(ppm)	(%)
Detection limit --						0.02	0.03	0.04	0.01	0.01	0.01	0.04	0.01	0.01	0.01	0.001	5	20	10	
Buffalo Head Hills																				
ABK01	4A-02	49.15	578380	6301519	11	36.89	0.17	3.47	27.59	1.02	0.09	0.3	0.01	0.12	0.05	0.115	133	611	2	30
ABK02	4B-01	140.65	578464	6300991	11	31.67	0.62	7.87	42.84	3.97	0.09	0.1	0.07	0.29	0.12	0.197	356	1535	4	11.9
ABK03	4C-01	63.00	578821	6301274	11	28.5	0.63	5.91	38.77	1.58	0.01	0.06	0.08	0.3	0.1	0.129	157	1309	7	23.6
ABK04	5A-02	84.23	582687	6306035	11	29.59	2.03	8.89	33.83	6.57	0.06	0.3	1.2	0.22	0.15	0.221	800	1279	12	16.7
ABK05	6-02	110.15	585550	6308383	11	29.72	2.77	8.94	32.3	7.54	0.04	0.2	0.9	0.5	0.16	0.158	326	1251	13	16.1
ABK06	7B-01	76.93	583131	6312089	11	22.29	3.47	9.08	18.03	15.48	0.4	0.46	1.24	0.63	0.17	0.09	1503	581	14	28
ABK07	7C-01	58.40	583052	6312455	11	12.66	2.99	7.64	14.02	23.09	0.21	0.17	1.44	0.7	0.17	0.103	1120	437	17	36.2
ABK08	11-01	55.50	619724	6320041	11	34.78	1.43	9.51	40.94	1.52	0.02	0.16	0.8	0.16	0.12	0.115	683	1702	7	10.1
ABK09	11-01	135.50	619724	6320041	11	32.93	2.13	8.97	36.91	3.58	0.08	0.23	0.47	0.25	0.14	0.142	763	1559	6	13.8
ABK10	14-01	14.56	582883	6315050	11	31.87	1.95	7.84	34.77	5.42	0.03	0.32	0.63	0.43	0.12	0.139	308	1601	9	15.9
ABK11	14B-03	30.17	582820	6315277	11	33.52	1.61	8.36	37.18	3.64	0.08	0.15	0.57	0.41	0.13	0.133	387	1621	8	13.8
ABK12	14C-06	54.30	583030	6315357	11	28.89	1.63	7.66	29.11	11.76	0.09	0.15	0.8	0.47	0.11	0.142	535	1524	10	18.6
ABK13	**14C-06**	**54.30**	**583030**	**6315357**	**11**	**28.92**	**1.62**	**7.77**	**29.34**	**11.46**	**0.09**	**0.14**	**0.84**	**0.51**	**0.1**	**0.153**	**559**	**1562**	**10**	**18.7**
ABK14	19-03	19.85	575034	6289104	11	41.35	5.93	5.7	19.83	7.06	0.08	1.54	0.46	0.47	0.09	0.092	1325	947	10	17
ABK15	91-03	84.93	581820	6317052	11	29.93	1.86	8.17	33.47	8.19	0.06	0.48	0.86	0.93	0.15	0.179	1437	1571	11	14.9
ABK16	155-01	102.50	581763	6293954	11	28.12	2.7	8.33	31.45	6.08	0.11	0.36	0.54	0.44	0.14	0.146	744	1007	11	21.2
ABK17	155-01	148.60	581763	6293954	11	29.47	2.54	8.62	35.41	6.02	0.09	0.22	0.48	0.41	0.14	0.146	959	1296	10	15.9
ABK18	**155-01**	**148.60**	**581763**	**6293954**	**11**	**30.49**	**1.95**	**8.55**	**30.06**	**5.41**	**0.07**	**0.15**	**0.45**	**0.38**	**0.14**	**0.151**	**909**	**1429**	**10**	**13.6**
ABK19	BM2-01	52.00	632349	6309823	11	70.12	11.53	4.32	1.9	1.36	1	1.94	0.62	0.18	0.03	0.014	1138	45	10	6.3
ABK20	BM2-01	79.50	632349	6309823	11	25.55	3.36	6.64	19.66	19.81	0.37	2.47	1.03	0.64	0.12	0.143	2494	791	12	19.7
ABK21	BM2-01	103.30	632349	6309823	11	28.36	2.62	9.03	32.23	7.82	0.11	0.23	1.4	0.89	0.19	0.2	2284	1143	16	15.8
ABK22	BM2-01	113.80	632349	6309823	11	27.47	2.81	8.18	29.45	12.03	0.14	0.25	1.32	0.96	0.17	0.182	2704	990	15	16.5
ABK23	BM3-01	124.90	631219	6314208	11	40.79	5.86	5.53	19.59	7.24	0.1	1.49	0.45	0.49	0.09	0.103	1386	1122	10	17.5
ABK24	BM3-01	144.90	631219	6314208	11	38.87	8.61	6.83	11.2	11.86	2.38	3.86	1.05	0.64	0.09	0.055	2474	245	16	13.4
ABK25	LL8-01	77.80	629936	6301692	11	17.24	0.41	4.56	33.66	2.97	0.06	0.25	0.05	0.15	0.07	0.128	274	1213	3	39.7
ABK26	LL8-01	121.50	629936	6301692	11	36.26	1.11	7.92	40.9	0.75	0.03	0.19	0.06	0.22	0.1	0.156	77	2091	4	11.7
ABK27	LL8-01	144.90	629936	6301692	11	35.39	0.66	8.23	44.94	1.6	0.02	0.4	0.07	0.32	0.13	0.168	158	2171	6	7.7
ABK28	K5 (surface)	surface O/C	582432	6306145	11	26.75	2.53	7.07	26.72	15.31	0.03	0.25	0.62	0.28	0.12	0.109	296	1343	9	19.8
ABK29	K6 (surface)	surface O/C	585317	6308651	11	29.76	2.47	8.06	27.33	11.78	0.15	0.34	0.77	0.37	0.15	0.144	553	1189	12	17.8
ABK30	K14 (surface)	surface O/C	582894	6315185	11	32.52	2.02	7.86	31.26	5.73	0.1	0.32	0.77	0.49	0.13	0.156	944	1376	10	18
Mountain Lake Diatreme																				
ABK31	ML95-1 (MLN)	7.22	454636	6145914	11	50.41	9.73	6.26	12.83	3.32	0.92	2.17	0.92	0.31	0.1	0.109	914	406	14	12.2
ABK32	ML95-1 (MLN)	35.00	454636	6145914	11	59.21	11.15	5.92	7.42	2.68	2.31	2.93	0.76	0.23	0.09	0.057	992	204	12	6.9
ABK33	**ML95-1 (MLN)**	**35.00**	**454636**	**6145914**	**11**	**59.99**	**11.49**	**5.44**	**6.97**	**2.67**	**2.29**	**3.1**	**0.79**	**0.22**	**0.08**	**0.062**	**1044**	**271**	**13**	**6.7**
ABK34	ML95-1 (MLN)	64.00	454636	6145914	11	31.96	6.56	3.62	2.45	27.55	1.33	1.03	0.56	0.44	0.22	0.053	1131	236	11	23.6
ABK35	ML95-1 (MLN)	95.00	454636	6145914	11	56.53	10.85	6.06	8.62	3.81	2.27	2.45	0.89	0.3	0.1	0.083	909	286	14	7.6
ABK36	ML95-1 (MLN)	134.10	454636	6145914	11	61.24	11.23	5.26	6.46	2.96	2.66	2.16	0.75	0.22	0.09	0.058	911	204	13	6.2
ABK37	**ML95-1 (MLN)**	**134.10**	**454636**	**6145914**	**11**	**61.61**	**11.35**	**5.38**	**6.48**	**2.71**	**2.55**	**2.15**	**0.73**	**0.2**	**0.09**	**0.056**	**945**	**197**	**13**	**6.1**
ABK38	ML95-1 (MLN)	161.90	454636	6145914	11	49.49	9.59	6.79	13.26	4.32	2.29	2.12	0.92	0.33	0.12	0.114	984	508	15	10
ABK39	ML95-3 (MLS)	7.45	454779	6145324	11	47.64	8.4	6.57	15.06	5.09	1.15	2.29	0.84	0.29	0.11	0.115	933	562	13	12.1
ABK40	ML95-3 (MLS)	29.80	454779	6145324	11	48	9.07	6.34	14.18	4.86	1.7	2.17	0.85	0.28	0.11	0.105	2641	479	13	11.7

Appendix 1. Major-element geochemical data from bulk rock samples collected from selected pipes in the Mountain Lake, Buffalo Head Hills and Birch Mountains fields.

Sample No.	Drillhole/ surface sample	Sample depth	UTM Easting	UTM Northing	UTM Zone	SiO$_2$ (%)	Al$_2$O$_3$ (%)	Fe$_2$O$_3$ (%)	MgO (%)	CaO (%)	Na$_2$O (%)	K$_2$O (%)	TiO$_2$ (%)	P$_2$O$_5$ (%)	MnO (%)	Cr$_2$O$_3$ (%)	Ba (ppm)	Ni (ppm)	Sc (ppm)	LOI (%)
Detection limit ----------						0.02	0.03	0.04	0.01	0.01	0.01	0.04	0.01	0.01	0.01	0.001	5	20	10	
ABK41	ML95-3 (MLS)	60.00	454779	6145324	11	46.2	7.58	7.78	16.39	4.4	1.35	1.71	0.79	0.29	0.11	0.135	837	712	12	12.6
ABK42	**ML95-3 (MLS)**	**60.00**	**454779**	**6145324**	**11**	**47.14**	**7.89**	**7.18**	**15.75**	**4.72**	**1.39**	**2.16**	**0.85**	**0.31**	**0.11**	**0.137**	**915**	**721**	**13**	**11.9**
ABK43	ML95-3 (MLS)	88.80	454779	6145324	11	45.98	7.46	6.95	16.74	5.01	1.37	1.65	0.85	0.31	0.12	0.138	829	701	13	13
ABK44	ML95-3 (MLS)	117.90	454779	6145324	11	47.08	8.31	6.79	15.53	4.75	1.43	2.24	0.84	0.3	0.12	0.13	971	601	13	12.2
ABK45	ML95-3 (MLS)	133.90	454779	6145324	11	47.09	8.64	6.63	16.22	3.86	1.61	1.98	0.86	0.31	0.12	0.115	913	580	14	11.8
ABK46	ML95-3 (MLS)	165.00	454779	6145324	11	51.37	9.29	6.43	13.71	3.24	1.92	2.44	0.89	0.3	0.1	0.119	959	507	14	9.6
ABK47	**ML95-3 (MLS)**	**165.00**	**454779**	**6145324**	**11**	**51.51**	**9.42**	**6.39**	**13.43**	**3.21**	**1.83**	**2.50**	**0.89**	**0.26**	**0.1**	**0.116**	**990**	**487**	**14**	**9.6**
Birch Mountains																				
ABK48	98DH-XE01	87.70	376850	6347300	12	17.33	5.41	7.9	4.51	27.97	0.34	2.47	1.36	0.91	0.23	0.093	3034	589	14	23
ABK49	98DH-XE01	153.96	376850	6347300	12	48.52	9.34	7.11	13.53	3.86	1.73	2.56	1.41	0.44	0.07	0.076	1344	355	14	11
ABK50	**98DH-XE01**	**153.96**	**376850**	**6347300**	**12**	**49.1**	**9.38**	**7**	**13.23**	**3.49**	**1.81**	**2.29**	**1.39**	**0.45**	**0.07**	**0.075**	**1114**	**337**	**14**	**11.4**
ABK51	98DH-R001	123.00	365051	6357585	12	37.77	7.78	7.1	12.25	11.28	0.41	3.06	1.32	0.51	0.24	0.048	1298	230	16	17.6
ABK52	98DH-PH02	137.00	351550	6330493	12	21.33	2.7	10.05	23.79	13.66	0.15	0.33	2.65	0.7	0.18	0.119	1606	496	16	23.8
ABK53	98DH-PE01	100.00	374692	6368251	12	31.87	3.5	9.79	23.41	8.86	0.19	0.61	2.08	0.43	0.17	0.197	611	834	16	18.7
ABK54	**98DH-PE01**	**100.00**	**374692**	**6368251**	**12**	**32.33**	**3.46**	**9.63**	**23.37**	**8.71**	**0.18**	**0.56**	**2.11**	**0.43**	**0.17**	**0.211**	**709**	**859**	**16**	**18.3**
ABK55	98DH-PE01	128.00	374692	6368251	12	44.78	11.42	7.92	17.39	1.78	0.4	1.92	0.61	0.27	0.05	0.018	496	31	12	13.4
ABK56	98DH-PE01	170.00	374692	6368251	12	29.2	3.76	11.78	20.29	12.38	0.25	0.75	2.24	0.66	0.19	0.185	2116	624	19	17.6
ABK57	98DH-LE01	12.20	386200	6340600	12	28.86	2.86	10.27	26.76	9.56	0.08	0.52	3.34	0.52	0.18	0.144	793	700	16	16.6
ABK58	98DH-LE01	22.00	386200	6340600	12	28.08	2.93	10.17	26.76	9.04	0.07	0.63	3.32	0.55	0.18	0.14	655	723	17	17.7
ABK59	98DH-LE01	44.00	386200	6340600	12	27.5	2.74	10.15	28.06	8.36	0.04	0.53	3.54	0.55	0.18	0.147	780	726	18	17.8
ABK60	**98DH-LE01**	**44.00**	**386200**	**6340600**	**12**	**27.42**	**2.74**	**10.25**	**28.04**	**8.54**	**0.03**	**0.58**	**3.53**	**0.54**	**0.19**	**0.145**	**769**	**712**	**18**	**17.6**
ABK61	98DH-LE01	58.00	386200	6340600	12	29.32	3.16	10.24	28.07	8.18	0.1	0.59	3.38	0.51	0.16	0.142	657	694	18	15.9
ABK62	98DH-LE01	81.90	386200	6340600	12	29.08	3.07	10.32	28.02	8.23	0.05	0.48	3.46	0.54	0.17	0.143	637	685	19	16.1
ABK63	98DH-LE01	104.20	386200	6340600	12	15.79	2.85	8.44	18.81	15.64	0.07	0.47	3.07	0.46	0.22	0.128	867	696	16	33.3
ABK64	98DH-LE01	111.00	386200	6340600	12	25.83	2.68	9.27	25.37	7.37	0.1	0.56	2.87	0.45	0.15	0.126	649	625	15	24.7
ABK65	98DH-LE01	120.00	386200	6340600	12	28.67	2.78	9.47	27.86	7.24	0.11	0.32	3.11	0.44	0.16	0.14	485	682	16	18.6
ABK66	98DH-LE01	137.00	386200	6340600	12	29.97	2.9	9.9	29.6	5.87	0.11	0.34	3.12	0.46	0.15	0.136	595	735	17	17
ABK67	98DH-LE01	159.00	386200	6340600	12	29.02	2.9	9.96	29.18	6.39	0.11	0.24	3.27	0.5	0.17	0.14	471	695	17	17.8
ABK68	98DH-LE01	187.00	386200	6340600	12	25.06	2.53	9.06	25.09	5.32	0.48	0.39	2.87	0.4	0.15	0.12	1225	618	15	28
ABK69	98DH-LE01	203.65	386200	6340600	12	13.07	2.62	7.83	19.14	16.02	0.18	0.19	3.15	0.46	0.19	0.128	532	551	15	36.4
ABK70	**98DH-LE01**	**203.65**	**386200**	**6340600**	**12**	**12.76**	**2.65**	**7.46**	**19.15**	**16.15**	**0.19**	**0.2**	**3.1**	**0.41**	**0.19**	**0.128**	**552**	**547**	**15**	**37**
ABK71	98DH-VA01B	129.50	362350	6355490	12	24.24	3.55	12.55	21.73	13.47	0.09	0.09	3.56	0.88	0.24	0.144	1115	608	20	18.5
ABK72	98DH-VA02	136.00	362350	6355490	12	22.89	4.43	14.98	18.83	12.87	0.12	0.04	4.76	0.56	0.32	0.165	1332	504	22	19.4
ABK73	98DH-VA02	147.00	362350	6355490	12	25.59	3.46	12.07	24.74	11.43	0.12	0.05	3.57	0.53	0.21	0.156	1494	704	19	17.4
ABK74	98DH-VA02	160.00	362350	6355490	12	25.31	3.59	12.72	24.66	11.19	0.12	0.06	3.68	0.53	0.2	0.163	930	701	19	17.3
ABK75	98DH-PH-01	105.00	351500	6330580	12	19.71	3.5	12.73	25.54	10.97	0.11	0.46	4.06	0.7	0.23	0.163	1661	552	25	20.9
ABK76	98DH-PH-01	130.00	351500	6330580	12	22.49	3.32	11.77	26.05	10.47	0.13	0.55	3.54	0.66	0.2	0.152	1816	522	22	20.1
ABK77	98DH-PH-01	159.00	351500	6330580	12	24.25	3.44	13.55	26.3	10.47	0.13	0.42	3.96	0.7	0.22	0.183	2628	674	26	15.4
ABK78	98DH-PH-01	175.00	351500	6330580	12	24.33	3.51	12.36	25.16	11.19	0.13	0.32	3.64	0.83	0.2	0.164	3038	596	22	17.1
ABK79	98DH-PH-01	218.00	351500	6330580	12	25.8	2.5	11.75	27.23	10.37	0.21	0.16	2.85	0.74	0.19	0.139	3040	772	18	17
ABK80	LE (surface)	Surface (till)	385924	6340845	12	57.39	11.26	6.97	7.04	5.17	3	4.62	0.54	0.59	0.21	0.04	3932	157	18	2
ABK81	Kendu	102.00	368561	6353407	12	38.86	5.06	8.55	26.52	3.68	0.35	0.95	1.13	0.35	0.11	0.107	632	1037	12	13.8
ABK82	Kendu	127.25	368561	6353407	12	37.38	4.42	7.66	23.9	7.73	0.45	0.78	0.88	0.33	0.15	0.106	666	1165	10	15.9
ABK83	Kendu	154.04	368561	6353407	12	37.43	4.65	8.02	23.03	7.95	0.45	0.99	1.05	0.34	0.12	0.091	665	978	10	15.8
▨	Duplicate sample (original sample is the previous sample)																			

Appendix 1. Major-element geochemical data from bulk rock samples collected from selected pipes in the Mountain Lake, Buffalo Head Hills and Birch Mountains fields.

Pipe	Sample No.	Drillhole ID	Depth (m)	UTM Easting	UTM Northing	UTM Zone	Co (ppm)	Cs (ppm)	Ga (ppm)	Hf (ppm)	Nb (ppm)	Rb (ppm)	Sn (ppm)	Sr (ppm)	Ta (ppm)	Th (ppm)	Tl (ppm)	U (ppm)	V (ppm)	W (ppm)	Zr (ppm)	Y (ppm)	La (ppm)
	Detection ------						0.1	0.1	0.1	0.1	0.05	0.02	0.5	0.1	0.1	0.1	0.1	0.1	5	0.5	0.5	0.1	0.1
Buffalo Head Hills																							
K4A	ABK01	4A-02	49.15	578380	6301519	11	39.2	0.1	< .5	4.5	23.1	2	< 1	239.5	1.8	5.5	0.2	1.3	17	< 1	164.5	0.7	13.1
K4B	ABK02	4B-01	140.65	578464	6300991	11	95.4	0.2	1	1.4	44.7	6.2	< 1	417.4	2.9	9.5	< .1	2	30	< 1	67.5	2.5	50.3
K4C	ABK03	4C-01	63.00	578821	6301274	11	67.6	0.2	1.4	1.6	93.2	3.9	< 1	216.9	7.8	27	< .1	5.2	18	< 1	87.8	2.6	50.9
K5A	ABK04	5A-02	84.23	582687	6306035	11	90.2	0.1	3.2	4.1	188.6	1.1	1	137.9	17.8	30.9	< .1	3.3	39	< 1	129.1	11.7	194.7
K6	ABK05	6-02	110.15	585550	6308383	11	87.4	0.2	3.2	3.1	172.3	7.6	1	419.2	12.6	23.2	< .1	3.9	66	1	120.8	10.9	163.6
K7B	ABK06	7B-01	76.93	583131	6312089	11	64.3	0.8	5.9	6.3	246	31.1	2	1279.1	17.2	31.7	< .1	7.4	90	< 1	241.6	16.8	233.6
K7C	ABK07	7C-01	58.40	583052	6312455	11	68.6	0.4	4.7	6.8	284.2	8.8	2	1581.8	21.4	37.1	< .1	6.2	78	< 1	323.5	19	320.7
K11	ABK08	11-01	55.50	619724	6320041	11	115.5	0.3	2.8	1.7	89	11.7	1	272.5	7.6	10.2	0.1	2	64	< 1	59.3	3.9	50.8
K11	ABK09	11-01	135.50	619724	6320041	11	96.6	0.5	3.7	3.9	116.8	15.5	1	601.3	7.1	14.7	0.2	3.8	57	< 1	141.8	5.4	101
K14	ABK10	14-01	14.56	582883	6315050	11	86.9	0.5	3.4	3.7	133	14.1	2	624.3	9.6	19	0.6	4.3	44	2	138.6	10.1	141.3
K14B	ABK11	14B-03	30.17	582820	6315277	11	100.1	0.2	3.1	3.4	117.1	6	1	336.8	8.2	15.4	0.1	3.3	41	< 1	124.6	8.7	118.4
K14C	ABK12	14C-06	54.30	583030	6315357	11	87.3	0.3	2.6	4.1	158.3	6.6	1	737.3	11.3	20.5	< .1	4.7	51	< 1	162.2	10.4	163.7
K14C	**ABK13**	**14C-06**	**54.30**	**583030**	**6315357**	**11**	**91.4**	**0.3**	**2.1**	**4.5**	**172.5**	**6.1**	**2**	**773.7**	**12.5**	**22.9**	**0.3**	**4.6**	**53**	**< 1**	**178**	**11.1**	**176.4**
K19	ABK14	19-03	19.85	575034	6289104	11	46.2	2.3	7.9	3	122	57	2	859.1	6.6	18.4	0.2	6.1	81	2	127.2	13.9	109.8
K91	ABK15	91-03	84.93	581820	6317052	11	88.6	0.4	2.7	5.8	208.8	22.6	2	1301.1	12.7	23.9	< .1	4.8	65	< 1	246.3	12.9	210.5
TQ155	ABK16	155-01	102.50	581763	6293954	11	84.5	0.8	4.6	2.3	135.7	22.6	2	566.3	9.4	26.3	< .1	3.1	77	< 1	88.9	7.2	145.1
TQ155	ABK17	155-01	148.60	581763	6293954	11	87.2	0.5	3.9	2	121.2	10	1	691.2	8.2	22.4	< .1	3	75	< 1	87.5	6.9	128.2
TQ155	**ABK18**	**155-01**	**148.60**	**581763**	**6293954**	**11**	**101.7**	**0.2**	**3.8**	**1.6**	**120.2**	**5.2**	**1**	**846.8**	**8.5**	**22.3**	**< .1**	**3**	**69**	**< 1**	**78.5**	**8.4**	**107.9**
BM2	ABK19	BM2-01	52.00	632349	6309823	11	10.4	5.1	15.1	7.5	11	87.4	2	179.5	1	8	0.2	3.1	156	1	286.1	21.6	28.2
BM2	ABK20	BM2-01	79.50	632349	6309823	11	62.5	1.9	5.7	3	183	122.6	2	1464.5	12.3	20.7	< .1	5.8	139	3	135.6	15.3	150.2
BM2	ABK21	BM2-01	103.30	632349	6309823	11	83.7	0.8	4.8	4	245.4	19.5	2	389.3	17.1	26.4	< .1	7.6	130	1	168.9	15.5	196.6
BM2	ABK22	BM2-01	113.80	632349	6309823	11	76.6	0.7	6.2	3.6	253.3	16.7	2	664.7	15.5	23.5	< .1	7.6	138	3	157.9	15.2	199.6
BM3	ABK23	BM3-01	124.90	631219	6314208	11	55.6	2.3	8	3	123.3	56.9	2	847.5	6.5	17.7	< .1	5.5	96	2	123	14.3	113.9
BM3	ABK24	BM3-01	144.90	631219	6314208	11	34.9	4.9	12.4	4.6	125.5	135.9	2	933.1	7.9	19.6	< .1	5.4	173	2	171.8	19	134.2
LL8	ABK25	LL8-01	77.80	629936	6301692	11	61.5	0.4	0.8	1	38	9.1	< 1	393.7	2.6	9.1	< .1	1.6	24	< 1	40.2	1.7	25.1
LL8	ABK26	LL8-01	121.50	629936	6301692	11	102.5	0.4	1.8	0.8	46.3	5.8	1	123.5	2.3	8.3	< .1	1.8	42	< 1	35.8	3.5	37.8
LL8	ABK27	LL8-01	144.90	629936	6301692	11	111.9	0.6	1.6	0.9	72.6	17.9	1	259.1	4.5	15	< .1	3.2	35	< 1	40.5	2.3	46.6
K5	ABK28	K5 (surface)	surface O/C	582432	6306145	11	80.8	1.5	4.2	2.8	108.3	10.3	1	450.8	8.5	15.1	< .1	2.9	64	< 1	107	9.1	109.9
K6	ABK29	K6 (surface)	surface O/C	585317	6308651	11	79.6	0.5	3.9	3.2	130.1	26.5	< 1	789.3	9.8	18.1	0.1	3.1	125	< 1	111.9	9.2	133.7
K14	ABK30	K14 (surface)	surface O/C	582894	6315185	11	80.7	0.3	2.9	3.9	147.2	14.6	< 1	1162.3	10.7	20.6	0.1	4.3	73	1	157.4	10.6	159.9
Mountain Lake																							
Mountain Lake North	ABK31	ML95-1 (MLN)	7.22	454636	6145914	11	32.1	3.2	13.3	3.8	83.6	76	1	443.2	5.7	15.6	0.2	3.4	138	2	146.6	16.8	74.9
Mountain Lake North	ABK32	ML95-1 (MLN)	35.00	454636	6145914	11	25.7	4	15.5	3.8	46.2	104.2	1	322.5	2.9	11.2	0.2	3.5	115	2	129.5	18.1	50.6
Mountain Lake North	**ABK33**	**ML95-1 (MLN)**	**35.00**	**454636**	**6145914**	**11**	**29.7**	**4.3**	**15**	**3.7**	**46.9**	**104.8**	**1**	**319**	**5**	**11**	**0.3**	**3.5**	**109**	**3**	**128.9**	**18.1**	**50.2**
Mountain Lake North	ABK34	ML95-1 (MLN)	64.00	454636	6145914	11	21.2	2.7	7.8	2.5	41.8	41.5	< 1	327.1	2.6	8.3	0.3	2.3	68	2	88.7	21.7	57.9
Mountain Lake North	ABK35	ML95-1 (MLN)	95.00	454636	6145914	11	33.5	3.6	14	3.7	75	80.9	1	441.7	4.5	13.2	0.5	3.8	126	2	146.5	18.3	69.7
Mountain Lake North	ABK36	ML95-1 (MLN)	134.10	454636	6145914	11	26.2	3.6	13.3	3.7	45.4	82.9	1	365.7	2.9	10.6	0.2	3.4	106	2	142.2	16.4	49
Mountain Lake North	**ABK37**	**ML95-1 (MLN)**	**134.10**	**454636**	**6145914**	**11**	**25.8**	**3.4**	**13.9**	**3.6**	**41.1**	**82.4**	**1**	**353**	**2.5**	**9.4**	**0.5**	**3.1**	**102**	**2**	**133.4**	**16.8**	**44.1**
Mountain Lake North	ABK38	ML95-1 (MLN)	161.90	454636	6145914	11	48.1	3.5	13.1	3.7	87.5	69.9	1	544.3	5.5	15	0.7	3.7	124	4	142	17.4	80.7
Mountain Lake South	ABK39	ML95-3 (MLS)	7.45	454779	6145324	11	46.5	2.8	11.2	3	80.2	72.7	1	487.9	5	12.6	0.2	3.4	115	2	115.1	14.8	70
Mountain Lake South	ABK40	ML95-3 (MLS)	29.80	454779	6145324	11	40.4	4	11.1	3.1	70.6	72.9	1	423.4	4.5	12.1	0.5	3.2	110	2	113	15.2	63.4
Mountain Lake South	ABK41	ML95-3 (MLS)	60.00	454779	6145324	11	54.9	1.9	13.5	3.2	77.2	55.9	2	428.9	4.9	12.9	0.6	3.1	103	4	121	13.7	66

Appendix 2. Trace-element geochemical data from bulk rock samples collected from selected pipes in the Mountain Lake, Buffalo Head Hills and Birch Mountains fields.

Pipe	Sample No.	Drillhole ID	Depth (m)	UTM Easting	UTM Northing	UTM Zone	Co (ppm)	Cs (ppm)	Ga (ppm)	Hf (ppm)	Nb (ppm)	Rb (ppm)	Sn (ppm)	Sr (ppm)	Ta (ppm)	Th (ppm)	Tl (ppm)	U (ppm)	V (ppm)	W (ppm)	Zr (ppm)	Y (ppm)	La (ppm)
	Detection ------						0.1	0.1	0.1	0.1	0.05	0.02	0.5	0.1	0.1	0.1	0.1	0.1	5	0.5	0.5	0.1	0.1
Mountain Lake South	**ABK42**	**ML95-3 (MLS)**	**60.00**	**454779**	**6145324**	**11**	**55.8**	**1.9**	**12.7**	**2.9**	**83.2**	**64.6**	**1**	**456.7**	**5.2**	**13.3**	**0.6**	**3**	**106**	**3**	**118.3**	**13.9**	**70.1**
Mountain Lake South	ABK43	ML95-3 (MLS)	88.80	454779	6145324	11	54	1.9	9.8	2.7	87.2	57.5	1	465.9	5.4	13.4	0.6	3.1	102	2	112.8	13.5	74.4
Mountain Lake South	ABK44	ML95-3 (MLS)	117.90	454779	6145324	11	50.1	2.6	10.5	2.9	80.3	75.5	1	466.3	5.1	12.9	0.3	3.3	110	2	114.9	14.8	70.1
Mountain Lake South	ABK45	ML95-3 (MLS)	133.90	454779	6145324	11	49.5	2.7	11.8	3.4	81.5	65.7	1	470.4	5	13.2	0.3	3	115	3	136.7	15	70.8
Mountain Lake South	ABK46	ML95-3 (MLS)	165.00	454779	6145324	11	44.1	3.7	12.1	3.6	79.2	79.2	1	432.4	4.8	13	0.2	3.6	117	2	133.1	15.4	68.9
Mountain Lake South	**ABK47**	**ML95-3 (MLS)**	**165.00**	**454779**	**6145324**	**11**	**43.5**	**3.8**	**12.2**	**3.4**	**78.7**	**84.9**	**< 1**	**419.6**	**5**	**13**	**0.2**	**3.6**	**123**	**2**	**132.7**	**15.9**	**69.5**
Birch Mountains																							
Xena	ABK48	98DH-XE01	87.70	376850	6347300	12	50.3	0.5	7.2	4.3	135.4	69.8	1	841.8	5.7	17.1	0.4	5.2	158	5	160.6	14.3	81
Xena	ABK49	98DH-XE01	153.96	376850	6347300	12	40.2	4.2	14.1	5	104.8	92.5	2	687.3	6.4	16.2	0.5	4.7	156	2	199.9	19.4	84.3
Xena	**ABK50**	**98DH-XE01**	**153.96**	**376850**	**6347300**	**12**	**37.5**	**4.1**	**12.4**	**4.9**	**97**	**85**	**1**	**592.3**	**6**	**15.1**	**0.4**	**4.2**	**148**	**2**	**183.1**	**18.6**	**77.3**
Roc	ABK51	98DH-R001	123.00	365051	6357585	12	50.8	2.9	10.4	5.6	187.7	95.1	2	880.6	9	25.4	0.3	4.9	149	1	234	21.9	189.8
Phoenix	ABK52	98DH-PH02	137.00	351550	6330493	12	73.8	0.3	5.9	4.7	280.6	18.6	2	1081.7	11.4	46.6	0.1	6.8	106	< 1	189.5	14.7	287.2
Pegasus	ABK53	98DH-PE01	100.00	374692	6368251	12	84.7	0.8	5.8	3.6	215.6	35.6	1	780	15.6	39	0.1	4.9	90	3	135.1	15.1	200.2
Pegasus	**ABK54**	**98DH-PE01**	**100.00**	**374692**	**6368251**	**12**	**91.8**	**0.9**	**6.5**	**3.9**	**219.8**	**33.3**	**2**	**776.8**	**16.0**	**38.6**	**0.2**	**5**	**90**	**3**	**137.4**	**15.2**	**207.0**
Pegasus	ABK55	98DH-PE01	128.00	374692	6368251	12	10.9	7.5	15.7	3.1	13	109.7	2	174.5	1.1	8.4	0.4	2.7	180	2	112.2	19.6	43
Pegasus	ABK56	98DH-PE01	170.00	374692	6368251	12	74.3	0.7	6.6	4.5	248	47.1	1	883.3	14.8	30.3	0.1	5	129	< 1	169	15.3	212
Legend	ABK57	98DH-LE01	12.20	386200	6340600	12	77.1	1	7.1	5.2	229.9	32.1	2	780.2	17.7	31.9	0.1	5.7	134	1	189.8	12.1	164.6
Legend	ABK58	98DH-LE01	22.00	386200	6340600	12	88.4	1.1	7.2	5.1	236.2	37.9	4	704.9	21	37.2	0.5	6.2	153	1	183.3	12.3	173.7
Legend	ABK59	98DH-LE01	44.00	386200	6340600	12	89.4	1	7.4	5.5	253.8	34.8	2	736.6	23.4	37.7	< .1	6	145	2	202.2	13.1	187.3
Legend	**ABK60**	**98DH-LE01**	**44.00**	**386200**	**6340600**	**12**	**90.4**	**1**	**8**	**5.5**	**266.5**	**37.5**	**3**	**809.7**	**22.1**	**37.3**	**0.5**	**6**	**138**	**1**	**201.9**	**14**	**202.6**
Legend	ABK61	98DH-LE01	58.00	386200	6340600	12	89.8	1.3	7.6	5.9	256.3	36.4	3	792.9	22.6	39.6	0.7	6.3	171	1	207.4	13.9	187.4
Legend	ABK62	98DH-LE01	81.90	386200	6340600	12	87	1	7.7	5.5	257.5	31.2	4	819.6	22.6	38.1	0.8	6.9	150	2	204.1	13.9	181
Legend	ABK63	98DH-LE01	104.20	386200	6340600	12	82.3	1.1	6.9	5	221.5	39.5	3	1099.4	14	33.7	0.6	7	131	1	181.6	11.8	150.7
Legend	ABK64	98DH-LE01	111.00	386200	6340600	12	76.3	1.3	6.6	5.1	216.3	39.5	2	675.5	20.5	33	< .1	5.5	120	1	173.8	10.9	141.6
Legend	ABK65	98DH-LE01	120.00	386200	6340600	12	80.2	0.9	6.8	5.6	230.3	23.3	2	433.4	21.9	35.2	0.6	5.9	123	1	187.7	11.6	153.7
Legend	ABK66	98DH-LE01	137.00	386200	6340600	12	84.5	0.9	6.7	5.5	237.6	22.7	2	399.6	20.6	36	0.1	6.2	98	< 1	188.5	11.8	153.4
Legend	ABK67	98DH-LE01	159.00	386200	6340600	12	82.8	0.6	7.4	5.2	230.9	17.6	2	330.7	21.3	34.8	0.2	5.8	115	1	180.6	11.8	157.8
Legend	ABK68	98DH-LE01	187.00	386200	6340600	12	76	1	6.4	4.8	203.9	26.7	2	454.7	18.5	31.1	< .1	5.3	92	< 1	167.6	9.7	132.9
Legend	ABK69	98DH-LE01	203.65	386200	6340600	12	72	0.7	5.8	4.4	223.9	14.2	2	775.3	13.9	31.3	< .1	3.9	104	< 1	172.7	9.9	133.6
Legend	**ABK70**	**98DH-LE01**	**203.65**	**386200**	**6340600**	**12**	**75.9**	**0.8**	**6.7**	**4.7**	**220.7**	**14.9**	**2**	**803**	**12.2**	**31.3**	**< .1**	**4.1**	**98**	**< 1**	**171.7**	**19.4**	**140**
Valkryie	ABK71	98DH-VA01B	129.50	362350	6355490	12	88.6	0.3	7.7	6.1	331.7	7.7	2	822.5	18	44.3	0.5	10.3	111	< 1	228.3	19.3	287.3
Valkryie	ABK72	98DH-VA02	136.00	362350	6355490	12	84.3	0.2	9.2	9.1	443.9	3.7	3	621.4	25.6	63.6	< .1	8.5	157	< 1	324.3	22.3	391.4
Valkryie	ABK73	98DH-VA02	147.00	362350	6355490	12	93.9	0.3	7.2	5.8	337	4.4	2	598.8	22.6	44.3	0.3	6.1	97	< 1	210.5	16.8	279.4
Valkryie	ABK74	98DH-VA02	160.00	362350	6355490	12	95.1	0.4	9	5.4	344.6	6	2	613.8	21.2	44.5	< .1	6	118	1	220.1	17.1	295.5
Phoenix	ABK75	98DH-PH-01	105.00	351500	6330580	12	83	0.5	9.1	7.3	414.6	26.3	3	822.4	11.2	88	0.2	8.5	94	1	284.1	18.5	442.1
Phoenix	ABK76	98DH-PH-01	130.00	351500	6330580	12	90.5	0.8	8.9	6.9	466.5	32	3	1019.3	25.3	85.9	0.1	8.9	113	2	286.3	19.2	448.5
Phoenix	ABK77	98DH-PH-01	159.00	351500	6330580	12	105.3	0.9	8.7	7.9	508.5	25.4	3	1161	32.2	97.3	< .1	10	104	2	310.5	20.3	487.6
Phoenix	ABK78	98DH-PH-01	175.00	351500	6330580	12	85.2	1.4	7.6	6.3	409.3	17	2	1352.8	26.1	71.6	0.1	9.2	126	1	245.8	19	422.4
Phoenix	ABK79	98DH-PH-01	218.00	351500	6330580	12	100.1	0.5	6.4	5.2	319.5	14.2	2	1408.7	21.6	53.3	< .1	7.3	105	2	198.6	15.5	333.2
Float in till	ABK80	LE (surface)	Surface (till)	385924	6340845	12	34	4.1	14.1	5.2	13.3	195.4	2	761.8	1.4	24.7	0.3	6.2	93	4	180.6	18.7	56.6
Kendu	ABK81	Kendu	102.00	368561	6353407	12	78.8	0.5	7.2	2.9	103.3	37.7	< 1	366	4.6	26.6	< .1	2.4	94	< 1	113	10.5	100.8
Kendu	ABK82	Kendu	127.25	368561	6353407	12	81.6	0.4	5.8	2.9	77.9	30.3	< 1	372	3.7	14.7	0.2	2	73	< 1	103.9	9	80.9
Kendu	ABK83	Kendu	154.04	368561	6353407	12	81.1	0.7	7.1	2.5	97	41.7	< 1	525.3	4.6	16.4	0.1	2.3	66	< 1	99.8	9.6	92.3
▨	Duplicate sample (original sample is the previous sample)																						

Appendix 2. Trace-element geochemical data from bulk rock samples collected from selected pipes in the Mountain Lake, Buffalo Head Hills and Birch Mountains fields.

Appendix 3. Petrographic Characteristics of Individual Samples

This Appendix includes the detailed description for samples selected for detailed petrography and isotopic analysis. The following Appendices 4 and 5 are intended to support the observations presented here. Electron microprobe backscatter and X-ray elemental images, or elemental distribution maps, are presented in Appendix 4. X-ray spectra, from X-ray diffraction analysis on whole-rock samples, are presented in Appendix 5 and summarized in Table A3-1. In general, the dominant minerals are olivine (forsterite, Mg_2SiO_4), serpentine (lizardite $[(Mg,Fe)_3SiO_5(OH)_4]$ and chrysotile $[Mg_3(Si_{2-x}O_5(OH)_{4-4x}])$, calcite ($CaCO_3$), dolomite (ankerite, $Ca(Fe^{+2},Mg)(CO_3)_2$), phlogopite ($KMg_3[Si_3Al]O_{10}[OH]_2$) and magnesite ($MgCO_3$).

Appendix 3. 1 Samples ABK01, ABK02 and ABK03 (Kimberlite K4, Buffalo Head Hills)

Discovered in February 1997, the K4 'complex' comprises three separate pipes, K4A, K4B and K4C, which correspond in this study to samples ABK01, ABK02 and ABK03, respectively. Pipes in the K4 complex have distinctly separate geophysical anomalies (Skelton and Bursey, 1998), but have only been tested by relatively shallow drillholes (≤200 m). Thus, it is not known whether the pipes are formed from three separate events or a single feeder system at depth. In contrast to the other pipes selected in the current report, which include two samples from different depths within the same pipe, the mineralogical descriptions for the three separate pipes within the K4 complex (i.e., samples ABK01, ABK02 and ABK03) are included as separate descriptions below.

Appendix 3.1. 1 Sample ABK01 (Kimberlite K4A, Buffalo Head Hills)

Drillhole 4A-2 penetrated altered, medium rusty brown to light grey-green kimberlitic rock from 26 m to the end of the hole at 52 m (Skelton and Bursey, 1998). Despite an extensively weathered, tan-brown appearance, sample ABK01, collected at 49 m, is relatively competent. Visible olivine pseudomorphs constitute about 20 vol. % and appear totally altered to carbonate and/or serpentine. The dominant portion of the rock (about 75 vol. %) is composed of a granular, fine-grained matrix. Country-rock xenoliths include both subrounded carbonate and angular shale clasts, the largest of which is a blade-like, 1 by 9 mm shale xenolith. No mantle xenoliths are present. Opaque minerals occur sporadically throughout the core as 1 to 2 mm xenocrysts, along with trace (<1%) amounts of light purple-red garnets (<1 mm).

In thin section, sample ABK01 is almost completely altered by variable amounts of carbonate and quartz (Figures A3-1A, A3-1B), such that it would be difficult to optically determine if the

Sample number/pipe	X-ray spectra identified minerals and mineral formula
ABK01/K4A	Quartz - SiO_2; Dolomite - $CaMg(CO_3)_2$; Magnesite - $MgCO_3$; Nimite-1MIIb - $(Ni,Mg,Al)_6(Si,Al)_4O_{10}(OH)_8$
ABK02/K4B	Dolomite - $CaMg(CO_3)_2$; Forsterite - Mg_2SiO_4; Lizardite-1M - $(Mg,Fe)_3Si_2O_5(OH)_4$; Phlogopite-2M1 - $KMg_3(Si_3Al)O_{10}(OH)_2$; Pyrite - FeS_2
ABK03/K4C	Quartz - SiO_2; Lizardite-6T1 - $Mg_3[(Si,Fe)_2O_5](OH)_4$; Dolomite - $CaMg(CO_3)_2$; Magnesite - $MgCO_3$
ABK05/K6	Calcite - $CaCO_3$; Lizardite-1M - $(Mg,Fe)_3Si_2O_5(OH)_4$; Forsterite - Mg_2SiO_4; Lizardite-6T1 - $Mg_3[(Si,Fe)_2O_5](OH)_4$
ABK29/K6	Calcite - $CaCO_3$; Lizardite-1M - $(Mg,Fe)_3Si_2O_5(OH)_4$; Forsterite - Mg_2SiO_4
ABK59/Legend	Ankerite - $Ca(Fe^{+2},Mg)(CO_3)_2$; Calcite - $CaCO_3$; Lizardite-6T1 - $Mg_3[(Si,Fe)_2O_5](OH)_4$ Magnetite - $Fe^{+2}Fe_2{}^{+3}O_4$
ABK68/Legend	Ankerite - $Ca(Fe^{+2},Mg)(CO_3)_2$; Magnesite - $(Mg,Fe)CO_3$; Lizardite-6T1 - $Mg_3[(Si,Fe)_2O_5](OH)_4$ Dolomite - $CaMg(CO_3)_2$; Beidellite-12A - $Na_{0.33}Al_2(Si,Al)_4O_{10}(OH)_2{\cdot}2H_2O$
ABK75/Phoenix	Ankerite - $Ca(Fe^{+2},Mg)(CO_3)_2$; Annite-1M - $KFe_3{}^{+2}(Si,Al)_4O_{10}(OH)_2$; Lizardite-6T1 - $Mg_3[(Si,Fe)_2O_5](OH)_4$; Magnetite - $Fe^{+2}Fe_2{}^{+3}O_4$
ABK76/Phoenix	Lizardite-1T - $(Mg,Al)_3[(Si,Fe)_2O_5](OH)_4$; Ankerite - $Ca(Fe^{+2},Mg)(CO_3)_2$; Phlogopite-2M1 - $KMg_3(Si_3Al)O_{10}(OH)_2$; Magnetite - $Fe^{+2}Fe_2{}^{+3}O_4$; Hematite - Fe_2O_3
ABK81/Kendu	Lizardite-1M - $(Mg,Fe)_3Si_2O_5(OH)_4$; Phlogopite-1M - $K(Mg,Fe)_3(Al,Fe)Si_3O_{10}(OH,F)_2$; Lizardite-6T - $Mg_3Si_2O_5(OH)_4$; Calcite - $CaCO_3$; Ankerite - $Ca(Fe^{+2},Mg)(CO_3)_2$; Clinochlore-1MIIb - $Mg_3Mn_2Al(Si_3Al)O_{10}(OH)_8$
ABK82/Kendu	Chrysotile - $Mg_3[Si_{2-x}O_5](OH)_{4-4x}$; Calcite - $CaCO_3$; Phlogopite-1M - $K(Mg,Fe)_3(Al,Fe)Si_3O_{10}(OH,F)_2$ Ankerite - $Ca(Fe^{+2},Mg)(CO_3)_2$; Anorthite - $(Ca,Na)(Al,Si)_2Si_2O_8$

Table A3-1. Results of x-ray diffraction analysis on selected bulk-rock northern Alberta kimberlitic rocks.

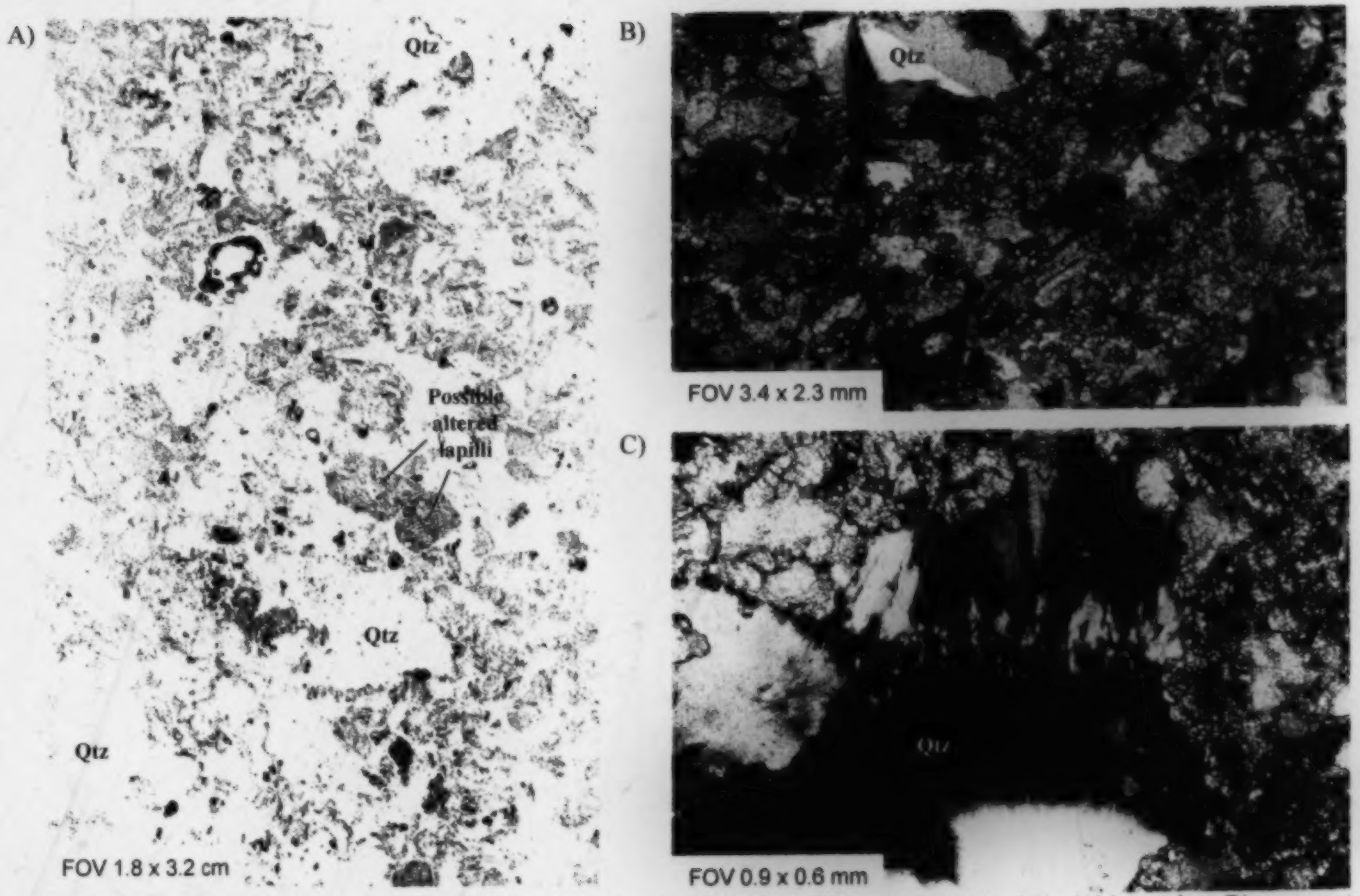
A)
Qtz
Possible altered lapilli
Qtz
Qtz
FOV 1.8 x 3.2 cm
B)
Qtz
FOV 3.4 x 2.3 mm
C)
Qtz
FOV 0.9 x 0.6 mm

Figure A3-1. Photomicrographs of sample ABK01, K4A pipe, Buffalo Head Hills: A) scan of polished thin section; B) representative matrix; and C) elongate, blocky textures indicative of secondary, hydrothermal emplacement. Abbreviation: FOV, field of view.

sample is kimberlite. Quartz constitutes up to 25 vol. %. Carlson et al. (1999) reported that silicification 'alteration caps' are prominent features in the upper parts of BHH pipes K4A, K4B, K7A and K7C. The quartz in sample ABK01 is commonly characterized by distinct elongate, blocky (jig-saw) textures that are often associated with secondary, hydrothermal emplacement (Figure A3-1C). Thus, the altered but competent nature of the sample is likely the result of silicification.

Possible olivine pseudomorphs and olivine-rich lapilli are completely altered and difficult to recognize optically. Where pseudomorphs of olivine xenocrysts are distinguishable, the olivine has been completely altered by late-stage dolomite and magnesite. The sample also includes rare opaque minerals (<2 vol. %). No phlogopite was seen.

The X-ray diffraction analysis shows that sample ABK01 is composed of quartz (SiO_2), dolomite ($CaMg[CO_3]_2$), magnesite and a nickeliferous sulphide (Table A3-1; Appendix 5). A whole-rock X-ray diffraction spectrum from ABK01 indicates the presence of nimite ($[Ni,Mg,Al]_6[Si,Al]_4O_{10}[OH]_8$), a member of the chlorite group. The most intense line (7.1 Å) for nimite, however, is absent and dominant peak at approximately 14.2Å would suggest chlorite.

Appendix 3.1. 2 Sample ABK02 (Kimberlite K4B, Buffalo Head Hills)

Drillhole 4B-1 penetrated olivine-rich kimberlitic rock from 8.5 m to the end of the hole at 200.25 m (Skelton and Bursey, 1998). Macroscopically, sample ABK02, collected at 141 m, is light grey-green, competent, medium grained and dominated by relatively unaltered olivine xenocrysts. The core is bitumen stained, with the bitumen intermixed within a fractionated matrix. Black, angular shale clasts account for approximately 5 vol. % of the rock and vary in size, with the largest observed clast being 1.3 cm in length. Mantle xenoliths were not observed. Trace amounts (<1%) of opaque (ilmenite) and sulphide minerals (pyrite) occur throughout the core.

In thin section, fresh olivine microphenocrysts constitute about 60 to 65 vol. % and range in size from less than 0.25 to 0.5 mm (Figures A3-2A, A3-2B). Olivine macrocrysts are also present, but are rare in comparison to the microphenocryst population. The majority of the olivine crystals are preserved, and sample ABK02 contains the freshest (least altered) olivine in samples selected for this study. The subhedral to anhedral olivine crystals have a variety of shapes and are generally poorly sorted, loosely packed and show no microscopic evidence of bedding. Skelton and Bursey

(1998) did not report bedding in drillhole 4B-1, although they did note distinct bedding in nearby inclined drillhole 4B-2.

Juvenile lapilli are uncommon (<10 vol. %) in comparison to olivine crystals, but do occur throughout the sample. The lapilli are easily identified on account of their dark, cryptocrystalline matrix (Figures A3-2C, A3-2D). At least two different types of lapilli exist. The lapillus in the upper left corner of Figure A3-2A has a rounded margin with subhedral to anhedral olivine, similar to the olivine distribution throughout the thin section, and a matrix devoid of opaque minerals. In contrast, the lapillus in Figure A3-2C is darker, has slightly curvilinear margins, euhedral to subhedral olivine and up to 10 vol. % opaque minerals.

The inter-clast matrix is composed mainly of serpentine (lizardite) with less common dolomite (Figures A3-2E, A3-3; Appendix 4). The dolomite preferentially replaces olivine and also occurs as blebs within the matrix. Pyrite, which is present in minor amounts (<3 vol. %), is commonly associated with the dolomite and often is present on the rim of the dolomite or within vugs (Figures A3-2E, A3-3). Small (<10 μm), discrete grains of apatite and chromite are rare and occur randomly in the matrix (Figure A3-3; Appendix 4).

Phlogopite occurs as isolated, elongate grains distributed throughout the thin section. The phlogopite constitutes up to 3 vol. %, with an average crystal size of 0.075 by 0.22 mm, and is randomly oriented. Irregular zoning in the ABK02 phlogopite observed on the microprobe is possibly a result of tetraferriphlogopite, which may result from changes in redox conditions during the final stages of crystallization (Mitchell, 1986).

The X-ray diffractogram indicates that sample ABK02 is composed of olivine (forsterite), serpentine (lizardite), dolomite, phlogopite and pyrite (FeS_2; Table A3-1; Appendix 5).

Appendix 3.1. 3 Sample ABK03 (Kimberlite K4C, Buffalo Head Hills)

Drillhole 4C-1 penetrated light brown to greyish yellow, altered kimberlite from 44 to 78 m, and light green to greyish green kimberlite from 78 m to the end of the hole at 106 m (Skelton and Bursey, 1998). In hand sample, ABK03, collected at 63 m, is tan to yellow-green, medium grained and has a highly altered, incompetent and vuggy appearance. The sample is dominated (up to 65 vol. %) by elongated, vermiform green to black crystals of random orientation.

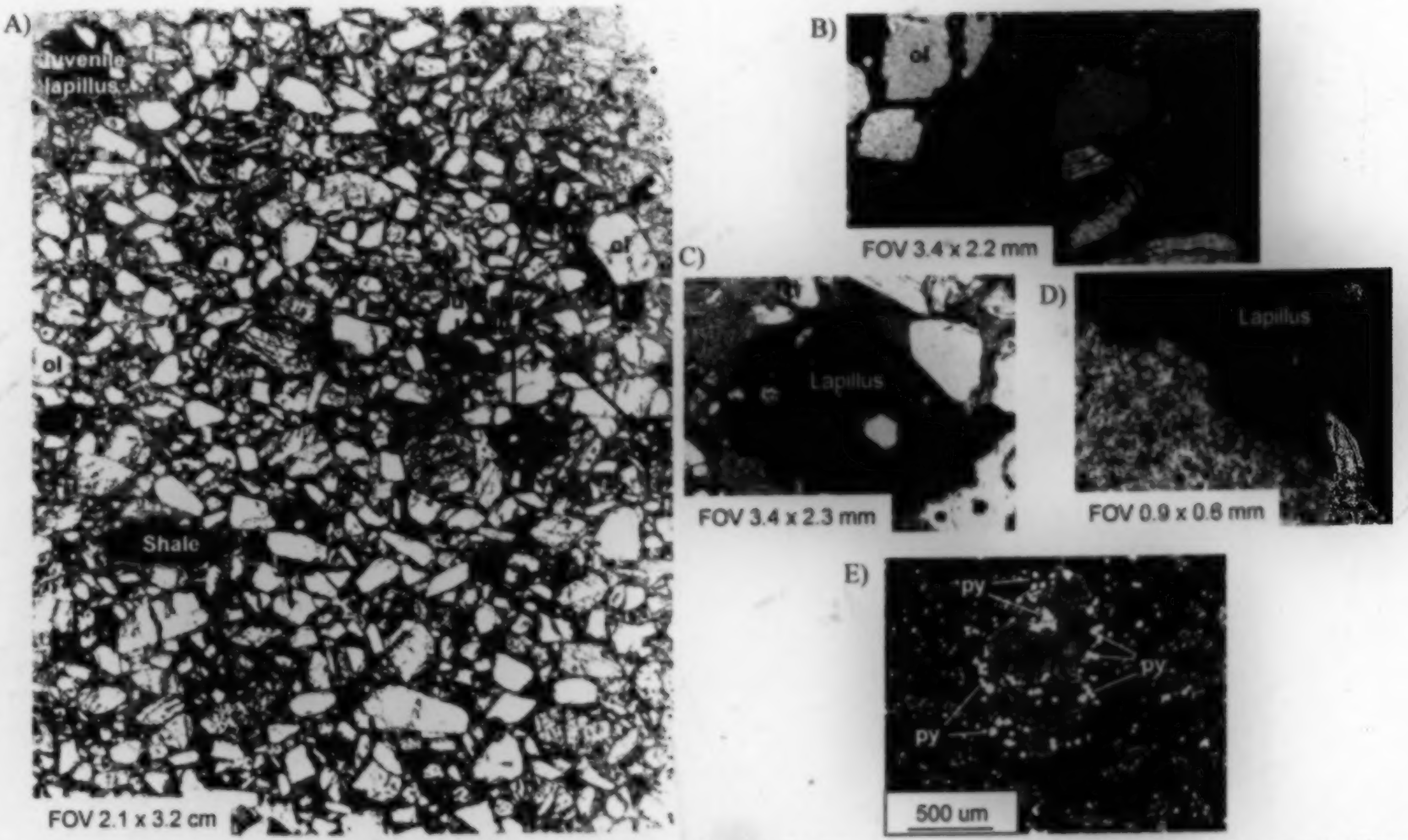
A)
Juvenile lapillus
ol
ol
Shale
FOV 2.1 x 3.2 cm
B)
ol
FOV 3.4 x 2.2 mm
C)
Lapillus
FOV 3.4 x 2.3 mm
D)
Lapillus
FOV 0.9 x 0.6 mm
E)
py
py
py
500 um

Figure A3-2. Photomicrographs of sample ABK02, K4B pipe, Buffalo Head Hills: A) scan of polished thin section; B) representative matrix; C) curvilinear lapillus; D) comparison between lapillus matrix and matrix that encompasses lapillus; and D) pyrite nucleating on dolomite. Abbreviation: FOV, field of view.

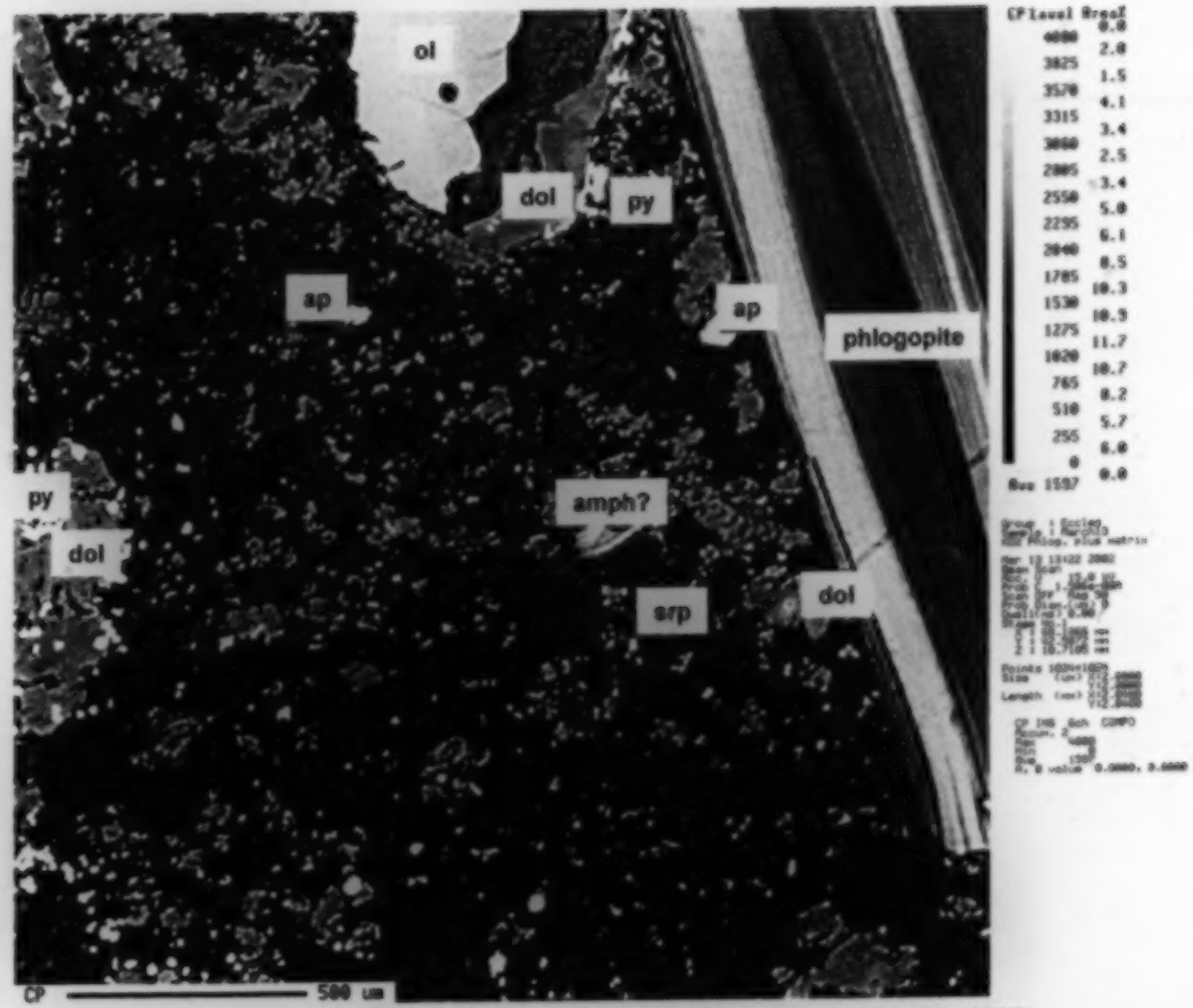
ol
dol
py
ap
ap
phlogopite
py
dol
amph?
dol
srp
CP
500 um
CP Level Area%
4080 2.0
3825 1.5
3570 4.1
3315 3.4
3060 2.5
2805 3.4
2550 5.0
2295 6.1
2040 8.5
1785 10.3
1530 10.3
1275 11.7
1020 10.7
765 8.2
510 5.7
255 6.0
0 0.0
Ave 1597

Figure A3-3. Backscatter image of representative area from sample ABK02, K4B pipe, Buffalo Head Hills.

In thin section, elongated (up to 3.5 mm long), vermiform crystals dominate the sample (Figure A3-4A). In thin section, the grains have similar characteristics to phlogopite (Figures A3-4B, A3-4C). Elemental analysis using the electron microprobe's energy-dispersive spectrometer (EDS) shows that these elongate grains with tabular cleavage are not phlogopite, but serpentine (lizardite). The genesis of this serpentine is unknown, although it may be similar to antigorite/clinochrysotile observed in the Sturgeon Lake kimberlite block and Fort à la Corne kimberlites, Saskatchewan (Scott Smith, 1995; B. Kjarsgaard, pers. comm., 2003). The serpentine is interpreted to result from the hydrous replacement of specific mineral grains. Small blebs of magnetite occur on the boundaries of the vermiform serpentine. The lath-like lizardite crystals are set in dark brown, fine-grained, serpentine-carbonate cement.

The X-ray diffractogram indicates that sample ABK03 is composed of serpentine (lizardite), quartz, dolomite and magnesite (Table A3-1; Appendix 5).

Appendix 3. 2 Samples ABK05 and ABK29 (Kimberlite K6, Buffalo Head Hills)

The K6 pipe was discovered in January 1997 when drillhole 6-1 intersected and bottomed out in 187 m of dark grey, volcaniclastic kimberlite. Sample ABK05 is from drillhole 6-2, which penetrated kimberlite from 74 to 127 m, and was collected at a depth of 100 m. Skelton and Bursey (1998) reported that several drillholes into K6 (e.g., drillholes K6-7, K6-8 and K6-10) penetrated cycles of kimberlite interlayered with mudstone with gradational contacts between kimberlite and underlying mudstone. The volcaniclastic kimberlite in drillhole 6-2 is underlain by 12 m of mudstone to the end of the hole at 139 m (Skelton and Bursey, 1998).

Macroscopically, sample ABK05 is characterized by light grey-green, competent volcaniclastic kimberlite. Olivine macrocrysts vary in size up to 1.1 cm and typically have altered, whitish (carbonate) cores and dark green rims. The matrix is medium to coarse grained and is comprised of mainly serpentine and inequigranular olivine crystals. Country-rock xenoliths in sample ABK05 constitute about 5 vol. % and include altered, subangular to rounded carbonate, siltstone and shale clasts up to 2.2 cm in size. Some sedimentary clasts appear to be internally 'sheared' and contain calcite veinlets.

Sample ABK29 was collected from an exposure of kimberlite K6 on the southeast flank of the BHH, where outcrop examinations shows numerous rock subtypes based on variations in textural and compositional characteristics, such as altered to fresh, and lapilli- and xenolith-rich kimberlite varieties. In outcrop, the rock is generally composed of grey-green, competent, coarse-

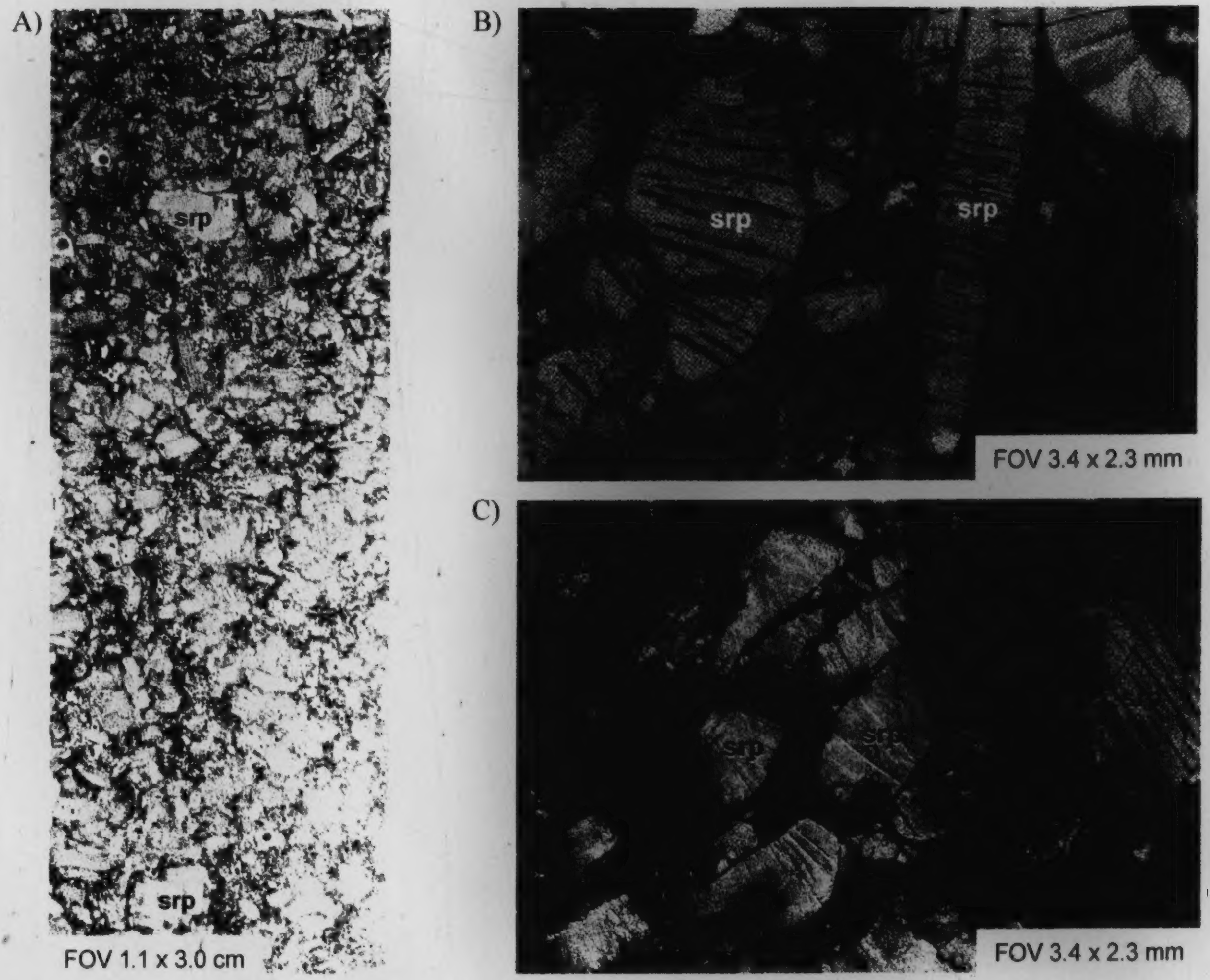
A)
srp
srp
FOV 1.1 x 3.0 cm
B)
srp
srp
FOV 3.4 x 2.3 mm
C)
srp
srp
FOV 3.4 x 2.3 mm

Figure A3-4. Photomicrographs of sample ABK03, K4C pipe, Buffalo Head Hills: A) scan of polished thin section; B) and C) selected images of tabular serpentine under plane and crossed polars, respectively. Abbreviation: FOV, field of view.

grained inequigranular kimberlite. The sample consists of olivine microphenocrysts and macrocrysts that constitute about 40 to 50 vol. %. Carbonate alteration is evident in outcrop, both in the matrix of the rock and preferentially in fractures, where calcite veins and stringers are up to 0.5 mm wide and typically striking at 135° and 100°. Despite carbonate alteration being evident, the outcrop has a higher modal amount of fresh olivine compared to the core sample ABK05, which was obtained at a depth of 110 m. Dark grey to black juvenile lapilli are evident. Mantle and basement xenoliths and mantle xenocrysts are randomly distributed throughout the outcrop. Sample ABK29 was chosen as being representative of the kimberlite outcrop.

In thin section, samples ABK05 and ABK29 have the classic inequigranular texture associated with kimberlite, caused by the presence of at least two generations of olivine: microphenocrysts less than 0.25 mm in size and occasional larger (up to 0.75 cm) macrocrysts (Figures A3-5A, A3-5B). Together, the olivine xenocrysts constitute approximately 40 vol. %. The macrocrysts are rounded to subrounded, moderately fractured, and contain fresh olivine with serpentine filling the fracture spaces. The smaller olivine microphenocrysts are mostly subhedral and altered by serpentine and calcite.

At least two types of lapilli are present. Large (up to 1 cm) juvenile lapilli occur throughout and are characterized by their dark colour, fine grain size, irregular lobate to curvilinear margins, multiple olivine crystals (often psedumorphed), and abundance of opaque matrix minerals (spinel and possibly perovskite; Figures A3-5, A3-6A). The mineralogical groundmass compositions of lapilli and the groundmass that encompasses the lapilli are similar (serpentine and calcite), but the dark-coloured lapilli matrix is finer grained and has higher CaO and lower Fe and Al_2O_3 contents (Appendix 4). In addition to these large amoeboid-shaped lapilli, juvenile pyroclasts (Figure A3-6B) occur in concentrated areas throughout the section. The juvenile pyroclasts are a significant feature of kimberlite K6, with excellent examples exposed on the eastward part of the outcrop (e.g., Figure A3-7A). Their size varies such that they may be described as ash- to lapilli-sized juvenile pyroclasts. The pyroclasts are formed when olivine phenocrysts / microphenocrysts, and less frequently macrocrysts, act as nuclei and are coated with variably sized 'skins' of magmatic material (Figure A3-7B).

The pyroclasts differ in petrographic character to pelletal lapillus associated with diatreme-facies kimberlite (e.g., Mitchell, 1986; Scott Smith, 1995) because the material surrounding olivine kernels does not contain clinopyroxene microcrysts with preferred orientations, the magmatic rinds do not encompass all of the olivine crystals present in the pyroclastic kimberlite, and the

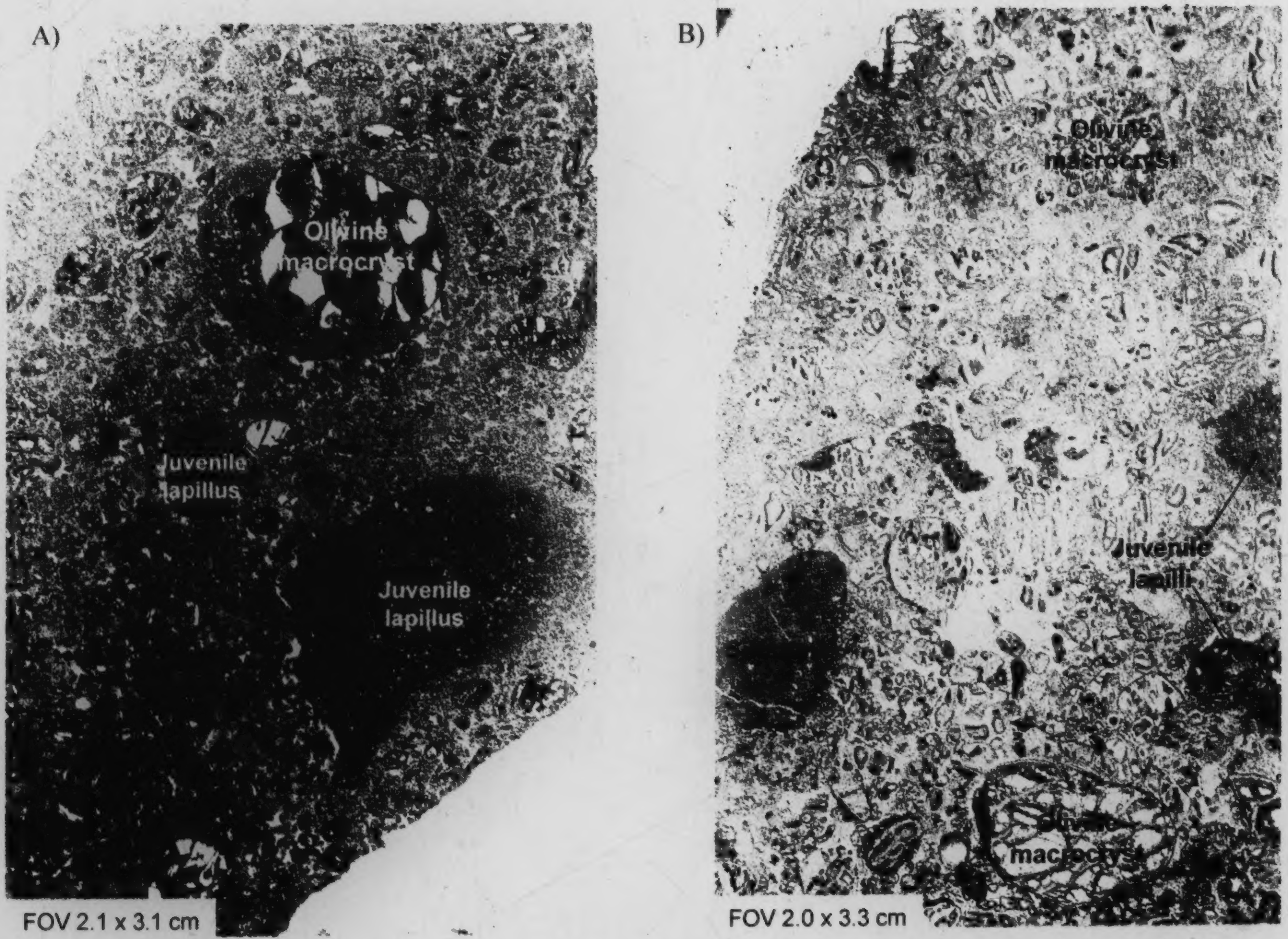
A)
Olivine macrocryst
Juvenile lapillus
Juvenile lapillus
FOV 2.1 x 3.1 cm
B)
Olivine macrocryst
Juvenile lapilli
Olivine macrocryst
FOV 2.0 x 3.3 cm

Figure A3-5. Scanned images of polished thin sections from samples ABK05 and ABK29, K6 pipe, Buffalo Head Hills. Abbreviation: FOV, field of view.

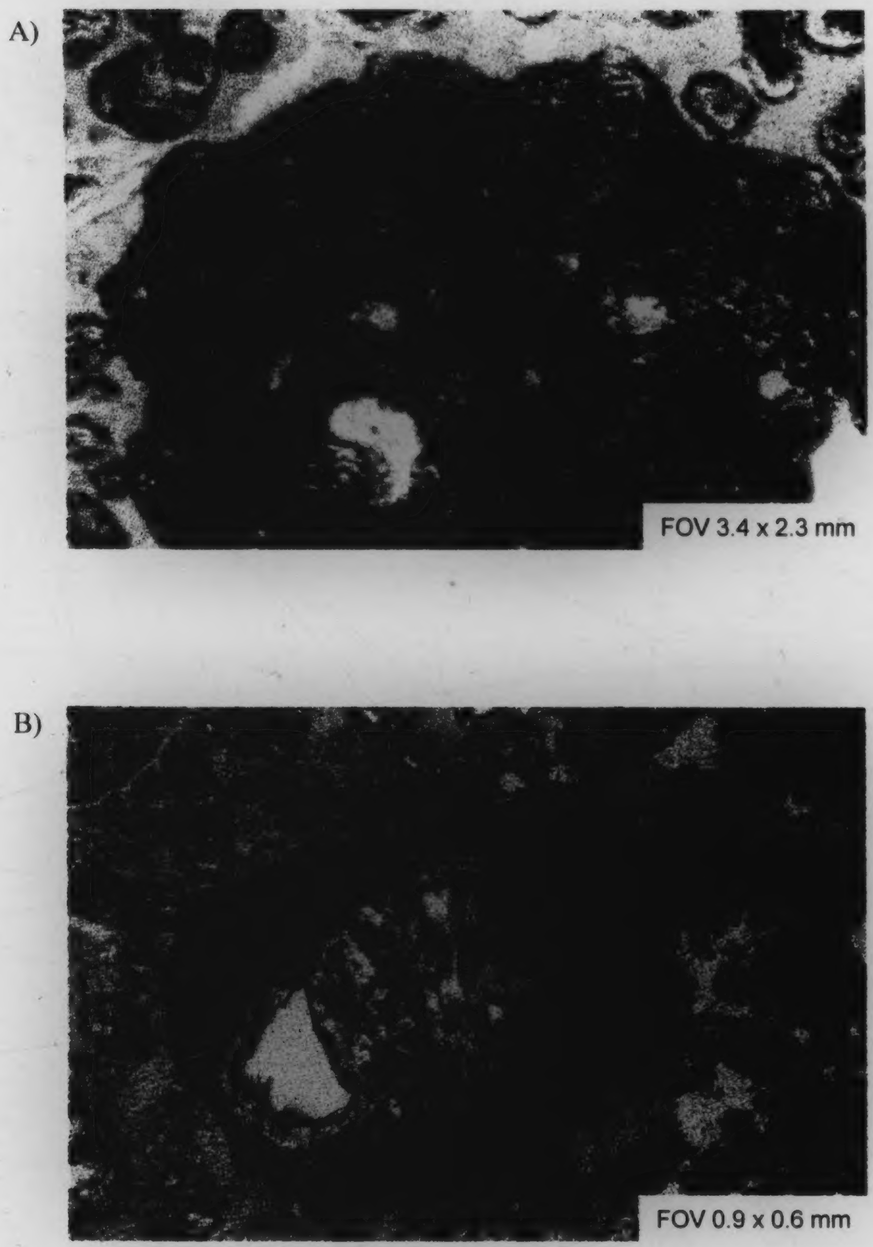
A)
FOV 3.4 x 2.3 mm
B)
FOV 0.9 x 0.6 mm

Figure A3-6. Variation between juvenile lapilli and ash-sized juvenile pyroclasts from the K6 pipe, Buffalo Head Hills: A) large, curvilinear lapillus; and B) ash-sized juvenile pyroclast. Abbreviation: FOV, field of view.

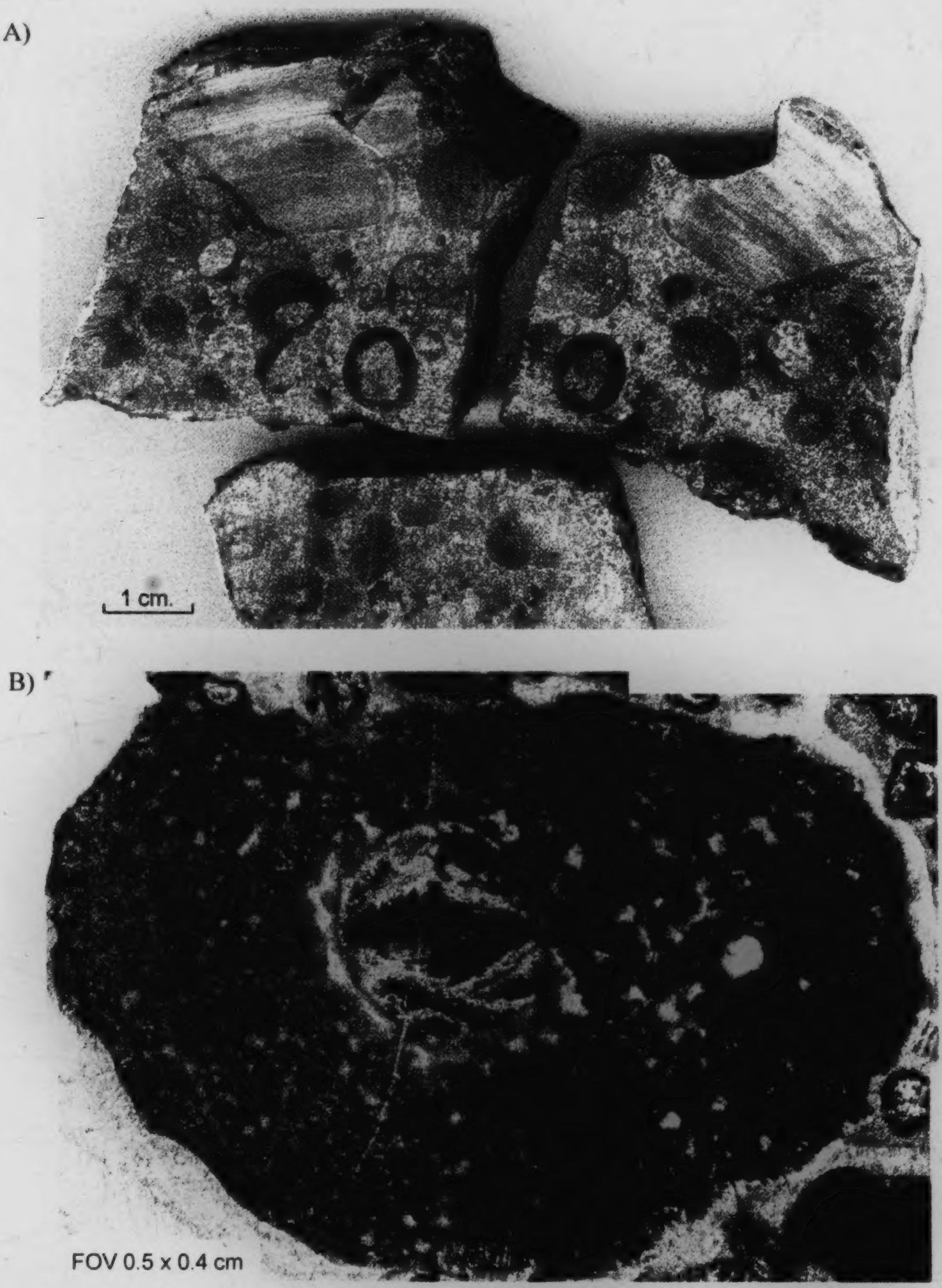

Figure A3-7. Ash- and lapilli-sized juvenile pyroclasts from the K6 pipe, Buffalo Head Hills: A) in hand sample; and B) photomicrograph mosaic capturing the entire pyroclast, in plane-polarized light. Abbreviation: FOV, field of view.

overall rock is calcitic. The mycrolitic material in the rinds of the pyroclasts are optically similar to the matrix material in the larger amoeboid lapilli, but differ in that the pyroclast mycrolitic material display some minor preferred orientation and circle the nuclei (Figure A3-7).

The groundmass encompassing the lapilli and pyroclasts is comprised of predominantly serpentine and calcite (Figure A3-8A; Appendix 4). The calcite occurs as pseudomorphs of earlier phases, mainly olivine. Other groundmass minerals include perovskite, spinel, apatite, magnetite and ilmenite. Phlogopite is rare. The pinkish brown perovskite is very small (often <3 μm) and difficult to identify (Figure A3-8B). Spinel and perovskite commonly form 'necklaces' around olivine crystals. Ilmenite occurs either as small dendritic crystals (Figure A3-8C) or together with chromite (Figure A3-8D).

Several small peridotite xenoliths (often 2 to 6 cm) were observed in outcrop. A fractured, altered xenolith, consisting of olivine, orthopyroxene and minor clinopyroxene in a serpentinized matrix, is shown in Figure A3-9. Based on macroscopic observation, mantle xenoliths are dominantly lherzolitic, pyroxenite and websterite in composition.

Based on EDS, a basement xenolith (Figure A3-10) consists of brownish green amphibolite. The boundary of the basement clast is minimally altered or distorted, indicative of either a relatively cool kimberlite magma or brief exposure to the magma. In places, there is secondary replacement of the amphibole by biotite; the timing of the replacement is not known.

The X-ray diffractograms indicate that samples ABK05 and ABK29 are composed of serpentine (lizardite), olivine (forsterite) and calcite (Table A3-1; Appendix 5).

Appendix 3. 3 Samples ABK59 and ABK68 (Legend Kimberlite, Birch Mountains)

Samples ABK59 and ABK68 were collected from drillhole 98DH-LE01 at depths of 44 m and 187 m, respectively. The lithology of the Legend pipes varies between alternating layers of coarse lapilli tuff and laminae of finer grained ash tuff, and bottoms out in light grey, competent kimberlite tuff.

In hand specimen, sample ABK59 is dark grey-green, competent, fine- to medium-grained and inequigranular. It is comprised of matrix-supported olivine pseudomorphs and xenocrysts and lapilli set in an aphanitic, dark green matrix. Olivine pseudomorphs dominate (about 40 vol. %); these are typically altered to carbonate, with only moderate (<10 vol. %) fresh olivine observed. Country rock xenoliths constitute about 5 vol. % and are dominated by white to whitish green,

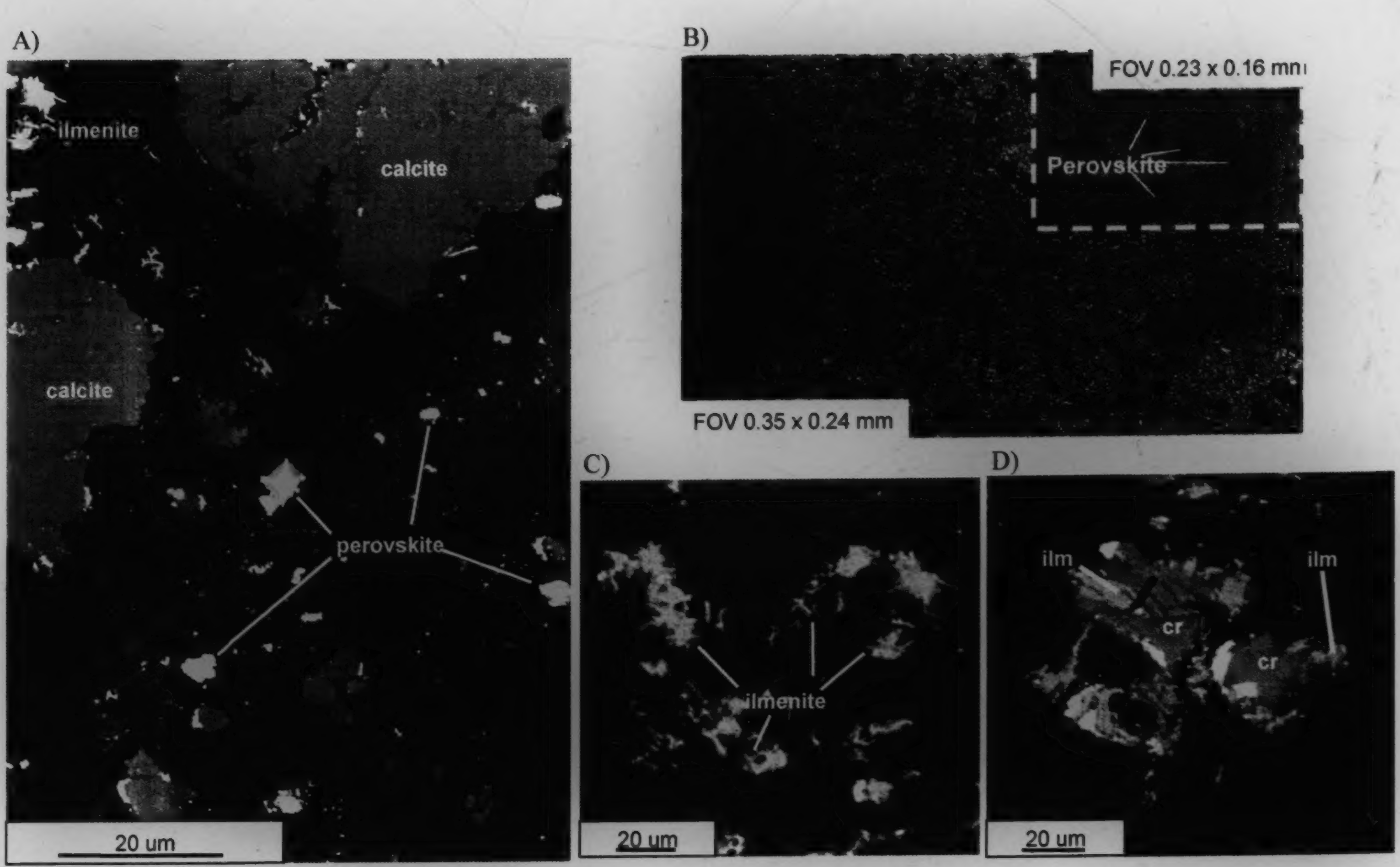
A)
ilmenite
calcite
calcite
perovskite
20 um
B)
FOV 0.23 x 0.16 mm
Perovskite
FOV 0.35 x 0.24 mm
C)
ilmenite
20 um
D)
ilm
ilm
cr
cr
20 um

Figure A3-8. Photomicrographs of sample ABK05, K6 pipe, Buffalo Head Hills: A) backscatter image of representative matrix; B) perovskite; C) dendritic crystals of ilmenite; and D) intergrown ilmenite (light grey) and chromite (dark grey). Abbreviation: FOV, field of view.

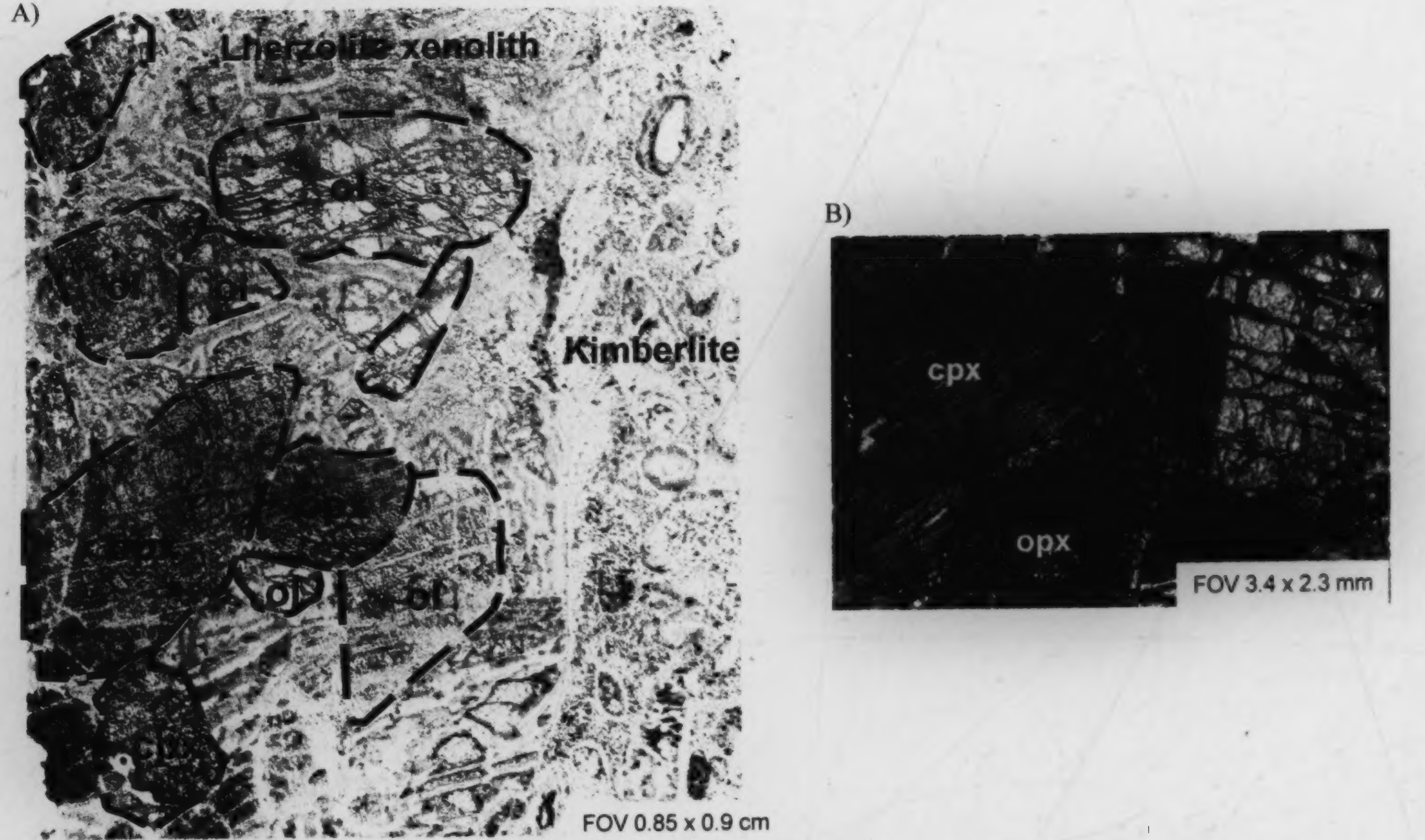
A)
Lherzolite xenolith
ol
ol
ol
Kimberlite
ol
ol
FOV 0.85 x 0.9 cm
B)
cpx
opx
FOV 3.4 x 2.3 mm

Figure A3-9. Mantle xenolith from sample ABK29, K6 pipe, Buffalo Head Hills: A) view of the xenolith in contact with kimberlite; B) expanded view of A showing clinopyroxene and orthopyroxene pair. Abbreviation: FOV, field of view.

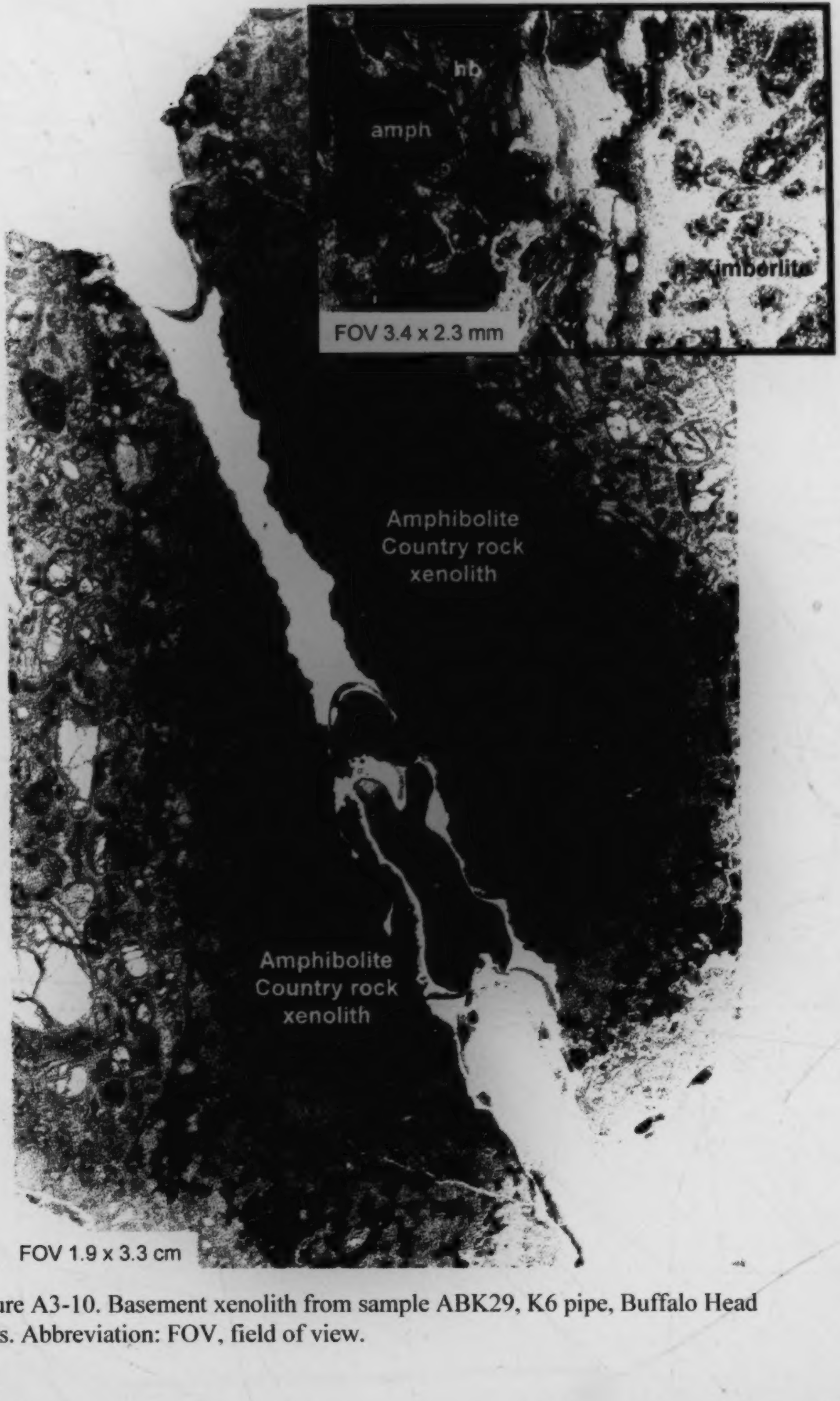
hb
amph
Kimberlite
FOV 3.4 x 2.3 mm
Amphibolite
Country rock
xenolith
Amphibolite
Country rock
xenolith
FOV 1.9 x 3.3 cm

Figure A3-10. Basement xenolith from sample ABK29, K6 pipe, Buffalo Head Hills. Abbreviation: FOV, field of view.

subrounded carbonate (up to 5 mm in length). Shale clasts are less common, and some have fractures filled with calcite. Other minerals include ilmenite and pyrite, which locally constitute up to 5 and 7 vol. %, respectively. Brown phlogopite macrocrysts are present, but rare.

In hand specimen, sample ABK68 is light grey, fine- to medium-grained and competent. The light colour may be related to carbonate enrichment, as the majority of olivine phenocrysts appear to be completely altered to carbonate. The matrix is fine grained and appears to consist of carbonate and serpentine. Like ABK59, ABK68 is comprised of about 5 vol. % country rock xenoliths. Ilmenite (up to 3 vol. %) is not as common as in sample ABK59, and sulphide minerals and phlogopite are rare.

In thin section, the Legend pipe samples ABK59 and ABK68 are characterized by their pervasive carbonate enrichment and high opaque-mineral (ilmenite) content. In comparison to the BHH samples described above, the olivine from these samples is restricted to the microphenocryst (often <0.25 mm) phase (Figures A3-11A, A3-11B). Pseudomorphed olivine microphenocrysts with relict euhedral features are by far the dominant feature and constitute about 40 to 55 vol. % of the sample. The olivine crystals have been replaced by serpentine, dolomite (ankerite) and magnesite. In rare instances, euhedral to subhedral olivine crystals are preserved and nonfractured.

Juvenile lapilli occur throughout the samples. The large lapilli have rounded to curvilinear boundaries and occur sporadically throughout the core (Figures A3-11B, A3-11C). Smaller ash- to lapilli-sized accretionary pyroclasts are also present and give the rock a distinct ovoid pyroclastic texture. Both types of lapilli consist of subhedral to euhedral microphenocrysts of serpentinized olivine pseudomorphs set in a calcite-serpentine matrix that is more carbonate-rich than the matrix external to the clasts. Dense, lapilli-rich layers typically consist of some large and many smaller lapilli.

The matrix consists mainly of serpentine and calcite (Appendix 4). Large (up to 0.15 mm) hexagonal apatite grains (Figure A3-11D) occur throughout, and especially in calcite-rich portions of the groundmass. Acicular sulphide grains are both disseminated and form clusters (e.g., Figure A3-11E). Optically these sulphide grains appear to be related to sulphosalt or Ni-sulphide minerals (e.g., millerite). When tested by the electron microprobe's EDS, the 'bladed' crystals in Figure A3-11E are FeS-rich sulphide mineral embedded possibly in an unidentified, LREE- and Re-rich mineral.

Opaque minerals include ilmenite and chromite. The ilmenite xenocrysts (Figure A3-11F) vary in size up to 1 cm and constitute up to 5 vol. %. Some of the ilmenite has a reddish-coloured alteration on the borders, which may be limonite or goethite. No phenocrysts and/or macrocrysts of phlogopite or perovskite were observed in thin section optically.

The X-ray diffractograms indicate that the Legend samples are composed mainly of serpentine (lizardite), magnesite, calcite, dolomite (ankerite) and a smectite-group clay mineral (beidellite [$Na_{0.33}Al_2(Si,Al)_4O_{10}(OH)_2 \cdot 2H_2O$]; Table A3-1; Appendix 5). Aravanis (1999) reported that glycolated X-ray diffractogram analysis on clay minerals from the Legend pipe identified a smectite-group mineral similar to saponite.

Appendix 3. 4 Samples ABK75 and ABK76 (Phoenix Kimberlite, Birch Mountains)

Samples ABK75 and ABK76 were collected from drillhole 98DH-PH01 at depths of 105 m and 130 m, respectively. Macroscopically, sample ABK75 is grey-green, competent, fine- to medium-grained, volcaniclastic kimberlitic rock. The sample contains abundant amber to dark brown phlogopite (up to 5 vol. %). Country rock xenoliths are a minor component (<3 vol. %) and include grey clay and mudstone.

Macroscopically, sample ABK76 is dark grey, competent, fine- to medium-grained volcaniclastic kimberlitic rock. Olivine xenocrysts are mainly altered, but some relatively fresh olivine macrocrysts are visible. Phlogopite is quite prominent in this sample and constitutes up to 8 vol. %. The matrix is generally fine grained and carbonate-rich.

Like samples from the Legend pipe, those from the Phoenix pipe are carbonate-rich. In thin section, carbonate is present in both the fine-grained matrix and partially to completely replaced olivine microphenocrysts (Figures A3-12A, A3-12B). Olivine pseudomorphs are typically subhedral, although some larger phenocrysts (up to 2.5 mm) are rounded. Olivine macrocrysts were not observed. Some fresh and nonfractured olivine is present in the larger phenocrysts, particularly from sample ABK76.

The samples from the Phoenix pipe contain two types of lapilli: ash-sized, single-kernel pyroclasts and larger multi-olivine crystal lapilli (Figures A3-12B, A3-12C). The lapillus in Figure A3-12C appears to have a secondary, lighter lapillus margin, which suggests that the original, dark lapillus has undergone a second eruption event.

The matrix consists mainly of serpentine with some dolomite and calcite (Appendix 4; Figure A3-

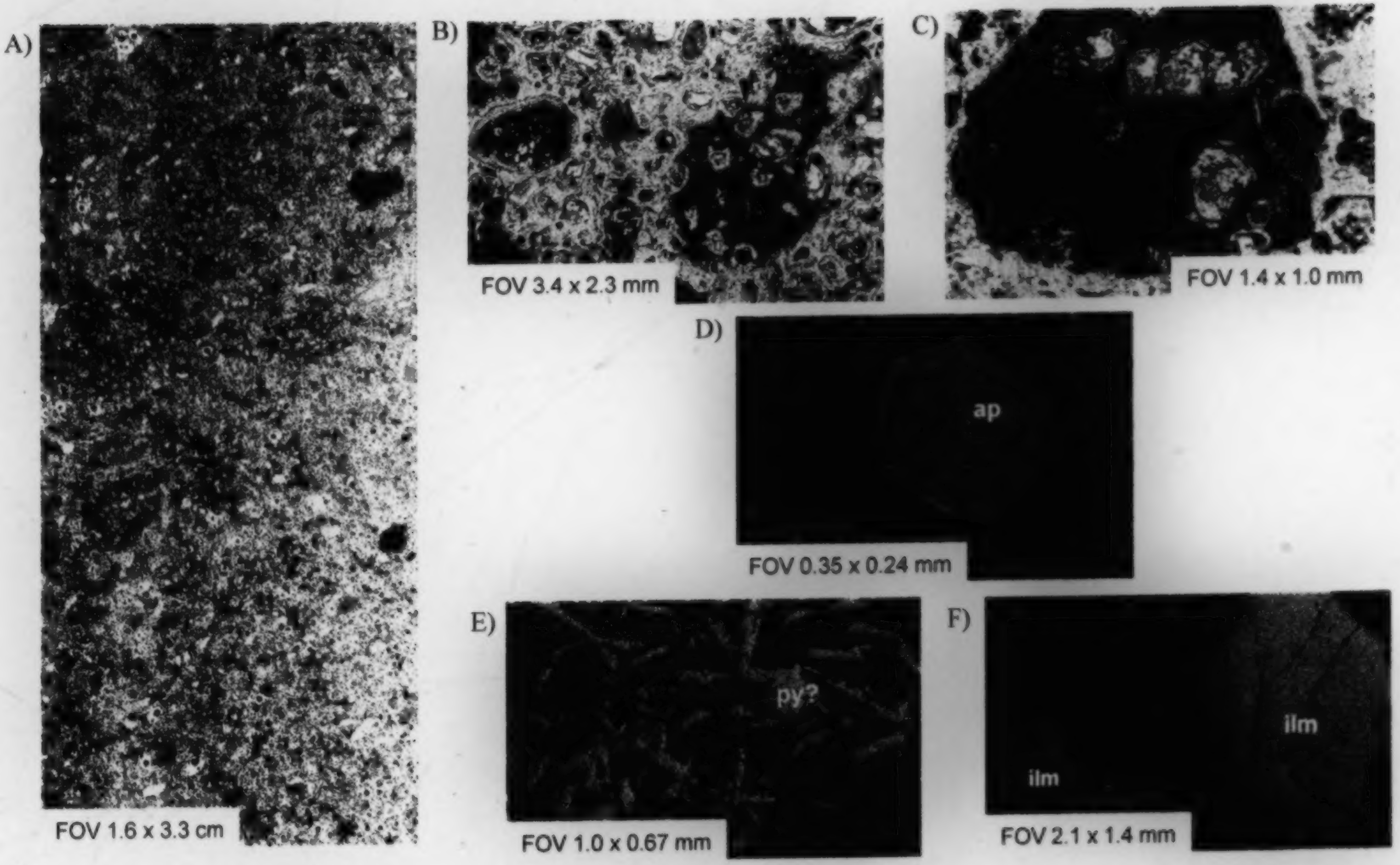
A)
FOV 1.6 x 3.3 cm
B)
FOV 3.4 x 2.3 mm
C)
FOV 1.4 x 1.0 mm
D)
ap
FOV 0.35 x 0.24 mm
E)
py?
FOV 1.0 x 0.67 mm
F)
ilm
ilm
FOV 2.1 x 1.4 mm

Figure A3-11. Photomicrographs of sample ABK59, Legend pipe, Birch Mountains: A) scan of polished thin section; B) blowup of image A, with lapillus; C) lapillus; D) hexagonal apatite; E) needle-textured sulphide mineral (?pyrite); and F) ilmenite. Abbreviation: FOV, field of view.

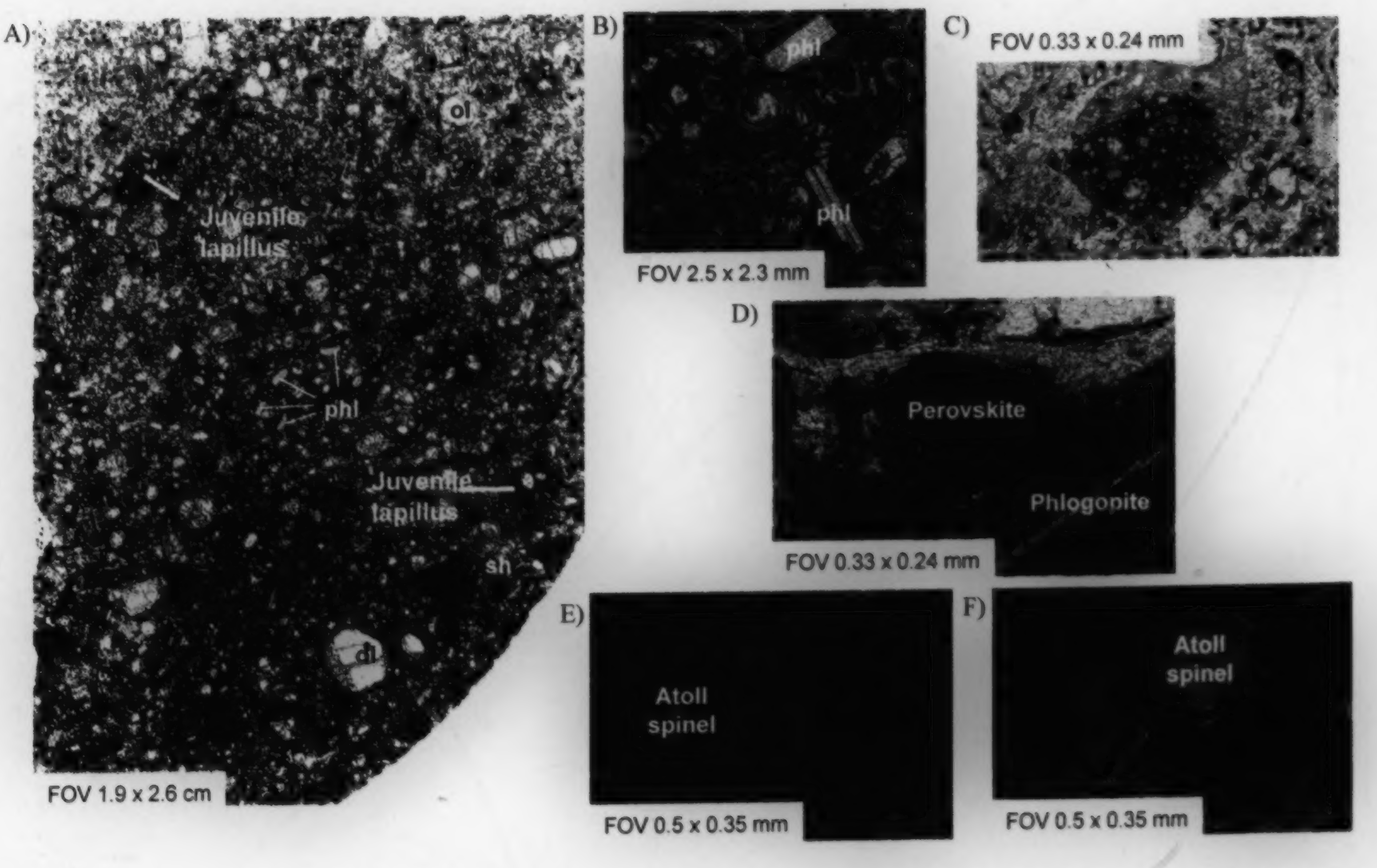
A)
Juvenile lapillus
ol
phl
Juvenile lapillus
sh
dl
FOV 1.9 x 2.6 cm
B)
phl
phl
FOV 2.5 x 2.3 mm
C)
FOV 0.33 x 0.24 mm
D)
Perovskite
Phlogopite
FOV 0.33 x 0.24 mm
E)
Atoll spinel
FOV 0.5 x 0.35 mm
F)
Atoll spinel
FOV 0.5 x 0.35 mm

Figure A3-12. Photomicrographs of sample ABK76, Phoenix pipe, Birch Mountains: A) scan of polished thin section; B) enlargement of image A; C) lapillus; D) matrix perovskite and phlogopite; and E) and F) atoll-textured spinel. Abbreviation: FOV, field of view.

13), but overall is characterized by an abundance of phlogopite macrocrysts and perovskite phenocrysts (Figures A3-12B, A3-12D) relative to the K4, K6 and Legend pipes. The phlogopite constitutes between 4 and 7 vol. %. The mica grains are typically isolated and have random orientation, although the grains, in places, appear aligned and at significant magnification, (Figure A3-13), the (<20 μm) phlogopite grains are also intergrown. In cross-polarized light, the greenish hue on some phlogopite grains is likely related to chloritization. Several phlogopite grains include inclusions of either a sulphide mineral or apatite. The perovskite grains are typically large (up to 0.12 mm and average about 0.08 mm) and have altered rims (Figure A3-12D).

Atoll-textured spinel grains are distributed throughout the sample (Figures A3-12E, A3-12F). The term 'atoll spinel' was used by Mitchell and Clarke (1976) to describe resorbed, complexly mantled spinel grains, believed to have formed by the instability of magnesian ulvöspinel–ulvöspinel–magnetite spinel with late-stage, carbonate-rich fluids that formed the groundmass. Optically, these spinel grains have a different reflectivity from core to border. The cores of the atoll spinel grains in the Phoenix pipe are most commonly magnetite, while the rims consist of Fe, Ti and relatively little Cr.

Other groundmass minerals include hexagonal apatite and highly altered Fe-oxide minerals (Figure A3-13). Ilmenite xenocrysts are rare.

Based on the X-ray diffractograms indicate that the Phoenix samples are composed mainly of dolomite (ankerite) and serpentine (lizardite), with magnetite (Fe_3O_4) and phlogopite (Table A3-1; Appendix 5). In addition, sample ABK76 contains hematite ($Fe_2O_{3(T)}$).

Appendix 3. 5. Samples ABK81 and ABK82 (Kendu Pipe, Birch Mountains)

Macroscopically, sample ABK81, collected at 102 m, is light to dark grey-green and fairly competent. In contrast to other samples studied, the Kendu core contains abundant mantle xenolith and xenocrystic material, lapilli and segregation-type textures as defined by agglomeration of different minerals. The matrix is fine grained to aphanitic, dark grey-green and carbonatized. Several mantle xenoliths were observed. The largest, a possible eclogitic mantle xenolith, is about 1.65 by 1.25 cm. Fresh xenocrysts of eclogite and pyrope garnet, phlogopite and diopside are randomly distributed throughout the sample.

Macroscopically, sample ABK82, collected at 127 m, is light to dark grey-green, fairly competent and mantle xenocryst–rich. Dark green-black, angular fragments (lapilli) occur throughout the

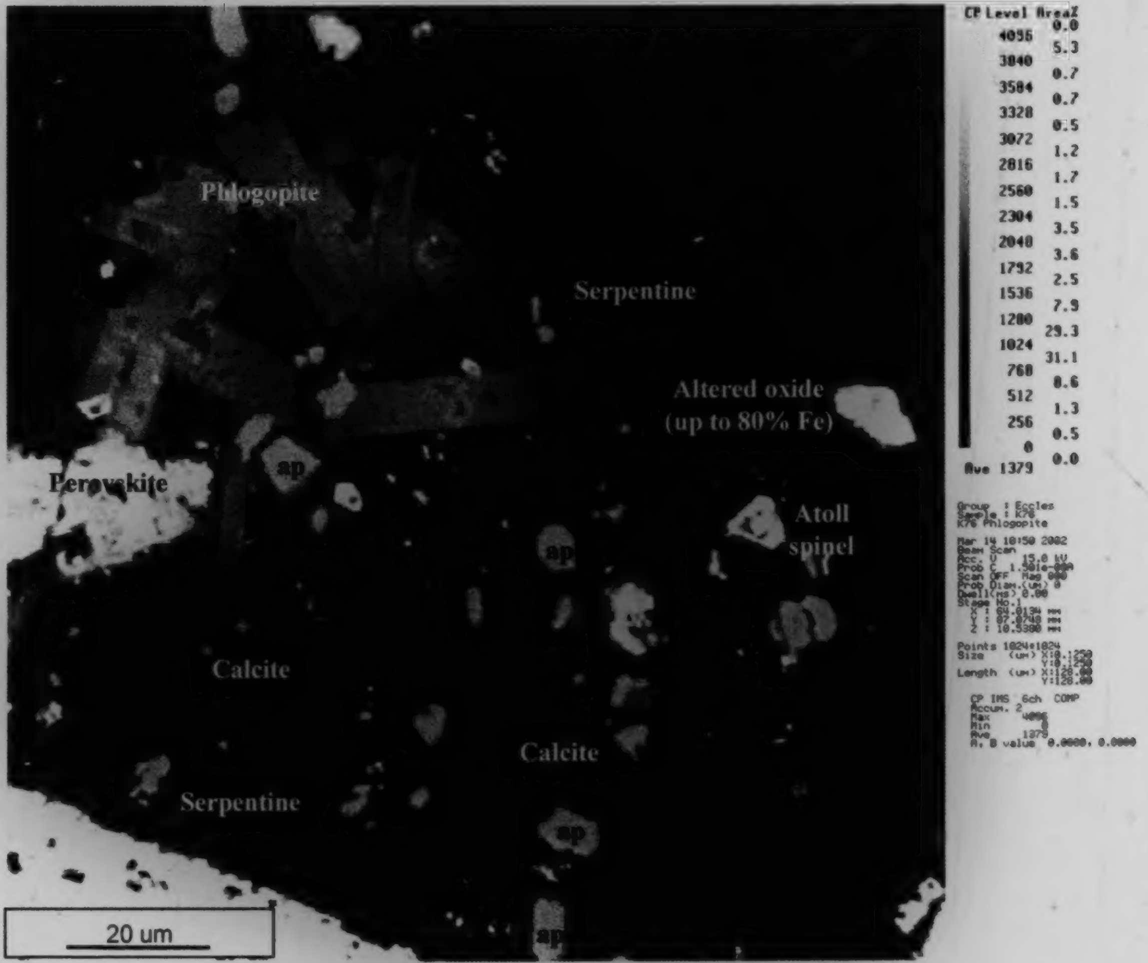
Phlogopite
Serpentine
Altered oxide
(up to 80% Fe)
Perovskite
ap
Atoll
spinel
ap
Calcite
Calcite
Serpentine
ap
ap
20 um
CP Level Area%
4096 0.0
3840 5.3
3584 0.7
3328 0.7
3072 0.5
2816 1.2
2560 1.7
2304 1.5
2048 3.5
1792 3.6
1536 2.5
1280 7.9
1024 29.3
768 31.1
512 8.6
256 1.3
0 0.5
Ave 1379 0.0
Group : Eccles
Sample : K76
K76 Phlogopite
Mar 14 10:50 2002
Beam Scan
Acc. V 15.0 kV
Scan OFF
Stage No.1
X : 64.0134 mm
Z : 10.5300 mm
Points 1024*1024
Length (um) X:128.00
Y:128.00
CP IMS 6ch COMP
Accum. 2
Ave 1379

Figure A3-13. Backscatter image of representative area from sample ABK76, Phoenix pipe, Birch Mountains.

sample. The matrix is grey-green and fine grained. Mantle xenoliths in this sample are up to 2.3 by 0.9 cm in size and typically consist of eclogite. There are also several smaller (<0.5 cm) xenoliths. The sample contains abundant mantle-indicator minerals (phlogopite, chrome diopside, eclogitic and pyrope garnet, ilmenite, clinopyroxene). Country rock xenoliths (possibly containing original plagioclase) constitute up to 8 vol. %, and are variably altered.

Compared to samples from the K4, K6, Legend and Phoenix pipes, the Kendu samples can easily be distinguished macroscopically and microscopically by the abundance of

1) mantle xenocrysts (mainly phlogopite, chrome diopside and garnet);
2) mantle xenoliths (possibly lherzolite and eclogite), which are set in a fine-grained, dark brown matrix;
3) dark, black-green juvenile lapilli; and
4) altered basement-rock xenoliths.

Mantle xenoliths and xenocrysts may locally constitute up to 30 vol. % of the samples. The xenoliths comprise mainly lherzolite and eclogite, (determined optically as electron microprobe analysis was not completed as part of this study). Their exact size is difficult to ascertain in drillcore, but they generally are less than 10 cm in diameter, with the majority being less than 5 cm. The xenoliths are ovoid to subangular, irregularly shaped and slightly to moderately altered (Figure A3-14A). The mantle xenocryst population occurs throughout the core and includes pyrope and eclogitic garnet, clinopyroxene, orthopyroxene, phlogopite, ilmenite and spinel. Garnet grains are up to, but rarely larger than, 0.5 mm in one direction. Complete or partial kelyphite rims are present on garnet xenocrysts.

In thin section, a phlogopite- and serpentine-rich microlitic material, which is very similar in mineralogy to the juvenile lapilli described below, is often concentrated by flow differentiation forming haloes around pre-existing country rock and mantle xenoliths, which give a superficial appearance to Group II kimberlite (Figure A3-15A). The phlogopite crystals are commonly oriented in a way that conforms to the shape of the xenolith.

Juvenile lapilli are another diagnostic feature in the Kendu samples and locally constitute up to 40 vol. %. The dark-coloured lapilli stand out in an aphanitic, almost indistinguishable matrix, and consist of microphenocrystic phlogopite (up to 40 vol. %) with vermiform-textured serpentine (similar to serpentine in K4, BHH), opaque minerals (mainly ilmenite), apatite and calcite-rich anhedral to euhedral spherical structures, which likely represent olivine

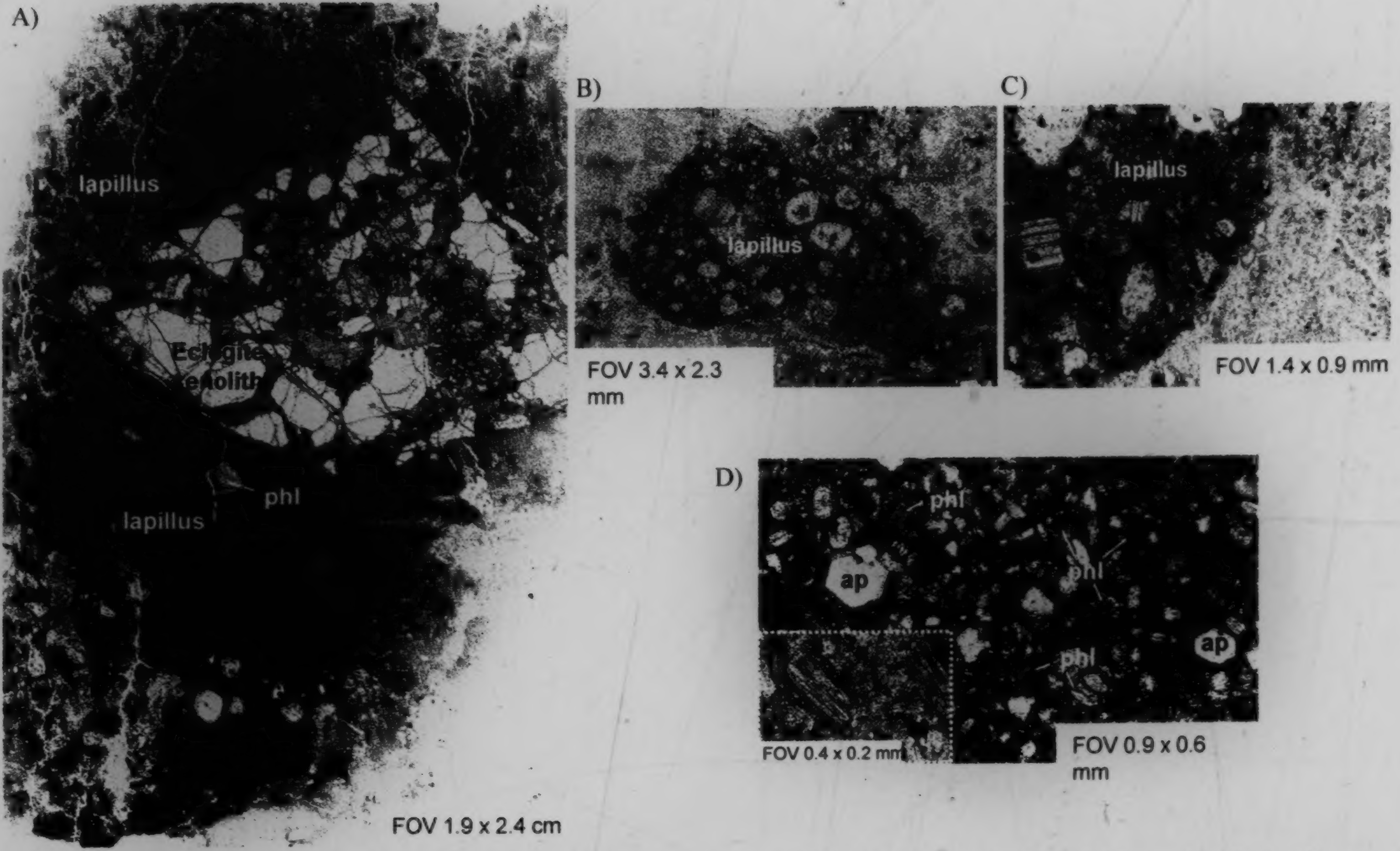
A)
lapillus
Eclogite xenolith
phl
lapillus
FOV 1.9 x 2.4 cm
B)
lapillus
FOV 3.4 x 2.3 mm
C)
lapillus
FOV 1.4 x 0.9 mm
D)
phl
ap
phl
phl
ap
FOV 0.4 x 0.2 mm
FOV 0.9 x 0.6 mm

Figure A3-14. Photomicrographs of sample ABK81, Kendu pipe, Birch Mountains: A) scan of polished thin section; B) lapillus in an aphanitic matrix; C) matrix comparison between lapillus and matrix external to lapillus; and D) magnified image of an lapillus. Abbreviation: FOV, field of view.

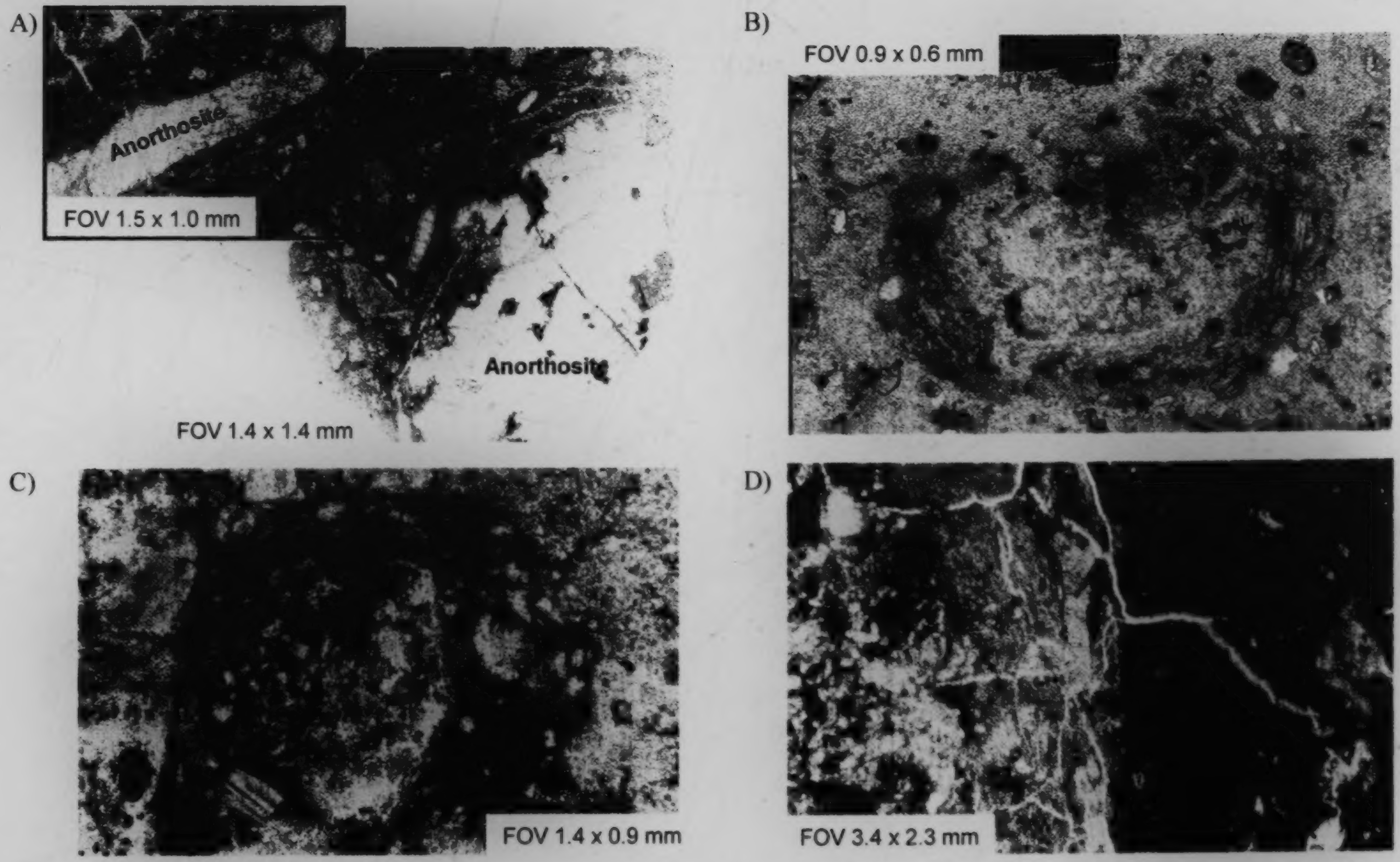
A)
Anorthosite
FOV 1.5 x 1.0 mm
Anorthosite
FOV 1.4 x 1.4 mm
B)
FOV 0.9 x 0.6 mm
C)
FOV 1.4 x 0.9 mm
D)
FOV 3.4 x 2.3 mm

Figure A3-15. Photomicrographs of the Kendu pipe, Birch Mountains: A) microphenocrystic kimberlitic rock haloes around altered basement xenoliths; B) and C) pelletal-textured lapilli with tangentially aligned phlogopite crystals; and D) matrix microsegregation textures. Abbreviation: FOV, field of view.

pseudomorphs (Figures A3-14B to A3-14D). The lapilli vary in diameter, up to 1.2 cm and more (the pyroclast in Figure A3-14 continues off the slide), and average about 0.25 mm. They vary drastically in shape, from rounded, spherical shapes to very irregular shapes.

Pelletal-textured lapilli are less common than the aforementioned juvenile lapilli, but occur throughout the sample. These lapilli consist of large (up to 0.2 mm), mostly altered olivine kernels that are surrounded by thin mantles of fine-grained cryptocrystalline kimberlitic material (mainly phlogopite, serpentine and apatite). Figures A3-15B and A3-15C illustrates an example of the pelletal lapilli, complete with tangentially aligned platy shards of phlogopite and serpentine around a remnant olivine kernel.

The groundmass consists mainly of serpentine and calcite, and has a heterogeneous appearance having, for example, aphanitic to coarse-grained serpentine-rich portions (Figure A3-15D), possibly a result of alteration. The olivine xenocrysts outside the lapilli are difficult to distinguish in plane-polarized light due to pervasive replacement. In addition, the groundmass contains a wide range of silicate (e.g., garnet, clinopyroxene and orthopyroxene), semi-opaque (e.g., perovskite), and opaque (e.g., spinel, ilmenite and sulphide) minerals (Figure A3-16). Rutile is also common, as observed in heavy-mineral concentrates. In thin section, rutile is commonly present in clinopyroxene and occurs as rod-like or needle-like inclusions, which are generally oriented parallel to crystal faces, and is therefore of mantle-derived xenocrystic origin (Figures A3-16A, A3-16B).

Basement xenoliths consist mainly of anorthosite. It is possible that they have undergone contact metamorphism, as indicated by their irregular, diffuse boundaries (Figure A3-15A). Trace amounts of possible labradorite and/or bronzite were also observed.

The X-ray diffractograms indicate that the Kendu samples are composed predominately of serpentine (lizardite and chrysotile $[Mg_3(Si_{2-x}O_5)(OH)_{4-4x}]$), dolomite (ankerite), phlogopite and calcite (Table A3-1; Appendix 5). The samples also contain contamination from bedrock material. Sample ABK81 contains clinochlore ($Mg_3Mn_2Al[Si_3Al]O_{10}[OH]_8$), which typically forms as a common hydrothermal alteration product of amphibole, pyroxene and biotite, and sample ABK82 contains anorthite ($CaAl_2Si_2O_8$).

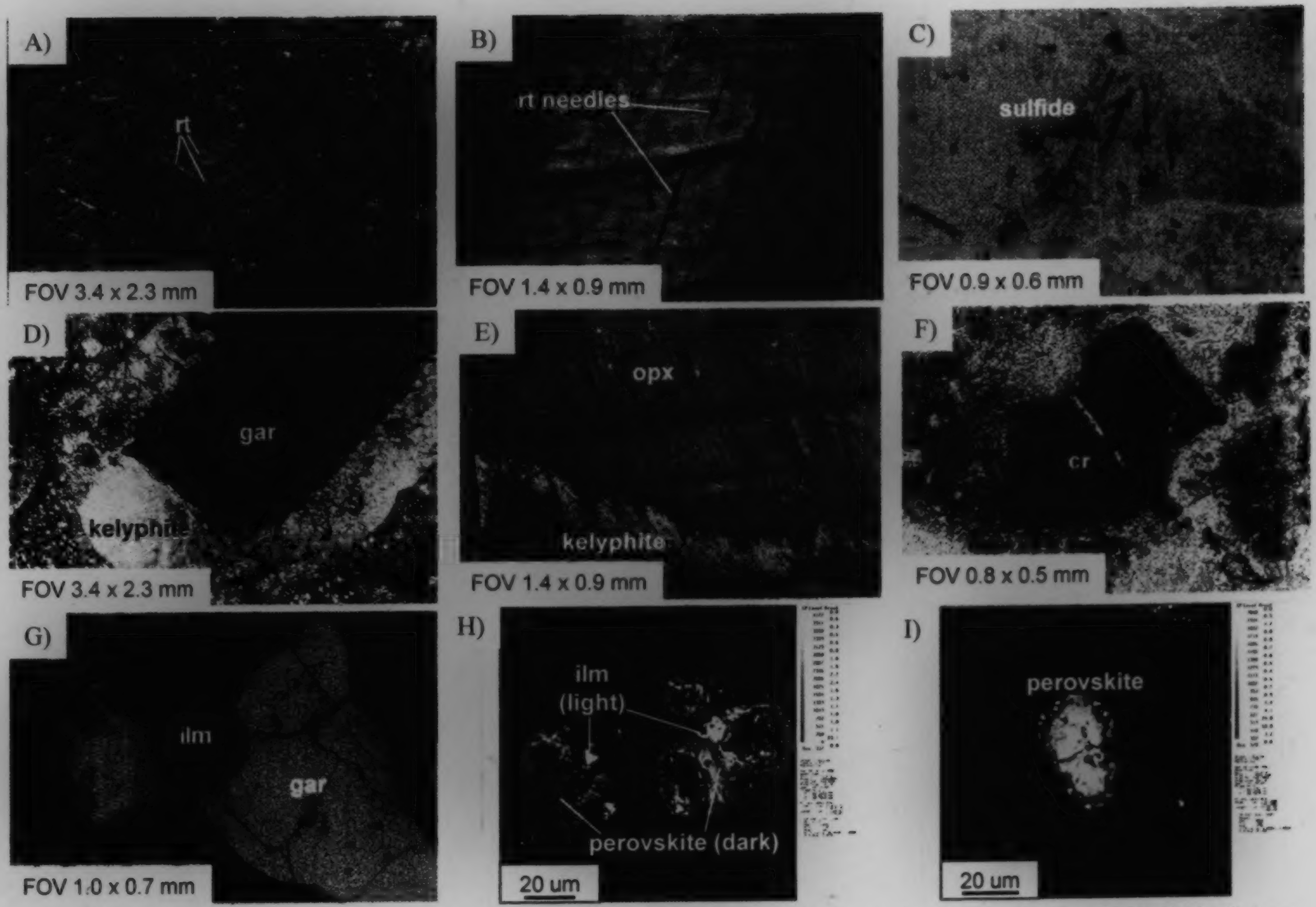
A)
rt
FOV 3.4 x 2.3 mm
B)
rt needles
FOV 1.4 x 0.9 mm
C)
sulfide
FOV 0.9 x 0.6 mm
D)
gar
kelyphite
FOV 3.4 x 2.3 mm
E)
opx
kelyphite
FOV 1.4 x 0.9 mm
F)
cr
FOV 0.8 x 0.5 mm
G)
ilm
gar
FOV 1.0 x 0.7 mm
H)
ilm
(light)
perovskite (dark)
20 um
I)
perovskite
20 um

Figure A3-16. Photomicrographs of mantle minerals from the Kendu pipe, Birch Mountains. Abbreviation: FOV, field of view.

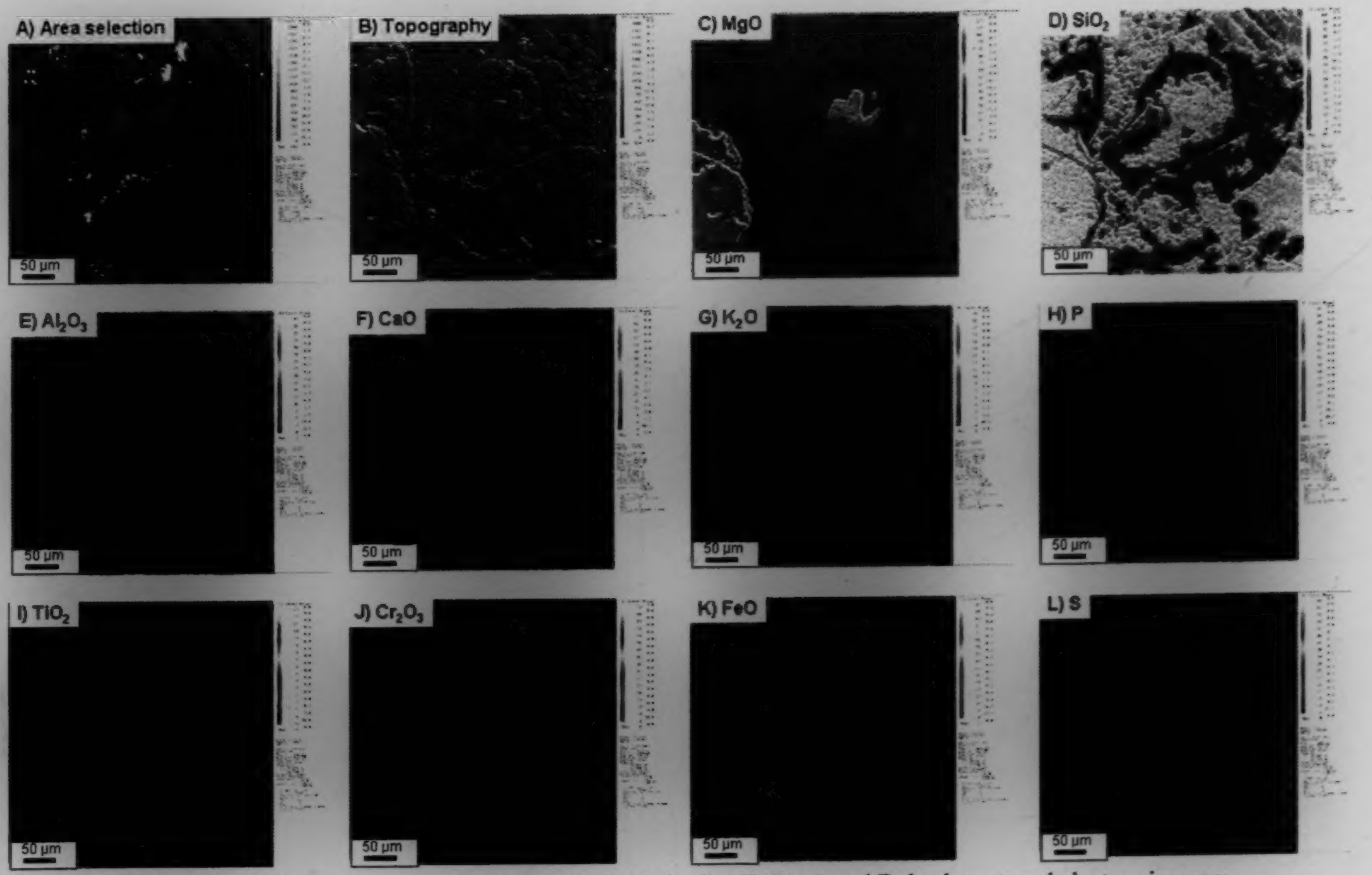
A) Area selection
B) Topography
C) MgO
D) SiO_2
E) Al_2O_3
F) CaO
G) K_2O
H) P
I) TiO_2
J) Cr_2O_3
K) FeO
L) S
50 µm

Appendix 4. Elemental distribution map of sample ABK02 (kimberlite K4B). A and B: back scattered electron images; C to L: x-ray elemental images

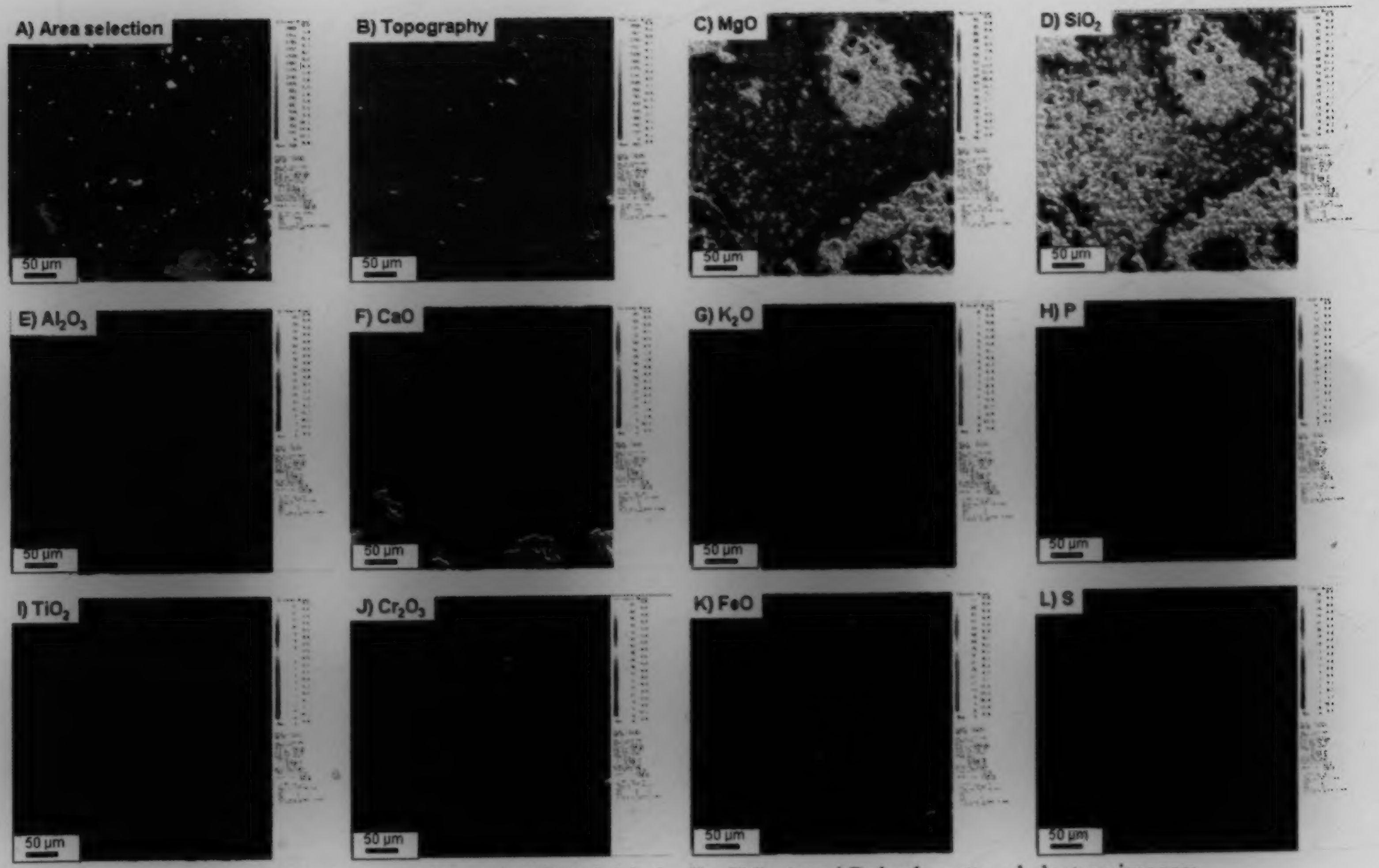
A) Area selection
B) Topography
C) MgO
D) SiO$_2$
E) Al$_2$O$_3$
F) CaO
G) K$_2$O
H) P
I) TiO$_2$
J) Cr$_2$O$_3$
K) FeO
L) S
50 µm

Appendix 4. Elemental distribution map of sample ABK05 (kimberlite K6). A and B: back scattered electron images; C to L: x-ray elemental images

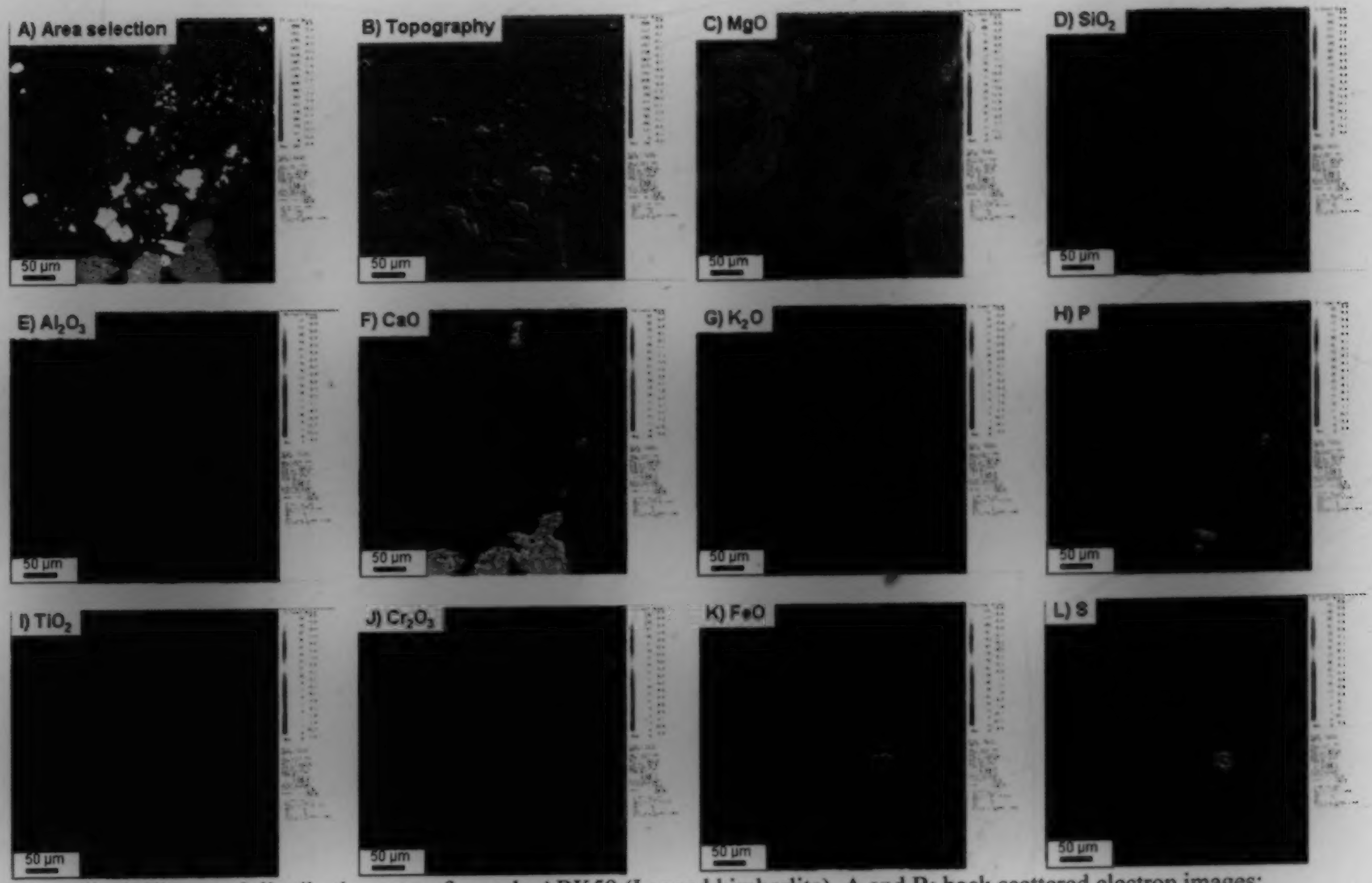
A) Area selection
B) Topography
C) MgO
D) SiO_2
E) Al_2O_3
F) CaO
G) K_2O
H) P
I) TiO_2
J) Cr_2O_3
K) FeO
L) S
50 µm

Appendix 4. Elemental distribution map of sample ABK59 (Legend kimberlite). A and B: back scattered electron images; C to L: x-ray elemental images

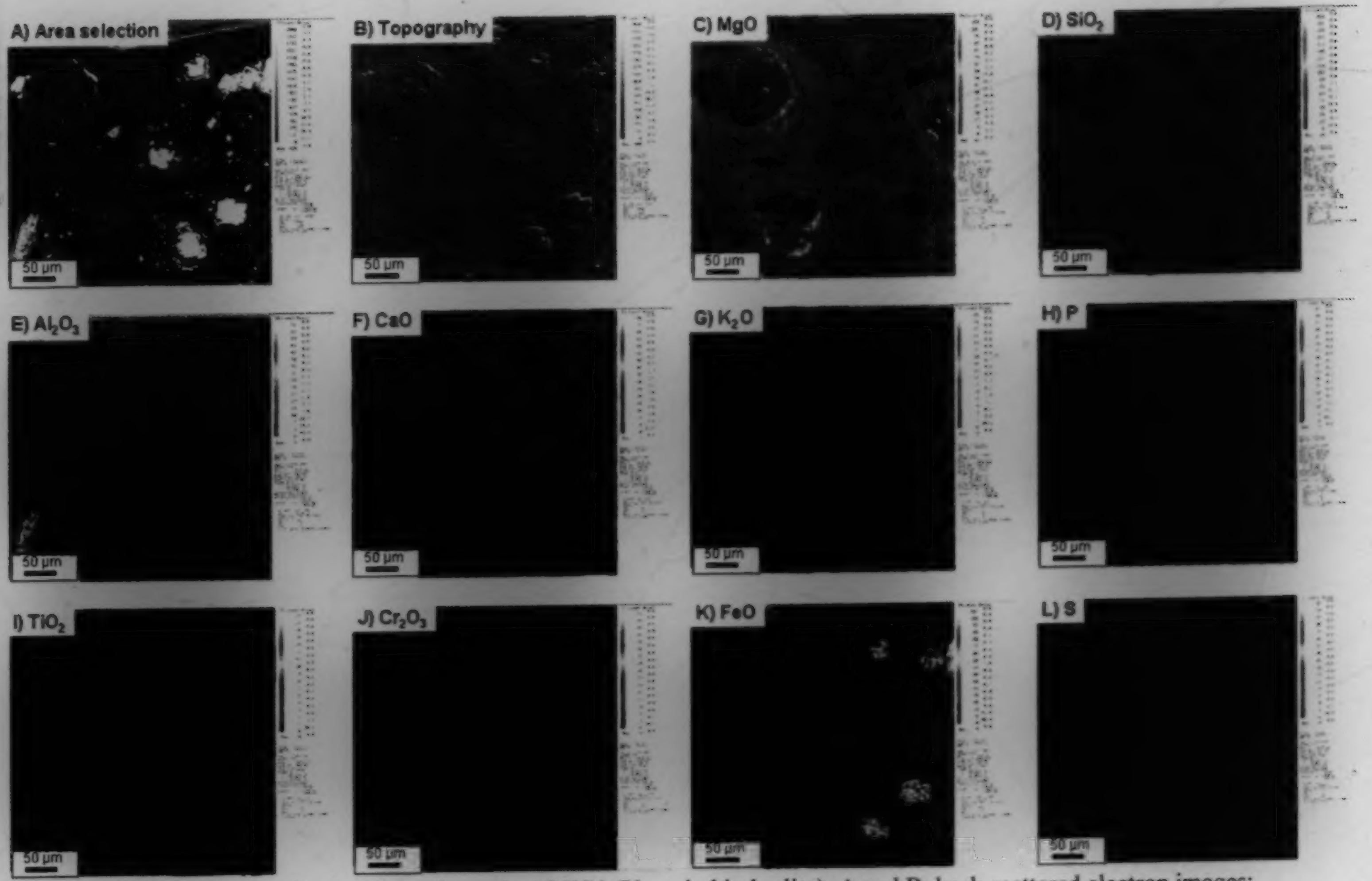
A) Area selection
B) Topography
C) MgO
D) SiO$_2$
E) Al$_2$O$_3$
F) CaO
G) K$_2$O
H) P
I) TiO$_2$
J) Cr$_2$O$_3$
K) FeO
L) S
50 µm

Appendix 4. Elemental distribution map of sample ABK76 (Phoenix kimberlite). A and B: back scattered electron images; C to L: x-ray elemental images

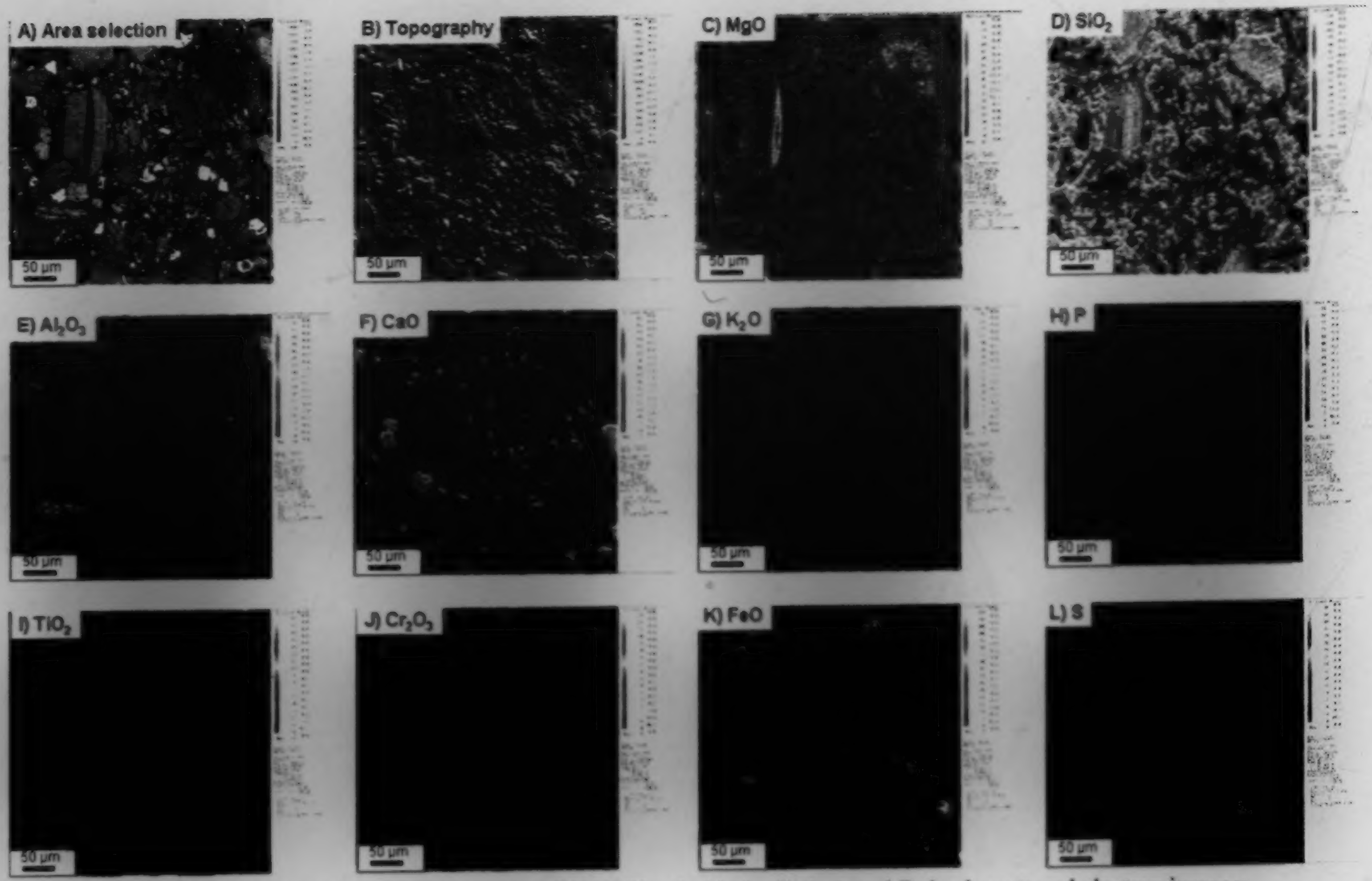
A) Area selection
B) Topography
C) MgO
D) SiO$_2$
E) Al$_2$O$_3$
F) CaO
G) K$_2$O
H) P
I) TiO$_2$
J) Cr$_2$O$_3$
K) FeO
L) S
50 µm

Appendix 4. Elemental distribution map of sample ABK81 (Kendu kimberlite). A and B: back scattered electron images; C to L: x-ray elemental images

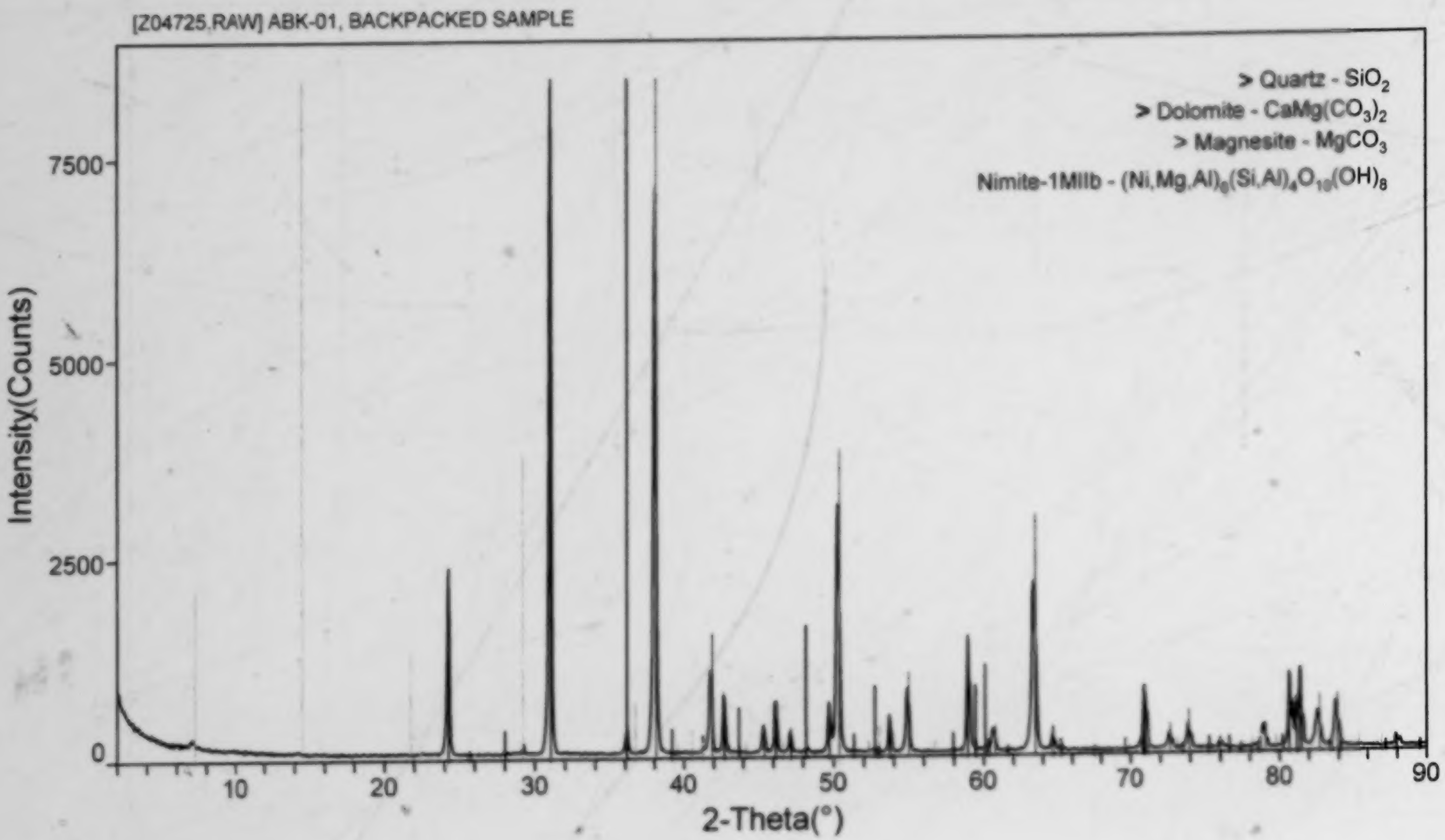

Appendix 5. X-ray diffractogram for sample ABK-01 (kimberlite K4A, Buffalo Head Hills).

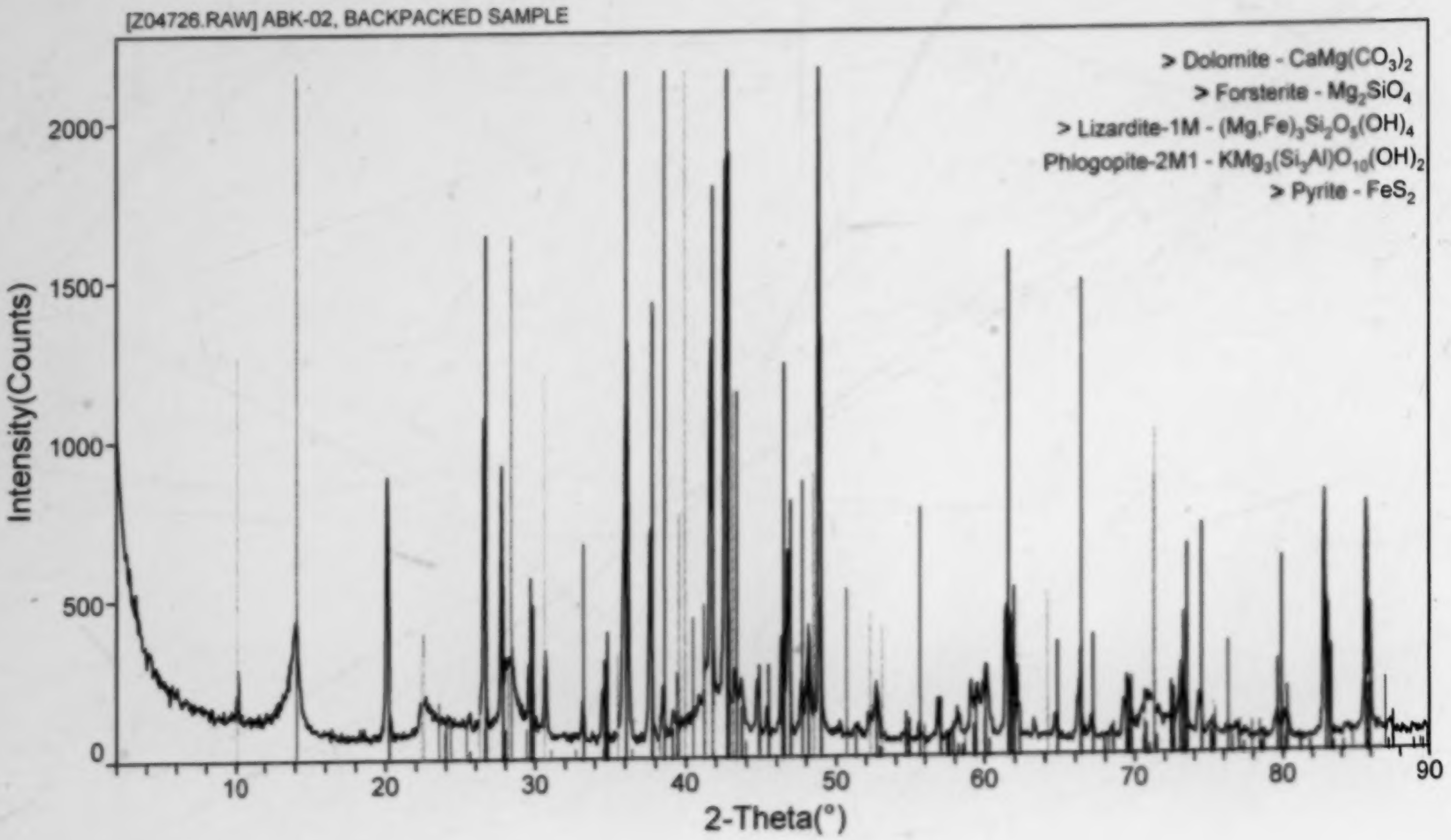

Appendix 5. X-ray diffractogram for sample ABK-02 (kimberlite K4B, Buffalo Head Hills).

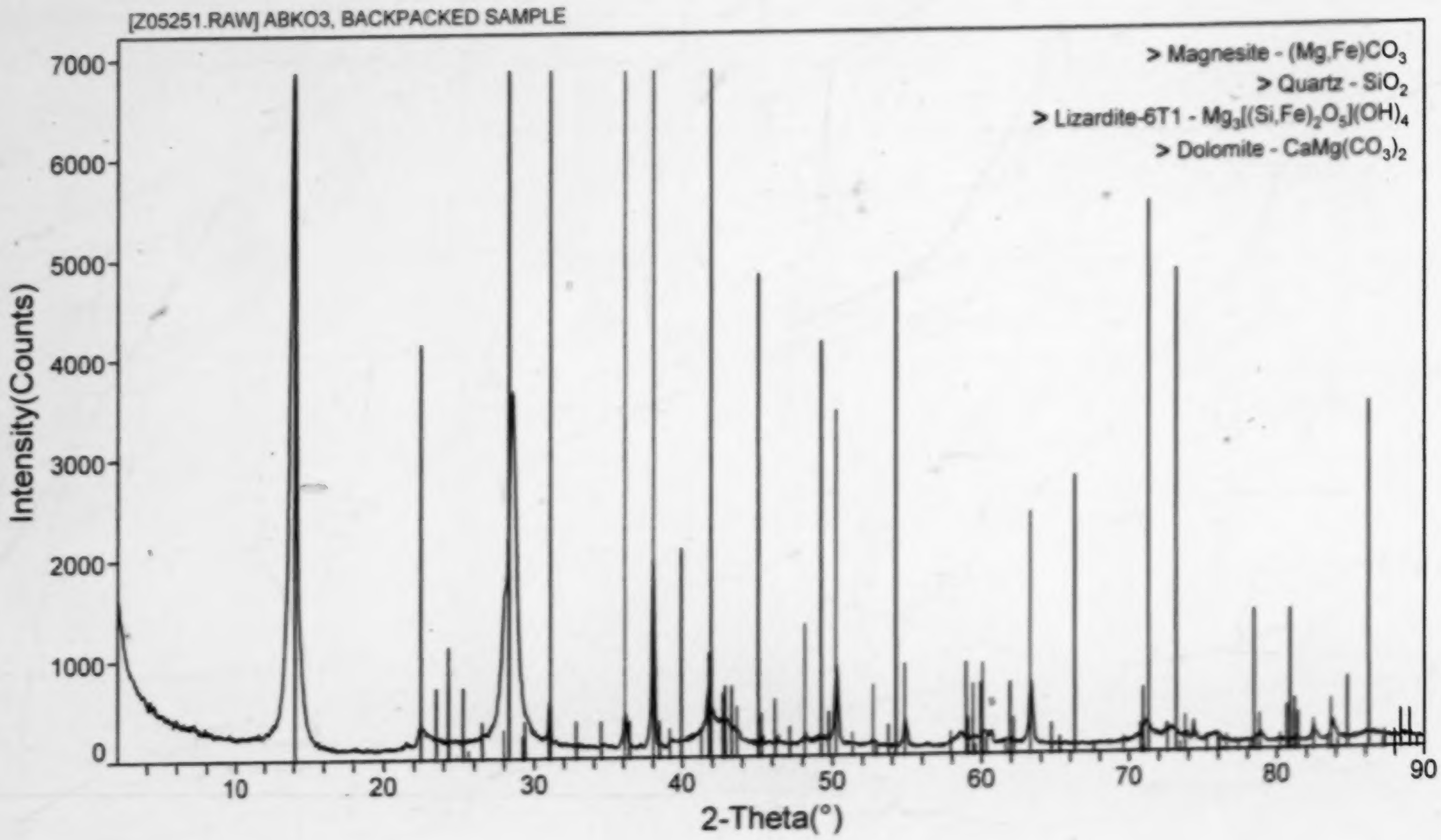

Appendix 5. X-ray diffractogram for sample ABK-03 (kimberlite K4C, Buffalo Head Hills).

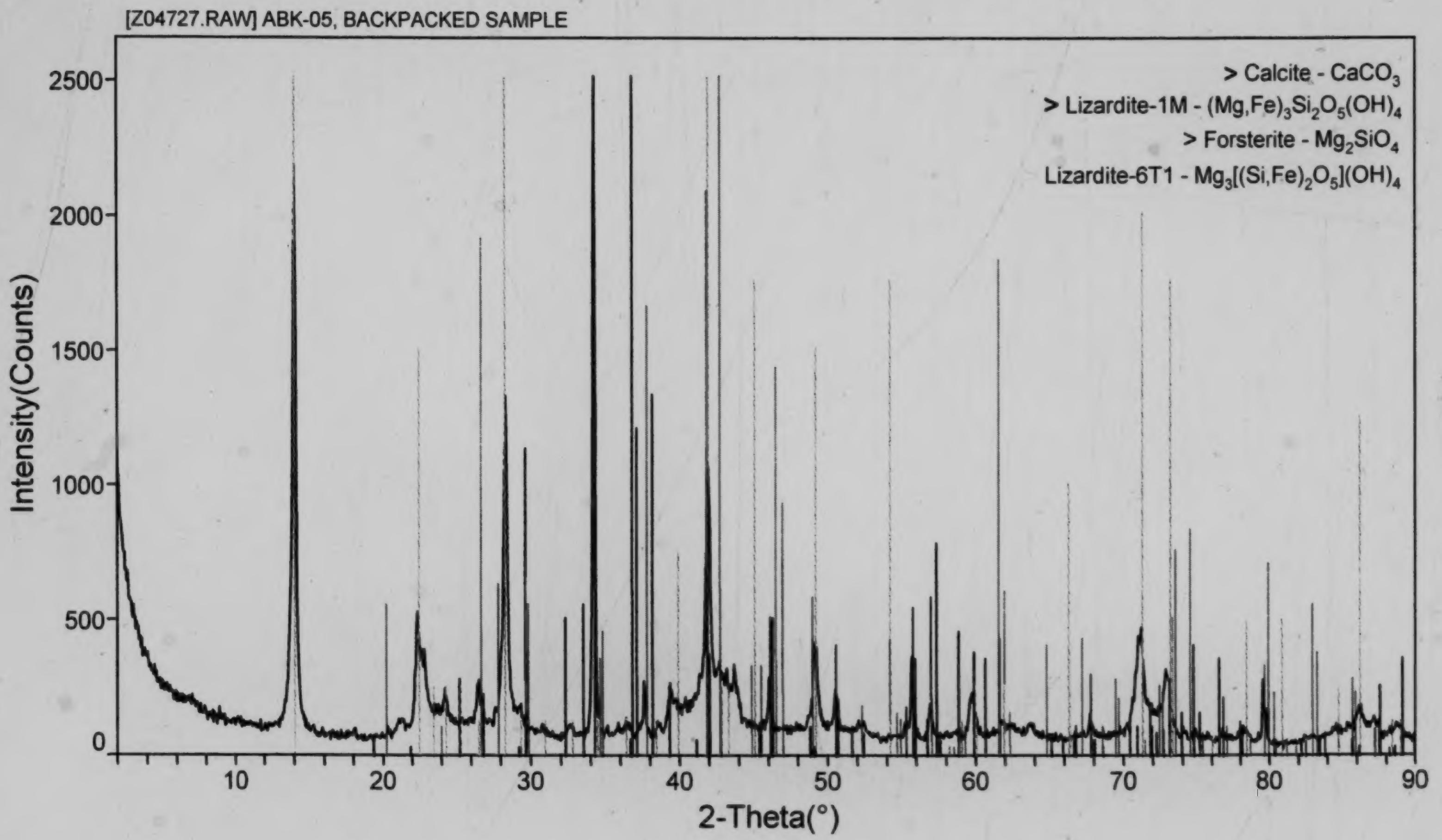

Appendix 5. X-ray diffractogram for sample ABK-05 (kimberlite K6, Buffalo Head Hills).

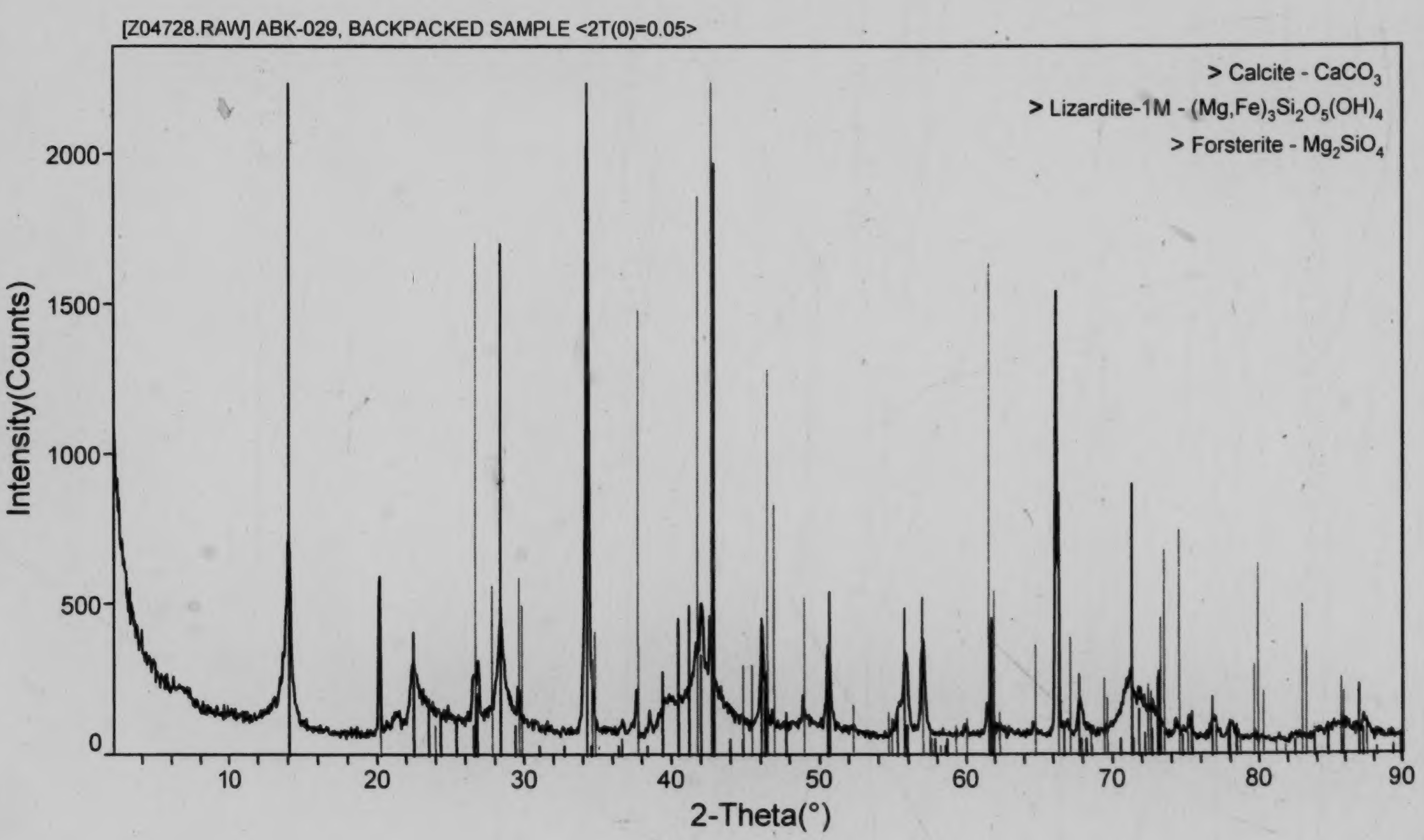

Appendix 5. X-ray diffractogram for sample ABK-29 (kimberlite K6, Buffalo Head Hills).

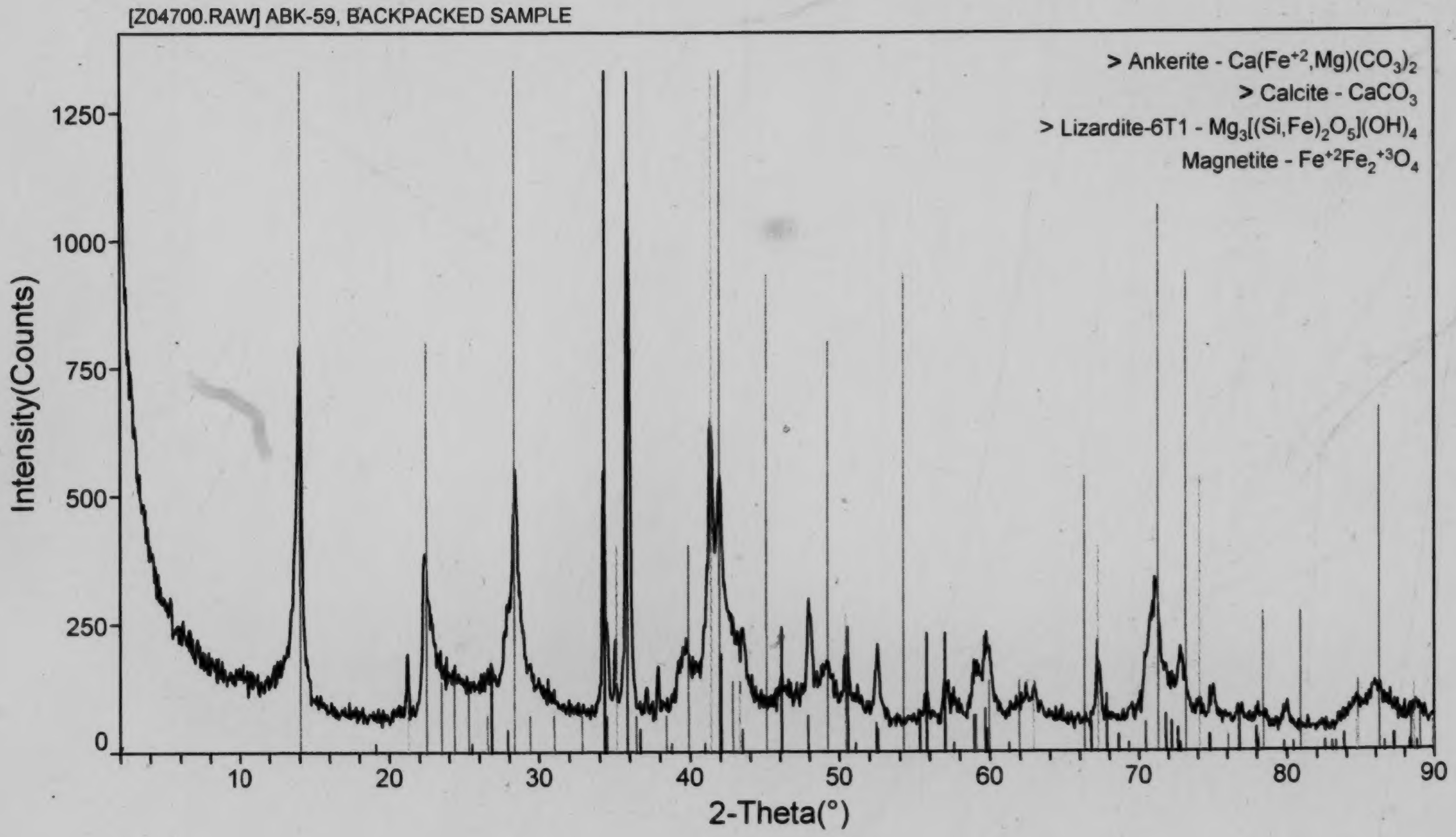

Appendix 5. X-ray diffractogram for sample ABK-59 (Legend kimberlite, Birch Mountains).

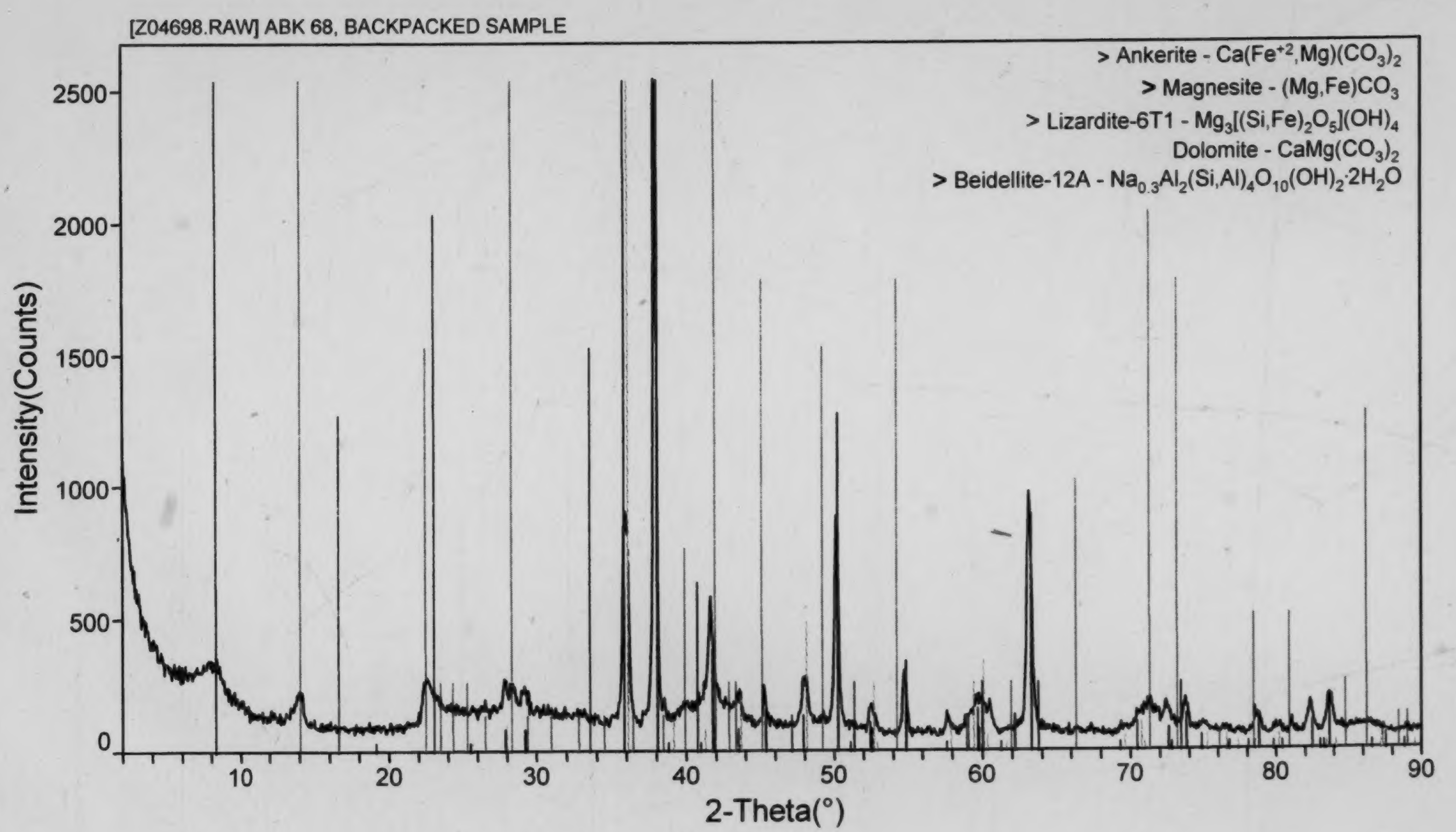

Appendix 5. X-ray diffractogram for sample ABK-68 (Legend kimberlite, Birch Mountains).

]

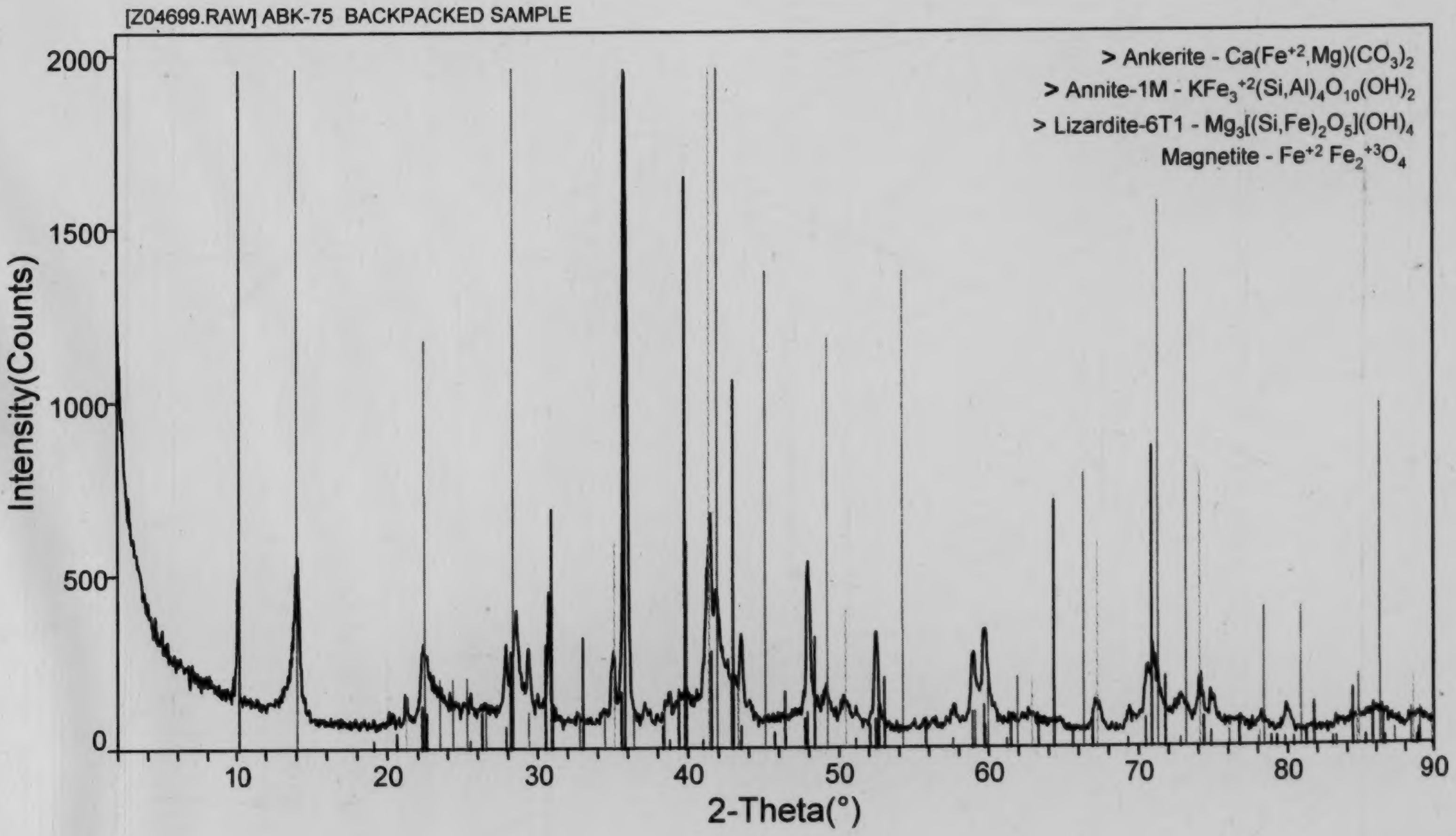

Appendix 5. X-ray diffractogram for sample ABK-75 (Phoenix kimberlite, Birch Mountains).

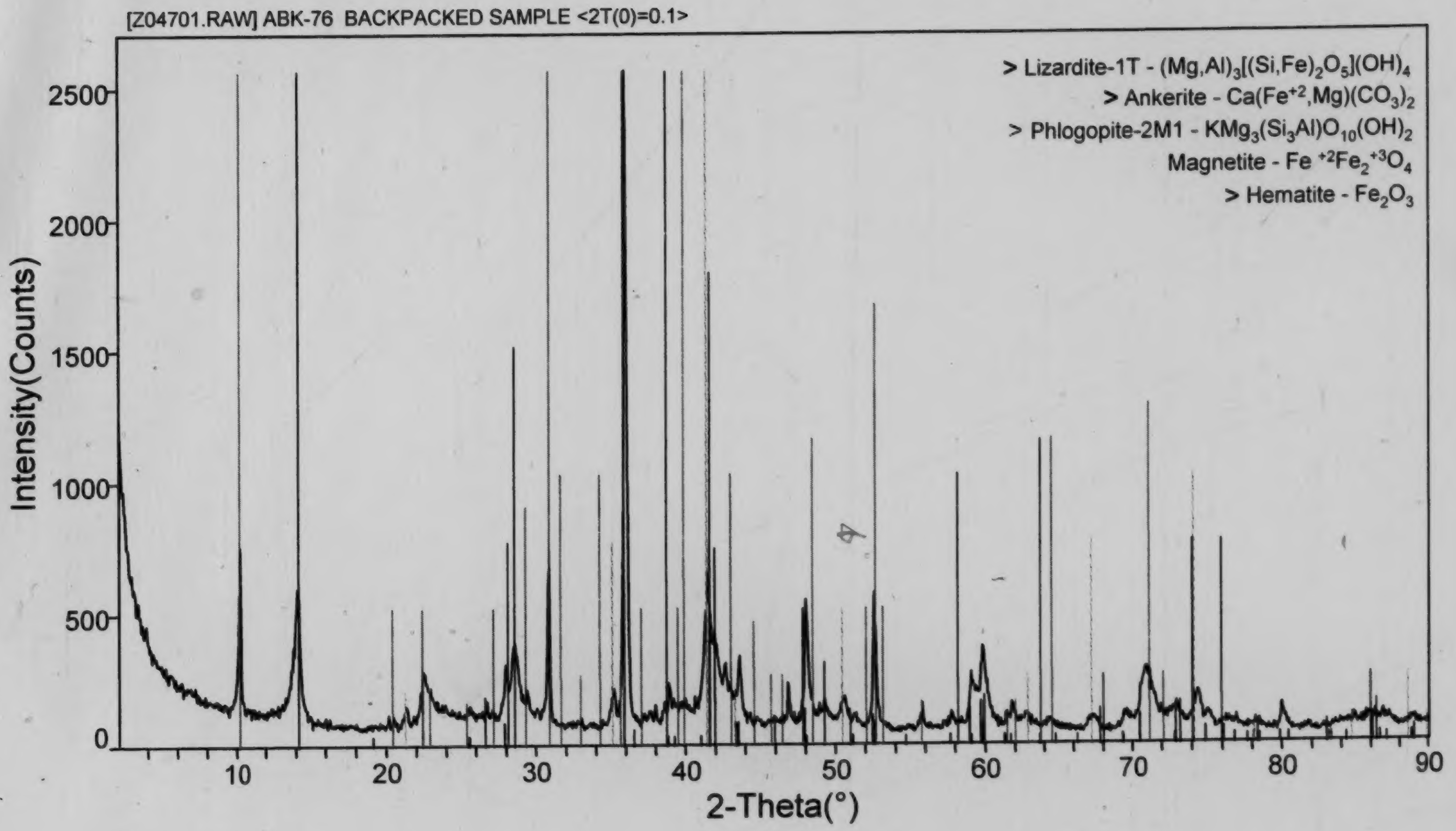

Appendix 5. X-ray diffractogram for sample ABK-76 (Phoenix kimberlite, Birch Mountains).

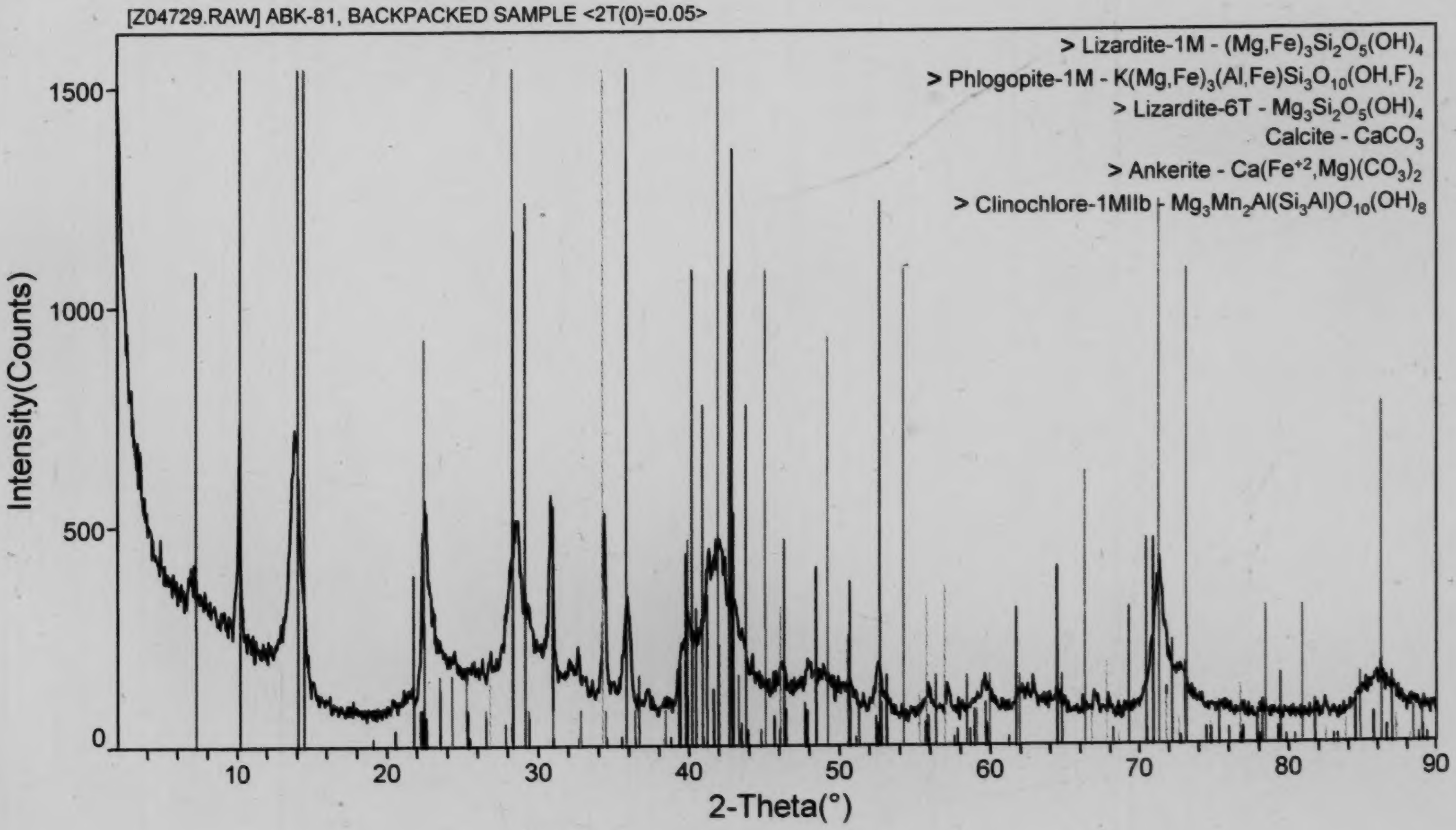

Appendix 5. X-ray diffractogram for sample ABK-81 (Kendu kimberlite, Birch Mountains).

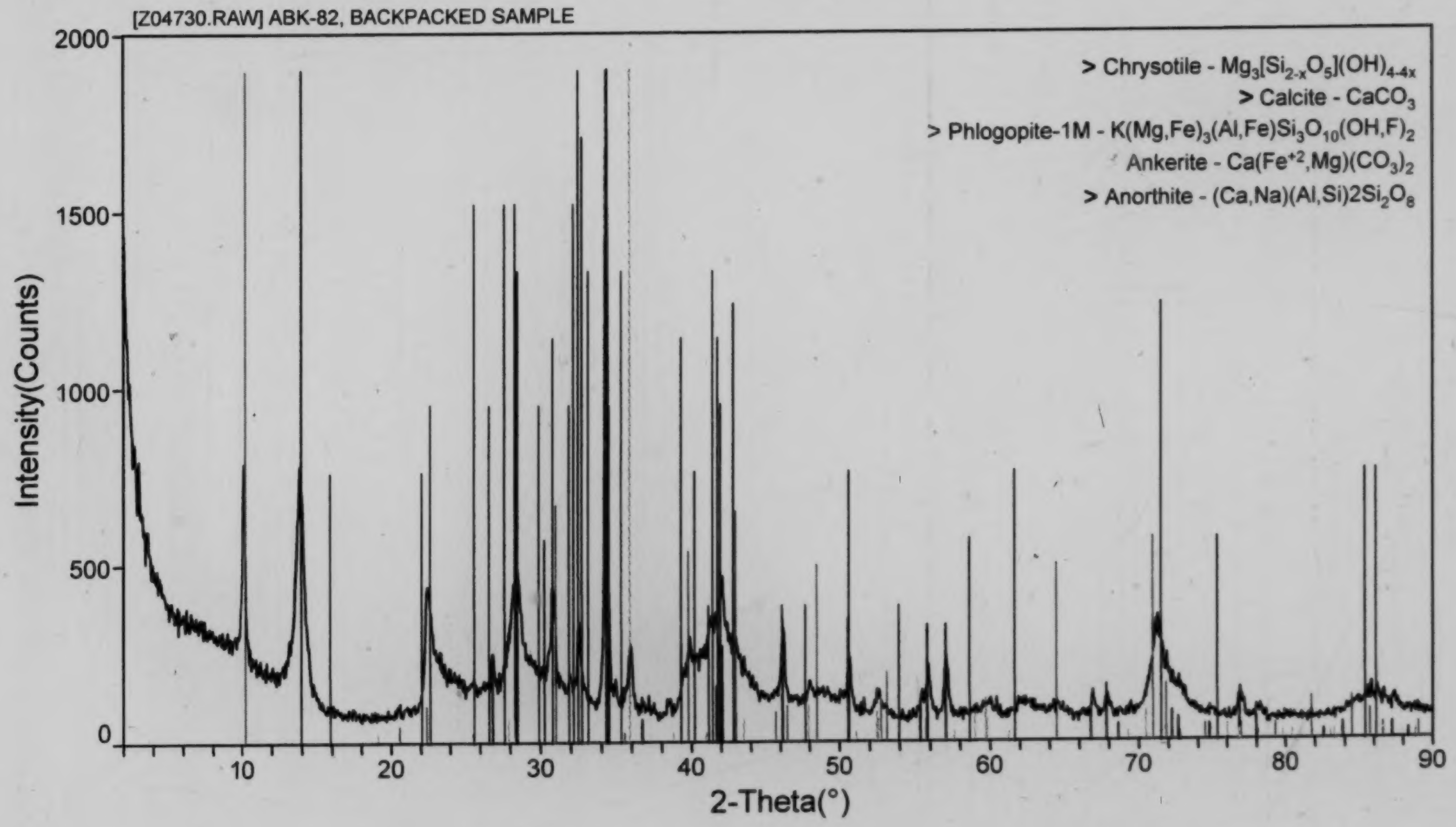

Appendix 5. X-ray diffractogram for sample ABK-82 (Kendu kimberlite, Birch Mountains).